Publication No. R80-26 Order No. 678

MIT

Evaluation of Seismic Safety of Buildings

Final Report

OVERALL SAFETY ASSESSMENT OF MULTISTORY STEEL BUILDINGS SUBJECTED TO EARTHQUAKE LOADS

by

SHIH-SHENG PAUL LAI

Supervised by Erik H. Vanmarcke

CIVIL ENGINEERING

SCHOOL OF ENGINEERING
MASSACHUSETTS INSTITUTE OF TECHNOLOGY
Cambridge, Massachusetts 02139

June 1980

Sponsored by
National Science Foundation
Division of Advanced Environmental Research and Technology
Grant 78-00658

Additional Copies May be Obtained From:

National Technical Information Service
U.S. Department of Commerce
5285 Port Royal Road
Springfield, Virginia 22161

50272-101

REPORT DOCUMENTATION PAGE	1. REPORT NO. NSF/RA-800204	2.	3. Recipient's Accession No. PB81 111718

4. Title and Subtitle
Overall Safety Assessment of Multistory Steel Buildings Subjected to Earthquake Loads (Evaluation of Seismic Safety of Buildings), Final Report

5. Report Date
June 1980

6.

7. Author(s)
S. -S. P. Lai

8. Performing Organization Rept. No.
R80-26

9. Performing Organization Name and Address
Massachusetts Institute of Technology
School of Engineering
Department of Civil Engineering
Constructed Facilities Division
Cambridge, MA 02139

10. Project/Task/Work Unit No.

11. Contract(C) or Grant(G) No.
(C) ENV7619021
(G) ENV7800658

12. Sponsoring Organization Name and Address
Engineering and Applied Science (EAS)
National Science Foundation
1800 G Street, N.W.
Washington, D.C. 20550

13. Type of Report & Period Covered
Final

14.

15. Supplementary Notes

16. Abstract (Limit: 200 words)

A set of 140 earthquake records was used to assess the uncertainties involved in ground motion representation. In particular, seismic input was characterized in terms of the Kanai-Tajimi power spectral density function and the strong-motion duration. Based on the method of spectral moments, key Kanai-Tajimi parameters were determined for the set of records. The statistics and interdependencies of these parameters were evaluated. The correlation between these K-T parameters, strong-motion duration, peak ground acceleration, epicentral distance and local magnitude was investigated. Based on an extensive simulation study, semi-empirical modifications were made to an existing random vibration solution for single-degree-of-freedom elasto-plastic systems. Similar modifications were incorporated in an approximate multi-degree-of-freedom elasto-plastic random vibration methodology for shear-beam systems, and its validity was assessed by a series of compatibility studies. By using the random vibration methodology, the overall inelastic seismic safety analysis of buildings was formulated. Also, for a hypothetical Boston site, the degree of overall seismic safety was assessed quantitatively for several multistory steel buildings designed by different procedures.

17. Document Analysis a. Descriptors

Earthquake resistant structures
Earthquakes
Buildings
Safety
Dynamic structural analysis
Damage
Ductility

b. Identifiers/Open-Ended Terms
Kanai-Tajimi parameters

c. COSATI Field/Group
Earthquake Hazards Mitigation

18. Availability Statement	19. Security Class (This Report)	21. No. of Pages
NTIS	20. Security Class (This Page)	22. Price

Massachusetts Institute of Technology
Department of Civil Engineering
Constructed Facilities Division
Cambridge, Massachusetts 02139

Evaluation of Seismic Safety of Buildings
Final Report

OVERALL SAFETY ASSESSMENT OF MULTISTORY STEEL BUILDINGS SUBJECTED TO EARTHQUAKE LOADS

by

SHIH-SHENG PAUL LAI

Supervised by
Erik H. Vanmarcke

June 1980

Sponsored by the National Science Foundation
Division of Advanced Engineering Research and Technology
Grants ENV 76-19021 and 78-00658

Publication No. R80-26 Order No. 678

ABSTRACT

A set of 140 earthquake records is used to assess the uncertainties involved in ground motion representation. In particular, seismic input is characterized in terms of the Kanai-Tajimi power spectral density function and the strong-motion duration. Based on the method of spectral moments, key Kanai-Tajimi parameters are determined for the set of records. The statistics and interdependencies of these parameters are evaluated. The correlation between these K-T parameters, strong-motion duration, peak ground acceleration, epicentral distance and local magnitude is investigated.

Based on an extensive simulation study, semi-empirical modifications are made to an existing random vibration solution for single-degree-of-freedom elasto-plastic systems. Similar modifications are incorporated in an approximate multi-degree-of-freedom elasto-plastic random vibration methodology for shear-beam systems, and its validity is assessed by a series of compatibility studies. The applicability of the methodology towards the inelastic component response prediction for structural frames is also evaluated.

By using the random vibration methodology, the overall inelastic seismic safety analysis of buildings is formulated. The sensitivity of local inelastic response w.r.t. the variabilities of the ground motion representation, the structural dynamic properties and the method of dynamic analysis is investigated. For a hypothetical Boston site, the degree of overall seismic safety is assessed quantitatively for several multistory steel buildings designed by different procedures. In particular, the conventional code-based design method, i.e., the Uniform Building Code, and a more complicated design method based on the "Inelastic Acceleration Response Spectrum" are considered.

PREFACE

This is the final report prepared under the research project entitled "Evaluation of Seismic Safety of Buildings" supported by National Science Foundation Grants ENV 76-19021 and 78-00658. This report is derived from a thesis written by Shih-sheng Paul Lai in partial fulfillment of the requirements for the degree of Doctor of Philosophy in the Department of Civil Engineering at the Massachusetts Institute of Technology, under the supervision of Professor Erik H. Vanmarcke.

The analysis and design of buildings for seismic effects involves a series of steps ranging from the prediction and specification of ground motions to the detailed design of structural components. The main objective of the project is to develop general methodology which permits quantitative assessment of the overall seismic safety of buildings provided by different design procedures. Earlier reports produced based on this research are as follows:

1. Arnold, P., Vanmarcke, E.H. and Gazetas, G., "Frequency Content of Ground Motions during the 1971 San Fernando Earthquake", M.I.T. Department of Civil Engineering Research Report R76-3, Order No. 526, January 1976.

2. Gasparini, D.A. and Vanmarcke, E.H., "Simulated Earthquake Motion Compatible with Prescribed Response Spectra", M.I.T. Department of Civil Engineering Research Report R76-4, Order No. 527, Jan. 1976.

3. Vanmarcke, E.H., Biggs, J.M., Frank, R., Gazetas, G., Arnold, P., Gasparini, D.A. and Luyties, W.H., "Comparison of Seismic Analysis Procedures for Elastic Multi-Degree Systems", M.I.T. Department of Civil Engineering Research Report R76-5, Order No. 528, Jan. 1976.

4. Frank, R., Anagnostopoulos, S.A., Biggs, J.M. and Vanmarcke, E.H., "Variability of Inelastic Structural Response due to Real and Artificial Ground Motions", M.I.T. Department of Civil Engineering Research Report R76-6, Order No. 529, January 1976.

5. Haviland, R., "A Study of the Uncertainties in the Fundamental Translational Periods and Damping Values for Real Buildings", Supervised by Professors J.M. Biggs and E.H. Vanmarcke, M.I.T. Department of Civil Engineering Research Report R76-12, Order No. 531, February 1976.

6. Luyties, W.H., Anagnostopoulos, S.A. and Biggs, J.M., "Studies on the Inelastic Dynamic Analysis and Design of Multi-Story Frames", M.I.T. Department of Civil Engineering Research Report R76-29, Order No. 548, July 1976.

7. Gazetas, G., "Random Vibration Analysis of Inelastic Multi-Degree-of-Freedom Systems Subjected to Earthquake Ground Motions", Supervised by Professor E.H. Vanmarcke, M.I.T. Department of Civil Engineering Research Report R76-39, Order No. 556, August 1976.

8. Haviland, R., Biggs, J.M. and Anagnostopoulos, S.A., "Inelastic Response Spectrum Design Procedures for Steel Frames", M.I.T. Department of Civil Engineering Research Report R76-40, Order No. 557, Sept. 1976.

9. Gasparini, D.A., "On the Safety Provided by Alternative Seismic Design Methods", Supervised by Professors J.M. Biggs and E.H. Vanmarcke, M.I.T. Department of Civil Engineering Research Report R77-22, Order No. 573, July 1977.

10. Vanmarcke, E.H. and Lai, S.P., "Strong-Motion Duration of Earthquakes", M.I.T. Department of Civil Engineering Research Report R77-16, Order No. 569, July 1977.

11. Robinson, J.H., "Inelastic Dynamic Design of Steel Frames to Resist Seismic Loads", Supervised by Professors J.M. Biggs and E.H. Vanmarcke, M.I.T. Department of Civil Engineering Research Report R77-23, Order No. 574, July 1977.

12. Lai, S.P., "On Inelastic Response Spectra for Aseismic Design", Supervised by Professors J.M. Biggs, and E.H. Vanmarcke, M.I.T. Department of Civil Engineering Research Report R78-18, Order No. 604, July 1978.

ACKNOWLEDGEMENTS

The author wishes to express the deepest appreciation for the invaluable inspiration and firm support of Professor Erik H. Vanmarcke throughout this research endeavor. The author is indebted to Professor John M. Biggs for his kind advice and encouragement and to Ms Elizabeth Augustine for the excellent typing of the report.

This research was supported by the U.S. National Science Foundation under Grant No. ENV 78-00658. Any opinions, findings and conclusions or recommendations expressed in this report are those of the author and do not necessarily reflect the views of the National Science Foundation.

TABLE OF CONTENTS

LIST OF FIGURES

LIST OF TABLES

LIST OF SYMBOLS

A_i	Amplitude of the ith Contributing Sinusoid
A_{kjt}	Cross Term Factor Between Mode k and Mode j
a	Ground Acceleration
a_{max}	Peak Ground Acceleration of an Earthquake Motion
a_o	Lower Bound Peak Ground Acceleration of Seismic Risk Curve
$B_{i,k}$	Probability of No Yielding Occurred in Story i, When Yielding State k Begins
C	An Event with Combination of Pertinent Random Variables
c_k	Contribution Coefficient to the Impulse-Response Function due to Mode k
D	Elasto-Plastic Interstory Deformation
D^*	Modified Elasto-Plastic Interstory Deformation
D_p	Peak Elasto-Plastic Interstory Deformation
$D^*_{i,k}$	Modified Elasto-Plastic Interstory Deformation of Story i During Yielding State k
d	Elasto-Plastic Response Threshold
d_i	Elasto-Plastic Response Threshold of Story i due to Yielding State k
DF	Damage Factor of a Building
E	Young's Modulus of Steel
$E[\cdot]$	Expected Value of a Random Variable
$F(\cdot)$	Cumulative Distribution Function of a Random Variable
F_y	Equivalent Story Yielding Strength
$f(\cdot)$	Probability Density Function of a Random Variable
f_k	Probability of Story k Yielding First
G	Power Spectral Density (PSD) Function
G_o	White Noise Excitation Intensity at Bedrock-Overburden Interface

G_y	Power Spectral Density Function of the Response
g	A Nonlinear Function Which Relates Random Variables Y and X_i
g_i'	Partial Derivative of Function g with respect to Random Variable X_i
H	Transfer Function of the System
H^*	Complex Conjugate of Transfer Function H
H_k	Transfer Function of Mode k
h	Impulse-Response Function
h_k	Impulse-Response Function for Mode k
I_C	Moment of Inertia of Column
I_G	Moment of Inertia of Girder
I_o	Arias Intensity
I_s	Modified Mercalli Intensity at the Site
J_i	Normalized ith Moment of the Kanai-Tajimi Power Spectral Density Function
$\underline{K}$	Far-Coupled Lateral Stiffness Matrix
$\underline{K}_L$	Close-Coupled Lateral Stiffness Matrix
K_i	Equivalent Lateral Story Stiffness of Story i
K_B^G	Girder Member Stiffness in the Adjacent Bottom Floor
K_T^G	Girder Member Stiffness in the Adjacent Top Floor
K^C	Member Stiffness of Column
L_C	Story Height
L_G	Girder Span
$\underline{M}$	Diagonal Story Mass Matrix
M^C	Column Design Moment
M_{EQ}^C	Average Column End Moment Due to Earthquake Load
M_{GR}^G	Average Girder End Moment Due to Earthquake Load

M^C_{GR}	Average Column End Moment Due to Gravity Load
M_L	Local Richter Magnitude of an Earthquake Motion
M^C_y	Moment Capacity of Column
M^G_y	Moment Capacity of Girder
m	Ratio of Transient Variances
m_i	ith Story Mass
$P[\cdot]$	Probability of a Random Variable
P^C	Maximum Column Axial Force
P_d	Probability of Peak Elasto-Plastic Deformation d_i Not Being Exceeded
P^C_{EQ}	Maximum Column Axial Force Due to Earthquake Load
P^C_{GR}	Maximum Column Axial Force Due to Gravity Load
$P_{i,k}$	Probability of Story i Yields During Yielding State k
P^C_y	Axial Force Capacity of Column
Q_k	Contribution Coefficient of Response Variance Due to Mode k
R	Epicentral Distance of an Earthquake Motion
R_L	Local Ductility Correction Factor
R_T	Natural Period Ratio
R_y	Yielding Strength Factor
r	Normalized Threshold Level
$r_{i,k}$	Normalized Response Threshold Level of Story i During Yielding State k
r_k	Normalized Response Threshold Level of Story k
$r_{S_o,P}$	Threshold Factor with Excitation Duration S_o and Probability Level P
S	Earthquake Duration Defined by Housner
S_k	Equivalent Steady-State Duration of Yielding State k

S_o	Equivalent Strong-Motion Duration
S_o^*	Equivalent Stationary Response Duration
t	Indicating Time
T_o	Predominant Period of an Earthquake Motion
u_1	Parameter of Gumbel Type I Extreme Value Distribution
u_2	Parameter of Gumbel Type I Extreme Value Distribution
V	Coefficient of Variation
w	Uniform Gravity Load
X_n	A Random Variable
$\bar{X}_n$	Mean Value of Random Variable X_n
Y	A Random Variable which Depends on X_n
y	Story Displacement at a Specific Point of the Structure
y_e	Elastic Response Limit
$y_{e,i}$	Elastic Response Limit of Story i
α	Decay Rate
α_k	Decay Rate of the Reliability for Story k
$\alpha_{i,k}$	Decay Rate of the Reliability for Story i During Yielding State k
Γ_k	Participation Factor of Mode k
γ_1	Coefficient of Skewness
γ_2	Coefficient of Kurtosis
Δ	Increment (or Discretization Interval)
δ	Shape Factor
δ_y	Shape Factor of the Response
ε	Modal Frequency Ratio
ζ_g	Kanai-Tajimi Damping Coefficient
ζ_k	Damping Coefficient of Mode k

ζ_{kt}	Time-Dependent Damping Coefficient of Mode k
ζ_s	Structural Damping Coefficient
η	Parameter Expressed by Eq. 3-12
κ	Empirical Economic Factor
λ_i	ith Spectral Moment
$\lambda_{i,y}$	ith Spectral Moment of the Response
$\lambda_{i,y,k}$	ith Spectral Moment of the Response During Yielding State k
μ	Local Component Ductility Ratio (or Story Ductility Ratio)
μ_{ult}	Ultimate Local Ductility Ratio of a Building
ν_i	Mean Rate of Zero Crossings for Story i
ν_o	Mean Rate of Zero Crossings
$\nu^*_{o,k}$	Reduced Mean Rate of Zero Crossings of Yielding State k
ξ_i	Reduction Factor for Story i
ρ	Normalized Second Slope of a Bilinear Spring Model
σ	Standard Deviation
σ_*	Root-Mean-Square Response Due to Random Phasing of Sinusoids
σ_o	Root-Mean-Square Acceleration
σ_{X_i}	Standard Deviation of Random Variable X_i
σ_Y	Standard Deviation of Random Variable Y
σ_y	Root-Mean-Square Response
$\sigma_{y,k}$	Elastic Root-Mean-Square Response of Story k
$\sigma_{y,i,k}$	Elastic Root-Mean-Square Response of Story i when Story k Yields First
σ_μ	Standard Deviation of Peak Ductility Ratio
τ	Time Integration Interval
$\underline{\Phi}_n$	nth Modal Shape Vector
ϕ_{1i}	First Modal Shape at Story i

ϕ_i Phase Angle of the ith Contributing Sinusoid

ψ Empirical Frequency Reduction Factor

Ω Ratio of ω to Kanai-Tajimi Frequency

Ω^* Ratio of ω^* to Kanai-Tajimi Frequency

Ω_y Average Response Frequency

$\Omega_{y,k}$ Central Frequency of Response for Story k

ω_i Natural Frequency of the ith Contributing Sinusoid

ω_c Central Frequency

ω^* Upper Integration Limit in Eq. 2-4

ω_g Kanai-Tajimi Frequency

CHAPTER 1

INTRODUCTION

1.1 Objectives and Scope

The analysis and design of a building subjected to earthquake loads requires a series of steps comprising the prediction and characterization of ground motions, the modeling of structural dynamic behavior and the detailed design of structural components. In recent years, extensive research efforts have been concentrated on the investigation of each of the above-mentioned steps. Different improved building design procedures with varying complexity have been developed, e.g., the response spectrum design approach (ATC-2) [3], and the seismic design provisions recently recommended by the Applied Technology Council (ATC-3) [4].

However, insufficient attention has been given to the building design process as a whole so that the actual degree of seismic protection provided by the alternative design approaches can be evaluated. Based on random vibration analysis, Gasparini [22] studied the seismic saftey of linear-elastic multi-degree-of-freedom systems. Limited effort was attempted by Binder [10] to evaluate the seismic safety of multi-degree elasto-plastic shear-beam structures.

The main objective of this research endeavor is to develop general methodology which permits quantitative assessment of the overall inelastic seismic safety of building frames provided by different design procedures. Specifically, principal research efforts are directed toward the investigation of the following topics:

- Characterization of strong ground motions
- Prediction of inelastic response for shear-beam systems by approximate multi-degree random vibration methodology
- Compatibility of inelastic response predictions for structural frames by random vibration and time-history analysis
- Formulation of overall inelastic seismic safety analysis for buildings
- Assessment of overall seismic safety of multistory steel buildings provided by the conventional code-based design method versus the inelastic design method

In this study, a set of 140 actual strong earthquake records is used to investigate the uncertainties involved in ground motion representation. In particular, seismic input is characterized in terms of the Kanai-Tajimi power spectral density function [34,55] and the strong-motion duration [61,63]. Based on the method of spectral moments, key Kanai-Tajimi parameters are determined for the set of records. The statistics and interdependencies of these parameters are investigated. The correlation between these pertinent seismic parameters and earthquake peak ground acceleration, epicentral distance and local magnitude is evaluated.

Based on an extensive simulation study, a semi-empirical modification is made to an existing random vibration analysis for one-degree elasto-plastic systems. The same modification is incorporated in an approximate multi-degree elasto-plastic random vibration solution for shear-beam systems, and its validity is assessed by a series of compatibility studies.

The applicability of the methodology towards the inelastic component response prediction for structural frames is also evaluated.

By using the random vibration methodology, the overall seismic safety analysis of buildings is formulated. By means of a series of sensitivity studies, the relative importance of different uncertainties involved in inelastic seismic safety analysis is investigated. For a hypothetical Boston site, the degree of overall seismic safety is assessed quantitatively for several multistory steel buildings designed by different procedures. In particular, the conventional code-based design method, i.e., the Uniform Building Code [58], and a more complicated design method based on the "Inelastic Acceleration Response Spectrum" [39] are considered.

1.2 Organization

Chapter 2 starts with a brief description of the Kanai-Tajimi spectral density function and the estimation method to determine its key parameters. The statistics of the Kanai-Tajimi parameters and of other pertinent seismic parameters are then reported for a set of 140 recorded strong ground motions. This is followed by a discussion of the influence of site conditions and a presentation of the results of correlation studies involving the Kanai-Tajimi parameters, strong-motion duration, peak ground acceleration, epicentral distance and local magnitude.

In Chapter 3, the linear-elastic random vibration solution for multi-degree shear-beam systems are first reviewed. This is followed by a brief description of a random vibration model for one-degree elasto-plastic systems. Based on extensive simulation studies, semi-empirical modifications to this model are reported. Based on similar modifications, an approximate multi-degree elasto-plastic random vibration methodology for shear-beam

systems is oulined.

The moment-resisting steel frames and the synthetic strong ground motions used in this study are briefly described in Chapter 4. The determination of equivalent story shear-springs parameters corresponding to a structural frame are discussed. The results of a series of compatibility studies aimed at quantifying different sources of uncertainty associated with the local inelastic response prediction of structural frames are presented next. A brief discussion on the effects of gravity loads is also included. Finally, the prediction of maximum lateral story displacement is discussed.

In Chapter 5, a method to predict inelastic seismic response of components in buildings is developed. The results of a series of sensitivity studies of local inelastic response with respect to the variabilities of the ground motion representation, the structural dynamic properties, and the method of dynamic analysis are then reported. The effect of ground motion intensity is also discussed.

Chapter 6 presents methodology for combining discrete response characteristics for the prediction of overall response statistics. The results of the conditional probability distributions of local ductility ratio (given peak ground acceleration) are presented for the steel frames under study. This is followed by a brief description of the seismic risk curves for the hypothetical Boston site. By incorporating this local seismic risk information, the degree of overall seismic safety is compared for several multistory steel buildings designed by different methods, i.e., the conventional code-based design method versus a more complicated inelastic design method. A brief discussion on the relationship between the predic-

ted local ductility ratio and the expected damage in a building is also included.

Finally, Chapter 7 summarizes major conclusions reached from this research endeavor. Recommendations for further study are also presented.

CHAPTER 2

CHARACTERIZATION OF STRONG GROUND MOTIONS FOR SEISMIC SAFETY ASSESSMENT

2.1 Introduction

The ultimate objective of earthquake-resistant design is to protect the structure and its contents, as well as to provide adequate safety for its occupants. In order to assess the overall seismic safety of constructed facilities, it is necessary to consider three major sources of uncertainty: i) the representation of earthquake environment, ii) the dynamic structural properties, and iii) the method of dynamic analysis. In this chapter, only the uncertainties of ground motion representation will be examined. The other two sources of uncertainty are discussed in Chapters 4 and 5.

There are two basic approaches to ground motion characterization. In the time domain approach, the design motion can be represented by time histories of ground acceleration, velocity or displacement. Although the method is generally applicable, it does not grasp the randomness of future earthquake motions. In order to account for this variability, multiple time-history analyses using a set of ground motions are often used, but this is often too expensive to be attractive for practical application.

This concern gives rise to a statistical approach to ground motion representation in the frequency domain in terms of the power spectral density (PSD) function. The PSD function can be obtained from the Fourier Transform of the acceleration time history of a ground motion record. Based on the PSD function, the probabilistic structural response can be predicted by random vibration methodology.

In this chapter, important statistical measures of the frequency content of strong motion excitation will first be discussed. This is followed by a brief description of the Kanai-Tajimi power spectral density function, and of the fitting method used to determine its key parameters. The method has been applied to a set of 140 recorded strong ground motions. The statistics of several pertinent seismic parameters will be presented. Moreover, ground motion parameter correlations involving strong-motion duration, Kanai-Tajimi parameters, peak ground acceleration, epicentral distance and local magnitude are investigated. Finally, a compatibility study concerning the prediction of strong-motion duration using different empirical relationships as suggested in this study will be included.

2.2 Kanai-Tajimi Power Spectral Density Function

Since the accelerogram of a strong ground motion has the appearance of a random process, it is commonly expressed in terms of a series of sinusoidal waves as follows:

$$a(t) = \sum_{i=1}^{n} A_i \sin(\omega_i t + \phi_i) \qquad (2\text{-}1)$$

where $a(t)$ is the ground acceleration, A_i is the amplitude and ϕ_i is the phase angle of the ith contributing sinusoid with frequency ω_i. The power

spectral density function $G(\omega)$ can be defined as:

$$G(\omega_i)\Delta\omega = A_i^2/2 \tag{2-2}$$

Based on Kanai's study [34] of the frequency content for several real strong ground motions, Tajimi suggested the following power spectral density function to characterize a ground motion [55]:

$$G(\omega) = \frac{[1 + 4\zeta_g^2(\omega/\omega_g)^2]G_o}{[1-(\omega/\omega_g)^2]^2 + 4\zeta_g^2(\omega/\omega_g)^2} \tag{2-3}$$

where ζ_g, ω_g and G_o are parameters to be determined from earthquake records.

Physically, the Kanai-Tajimi (K-T) PSD function can be interpreted as corresponding to an "ideal white noise" excitation at the bedrock subjected to one-degree-amplification through the overlaying soil deposits. Therefore, the three Kanai-Tajimi parameters can be interpreted as: ζ_g, the ground "viscous damping coefficient"; ω_g, the ground "natural frequency" (assuming single-degree-of-freedom); and G_o, the "intensity of the ideal white noise excitation" at the bedrock-overburden interface. Since only three parameters are needed to define the frequency content of strong ground motion, the Kanai-Tajimi power spectral density spectrum has been widely used by researchers [9,10,22,40]. It has also been employed in this study to characterize strong ground motion.

However, due to the fact that most estimated power spectra of ground motions are very erratic, it is difficult to determine the parameters of the corresponding smooth K-T PSD function. Binder [9] tried two different fitting methods, namely, the "least square method" and the "moments method", to compute the Kanai-Tajimi parameters. Based on the study of 39 real earthquake records, he concluded that the method of moments should

yield the most satisfactory results.

In this study, the spectral moments method used by Binder is employed to calculate the Kanai-Tajimi parameters for a set of 140 strong ground motions. A brief overview of the method is presented below.

For frequency domain analysis, the spectral moments of a PSD function are key statistical parameters. The ith spectral moment λ_i is defined as [60]:

$$\lambda_i = \int_0^\infty \omega^i \, G(\omega) \, d\omega \tag{2-4}$$

The variance of the excitation is the zero spectral moment λ_o:

$$\lambda_o = \sigma_o^2 = \int_0^\infty G(\omega) \, d\omega \tag{2-5}$$

The central frequency, ω_c, and the shape factor, δ, of the random process can be directly evaluated from the first few spectral moments:

$$\omega_c = \sqrt{\lambda_2/\lambda_o} \tag{2-6}$$

$$\delta = \sqrt{1 - (\lambda_1^2/\lambda_o\lambda_2)} \tag{2-7}$$

The method of spectral moments computes the Kanai-Tajimi parameters in such a way that the spectral moments, i.e., λ_o, λ_1, and λ_2, of the actual ergodic power spectrum and those of the fitted K-T PSD function are the same. Since σ_o^2, ω_c and δ are functions of the spectral moments as expressed in Eqs. 2-5, 2-6 and 2-7, respectively, this suggests that the moments method will lead to a K-T PSD function with the same variance, central frequency and shape factor as the actual power spectrum. This consistency in

the pertinent statistical parameters is clearly desirable.

As an extension of the work by Pulgrano and Ablowitz [50], spectral moments of the Kanai-Tajimi PSD function can be expressed as:

$$\lambda_o = \frac{\pi G_o \omega_g}{4\zeta_g} \; J_o(\Omega^*)(1 + 4\zeta_g^2) \tag{2-8}$$

$$\lambda_1 = \frac{\pi G_o \omega_g^2}{4\zeta_g} \left\{ J_1(\Omega^*) + 4\zeta_g^2 \; J_3(\Omega^*) - \frac{1 + 4\zeta_g^2 - 8\zeta_g^4}{\pi\sqrt{1 - \zeta_g^2}} \; \tan^{-1}\left(\frac{2\zeta_g\sqrt{1 - \zeta_g^2}}{1 - 2\zeta_g^2} \right) \right\} \tag{2-9}$$

$$\lambda_2 = \frac{\pi G_o \omega_g^3}{4\zeta_g} \left| J_2(\Omega^*) + 4\zeta_g^2 \; J_4(\Omega^*) \right| \tag{2-10}$$

where

$$J_i(\Omega) = \frac{4\zeta_g}{\pi} \int_0^{\Omega} \frac{\Omega^i d\Omega}{[1 - \Omega^2]^2 + 4\zeta_g^2\Omega^2} \tag{2-11}$$

The expressions J_o, J_1, J_2, J_3 and J_4 are tabulated in Appendix A.

Ω^* is defined as ω^*/ω_g, where ω^* is the upper integration limit in Eq. 2-4 and is theoretically equal to infinity. As expressed in Eqs. 2-9 and 2-10, the evaluation of λ_1 and λ_2 requires $J_3(\Omega^*)$ and $J_4(\Omega^*)$. However, both values are infinite when Ω^* approaches infinity (see Appendix A). Therefore, it is necessary to use a finite value for the upper limit of integration.

Given that high frequency sinusoids contribute negligible excitation to most strong ground motions, the standard C.I.T. earthquake record digitization procedure uses a cut-off frequency of 25 Hz [13]. Since the natural frequencies of most structures of interest lie in the range of $0 \sim 25\ \pi$ rad/sec, the value of $25\ \pi$ rad/sec is assumed for ω^* in this

study. This implies $\Omega^* = 25\pi/\omega_g$.

Because the central frequency and shape factor are functions of the spectral moments (λ_o, λ_1, and λ_2), they can be expressed in terms of the Kanai-Tajimi parameters, i.e., ω_g, ζ_g and G_o. Hence, the K-T parameters can be computed by matching the variance of acceleration (Eq. 2-5), the central frequency (Eq. 2-6), and the shape factor (Eq. 2-7).

2.3 Ground Motion Parameters for a Set of 140 Records

2.3.1 Background

The method of spectral moments has been applied to two horizontal components for each of 70 California strong motion records. The record set was originally selected by McGuire and Barnard [44] so as to be representative of a broad range of earthquake magnitudes, epicentral distances, motion intensities and site conditions. Eleven sites (22 records) were classified by McGuire and Barnard as "rock" sites, and 59 sites (118 records) as "soil" sites. Pertinent characteristics of these records are listed in Table 2-1.

As mentioned in Chapter 1, the "strong-motion duration" is also a relevant parameter for seismic safety analysis. The definition of strong-motion duration proposed by Vanmarcke and Lai [61,63] has been employed in this study. It is based on the following relationships:

$$I_o = \sigma_o^2 \, S_o \tag{2-12}$$

$$a_{max} = \sqrt{2 \, \ell n(2S_o/T_o)} \;\; \sigma_o \quad ; \quad S_o \geq 1.36 \, T_o \tag{2-13}$$

where S_o = equivalent strong-motion duration, I_o = Arias Intensity, i.e., the integral of the squared accelerations [5], σ_o = root-mean-square acceleration, a_{max} = peak ground acceleration, and T_o = predominant period

of the earthquake motion.

For each strong ground motion, I_o and a_{max} can readily be computed. By assuming a predominant period T_o, the strong-motion duration and the r.m.s. acceleration can be solved from the above two equations. The advantages of using this approach are: i) the total energy of the motion is preserved, ii) a consistent relationship exists between a_{max}, σ_o, and S_o. (For a stationary Gaussian random process with mean-squared acceleration σ_o^2, Eq. 2-13 implies that a_{max} occurs <u>once on the average</u> during the duration S_o.)

Using the C.I.T. ground motion identification labels, Table 2-1 lists the results for the set of 140 real strong ground motions. They comprise: local Richter magnitudes (M_L), epicentral distances (R), peak ground accelerations (a_{max}), r.m.s. accelerations (σ_o), strong-motion durations (S_o), central frequencies (ω_c), shape factors (δ), Kanai-Tajimi frequencies (ω_g), Kanai-Tajimi damping coefficients (ζ_g), white noise bedrock excitation intensities (G_o) and site conditions (soil versus rock).

2.3.2 Histograms of S_o, ω_g, and ζ_g

The assessment of overall seismic safety of a structure requires probabilistic representation of the ground motion. The statistics of several pertinent seismic parameters have been computed; they are listed in Table 2-2. In this section, the variability of strong-motion duration, Kanai-Tajimi frequency and damping coefficient will be presented in the form of histograms.

<u>Strong-Motion Duration</u>

As shown in Table 2-2, the mean strong-motion duration for the set of records is 9.27 sec, with standard deviation (σ) = 8.77 sec, coefficient

TABLE 2-1

PERTINENT SEISMIC PARAMETERS FOR THE 140 STRONG GROUND MOTIONS

C.I.T. NO.	EARTHQUAKE	COMP.	M	R (km)	SITE	a_{max} (g)	σ_o (g)	ω_c (rad/sec)	δ	ω_g (rad/sec)	ζ_g	G_o (cm^2/sc^3)	s_o (sec)
A002-1	Northwest	S44W	6.0	53	s	0.104	0.0376	29.48	0.46	28.39	0.32	14.42	4.11
A002-2	California	N46W				0.112	0.0424	24.46	0.48	22.86	0.29	21.59	4.12
A003-1	Kern County	S00E	7.2	127	s	0.047	0.0162	12.95	0.54	11.18	0.25	5.70	16.00
A003-2		S90W				0.053	0.0177	11.06	0.53	9.71	0.22	7.24	23.59
A004-1	Kern County	N21E	7.2	43	s	0.156	0.0511	22.07	0.55	18.46	0.36	42.85	13.66
A004-2		S69E				0.179	0.0599	21.97	0.54	18.81	0.35	56.60	10.72
A005-1	Kern County	N42E	7.2	89	s	0.090	0.0303	12.31	0.55	10.60	0.24	20.95	16.80
A005-2		S48E				0.131	0.0545	9.65	0.55	8.36	0.21	78.23	6.62
A006-1	Kern County	S00W	7.2	119	s	0.055	0.0182	15.71	0.52	13.90	0.26	5.99	19.32
A006-2		N90E				0.044	0.0138	13.76	0.61	10.52	0.32	5.09	35.41
A007-1	Kern County	S00W	7.2	119	s	0.059	0.0195	17.93	0.56	14.90	0.32	7.23	17.09
A007-2		N90E				0.042	0.0128	15.90	0.65	10.68	0.40	4.72	40.08
A008-1	Eureka	N11W	6.6	24	s	0.168	0.0628	18.15	0.59	14.16	0.36	83.17	5.47
A008-2		N79E				0.258	0.1046	20.75	0.50	18.76	0.29	157.53	4.23
A009-1	Eureka	N44E	6.6	40	s	0.159	0.0557	11.45	0.69	7.47	0.35	120.84	11.53
A009-2		N46W				0.201	0.0829	13.36	0.66	9.09	0.36	223.56	3.52
A010-1	San Jose	N31W	5.8	10	s	0.102	0.0405	21.98	0.40	21.77	0.18	14.84	2.97
A010-2		N59E				0.108	0.0444	30.65	0.23	31.12	0.06	4.89	1.78
A014-1	San	N09W	5.3	15	s	0.043	0.0158	26.92	0.42	26.69	0.23	2.21	4.07
A014-2	Francisco	N81E				0.046	0.0184	26.16	0.38	26.35	0.18	2.49	2.42
A015-1	San	N10E	5.3	12	k	0.083	0.0351	32.71	0.39	33.50	0.22	8.41	1.34
A015-2	Francisco	S80E				0.105	0.0411	35.98	0.37	37.45	0.20	9.61	2.02
A016-1	San	S09E	5.3	14	s	0.085	0.0348	25.69	0.37	25.92	0.16	8.48	2.76
A016-2	Francisco	S81W				0.056	0.0207	24.24	0.52	21.41	0.35	5.96	5.16
A017-1	San	N26E	5.3	24	s	0.040	0.0159	28.52	0.37	28.93	0.18	1.73	2.48
A017-2	Francisco	S64E				0.024	0.0088	28.73	0.46	27.83	0.30	0.76	4.82
A018-1	Hollister	S01W	5.6	21	s	0.065	0.0219	15.87	0.54	13.65	0.28	9.25	18.05
A018-2		N89W				0.179	0.0772	18.79	0.41	18.40	0.18	62.50	2.72
A019-1	Borrego	S00W	6.5	64	s	0.130	0.0485	13.00	0.74	6.38	0.48	115.54	7.07
A019-2	Mountain	N90E				0.057	0.0178	16.50	0.69	9.29	0.49	10.78	31.55
A020-1	Borrego	S00W	6.5	96	s	0.030	0.0104	15.31	0.70	8.69	0.47	3.90	12.90
A020-2	Mountain	S90W				0.029	0.010	14.40	0.65	9.84	0.38	3.08	18.73
B021-1	Long Beach	S08W	6.3	53	s	0.133	0.0483	25.18	0.64	12.63	0.75	56.20	6.44
B021-2		N82W				0.154	0.0638	20.82	0.62	14.05	0.48	91.32	2.91
B023-1	Southern	N00E	5.4	38	s	0.033	0.0136	21.42	0.43	20.85	0.21	1.91	3.53
B023-2	California	N90W				0.027	0.0101	19.42	0.47	18.15	0.24	1.37	6.76

(TABLE 2-1 CONTINUED)

C.I.T. NO.	EARTHQUAKE	COMP.	M	R (km)	SITE	a_{max} (g)	σ_o (g)	ω_c (rad/sec)	δ	ω_g (rad/sec)	ζ_g	C_o (cm^2/sc^3)	s_o (sec)
B024-1	Lower	S00W	6.5	64	s	0.160	0.0519	25.68	0.50	23.16	0.35	33.72	13.30
B024-2	California	S90W				0.183	0.0629	24.45	0.46	23.39	0.26	42.58	10.19
B026-1	1st N.W.	N45E	5.5	55	s	0.144	0.0656	25.77	0.45	25.01	0.26	43.49	1.74
B026-2	California	S45E				0.089	0.0319	26.96	0.42	26.75	0.23	8.96	4.64
B027-1	2nd N.W.	N45E	6.6	104	s	0.062	0.0224	21.86	0.44	21.06	0.23	5.54	4.34
B027-2	California	S45E				0.039	0.0136	22.15	0.45	21.23	0.24	2.08	11.23
B030-1	Northern	N44E	5.4	43	s	0.054	0.0185	21.55	0.53	18.53	0.34	5.40	9.67
B030-2	California	S46E				0.075	0.0283	25.14	0.46	24.11	0.27	8.70	4.01
B031-1	Wheeler	N21E	5.9	43	s	0.065	0.0264	21.89	0.49	20.13	0.28	9.25	3.64
B031-2	Ridge	S69E				0.068	0.0256	26.00	0.39	26.08	0.19	5.13	4.12
B034-1	Parkfield	N05W	5.3	5	s	0.355	0.1543	22.59	0.49	20.81	0.29	309.51	1.66
B034-2		N85E				0.434	0.2535	25.74	0.49	23.60	0.33	793.66	0.95
B035-1	Parkfield	N50E	5.3	9	s	0.237	0.0898	40.98	0.41	43.89	0.31	53.07	2.37
B035-2		N40W				0.275	0.1085	31.82	0.39	32.47	0.22	82.46	1.99
B036-1	Parkfield	N50E	5.3	38	s	0.053	0.0171	32.32	0.57	21.23	0.78	4.48	12.60
B036-2		N40W				0.064	0.0210	34.62	0.51	30.97	0.53	4.98	9.55
B037-1	Parkfield	N65W	5.3	6	k	0.269	0.1193	24.37	0.36	24.61	0.15	97.23	1.39
B037-2		S25W				0.347	0.2026	21.46	0.40	21.21	0.18	379.84	0.65
B038-1	Parkfield	N36W	5.3	77	k	0.014	0.0049	29.76	0.53	25.11	0.48	0.33	8.27
B038-2		S54W				0.012	0.0040	31.89	0.49	29.73	0.41	0.17	8.07
B039-1	2nd Northern	S11E	5.8	51	s	0.021	0.0080	19.63	0.54	16.80	0.32	1.08	4.77
B039-2	California	N79E				0.020	0.0076	17.26	0.57	13.91	0.33	1.19	5.58
B040-1	Borrego	N33E	6.5	134	k	0.041	0.0150	21.62	0.47	20.47	0.25	2.72	7.01
B040-2	Mountain	N57W				0.046	0.0162	22.93	0.49	21.22	0.29	3.35	5.65
C048-1	San	N00W	6.6	20	s	0.255	0.0923	16.12	0.59	12.55	0.34	196.95	9.93
C048-2	Fernando	S90W				0.134	0.0437	17.99	0.66	11.02	0.48	55.19	22.88
D056-1	San	N21E	6.6	29	k	0.315	0.1287	25.83	0.49	23.96	0.32	198.61	2.71
D056-2	Fernando	N69W				0.271	0.0954	24.32	0.59	17.29	0.51	173.13	7.07
E071-1	San	S00W	6.6	89	s	0.027	0.0094	45.45	0.42	51.75	0.37	0.57	4.77
E071-2	Fernando	N90E				0.026	0.0087	32.68	0.50	30.09	0.44	0.84	6.14
F086-1	San	N83E	6.6	46	s	0.107	0.0387	18.72	0.61	13.51	0.41	34.49	8.09
F086-2	Fernando	S07W				0.082	0.0277	22.43	0.52	19.64	0.33	11.39	11.09
G114-1	San	S60E	6.6	33	s	0.113	0.0364	29.23	0.66	13.66	0.95	29.06	16.42
G114-2	Fernando	S30W				0.139	0.0465	35.17	0.49	32.66	0.49	23.41	7.51
T286-1	Borrego	North	6.5	48	s	0.060	0.0191	26.83	0.51	23.68	0.38	4.77	17.63
T286-2	Valley	East				0.047	0.0150	24.55	0.55	20.29	0.41	3.49	20.24

(TABLE 2-1 CONTINUED)

C.I.T. NO.	EARTHQUAKE	COMP.	M	R (km)	SITE	a_{max} (g)	σ_o (g)	ω_c (rad/sec)	δ	ω_g (rad/sec)	ζ_g	G_o (cm^2/sc^3)	s_o (sec)
T287-1	Imperial Valley	North	5.6	30	s	0.031	0.0103	22.56	0.57	17.62	0.42	1.88	13.90
T287-2		East				0.028	0.0094	16.36	0.56	13.55	0.31	1.79	17.72
T288-1	Imperial Valley	North	5.5	11	s	0.007	0.0026	28.49	0.53	24.27	0.44	0.09	8.99
T288-2		East				0.036	0.0118	20.91	0.59	15.97	0.41	2.76	16.26
T289-1	Lower California	North	6.3	150	s	0.025	0.0083	16.51	0.60	12.59	0.35	1.62	13.28
T289-2		East				0.028	0.0096	15.21	0.60	11.78	0.33	2.23	11.37
T290-1	Imp. County Foreshock	North	4.3	22	s	0.031	0.0126	38.01	0.29	39.34	0.11	0.52	1.37
T290-2		East				0.016	0.0053	30.97	0.34	31.77	0.15	0.15	9.95
T293-1	Gulf of California	North	6.3	147	s	0.014	0.0043	15.77	0.61	11.96	0.35	0.45	48.70
T293-2		East				0.015	0.0048	15.93	0.53	13.99	0.26	0.42	35.85
U298-1	Humboldt Bay	N45W	5.75	80	s	0.039	0.0146	20.55	0.52	18.18	0.30	3.24	6.86
U298-2		S45W				0.037	0.0131	22.59	0.44	21.90	0.23	1.82	6.10
U299-1	Santa Barbara	N45E	5.9	16	s	0.238	0.1015	22.08	0.45	21.25	0.23	113.49	2.03
U299-2		S45E				0.176	0.0747	16.52	0.45	15.72	0.20	75.43	2.80
U300-1	Northern California	N45W	6.4	50	s	0.121	0.0484	22.61	0.49	20.83	0.29	30.47	2.79
U300-2		S45W				0.116	0.0458	24.34	0.46	23.32	0.26	22.99	3.33
U301-1	Northern California	N89W	5.3	21	s	0.197	0.1322	20.67	0.33	20.77	0.12	118.37	0.78
U301-2		S01W				0.122	0.0469	19.38	0.40	19.07	0.17	21.71	5.08
U305-1	Central California	N89W	5.3	27	s	0.053	0.0188	18.62	0.53	16.30	0.29	5.88	8.70
U305-2		S01W				0.050	0.0172	19.31	0.55	16.28	0.33	5.22	10.82
U307-1	Central California	N89W	5.0	6	s	0.057	0.0207	20.42	0.47	19.28	0.24	5.37	7.12
U307-2		S01W				0.036	0.0124	23.34	0.53	20.16	0.36	2.30	10.25
U308-1	Northern California	N46W	5.7	59	s	0.059	0.0222	28.97	0.41	29.13	0.22	3.92	4.00
U308-2		S44W				0.075	0.0312	28.09	0.41	28.12	0.22	8.03	2.54
U309-1	Central Cal. Aftershock	N89W	5.6	21	s	0.172	0.0770	23.04	0.55	19.05	0.39	92.71	1.43
U309-2		S01W				0.076	0.0281	17.28	0.45	16.49	0.20	10.32	8.46
U311-1	Parkfield	N21E	5.3	131	s	0.008	0.0030	11.01	0.59	8.91	0.26	0.26	21.04
U311-2		S69E				0.011	0.0043	12.24	0.59	9.94	0.27	0.48	13.49
U312-1	Ferndale	N46W	5.8	32	s	0.105	0.0432	24.66	0.66	10.55	0.85	52.82	2.66
U312-2		S44W				0.237	0.1160	29.73	0.45	29.15	0.29	126.79	0.30
U313-1	Northern California	N89W	5.2	39	s	0.013	0.0045	16.70	0.52	14.72	0.27	0.35	18.60
U313-2		S01W				0.017	0.0057	15.43	0.52	13.61	0.26	0.60	14.74
V314-1	Long Beach	N39E	6.3	59	k	0.064	0.0222	11.59	0.67	7.88	0.34	17.90	21.62
V314-2		N51W				0.097	0.0335	15.84	0.74	6.54	0.61	52.65	13.48
V315-1	Long Beach	South	6.3	27	s	0.196	0.0724	22.58	0.59	16.87	0.45	96.16	5.81
V315-2		West				0.159	0.0548	25.62	0.52	22.57	0.37	39.21	8.88

(TABLE 2-1 CONTINUED)

C.I.T. NO.	EARTHQUAKE	COMP.	M	R (km)	SITE	a_{max} (g)	σ_o (g)	ω_c (rad/sec)	δ	ω_g (rad/sec)	ζ_g	G_o (cm^2/sc^3)	s_o (sec)
V316-1	Torrance	North	5.4	6	s	0.040	0.0152	19.06	0.46	18.05	0.22	2.93	6.47
V316-2	Gardena	East				0.055	0.0362	6.99	0.59	5.74	0.21	49.33	1.52
V317-1	Torrance	S50E	5.4	27	s	0.015	0.0056	16.76	0.49	15.42	0.23	0.49	7.07
V317-2	Gardena	S40W				0.011	0.0039	17.93	0.52	15.80	0.28	0.26	13.64
V319-1	Southern	N36W	6	77	k	0.054	0.0216	23.68	0.50	21.49	0.32	6.22	3.40
V319-2	California	S54W				0.036	0.0132	21.25	0.56	17.11	0.38	3.12	7.05
V329-1	Southern	South	5	6	s	0.167	0.1007	16.53	0.48	15.28	0.23	153.53	0.67
V329-2	California	West				0.089	0.0479	19.31	0.66	11.62	0.51	63.07	0.49
V330-1	Northern	N79E	5	19	s	0.046	0.0192	20.18	0.40	19.92	0.17	3.50	2.31
V330-2	California	S11E				0.048	0.0239	20.48	0.37	20.42	0.15	4.80	1.52
V331-1	Southern	South	4.5	18	k	0.041	0.0176	34.29	0.47	33.06	0.41	2.91	1.63
V331-2	California	East				0.037	0.0154	43.01	0.33	45.80	0.17	0.99	1.27
V332-1	Northern	South	6.25-	151	s	0.015	0.0054	20.18	0.47	18.95	0.25	0.38	8.59
V332-2	California	East	6.5			0.013	0.0047	18.93	0.54	16.09	0.32	0.39	9.07
W334-1	Lytle	S65E	5.4	13	k	0.142	0.0600	25.66	0.59	18.12	0.54	64.65	2.42
W334-2	Creek	S25W				0.198	0.0787	31.62	0.54	25.02	0.58	85.44	1.26
W335-1	Lytle	S85E	5.4	19	k	0.071	0.0254	39.92	0.43	42.21	0.34	4.42	2.98
W335-2	Creek	S05W				0.056	0.0208	43.08	0.34	45.99	0.18	1.73	2.26
W336-1	Lytle	S54E	5.4	22	k	0.057	0.0209	35.21	0.43	35.99	0.30	3.39	3.36
W336-2	Creek	S36W				0.071	0.0279	34.61	0.48	32.96	0.44	7.65	1.90
W339-1	Lytle	South	5.4	18	s	0.041	0.0144	28.58	0.39	28.89	0.20	1.55	7.32
W339-2	Creek	East				0.036	0.0123	29.13	0.35	29.71	0.16	0.91	9.12
W342-1	Lytle	North	5.4	56	s	0.020	0.0068	30.64	0.45	30.19	0.30	0.43	8.18
W342-2	Creek	East				0.019	0.0065	35.33	0.46	34.78	0.40	0.40	7.05
Y370-1	Borrego	South	6.5	144	s	0.022	0.0072	25.87	0.54	21.34	0.43	0.79	15.41
Y370-2	Mountain	East				0.029	0.0103	23.45	0.56	18.72	0.42	1.80	6.57
Y371-1	Borrego	S04E	6.5	174	s	0.013	0.0044	10.31	0.71	6.38	0.35	0.90	34.50
Y371-2	Mountain	S86W				0.012	0.0039	11.86	0.60	9.46	0.27	0.41	38.51
Y373-1	Borrego	S82E	6.5	205	s	0.008	0.0028	12.13	0.56	10.19	0.25	0.20	12.01
Y373-2	Mountain	S08W				0.007	0.0025	13.06	0.57	10.83	0.27	0.15	13.95
Y379-1	Borrego	N83W	6.5	214	s	0.019	0.0066	10.63	0.66	7.61	0.30	1.56	22.21
Y379-2	Mountain	S07W				0.019	0.0067	10.40	0.66	7.46	0.30	1.65	18.62

TABLE 2-2 STATISTICS FOR PERTINENT SEISMIC PARAMETERS

SEISMIC PARAMETERS	MEAN	STANDARD DEVIATION (σ)	COEF. OF VARIATION (V)	COEF. OF SKEWNESS (γ_1)	COEF. OF KURTOSIS (γ_2)
a_{max} (g)	0.0883	0.0817	0.925	1.621	5.636
σ_o (g)	0.0357	0.0391	1.094	2.476	11.207
S_o (sec)	9.27	8.77	0.945	1.922	7.3
ω_c (rad/sec)	22.7	7.59	0.335	0.549	3.164
δ	0.51	0.097	0.19	0.035	2.836
ω_g (rad/sec)	20.3	8.97	0.443	0.852	3.828
ζ_g	0.32	0.13	0.421	1.697	7.736
G_o (cm^2/sec^3)	37.8	87.2	2.307	5.52	43.15
ω_c/ω_g	1.19	0.26	0.22	2.42	11.65

of variation (V) = 0.945, coefficient of skewness (γ_1) = 1.922, and coefficient of kurtosis (γ_2) = 7.3.

Since γ_1 is approximately equal to 2V, the probability density function (PDF) of strong-motion duration can be assumed as Gamma-distributed [8]. The histogram and the fitted analytical PDF of strong-motion duration are plotted in Fig. 2-1. The Gamma PDF appears to fit the histogram quite well:

$$f_{S_o}(S_o) = 0.0994\ S_o^{0.12}\ \exp(-0.121\ S_o) \tag{2-14}$$

Kanai-Tajimi Frequency

The mean Kanai-Tajimi frequency of the set of 140 records is 20.3 rad/sec. The other statistics are: σ = 8.97 rad/sec, V = 0.443, γ_1 = 0.852, and γ_2 = 3.828. The fitted Gamma probability density function is:

$$f_{\omega_g}(\omega_g) = 3.18 \times 10^{-5}\ \omega_g^{4.1}\ \exp(-0.252\ \omega_g) \tag{2-15}$$

where ω_g is in rad/sec. The histogram as well as the Gamma PDF are presented in Fig. 2-2.

Kanai-Tajimi Damping Coefficient

Based on the 140 strong ground motions used in this study, the mean Kanai-Tajimi damping coefficient is 0.32, and σ = 0.13, V = 0.421, γ_1 = 1.697, γ_2 = 7.736. Fig. 2-3 shows the histogram and the fitted Lognormal probability density function, which takes the following form:

$$f_{\zeta_g}(\zeta_g) = \frac{1}{1.01\ \zeta_g}\ \exp\{-3.063[\ln\ \zeta_g + 1.221]^2\} \tag{2-16}$$

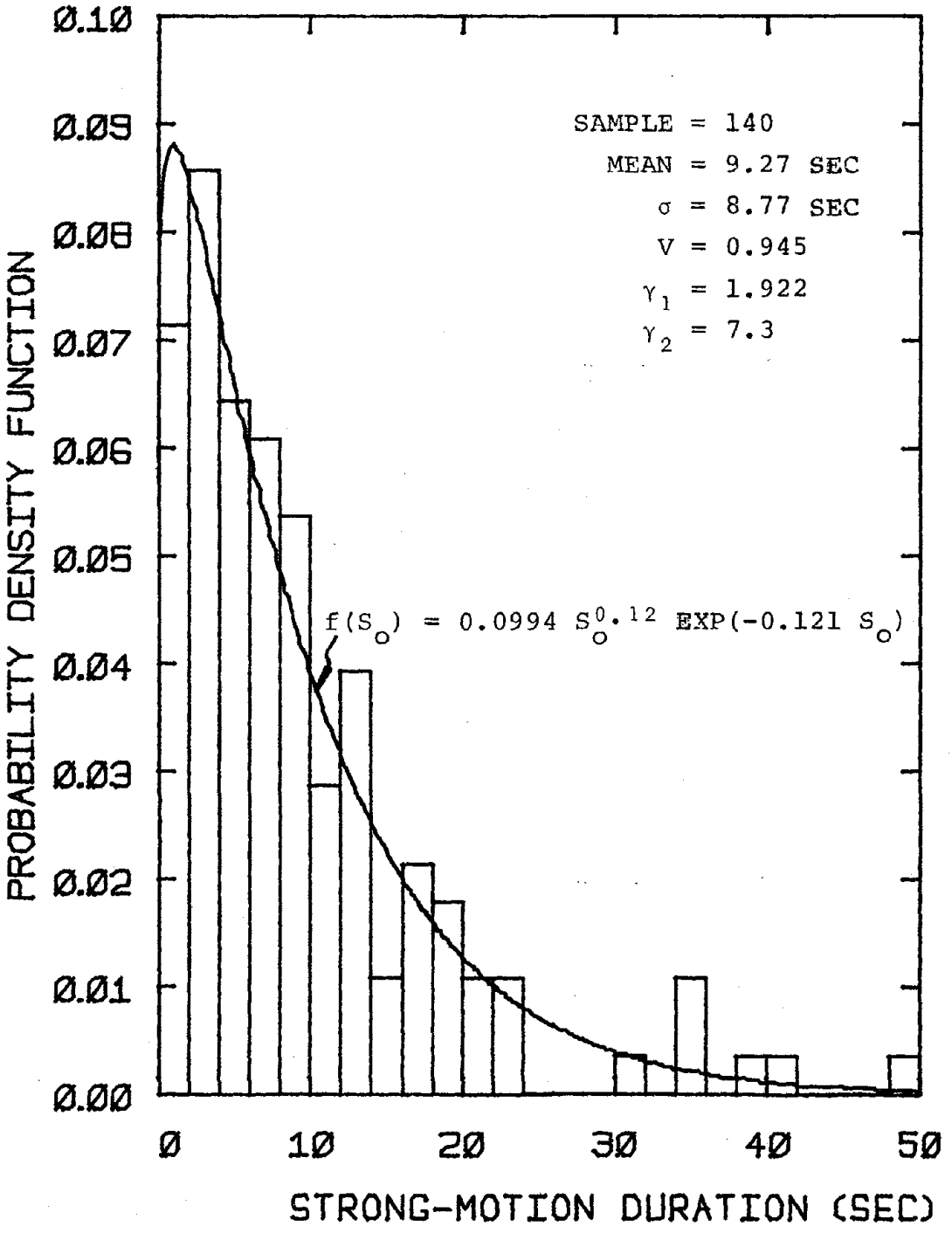

FIG. 2-1 HISTOGRAM OF STRONG-MOTION DURATION

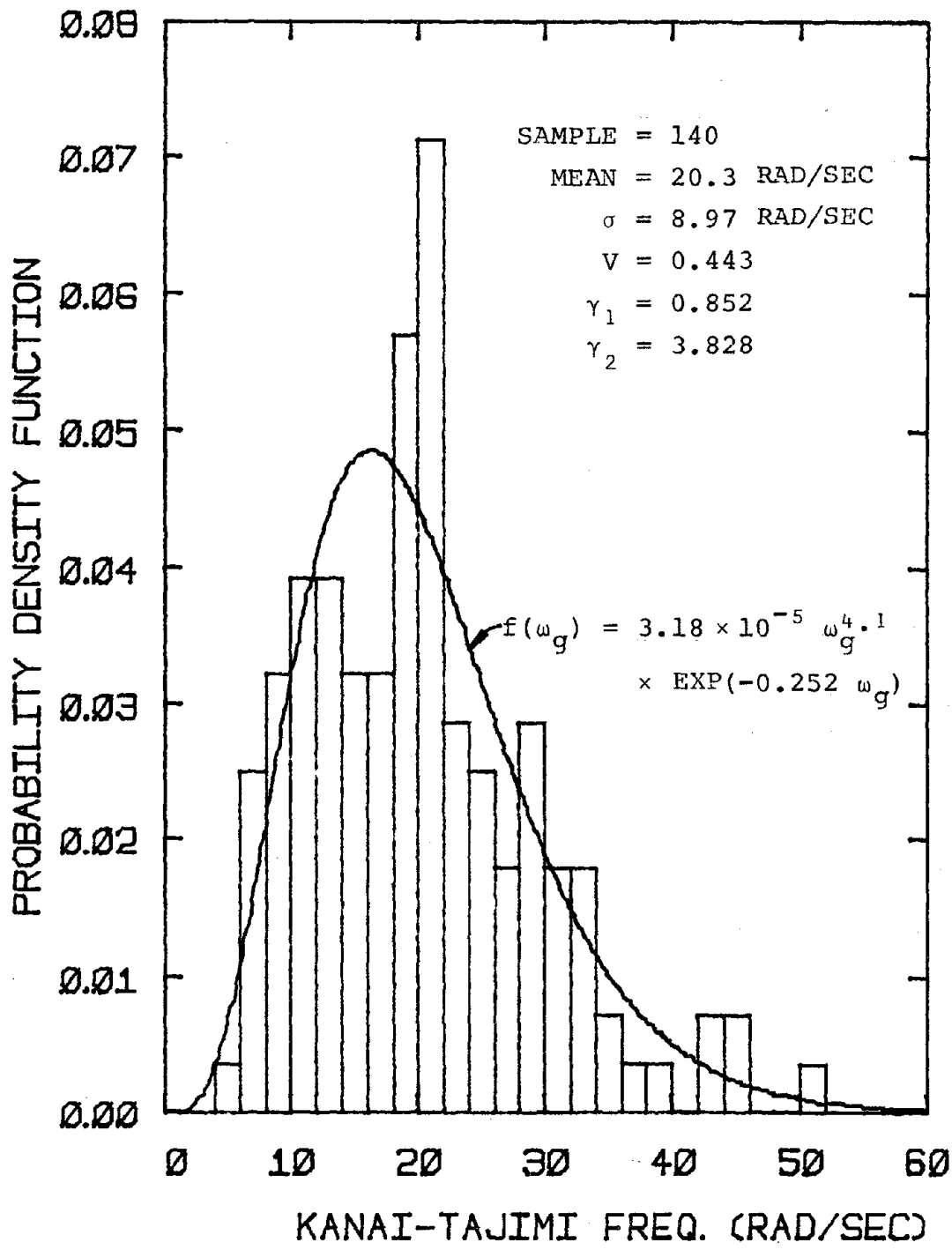

FIG. 2-2 HISTOGRAM OF KANAI-TAJIMI FREQUENCY

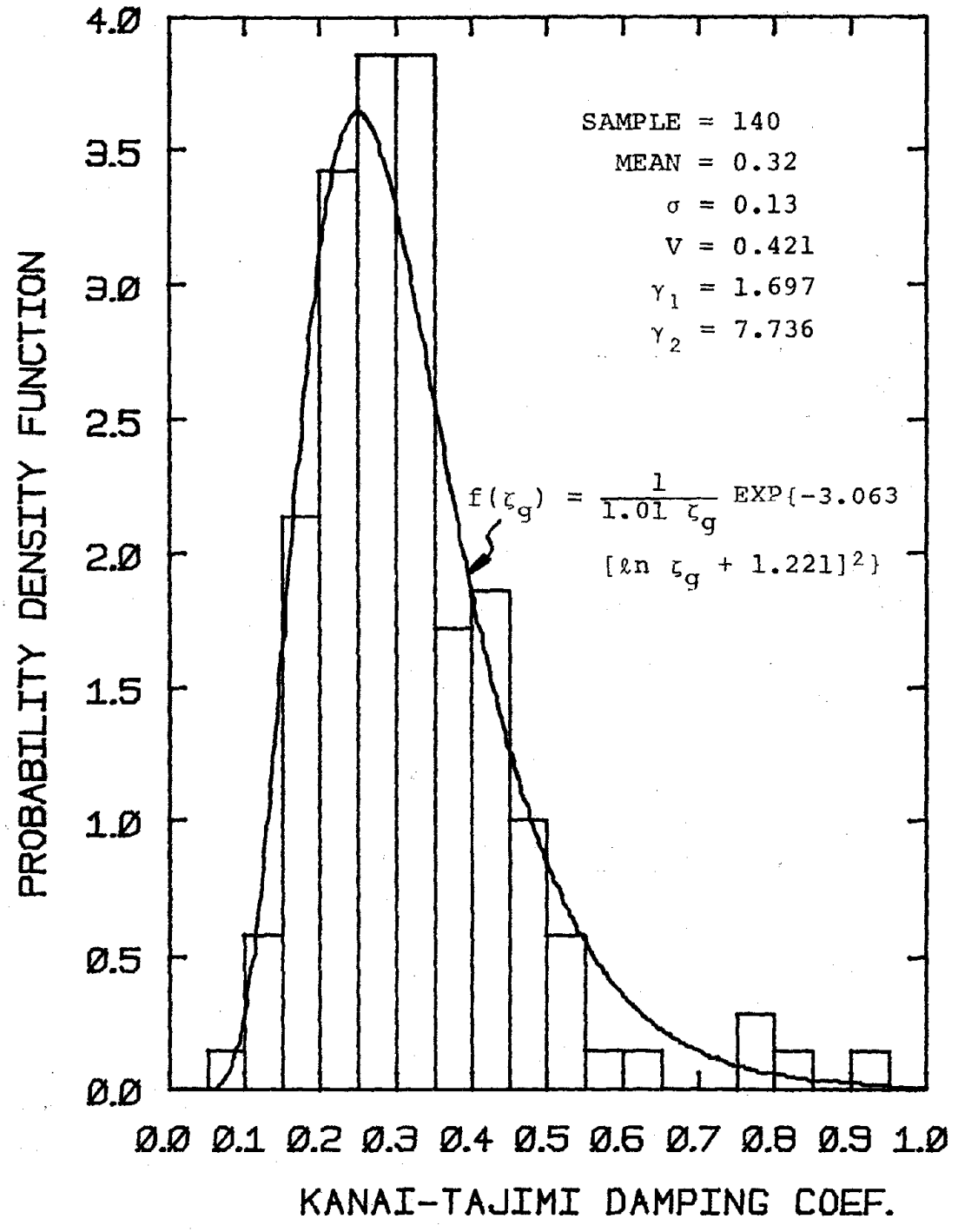

FIG. 2-3 HISTOGRAM OF KANAI-TAJIMI DAMPING COEFFICIENT

2.3.3 Scattergrams of Pertinent Ground Motion Parameters

In this section, the correlations between several important seismic parameters will be studied based on scatter plots. Included are the scattergrams of central frequency versus Kanai-Tajimi frequency, K-T damping coefficient versus frequency, strong-motion duration versus K-T frequency, and strong-motion duration versus K-T damping coefficient.

Central Frequency Versus Kanai-Tajimi Frequency

In his seismic safety investigation, Gasparini [22] assumed $\omega_c = 2.1\ \omega_g$. From the results of 140 strong ground motions, statistics of the ratio ω_c/ω_g have been computed and are listed in Table 2-2. The resulting mean ratio is 1.19. The other statistics are: $\sigma = 0.26$, $V = 0.22$, $\gamma_1 = 2.42$, $\gamma_2 = 11.65$.

The scattergram of central frequency versus Kanai-Tajimi frequency is presented in Fig. 2-4. The relationship used by Gasparini is also plotted in the figure. It is quite obvious that the coefficient of 2.1 is too high. Based on linear regression, the relationship between the K-T frequency and the central frequency can be expressed as follows:

$$\omega_g = 1.12\ \omega_c - 5.15 \qquad (2\text{-}17)$$

where the standard error is 2.87 rad/sec, and the correlation coefficient is 0.948. Eq. 2-17 can be easily employed to predict the Kanai-Tajimi frequency for a given strong ground motion record.

Kanai-Tajimi Damping Coefficient Versus Frequency

Fig. 2-5 shows the scattergram of Kanai-Tajimi damping coefficient versus frequency for the set of 140 strong ground motions. As depicted in the figure, there exists no obvious trend between the two seismic parameters. Hence, it seems reasonable to assume that the K-T damping co-

efficient and frequency are uncorrelated. This conclusion is consistent with the results based on 39 scaled earthquake records reported by Binder [9].

Strong-Motion Duration Versus Kanai-Tajimi Frequency

The scattergram of strong-motion duration versus Kanai-Tajimi frequency is plotted in Fig. 2-6. It appears that the K-T frequency decreases with increasing strong-motion duration. This can be explained by the dependence of both of these two parameters on the earthquake epicentral distance. A detailed discussion will be presented in Section 2.4.3.

Strong-Motion Duration Versus Kanai-Tajimi Damping Coefficient

Fig. 2-7 shows the scattergram of strong-motion duration versus Kanai-Tajimi damping coefficient for the entire set of records. There exists no clear trend in the relationship between these two seismic parameters. The only observation worth making is that the variability of K-T damping coefficient appears to decrease somewhat with increasing duration.

2.3.4 Influence of Site Conditions

The effects of site conditions on seismic parameters have been widely studied in earthquake engineering. Notice that there are 22 rock site records in the set of ground motions used in this study. The statistics of strong-motion duration, central frequency, Kanai-Tajimi frequency and damping coefficient were computed for two different site conditions, i.e., rock and soil. The results are listed in Table 2-3. Some interesting observations concerning the influence of site conditions on the seismic parameters are presented below.

Strong-Motion Duration

As shown in Table 2-3, the mean strong-motion duration for soil sites

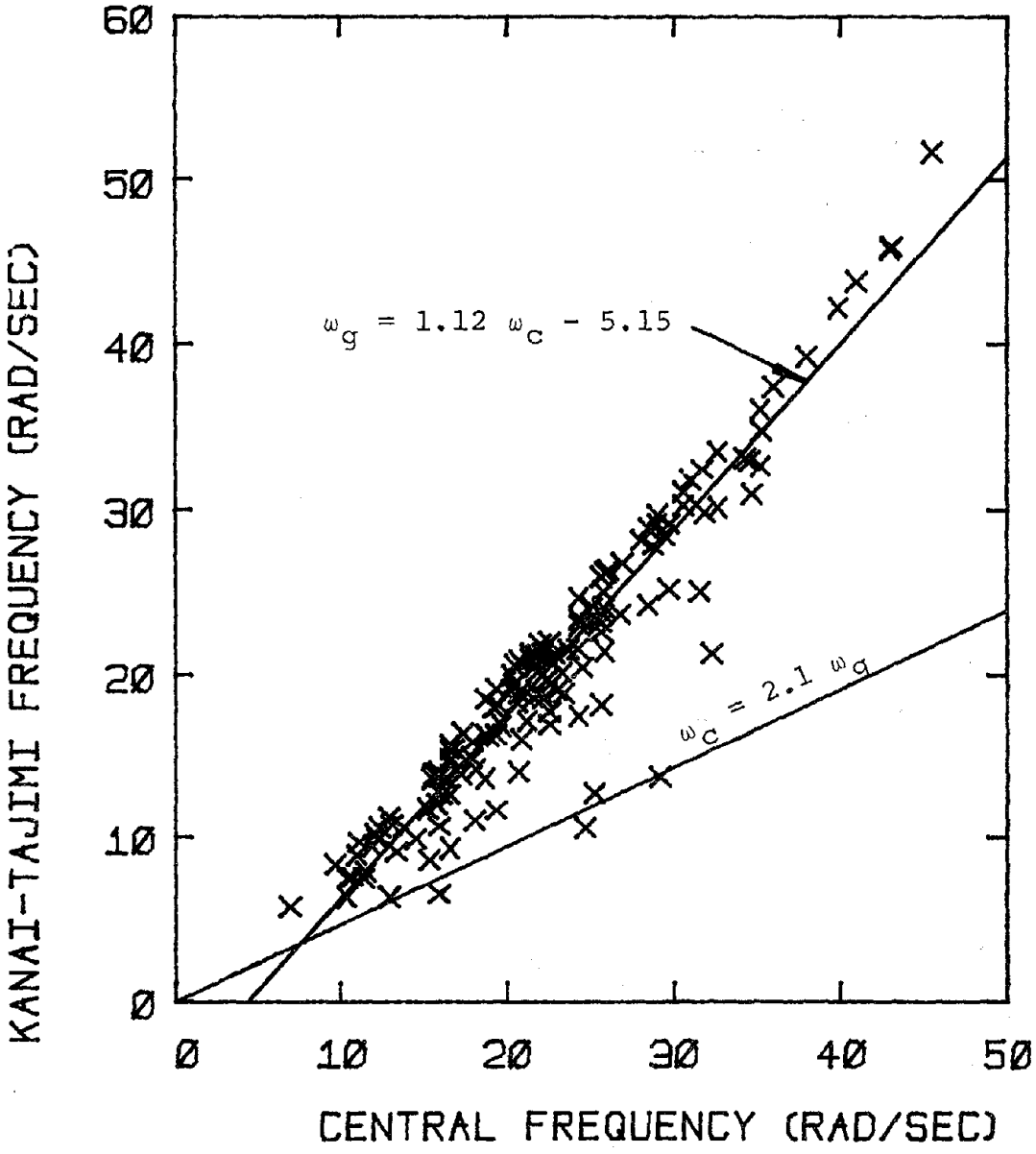

FIG. 2-4 SCATTERGRAM OF CENTRAL FREQUENCY VERSUS KANAI-TAJIMI FREQUENCY

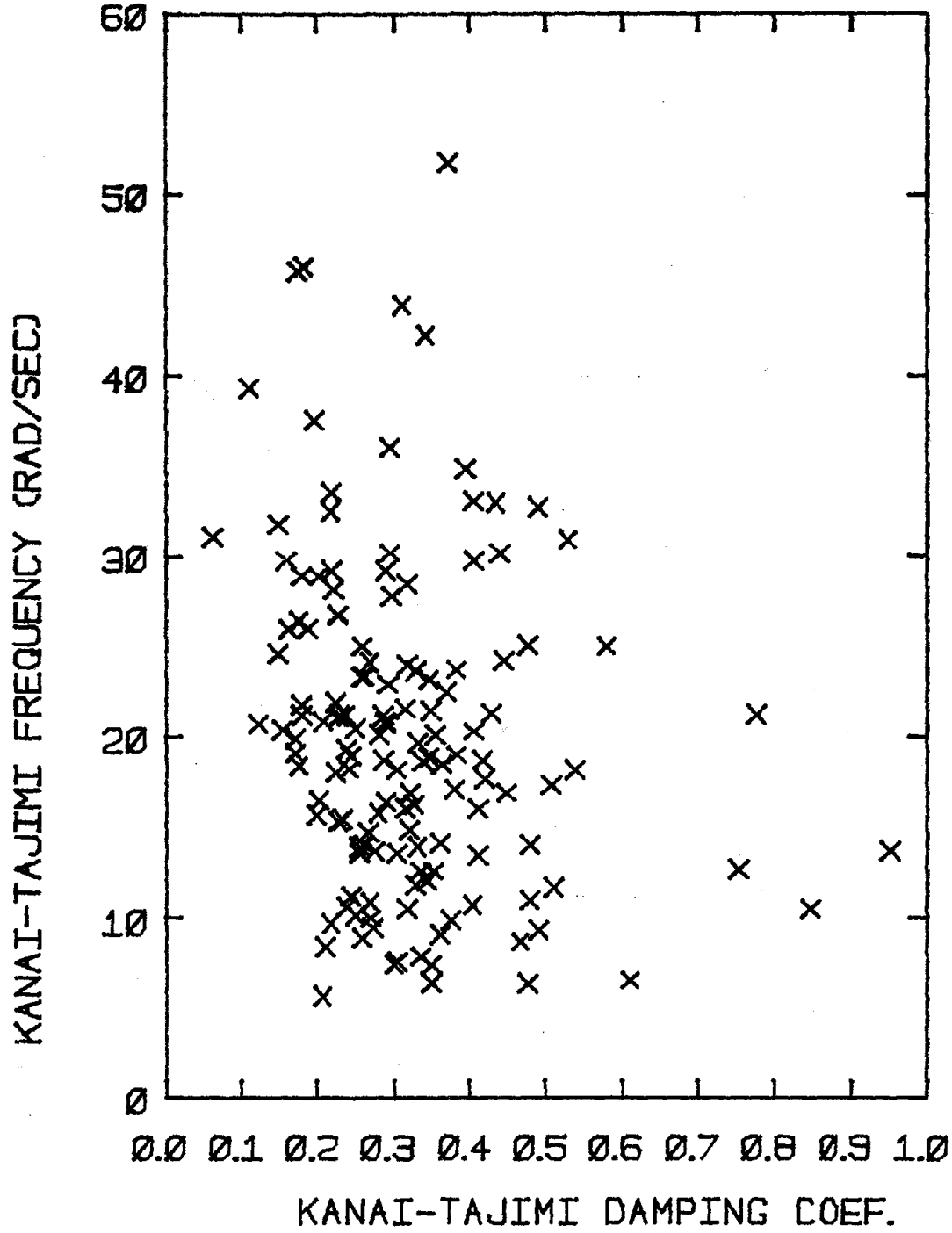

FIG. 2-5 SCATTERGRAM OF KANAI-TAJIMI DAMPING COEFFICIENT VERSUS FREQUENCY

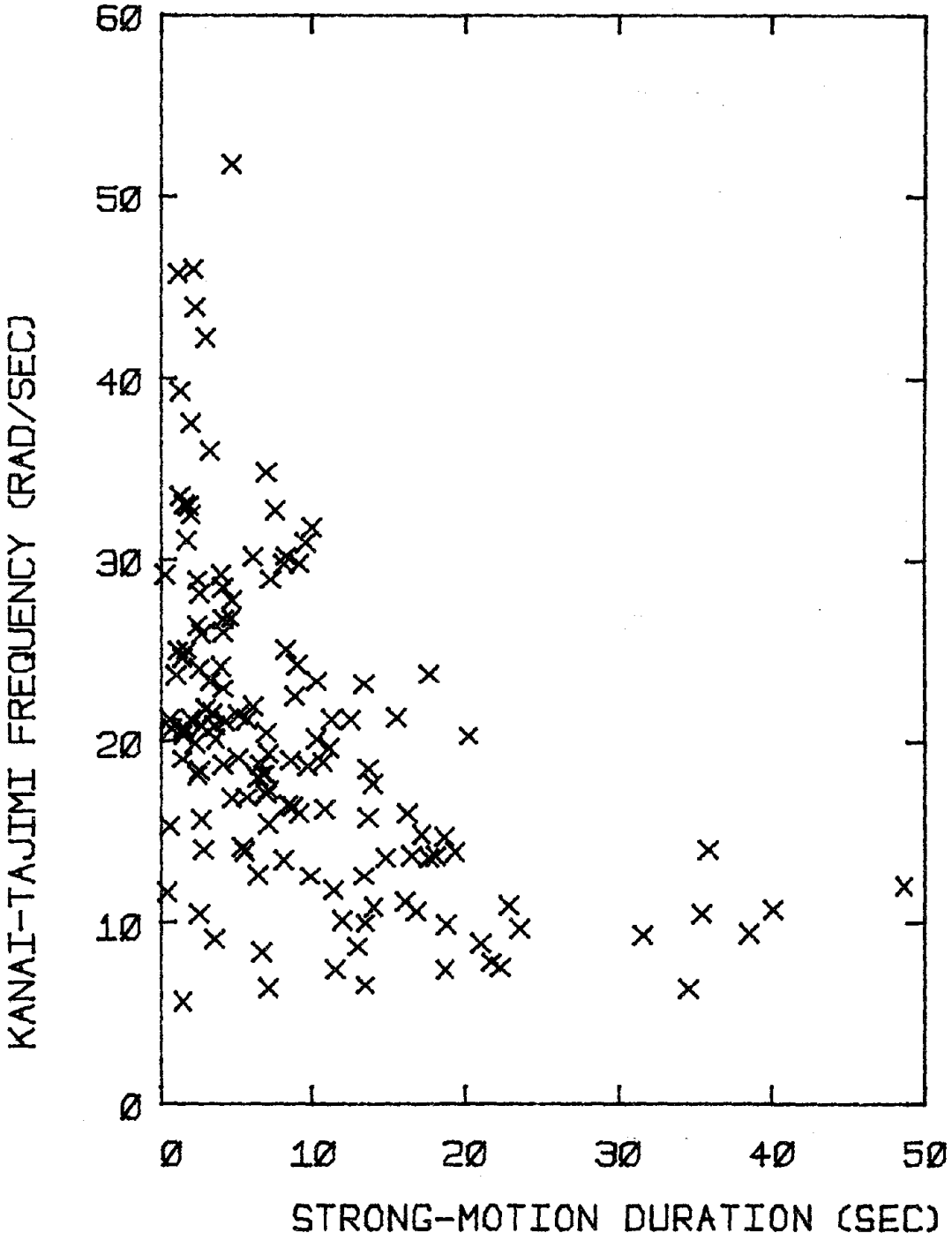

FIG. 2-6 SCATTERGRAM OF STRONG-MOTION DURATION VERSUS KANAI-TAJIMI FREQUENCY

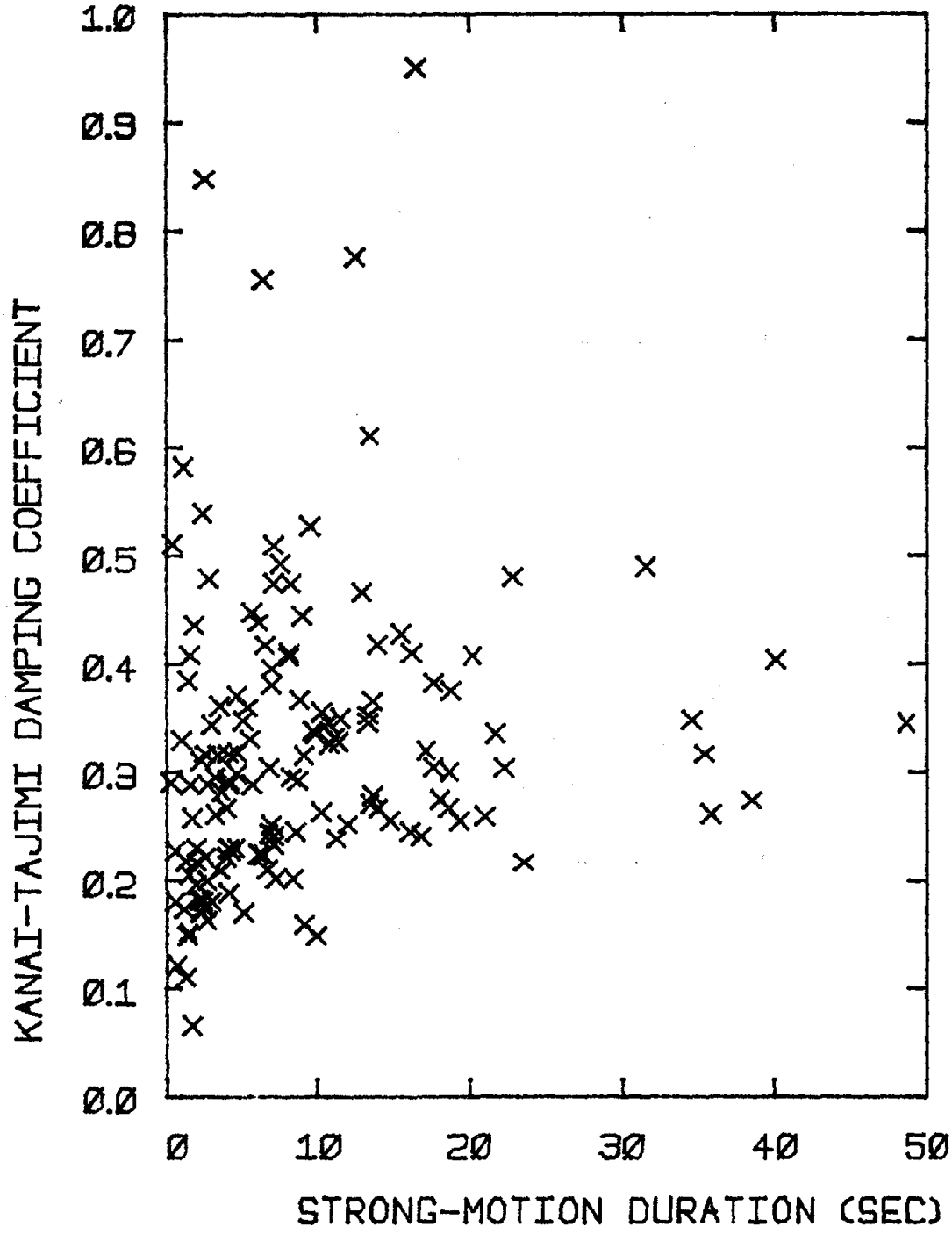

FIG. 2-7 SCATTERGRAM OF STRONG-MOTION DURATION VERSUS KANAI-TAJIMI DAMPING COEFFICIENT

is about twice that for rock sites (10.16 sec versus 5.07 sec). The other statistics are as follows: for rock sites, σ = 4.92 sec, V = 0.971, γ_1 = 1.858, γ_2 = 6.436; and for the soil sites, σ = 9.22 sec, V = 0.907, γ_1 = 1.917, γ_2 = 7.338.

Kanai-Tajimi Frequency

It has been suggested that the Kanai-Tajimi frequency is equal to 4π rad/sec for typical firm ground sites [48,60]. From this study, the mean value of ω_g for 22 rock site records is 26.67 rad/sec, and σ = 10.6 rad/sec, V = 0.398, γ_1 = 0.116, γ_2 = 2.42. This clearly indicates that the suggested value of 4π rad/sec is too small.

Observations during past earthquakes have led to the conclusion that the higher frequency components of an earthquake would be filtered out when the strong ground motion waves travel through soil deposits [45]. The results obtained herein tend to support this argument. For example, the mean value of ω_g for soil sites is equal to 19.06 rad/sec, and σ = 8.09 rad/sec, V = 0.425, γ_1 = 0.923, γ_2 = 4.523.

Kanai-Tajimi Damping Coefficient

Since the Kanai-Tajimi damping coefficient controls the flatness of the PSD function, it is implicitly related to the shape factor δ. Based on the study of six real firm ground earthquake records, Sixsmith and Roesset [54] reported a mean value of δ equal to 0.66. This corresponds to the K-T damping coefficient of approximately 0.6 as suggested by Gasparini [22]. However, from the results of this study, the mean ζ_g for rock sites is equal to 0.35, with σ = 0.14, V = 0.391, γ_1 = 0.36, and γ_2 = 2.087. Note that the mean value is much smaller than the 0.6 value frequently assumed [48,60].

TABLE 2-3 STATISTICS OF PERTINENT SEISMIC PARAMETERS FOR DIFFERENT SITE CONDITIONS

		S_o (sec)	ω_c (rad/sec)	ω_g (rad/sec)	ζ_g
ROCK SITES	MEAN	5.07	28.66	26.67	0.35
	STANDARD DEVIATION	4.92	8.16	10.60	0.14
	COEF. OF VARIATION	0.971	0.285	0.398	0.391
	COEF. OF SKEWNESS	1.858	-0.015	0.116	0.360
	COEF. OF KURTOSIS	6.436	2.375	2.420	2.087
SOIL SITES	MEAN	10.16	21.56	19.06	0.32
	STANDARD DEVIATION	9.22	6.93	8.09	0.13
	COEF. OF VARIATION	0.907	0.322	0.425	0.426
	COEF. OF SKEWNESS	1.917	0.559	0.923	1.969
	COEF. OF KURTOSIS	7.338	3.515	4.523	9.114

The mean K-T damping coefficient for soil sites is equal to 0.32, and $\sigma = 0.13$, $V = 0.426$, $\gamma_1 = 1.969$, $\gamma_2 = 9.114$. Notice that there is a slight decrease in the mean K-T damping coefficient from rock sites to soil sites.

2.4 Correlation Studies of Seismic Parameters

2.4.1 Background

Ideally, a seismic safety analysis should include all the uncertainties related to ground motion representation, with all the seismic parameters expressed in probabilistic terms. However, for convenience and simplicity, it is common to consider some parameters as deterministic and others in terms of a conditional distribution given, say, peak ground acceleration [10,22].

The probability distributions as well as the interdependencies of the strong-motion duration and the Kanai-Tajimi frequency and damping coefficient have been discussed in the preceding sections. In this section, the correlations that may exist between these seismic parameters and peak ground acceleration, epicentral distance, and local magnitude will be examined. Several useful empirical relationships will be suggested.

There are many ways of assessing relationships among random variables, e.g., statistical regression techniques. In this study, the correlations are evaluated based on the "moving average" method which is quite effective in revealing trends that may exist between seismic parameters. Statistics are presented, based on a "moving average window" comprising 20 data points for strong-motion duration, Kanai-Tajimi frequency and damping coefficient as functions of peak ground acceleration, epicentral distance as well as earthquake local magnitude.

2.4.2 Correlations Versus Peak Ground Acceleration

Moving average statistics of the strong-motion duration, Kanai-Tajimi frequency and damping coefficient are plotted as functions of peak ground acceleration in Figures 2-8, 2-9, and 2-10, respectively. A point on these curves corresponding to a specific a_{max} is obtained by averaging the seismic parameter considered for a subset of 20 accelerograms with peak ground acceleration clustered around the median value a_{max}. Since there are only 10 records with peak ground acceleration greater than 0.25 g, the moving average statistics are computed only up to this value of a_{max}.

As depicted in Fig. 2-8, the strong-motion duration and the peak ground acceleration show a clear negative correlation, i.e., the strong-motion duration tends to decrease with increasing peak acceleration. This can be explained by the common dependence of S_o and a_{max} on the epicentral distance. Further discussion of this point is presented in Section 2.4.3.

The following approximate empirical relationship is suggested between mean strong-motion duration and peak ground acceleration (in g's):

$$S_{o|a_{max}} = 30 \exp(-3.254\ a_{max}^{0.35}) \qquad (2\text{-}18)$$

This equation implies an upper bound of 30 sec on the mean value of strong-motion duration. This is not unreasonable based on historical data. The relationship is plotted in Fig. 2-8 for comparison.

From the mean and mean plus one standard deviation curves, shown in Fig. 2-8, the "moving average" coefficient of variation, $V_{S_o|a_{max}}$, can be computed. The result indicates that except for the range of low peak ground accelerations, the variability of strong-motion duration remains almost the same. In particular, the overall moving average $V_{S_o|a_{max}}$ is

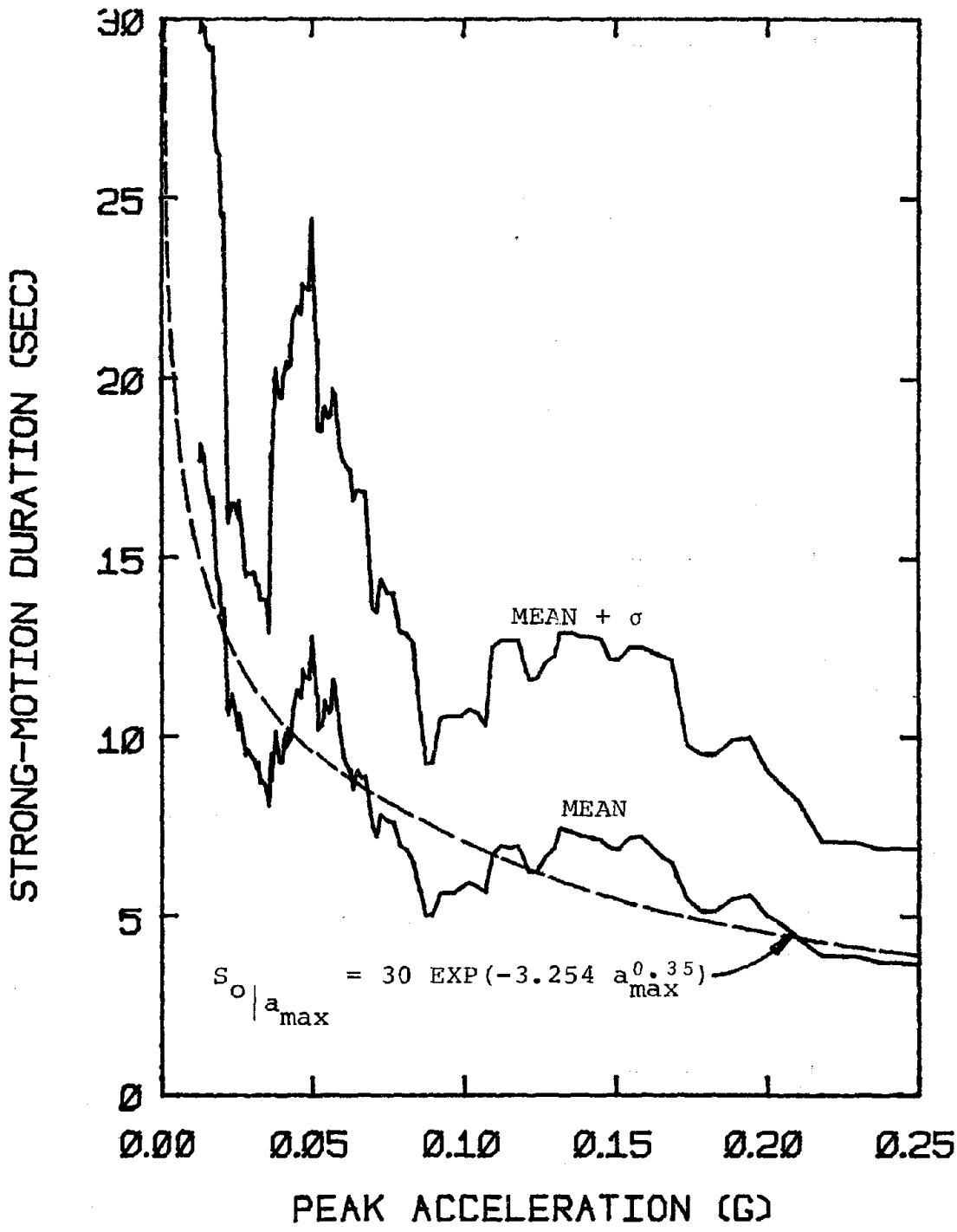

FIG. 2-8 MOVING AVERAGE STATISTICS FOR STRONG-MOTION DURATION VERSUS PEAK GROUND ACCELERATION

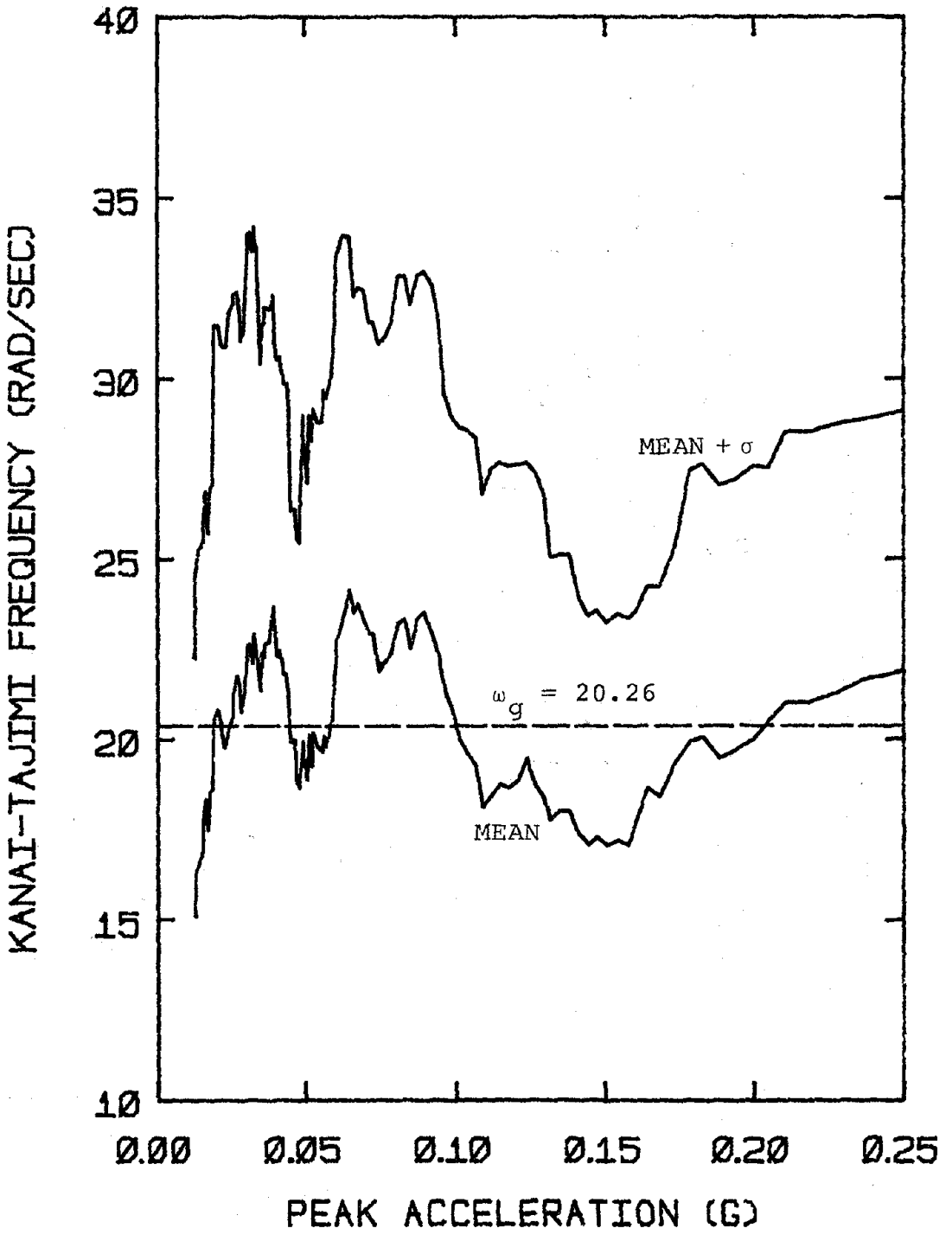

FIG. 2-9 MOVING AVERAGE STATISTICS FOR KANAI-TAJIMI FREQUENCY VERSUS PEAK GROUND ACCELERATION

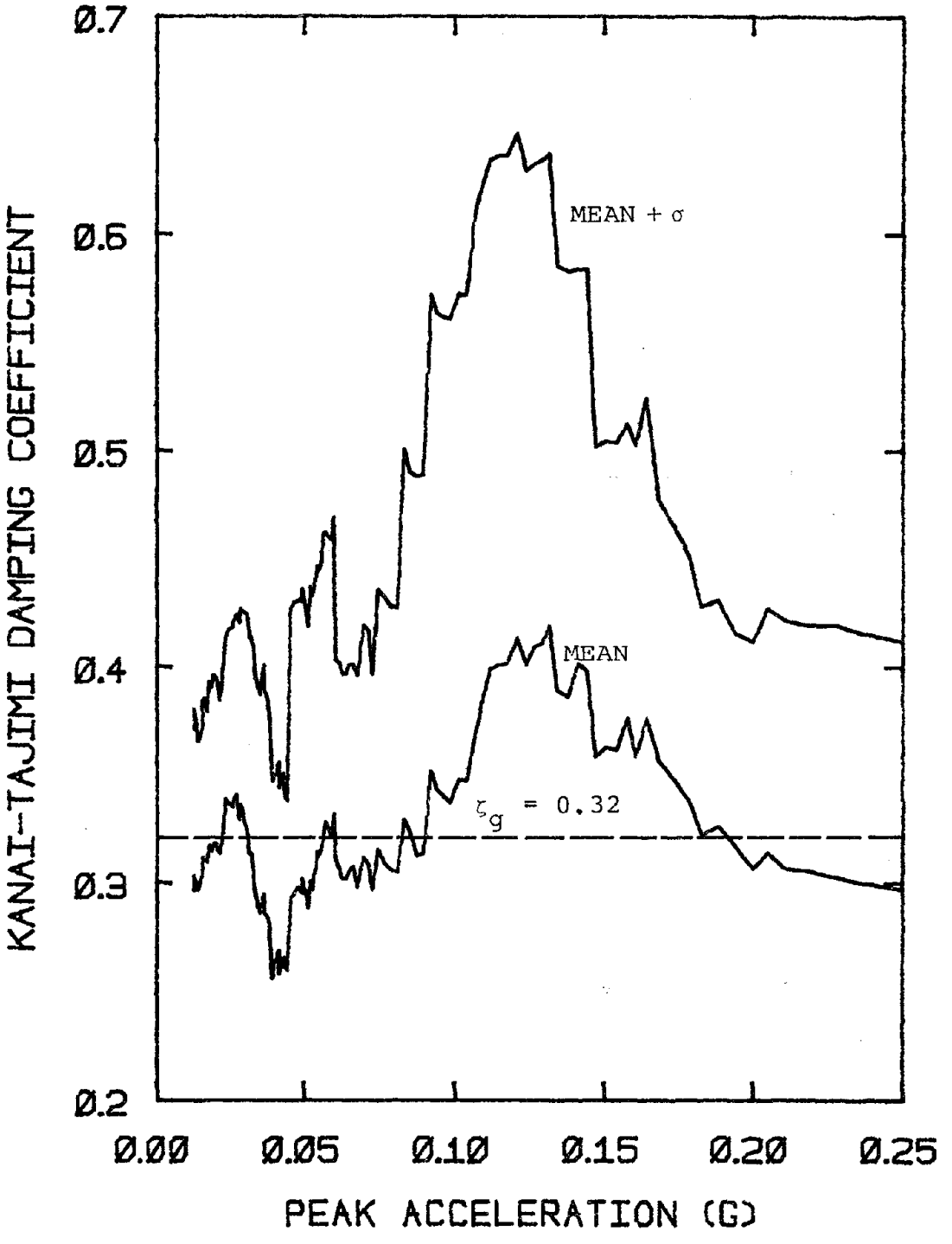

FIG. 2-10 MOVING AVERAGE STATISTICS FOR KANAI-TAJIMI DAMPING COEFFICIENT VERSUS PEAK GROUND ACCELERATION

equal to 0.804. This is smaller than the "unconditional" coefficient of variation of 0.945 reported earlier. The same procedure can be applied to find the moving average coefficient of skewness $\gamma_{1_{S_o|a_{max}}}$.

By studying the relationship between $V_{S_o|a_{max}}$ and $\gamma_{1_{S_o|a_{max}}}$, it can be concluded that the marginal distribution of strong-motion duration for different levels of peak acceleration is also approximately Gamma-distributed. Moreover, by assuming $V_{S_o|a_{max}}$ to be constant, the marginal distribution can be determined. For example, given a_{max} equal to 0.1 g, the conditional mean duration $S_{o|a_{max}}$ is 7.01 sec (Eq. 2-18). Assuming $V_{S_o|a_{max}} = 0.804$, then $\sigma_{S_o|a_{max}} = 5.64$ sec. Hence, the marginal distribution for strong-motion duration can be estimated.

As shown in Fig. 2-9, the moving average of the Kanai-Tajimi frequency is quite uniform for different levels of ground acceleration. The overall mean K-T frequency is 20.26 rad/sec. The coefficient of variation decreases with increasing acceleration, but it averages $V_{\omega_g|a_{max}} \simeq 0.429$.

Fig. 2-10 depicts the moving average statistics for Kanai-Tajimi damping coefficient versus peak ground acceleration. Again, ζ_g averages 0.32 and has an approximate conditional coefficient of variation $V_{\zeta_g|a_{max}} \simeq 0.385$.

2.4.3 Correlations Versus Epicentral Distance

Figures 2-11, 2-12 and 2-13 present the moving average statistics of S_o, ω_g, and ζ_g versus epicentral distance R for the 140 strong ground motions. As in the preceding section, each data point plotted represents the statistics of 20 motions recorded at epicentral distances that are clustered around a given median value.

Interestingly, the results shown in Fig. 2-11 suggest that the moving

average mean value of strong-motion duration increases almost linearly with epicentral distance. In fact, the following simple relationship can be derived:

$$S_{o|R} = 0.115(R + 30) \quad ; \quad 10 \text{ km} \leq R \leq 160 \text{ km} \tag{2-19}$$

where R is the epicentral distance in kilometers. The standard deviation also increases approximately linearly with R. This leads to a constant $V_{S_o|R} \simeq 0.65$.

Based on Eq. 2-19, one can crudely estimate the strong-motion duration given the value of epicentral distance. However, it is expected that the relationship will also be influenced by local magnitude. Further discussion is presented in the next section.

As shown in Fig. 2-12, the moving average mean Kanai-Tajimi frequency decreases with increasing epicentral distance. This is not surprising, since the higher frequency contents of the travelling seismic waves would be filtered out through soils. With increasing distance, the frequency content of the ground motion should shift to the lower side. For example, for R increasing from 10 km to 160 km, ω_g decreases from approximately 28 rad/sec to 13 rad/sec. Notice that the conditional coefficient of variation $V_{\omega_g|R}$ averages 0.39, which is only slightly below the unconditional coefficient of variation of 0.443.

Fig. 2-13 shows the moving average statistics of the K-T damping coefficient versus epicentral distance for the 140 strong ground motions. For practical purposes, ζ_g can be assumed to be constant and equal to about 0.32 for varying earthquake epicentral distances.

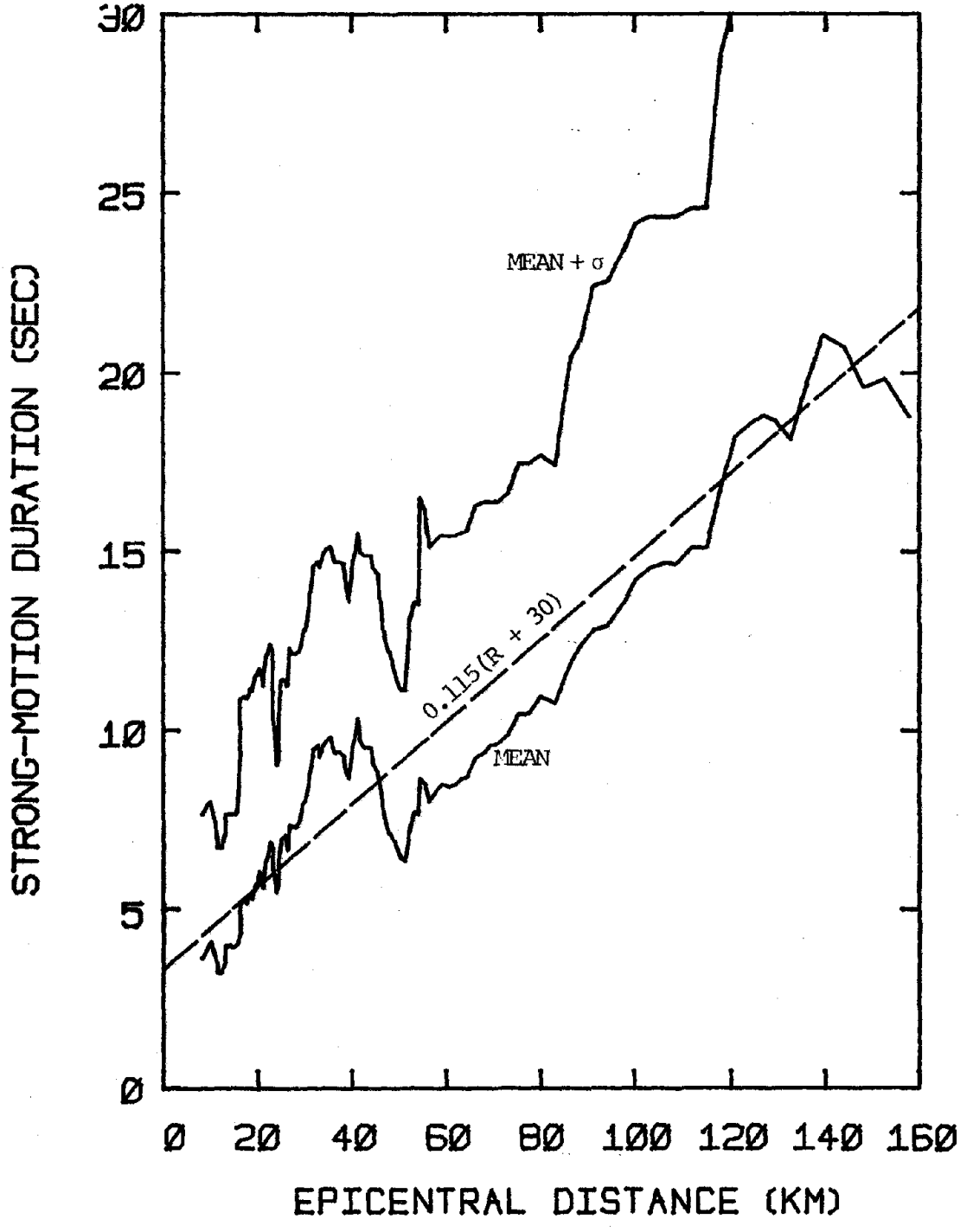

FIG. 2-11 MOVING AVERAGE STATISTICS FOR STRONG-MOTION DURATION VERSUS EPICENTRAL DISTANCE

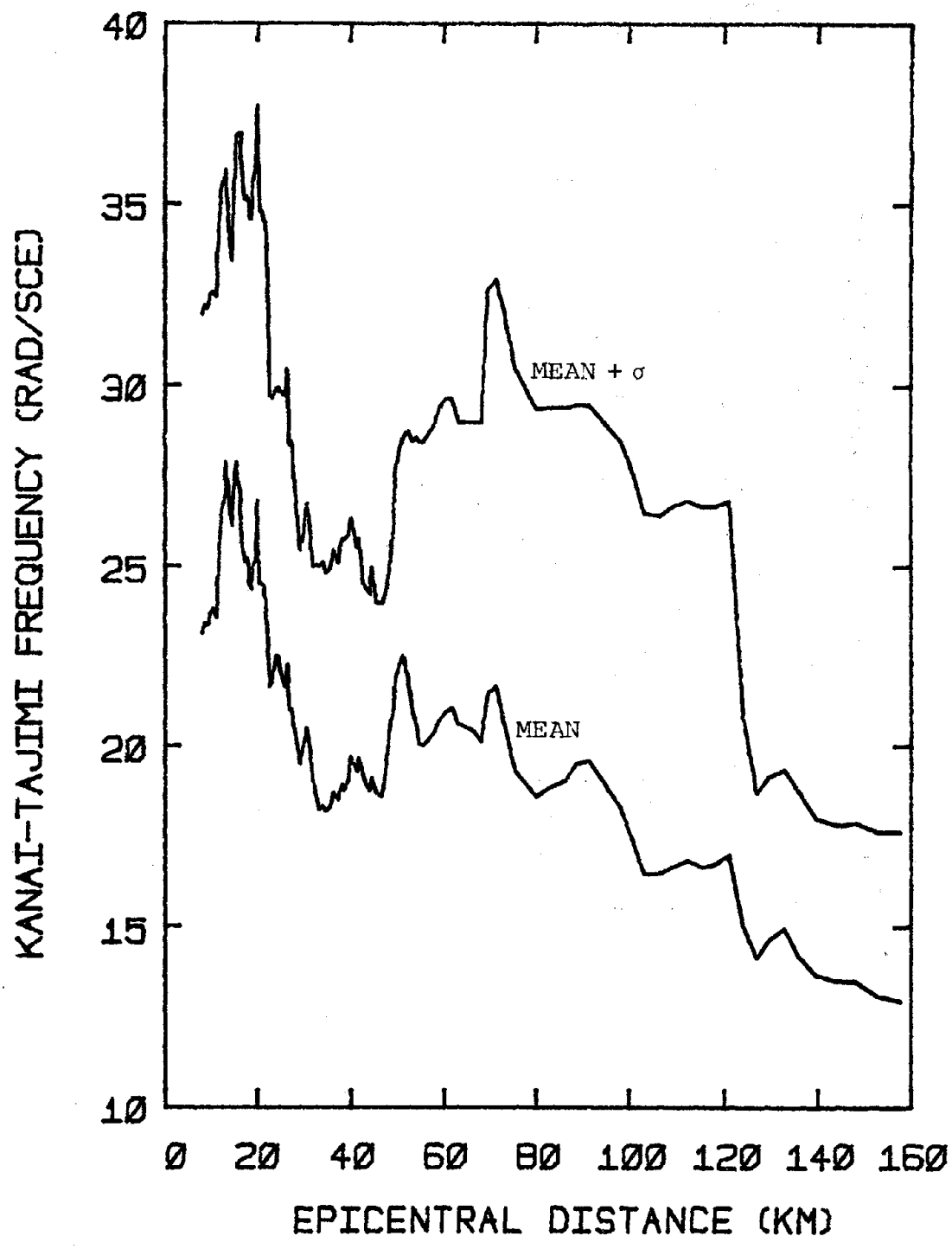

FIG. 2-12 MOVING AVERAGE STATISTICS FOR KANAI-TAJIMI FREQUENCY VERSUS EPICENTRAL DISTANCE

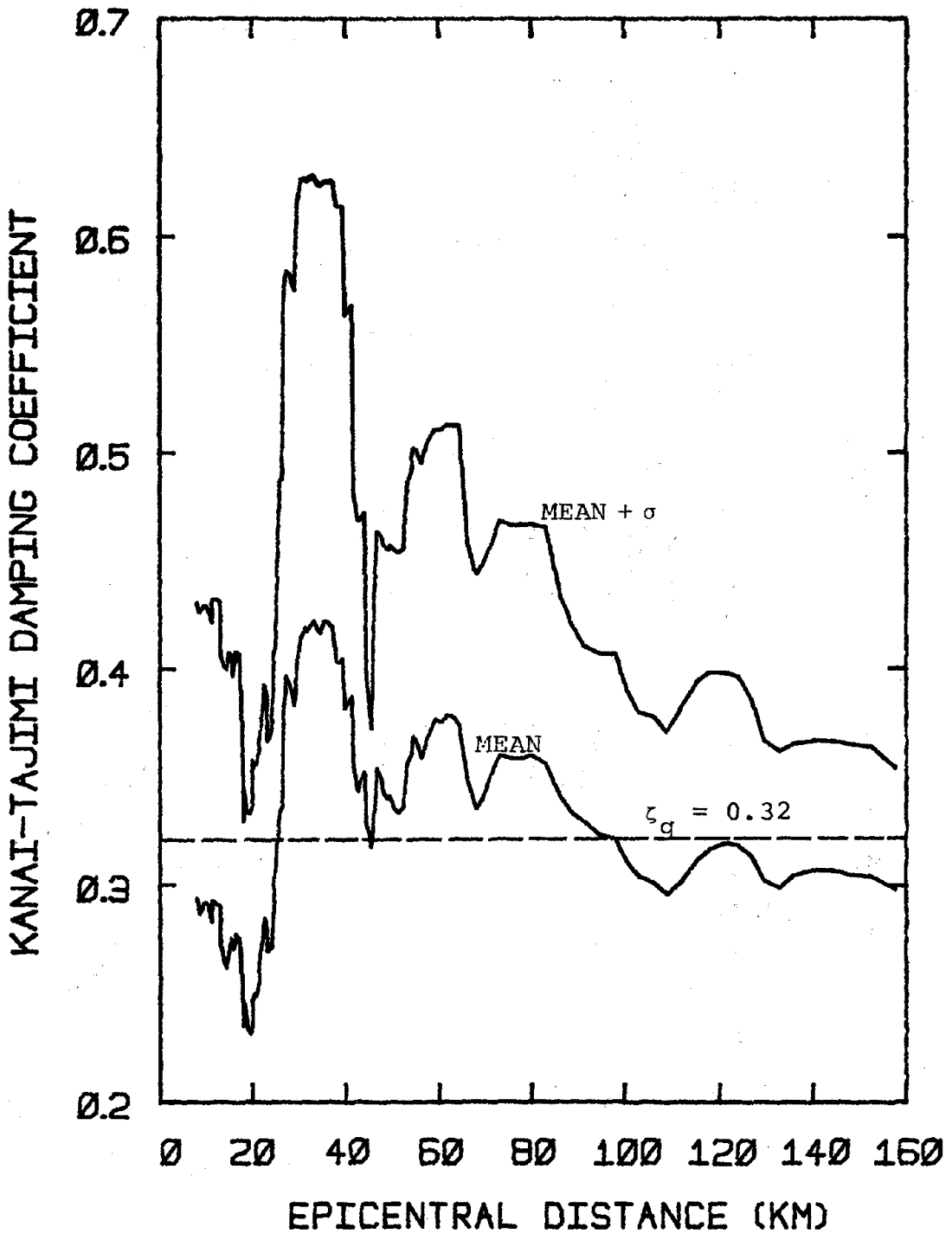

FIG. 2-13 MOVING AVERAGE STATISTICS FOR KANAI-TAJIMI DAMPING COEFFICIENT VERSUS EPICENTRAL DISTANCE

2.4.4 Correlations Versus Earthquake Local Magnitude

The moving average statistics for the strong-motion duration and the Kanai-Tajimi frequency and damping versus Richter magnitude are plotted in Figures 2-14, 2-15 and 2-16, respectively. Since many records have the same local magnitude, the moving average results presented below are expected to be very irregular at times, but certain important trends can still be identified. As shown in Fig. 2-14, the "moving average" strong-motion duration increases with the earthquake local magnitude. This trend has been observed by Housner, who proposed [31]:

$$S = 11\, M_L - 53 \tag{2-20}$$

where M_L is the Richter magnitude and S is the earthquake duration, which is however not quantitatively defined.

Based on the results of the 140 strong motion records used in this study, the following expression is suggested:

$$S_{o|M_L} = 4.4(M_L - 4.2) \quad ; \quad 5 \leq M_L \leq 7 \tag{2-21}$$

This permits a very crude estimate of strong-motion duration for given earthquake local magnitude. For comparison, both equations are plotted in Fig. 2-14. Notice that the conditional coefficient of variation, $V_{S_o|M_L}$, is equal to 0.79.

For an earthquake with given magnitude, as the epicentral distance increases, the peak ground acceleration tends to decrease, whereas the strong-motion duration tends to increase. The net effect is that strong-motion duration tends to be negatively correlated with peak acceleration. This is consistent with the result of this study as reported in Sec. 2.4.2.

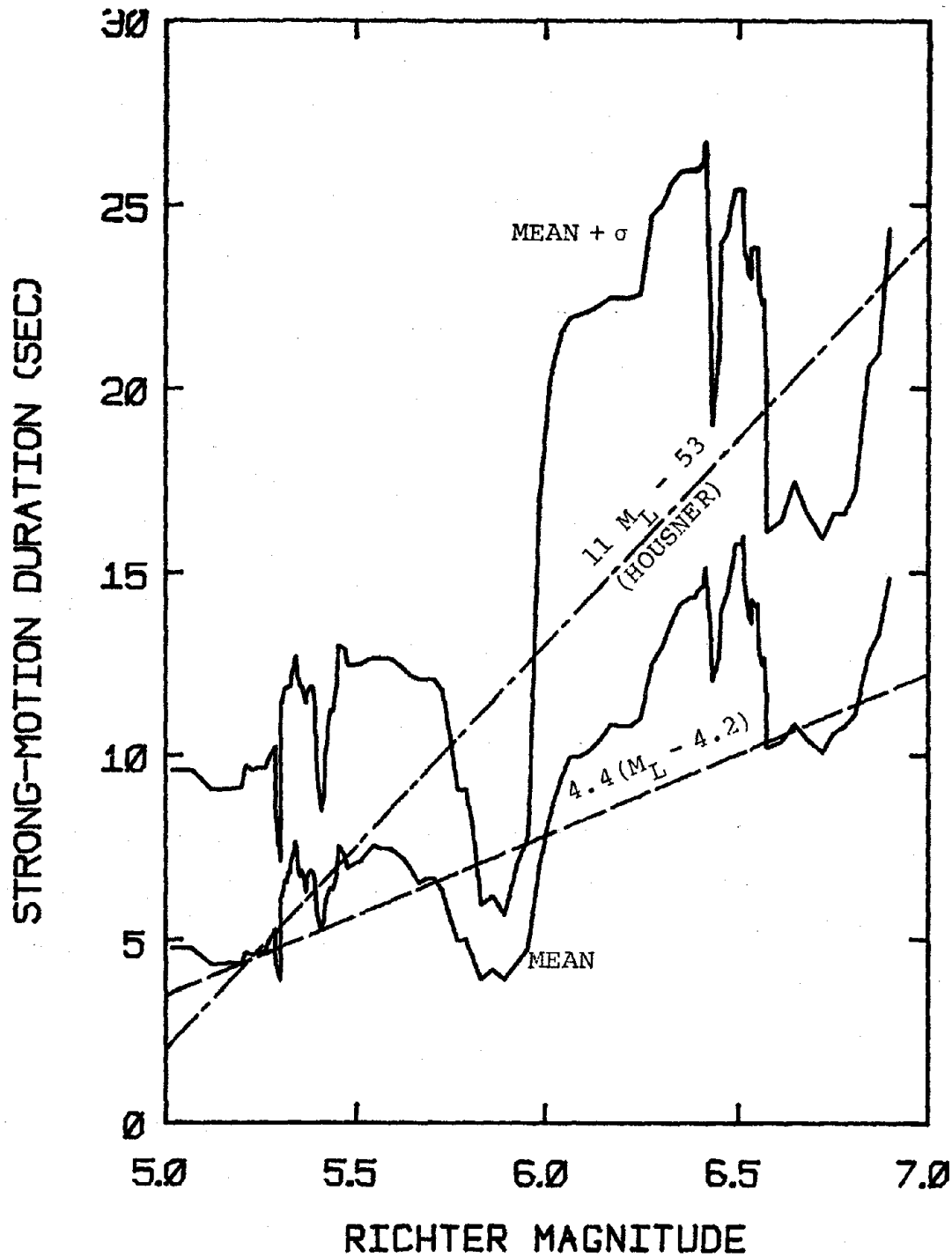

FIG. 2-14 MOVING AVERAGE STATISTICS FOR STRONG-MOTION DURATION VERSUS LOCAL RICHTER MAGNITUDE

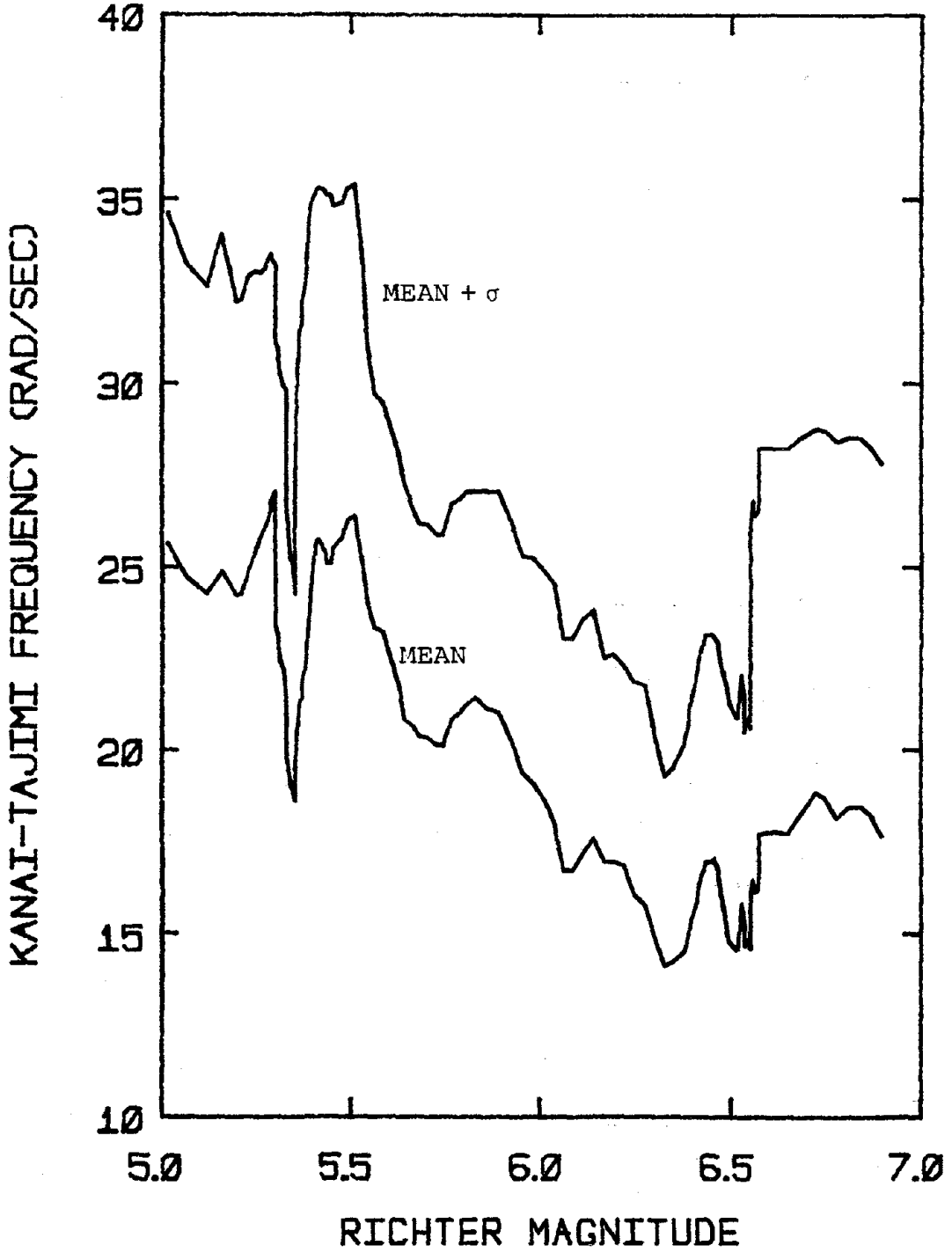

FIG. 2-15 MOVING AVERAGE STATISTICS FOR KANAI-TAJIMI FREQUENCY VERSUS LOCAL RICHTER MAGNITUDE

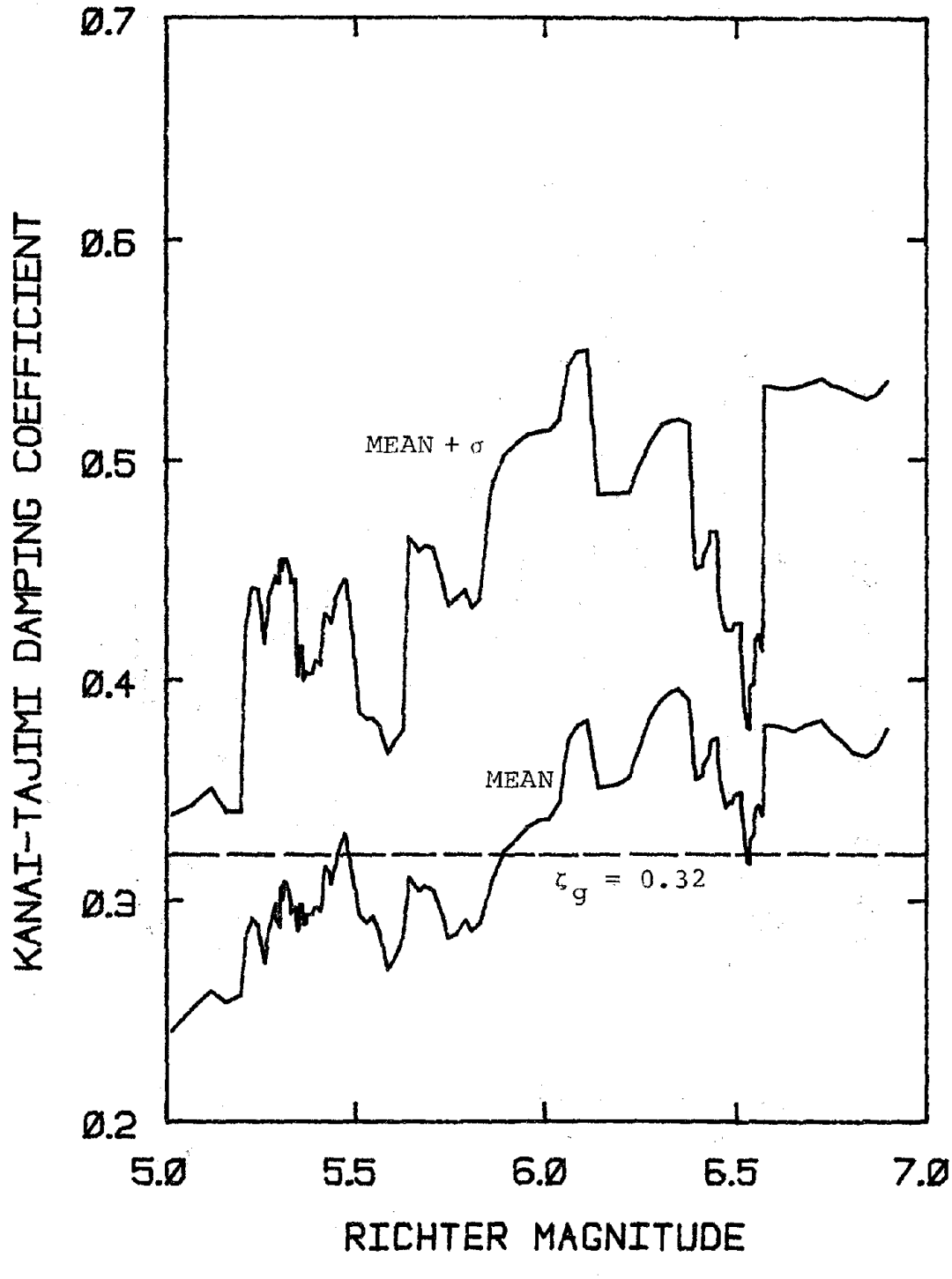

FIG. 2-16 MOVING AVERAGE STATISTICS FOR KANAI-TAJIMI DAMPING COEFFICIENT VERSUS LOCAL RICHTER MAGNITUDE

Fig. 2-15 shows that the moving average of the Kanai-Tajimi frequency generally decreases with increasing local magnitude except when M_L is greater than 6.5. This can also be explained by the common dependence of ω_g and M_L on the epicentral distance: ω_g decreases with increasing R, whereas M_L generally increases with R. This tends to introduce a negative correlation of ω_g on M_L. The sudden increase of the variability of ω_g when M_L exceeds 6.5 is probably because a large number of records, 36 to be exact, have magnitude in the range from 6.5 to 6.6. The conditional coefficient of variation, $V_{\omega_g|M_L}$, averages 0.383.

As shown in Fig. 2-16, the moving average Kanai-Tajimi damping coefficient increases slightly with the local Richter magnitude. However, it is still reasonable to assume a constant value of 0.32. The conditional coefficient of variation, $V_{\zeta_g|M_L}$, averages 0.392.

2.4.5 Alternate Ways to Predict Strong-Motion Duration

Based on the empirical relationships proposed in this chapter, the strong-motion duration of a ground motion can be determined in straightforward ways. For example, with given earthquake local magnitude, the strong-motion duration can be roughly predicted by Eq. 2-21. For given epicentral distance, Eq. 2-19 will also give an estimate of S_o. Alternatively, by using a particular attenuation law, one can compute the peak ground acceleration. Then, based on Eq. 2-18, the strong-motion duration can be predicted. These three different approaches are depicted in Fig. 2-17.

To study the compatibility between these approaches, the strong-motion durations for two levels of earthquake magnitude, i.e., 5.5 and 6.5, with varying epicentral distances, have been computed. The results are listed

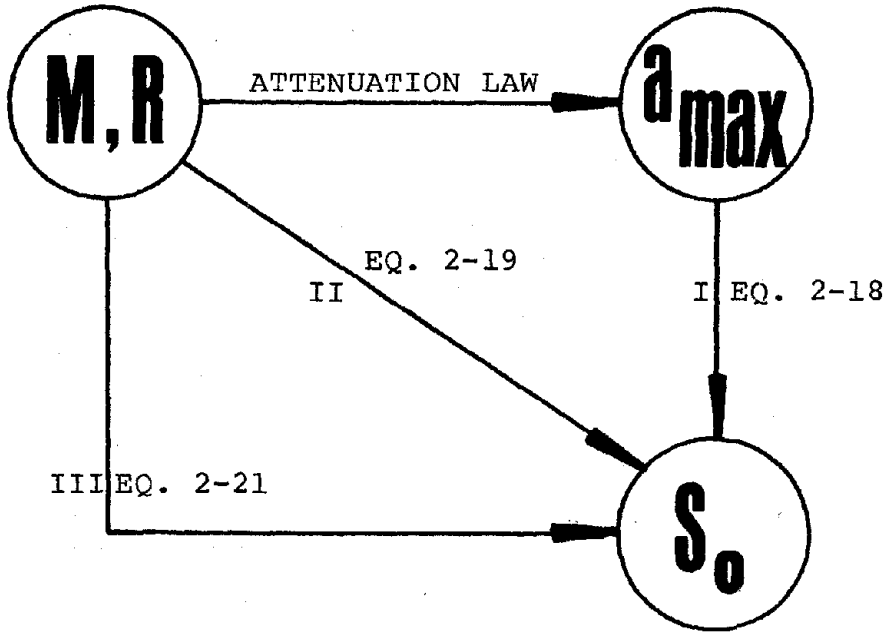

FIG. 2-17 DIFFERENT APPROACHES FOR PREDICTING STRONG-MOTION DURATION

---

in Table 2-4, where S_o^I represents the strong-motion duration predicted by Eq. 2-18, S_o^{II} is the duration based on Eq. 2-19, and S_o^{III} corresponds to Eq. 2-21.

Many expressions have been proposed in the literature for the attenuation of ground motion intensity, and each expression may predict a different peak ground acceleration. For purposes of illustration, the attenuation law proposed by Esteva and Villaverde was used in this study [20]:

$$a_{max} = 5.7\, e^{0.8\, M_L}\, (R + 40)^{-2} \qquad (2\text{-}22)$$

where a_{max} is in g's, R is in kilometers, M_L is the local Richter magnitude.

As shown in Table 2-4, the strong-motion durations predicted by Eqs.

TABLE 2-4 STRONG-MOTION DURATIONS PREDICTED BY DIFFERENT APPROACHES

M_L	R (km)	a_{max} (g)	S_o^I (sec)	S_o^{II} (sec)	S_o^{III} (sec)
5.5	10*	0.1857	4.93	4.60	5.72
	20	0.1289	6.13	5.75	
	40	0.0725	8.18	8.05	
	80	0.0322	11.28	12.65	
	120	0.0181	13.48	17.25	
	160	0.0116	15.14	21.85	
6.5	10*	0.4133	2.75	4.60	10.12
	20*	0.2870	3.67	5.75	
	40	0.1614	5.38	8.05	
	80	0.0718	8.23	12.65	
	120	0.0404	10.41	17.25	
	160	0.0258	12.14	21.85	

* Near Field Earthquake as Classified by Krinitzsky and Chang [38].

2-18 and 2-19 are quite compatible, especially for M_L = 5.5. Since information about the epicentral distance is not used, Eq. 2-21 provides only a rough estimate of the strong-motion duration. Considering the variability inherent in duration prediction, it appears that the first two approaches (Eqs. 2-18 and 2-19) will lead to satisfactory predictions of strong-motion duration.

Ideally, one should consider the joint effects of earthquake local magnitude and epicentral distance on strong-motion duration. The data set used in this study should preferably be divided into several subsets, each with different magnitude and epicentral distance ranges. Since the sample space used in this study is rather small, no attempt has been made herein. (Limited results of this type are reported in Ref. 40.)

2.5 Summary

In this chapter, the uncertainties in ground motion representation were investigated. Specifically, the characterization of strong ground motion in terms of the Kanai-Tajimi power spectral density function was studied. Based on the method of spectral moments, the parameters of the K-T PSD function were determined for a set of 140 earthquake records. Statistics of the strong-motion duration and the K-T frequency and damping were computed. Correlation studies of these parameters versus peak ground acceleration, epicentral distance, as well as local magnitude were performed. The results can be summarized as follows:

(1) Strong-motion duration, Kanai-Tajimi frequency and damping are approximately statistically independent. Both the strong-motion duration and the K-T frequency may be assumed Gamma-distributed, whereas the K-T damping is approximately Lognormal-distributed.

(2) The influence of site conditions on strong-motion duration is significant. The mean duration for records on soil is twice that for records on rock. The mean Kanai-Tajimi frequency for rock site records is 26.7 rad/sec, which is much higher than the value of 4π rad/sec often suggested in the literature [48,60].

(3) The assumed value of 0.6 for the Kanai-Tajimi damping as mentioned in the literature [22,55,60] is too high. The result of this study suggests that the mean value of K-T damping is equal to 0.32, and the coefficient of variation is 0.426.

(4) By calculating the moving average statistics, it is concluded that the strong-motion duration and the peak ground acceleration are negatively correlated. The moving averages of Kanai-Tajimi frequency and damping are quite uniform for different levels of peak acceleration.

(5) The moving average of the strong-motion duration increases almost linearly with the epicentral distance and the local magnitude. Empirical relationships for these parameters have been suggested. Based on a brief compatibility study, it is concluded that the relationships will predict duration consistently for given local magnitude and epicentral distance.

(6) The K-T frequency decreases with increasing epicentral distance. This confirms the observation that higher frequency components of seismic waves travelling through the earth's crest tend to be filtered out.

The results reported herein provide a better understanding of the variability of ground motion representation. Moreover, the findings constitute the basis for characterizing seismic input for overall seismic safety assessment.

CHAPTER 3

MULTI-DEGREE-OF-FREEDOM RANDOM VIBRATION INELASTIC RESPONSE PREDICTION FOR SHEAR-BEAM SYSTEMS

3.1 Introduction

As part of the effort to evaluate quantitatively the overall safety of earthquake-resistant structures, the conditional structural performance given a description of ground motion must be investigated. Random vibration methodology predicts the distribution of structural response, and permits direct assessment of the exceedance probability of a given response threshold. Within the context of seismic safety evaluation, this methodology is therefore superior to conventional step-by-step time integration techniques.

Using the first- and second-order statistics of stationary random processes, rigorous random vibration treatment of the linear-elastic simple systems is possible (see for example, Crandall and Mark, Ref. 19), and applications to the complex multi-degree-of-freedom (MDOF) structural systems have been proposed (e.g., Refs. 22, 60). Unfortunately, application of the methodology to nonlinear systems has been limited, as very few exact random vibration solutions to nonlinear systems exist.

Various approximate formulations for small inelastic deformation of single-degree-of-freedom (SDOF) systems have been suggested. For example, Crandall [18] proposed the perturbation method for stationary response prediction. Caughey [14] and Kobori et al. [37] suggested the equivalent linearization techniques, and Lutes [41] studied an equivalent non-linearization method for energy-dissipating systems.

Based on a substitute structure concept, and using the ductility-dependent stiffness and damping (Gates [23], Gulkan and Sozen [26]), Wen [66] suggested an approximate solution for MDOF systems. Kaul and Penzien [36] tried a third-order equivalent linearization procedure for bilinear offshore structures. Numerous approaches have also been attempted for different hysteretic oscillators, e.g., Paez and Yao [47], Iyengar and Iyengar [33], Iwan and Gates [32], Grossmayer and Iwan [25]. However, most of the above-mentioned models are quite complicated and it is difficult, if not impossible, to incorporate these techniques in practical seismic safety evaluation of structures.

As an extension of the energy conservation principle by Karnopp and Scharton [35], Vanmarcke [59] suggested an approximate stochastic model to estimate the average rate of energy dissipation due to yielding of an elasto-plastic system undergoing stationary ground excitation. The mean, variance and probability distribution of the E-P structural response can be conveniently predicted. Since the formulation is simple and readily applicable, this model has been extended into the nonlinear response prediction of MDOF systems by Gazetas [24]. The same methodology, with some important modifications, is incorporated in this study.

In this chapter, the pertinent statistical parameters of linear-elas-

tic random vibration solution strategy are first presented. Based upon extensive simulation study of a series of SDOF elasto-plastic systems, semi-empirical modification to the methodology is suggested. This is followed by a brief discussion of the key aspects of MDOF random vibration E-P response prediction.

3.2 Elastic Response Prediction by Random Vibration

As mentioned earlier, the response prediction of MDOF elastic shear-beam systems has been treated by Vanmarcke [59]. The solution strategy is briefly outlined below.

The input ground acceleration a(t) and the output story displacement y(t) at a specific point of the structure can be related by convolution as follows:

$$y(t) = a(t) * h(t) \tag{3-1}$$

h(t) is the impulse-response function which can be expressed as the summation of all the modal contributions:

$$h(t) = \sum_{k=1}^{n} c_k \, h_k(t) = \sum_{k=1}^{n} \Gamma_k \, \Phi_k \, h_k(t) \tag{3-2}$$

where $h_k(t)$ is the impulse-response function for the kth mode. Γ_k is the participation factor and Φ_k is the characteristic shape ordinate for mode k. Based on the Fourier transformation, the time-dependent transfer function of the system can be determined:

$$H(\omega,t) = \int_0^t h(t-\tau) \, \exp(-i\omega\tau) \, d\tau = \sum_{k=1}^{n} c_k \, H_k(\omega,t) \tag{3-3}$$

If the input motion is now modeled as a limited duration segment of a stationary stochastic process with PSD function $G(\omega)$, then the time-dependent PSD function of the response may be expressed as follows:

$$G_y(\omega,t) = G(\omega)\left|H(\omega,t)\right|^2 = G(\omega)\sum_{k=1}^{n}\sum_{j=1}^{n} c_k c_j\, H_k(\omega,t)\, H_j^*(\omega,t) \qquad (3\text{-}4)$$

where $H_j^*(\omega,t)$ is the complex conjugate of $H_j(\omega,t)$. The double summations involved in Eq. 3-4 are difficult to evaluate exactly.

For systems with small damping and with modal frequencies well separated, the following approximation has been suggested by Vanmarcke [60]:

$$G_y(\omega,t) \simeq G(\omega)\sum_{k=1}^{n}\left|H(\omega,t)\right|^2\left(c_k^2 + \sum_{j\neq k} c_j c_k\, A_{kjt}\right) \qquad (3\text{-}5)$$

where

$$A_{kjt} = \frac{8\varepsilon\,\zeta_{kt}(\zeta_{jt}+\zeta_{kt}\varepsilon)[(1-\varepsilon^2)^2 - 4\varepsilon(\zeta_{kt}-\zeta_{jt}\varepsilon)(\zeta_{jt}-\zeta_{kt}\varepsilon)]}{8\varepsilon[(\zeta_{kt}^2+\zeta_{jt}^2)(1-\varepsilon^2)^2 - 2(\zeta_{jt}^2-\zeta_{kt}^2\varepsilon^2)(\zeta_{kt}^2-\zeta_{jt}^2\varepsilon^2)] + (1-\varepsilon^2)^4} \qquad (3\text{-}6)$$

$$\zeta_{kt} = \frac{\zeta_k}{1-\exp(-2\zeta_k\omega_k t)} \qquad (3\text{-}7)$$

$$\zeta_{jt} = \frac{\zeta_j}{1-\exp(-2\zeta_j\omega_j t)} \qquad (3\text{-}8)$$

ε is the modal frequency ratio ω_j/ω_k, whereas ζ_{kt} and ζ_{jt} are the fictitious time-dependent modal dampings that take into account the nonstationarity of the system response.

Based on Eq. 3-5, the response variance $\sigma_y^2(t)$ can then be expressed

in terms of all the contributing modal response variances:

$$\sigma_y^2(t) = \int_0^\infty G_y(\omega,t)\, d\omega$$

$$\simeq \int_0^\infty G(\omega) \sum_{k=1}^{n} |H_k(\omega,t)|^2 \left(c_k^2 + \sum_{j\neq k} c_j c_k A_{kjt}\right) d\omega \qquad (3\text{-}9)$$

$$= \sum_{k=1}^{n} \left(c_k^2 + \sum_{j\neq k} c_j c_k A_{kjt}\right) \sigma_{y,k}^2(t)$$

Similarly, the ith spectral moment of the response $\lambda_{i,y}$ can be generalized as follows:

$$\lambda_{i,y}(t) \simeq \sum_{k=1}^{n} \left(c_k^2 + \sum_{j\neq k} c_j c_k A_{kjt}\right) \lambda_{i,y,k}(t) \qquad (3\text{-}10)$$

For most engineering applications, the peak response is of primary interest. In order to arrive at the peak response prediction, the root-mean-square response $\sigma_y(t)$ must be multiplied by a threshold factor $r_{S_o,P}$. For given excitation duration S_o and a probability level P, $r_{S_o,P}$ can be computed based on the first-passage theory:

$$r_{S_o,P} = [2\, \ell n\{2\eta[1 - \exp(-\delta_y^{1.2}\sqrt{\pi \ell n\, 2\eta})]\}]^{\frac{1}{2}} \qquad (3\text{-}11)$$

$$\eta = (\Omega_y S_o/2\pi)(-\ell n\ P)^{-1} \qquad (3\text{-}12)$$

where Ω_y is the average response frequency and δ_y is the response shape factor. They can be expressed in terms of the modal frequencies ω_k and modal shape factors δ_k, both evaluated at the end of the ground excita-

tion ($t = S_o$):

$$\Omega_y = \left(\sum_{k=1}^{n} Q_k \omega_k^2 \right)^{\frac{1}{2}} \tag{3-13}$$

$$\delta_y = \left\{ 1 - \left[\sum_{k=1}^{n} Q_k (\omega_k / \Omega_y) \sqrt{1 - \delta_k^2} \right]^2 \right\}^{\frac{1}{2}} \tag{3-14}$$

$$Q_k = \frac{\left(c_k^2 + \sum_{j \neq k} c_j c_k A_{kjt} \right) \sigma_{y,k}^2(S_o)}{\sum_{i=1}^{n} \left(c_i^2 + \sum_{j \neq i} c_j c_i A_{ijt} \right) \sigma_{y,i}^2(S_o)} \tag{3-15}$$

Note that $\delta_k = (4\zeta_{kt}/\pi)^{\frac{1}{2}}$, which is also evaluated at $t = S_o$. The weight Q_k is the ratio of modal response variance contribution to the overall response variance.

Since the duration of a strong ground motion is usually not very long compared to the lower-mode natural periods of structures, the above-mentioned steady-state solution is seldom reached. This is especially true when the structural damping is small. Hence, the random vibration methodology as outlined herein must be modified. Vanmarcke [60] has suggested an "equivalent stationary response duration", denoted by S_o^*. It is defined as a fraction of the input strong-motion duration S_o:

$$S_o^* \simeq S_o \exp[-2(m - 1)] \tag{3-16}$$

$$m = \sigma_y^2(S_o) / \sigma_y^2(0.5\, S_o) \tag{3-17}$$

where m is the ratio of the transient variances at time $t = S_o$ and $0.5\, S_o$ respectively. For simplicity, the asterisk will be dropped in the following discussion. Except when specifically mentioned otherwise, S_o re-

presents the equivalent stationary duration.

3.3 Inelastic Response Prediction by Random Vibration

3.3.1 Background

When an elasto-plastic SDOF system starts to yield, the kinetic energy will dissipate by hysteretic yielding action. Based on the balance of these energies, Karnopp and Scharton [35] suggested that the expected amount of E-P deformation, E[D], for a single crossing of the yielding threshold y_e can be expressed as follows:

$$E[D] = \sigma_y^2/2y_e = \sigma_y/2r \tag{3-18}$$

where $r = y_e/\sigma_y$ is the normalized factor of the yielding threshold divided by the root-mean-square of the response for the "associated elastic system".

As an extension of the work by Karnopp and Scharton, Vanmarcke [59] argued that the elasto-plastic response could be divided into two components: a component of permanent set, and an equivalent elastic response component. He further suggested that the nonlinear effect could be modeled as a first threshold passage problem for the associated elastic system. Specifically, the probability of the peak E-P deformation D_p not exceeding a given plastic threshold d has been approximated as follows [60,64]:

$$P[D_p \leq d] = \exp\{[1 - \exp(\alpha S_o)] \exp(-d/E[D])\} \tag{3-19}$$

where S_o is the excitation duration and α is the decay rate which can be determined as follows:

$$\alpha = \frac{2\nu_o[1 - \exp(-\sqrt{\pi/2}\ r\ \delta_y^{1.2})]}{\exp(r^2/2) - 1} \tag{3-20}$$

and $\nu_o = (\lambda_2/\lambda_o)^{\frac{1}{2}}/2\pi$ = mean rate of zero crossings.

Alternatively, Eq. 3-19 can be expressed as the expected peak elasto-plastic deformation d with probability P_d of not being exceeded:

$$d = E[D]\{\ell n[1 - \exp(\alpha S_o)] - \ell n(-\ell n\ P_d)\} \tag{3-21}$$

The commonly used "peak ductility ratio" μ is a simple function of d and the elastic response limit y_e, and is expressed as follows:

$$\mu = \frac{d}{y_e} + 1 \tag{3-22}$$

The probabilistic prediction of SDOF inelastic action in terms of the peak ductility ratio is derived as follows:

$$\mu = \frac{E[D]}{y_e}\{\ell n[1 - \exp(\alpha S_o)] - \ell n(-\ell n\ P_d)\} + 1 \tag{3-23}$$

3.3.2 Single-Degree-of-Freedom Simulation Study

Based on the Karnopp-Scharton energy conservation equation (Eq. 3-18) and confirmed by Yanev's simulation study [70] for the white noise Gaussian excitation, the average amount of elasto-plastic deformation, E[D], is predicted to be equal to $\sigma_y/2r$. All the previous random vibration analysis of SDOF E-P systems by Vanmarcke et al. [59,60,64], and of MDOF systems by Gazetas [24] were based on this relationship. The validity of this relationship, especially at low values of r, was investigated by an extensive simulation study described below.

As mentioned in the preceding section, given the ground motion PSD function and the duration of the strong motion, the elasto-plastic defor-

mation corresponding to a non-exceedance probability P_d can be computed (Eq. 3-21). The 50% probability level is used throughout the simulation study.

For a given natural period and ductility demand of a one-degree E-P system, the corresponding elastic response limit y_e can be determined directly from time-history analysis of a set of accelerograms. With this information, one can calculate the expected plastic deformation which would achieve agreement between the random vibration solution and the time-history results. The back-figured expected plastic deformation is denoted by $E[D^*]$. By comparing the required value $E[D^*]$ with the original value of $E[D]$ obtained from Eq. 3-18, the adequacy of the Karnopp-Scharton equation can be assessed, and a "semi-empirical" correction factor can be determined.

A set of SDOF elasto-plastic systems has been selected for the simulation study. It comprises ten natural periods varying from 0.1 to 7.0 seconds. Each system has four different levels of spring resistance, corresponding to ductility ratios of 2, 3, 4 and 5. These 40 systems have been subjected to two sets of artificial ground motions with varying durations, i.e., S_o = 10 sec and 20 sec. Each set comprises five different synthetic ground motions. Two corresponding PSD functions have also been used for the random vibration analysis. Detailed description of the artificial ground motions as well as the associated PSD functions is presented in Sec. 4.3.

The values of $E[D^*]$ can be normalized with respect to $E[D]$. The resulting values of the elasto-plastic deformation ratio $E[D^*]/E[D]$ are plotted versus the response threshold r in Fig. 3-1. As shown in the figure,

the results for S_o = 10 sec are generally greater than those corresponding to S_o = 20 sec. Moreover, the results do tend to suggest that $E[D^*]/E[D]$ is dependent on the response threshold r.

For comparison, the simulation results for the white noise Gaussian excitation by Yanev [70] are also plotted in the figure. Notice that these data are much higher than those obtained in this study. This suggests that Eq. 3-18 is valid only when the system "r value" is greater than about 2. In other words, the Karnopp-Scharton energy conservation equation is adequate only when the system has a high yielding theshold r. For the range of r of most interest in earthquake engineering, i.e., $0.2 \leq r \leq 2.0$, the method must be modified.

For the purpose of improving random vibration prediction of elasto-plastic response, a quadratic relationship between $E[D^*]/E[D]$ and the response threshold r is proposed:

$$E[D^*]/E[D] = 0.5\ r - 0.06\ r^2 \tag{3-24}$$

Since $E[D] = \sigma_y/2r$, (Eq. 3-18), this leads to the following modified prediction of average amount of plastic deformation:

$$E[D^*] = (0.25 - 0.03\ r)\sigma_y \tag{3-25}$$

Eq. 3-24 is also plotted in Fig. 3-1. Note that when r is large, the value of $E[D^*]/E[D]$ calculated by Eq. 3-24 is close to that predicted by Eq. 3-18 within the range of the data. Hence, this semi-empirical relationship appears compatible with the original formulation for high response thresholds.

3.3.3 Response Prediction of a Yielding State

Except for the above-mentioned modification, the multi-degree-of-free-

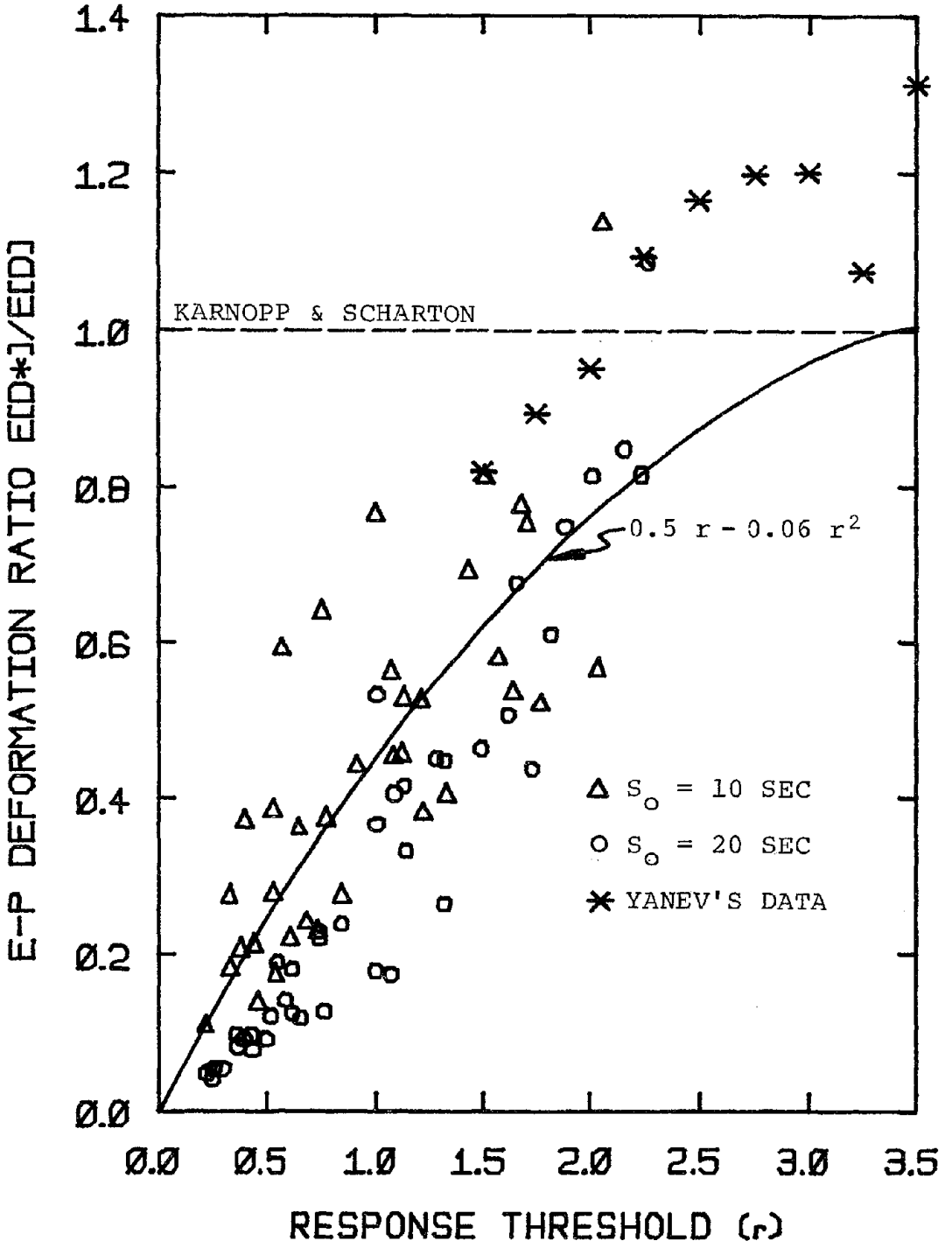

FIG. 3-1 COMPARISON OF SIMULATED AND THEORETICAL VALUES FOR AVERAGE AMOUNT OF E-P DEFORMATION VERSUS RESPONSE THRESHOLD LEVEL r

dom elasto-plastic random vibration solution strategy used in this study generally follows that proposed by Gazetas [24]. Key aspects of the MDOF elastic random vibration methodology have been presented in Sec. 3.2. Its extension into the elasto-plastic response prediction of MDOF systems is briefly discussed below.

By studying the response time histories of three 4-story and two 2-story shear-beam models, Gazetas observed that the inelastic action in each story tends to occur in several consecutive "clumps" of yield level crossings. He further suggested that the inelastic structural behavior can be modeled as a sequence of "yielding states", defined by the story which yields first after an elastic interval. Based on the first-passage theory, the probability that a story yields within a given time interval is found to be exponentially distributed with decay rate α. In particular, the probability of story k yielding first (i.e., before the other stories), can be expressed as [24]:

$$f_k = \frac{\alpha_k}{\sum_{j=1}^{n} \alpha_j} \tag{3-26}$$

where α_k is the decay rate of the reliability for the kth story, as defined in Eq. 3-20.

Assuming that the kth story starts yielding first, the response of the other stories would decrease. Based on the simulation study, Gazetas suggested that the reduction in energy received by the other stories should be proportional to their "elastic energy rate" just before yielding occurred in story k. The elastic energy rate of story i is defined as $\nu_i K_i \sigma^2_{y,i}$, where ν_i is the rate of zero-crossings, K_i is the story stiff-

ness, and $\sigma^2_{y,i}$ is the elastic response variance of story i. Specifically, the following reduction formula is suggested for story i when story k yields first:

$$\sigma^2_{y,i,k} = \sigma^2_{y,i}\ \xi_i^2 \tag{3-27}$$

where

$$\xi_i = \left(1 - \frac{\nu_i\ K_i\ \sigma^2_{y,i}}{\sum_{j=1}^{n} \nu_j\ K_j\ \sigma^2_{y,j}}\right)^{\frac{1}{2}} \tag{3-28}$$

Gazetas [24] further observed that the central frequencies of vibration for those stories above the first-yield story, k, would increase as if a separate structure exists on top of the yielding story (with n minus k degrees of freedom). Moreover, the central frequency of vibration of story k should decrease as a function of the yielding action. Based on a simulation study, he suggested an empirical frequency reduction factor, ψ, as a function of the peak story ductility μ:

$$\Omega^*_{y,k} = \psi\ \Omega_{y,k} \tag{3-29}$$

This empirical frequency reduction factor is plotted in Fig. 3-2.

By studying the nonlinear behavior of non-deteriorating systems, e.g., steel structures, Gates proposed a similar ductility-dependent frequency reduction factor [23,66]:

$$\psi = \left[\frac{1-\rho}{\mu}\ (1 + \ell n\ \mu) + \rho\right]^{\frac{1}{2}} \tag{3-30}$$

where ρ is the second slope normalized to the initial stiffness of a bi-linear spring model. For comparison, the empirical values for the elas-to-plastic spring (i.e., $\rho = 0\%$) and for a 5% bilinear spring are also

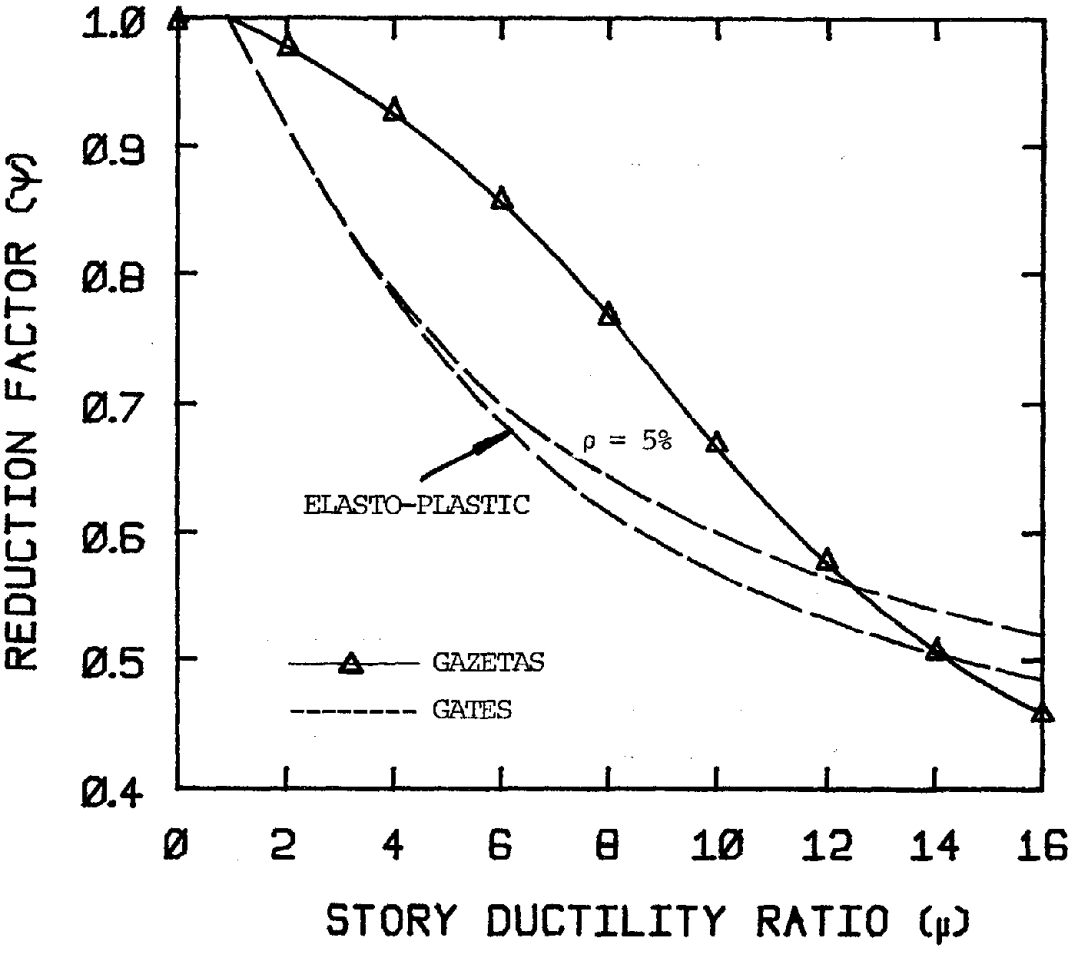

FIG. 3-2 EMPIRICAL FREQUENCY REDUCTION FACTOR AS A FUNCTION OF STORY DUCTILITY RATIO

---

presented in Fig. 3-2.

As shown in the figure, the empirical frequency reduction factor suggested by Gates is generally smaller, implying greater reduction than that proposed by Gazetas. The difference is not large; it is most pronounced (19% greater reduction) when μ is about 6. Since the Gates study was only based on the results of five cases, the frequency reduction factor sugges-

ted by Gazetas is considered to be more reliable. Hence, it is incorporated in this study.

Thus far, only the response prediction of a particular yielding state has been discussed. During each yielding state, yielding may also occur in the other stories. Therefore, one must compute the resulting changes of response characteristics due to these so-called "substates".

Using the same methodology presented earlier, the computation is necessarily iterative for each yielding state. Based on the first-passage formulation, the probability that story i will yield during the kth yielding state has been derived [24]:

$$P_{i,k} = 1 - B_{i,k} \exp(-\alpha_{i,k} S_k) \tag{3-31}$$

$$B_{i,k} = 1 - \exp(-r_{i,k}^2/2) \tag{3-32}$$

$$S_k = \frac{1}{2\nu_{o,k}^*[1 - \exp(-\sqrt{\pi/2}\ \delta_k\ r_k)]} \tag{3-33}$$

where $\nu_{o,k}^*$ is the reduced zero-crossing rate, $\alpha_{i,k}$ is the decay rate (Eq. 3-20), and S_k is the expected duration of yielding state k. $B_{i,k}$ is the probability that no yielding occurred in story i, when yielding state k begins.

Having obtained the story response statistics for each yielding substate, the yielding state response can be obtained by combining the substate results according to their relative likelihood. The final combination of all yielding states is presented next.

3.3.4 Yielding States Combination

In order to predict the overall response characteristics, the elasto-

plastic response of each yielding state must be combined. Based on a simulation study, Vanmarcke et al. [65] confirmed that the probability density function for the permanent plastic deformation, d, is approximately exponentially distributed:

$$f_{|D|}(d) = \frac{1}{E[D^*]} \exp(-d/E[D^*]) \tag{3-34}$$

Gazetas [24] suggested that the "maximum" plastic deformation can also be assumed exponentially distributed. Moreover, the exceedance probability of the maximum plastic deformation of a story i due to the yielding state k can be estimated by:

$$\begin{aligned} P_k[D_p \leq d_i] &= [1 - F_{|D|}(d_i)]^{\alpha_{i,k} S_k f_k P_{i,k}} \\ &= [\exp(-d_i/E[D^*_{i,k}])]^{\alpha_{i,k} S_k f_k P_{i,k}} \\ &= \exp(-\alpha_{i,k} S_k f_k P_{i,k} d_i/E[D^*_{i,k}]) \end{aligned} \tag{3-35}$$

where $F_{|D|}(d)$ is the cumulative distribution function of d; $\alpha_{i,k}$ = elastic decay rate (Eq. 3-20); S_k = equivalent steady-state duration (Eq. 3-16); f_k = probability that story k yields first (Eq. 3-26); $P_{i,k}$ = probability that story i yields during yielding state k (Eq. 3-31), and $E[D^*_{i,k}]$ = expected plastic deformation of story i during yielding state k (Eq. 3-25).

Based on the argument that the overall maximum elasto-plastic deformation is the largest of all the maxima of each yielding state, the exceedance probability of the overall peak E-P deformation of story i can be crudely estimated by the following equation (assuming independence among successive maximum values):

$$P[D_p \leq d_i] = \prod_{k=1}^{n} P_k[D_p \leq d_i]$$

$$= \prod_{k=1}^{n} \exp(-\alpha_{i,k} S_k f_k P_{i,k} d_i / E[D^*_{i,k}]) \qquad (3\text{-}36)$$

Π represents the product of all the yielding states.

From the above probability distribution, the mean and the standard deviation of the maximum E-P deformation of story i, i.e., $E[d_i]$ and σ_{d_i}, can be obtained numerically. The mean and the standard deviation of the peak ductility ratio for story i can then be obtained as follows:

$$E[\mu] = \frac{E[d_i]}{y_{e,i}} + 1 \qquad (3\text{-}37)$$

$$\sigma_\mu = \frac{\sigma_{d_i}}{y_{e,i}} \qquad (3\text{-}38)$$

By the simulation study, Gazetas concluded that the peak story ductility ratio may be expected to have a Gumbel type I extreme value distribution as follows [24]:

$$F_\mu(\mu) = \exp\{-\exp[-u_1(\mu - u_2)]\} \qquad (3\text{-}39)$$

The parameters u_1 and u_2 can be directly estimated from the mean and the standard deviation of μ [8]:

$$E[\mu] \simeq u_2 + \frac{0.5772}{u_1} \qquad (3\text{-}40)$$

$$\sigma_\mu = \frac{\pi}{\sqrt{6}\, u_1} \qquad (3\text{-}41)$$

In this way, the conditional structural performance is predicted in terms

of the peak story ductility ratio by appropriate MDOF random vibration analysis.

3.4 Summary

Important aspects of the approximate random vibration-based approach to seismic analysis of multi-degree-of-freedom elasto-plastic systems have been presented in this chapter. The results of an extensive simulation study indicate that the Karnopp-Scharton energy conservation equation, which predicts yielding in one-degree E-P systems, is valid only for high yielding thresholds. In the range of ductilities of earthquake engineering interest (say, about 5), the method must be modified. A semi-empirical modification has been suggested in this chapter.

The validity of the modified multi-degree elasto-plastic random vibration methodology will be assessed through comparison with the results of time-history analysis. This is presented in the next chapter.

CHAPTER 4

COMPATIBILITY OF INELASTIC RESPONSE PREDICTIONS BY RANDOM VIBRATION AND TIME-HISTORY ANALYSIS

4.1 Introduction

This chapter describes the results of a series of compatibility studies aimed at quantifying three major components of uncertainty associated with the inelastic response prediction of structural frames. These uncertainties are briefly described below:

(I) Assuming the moment-resisting frame behaves as an elasto-plastic multi-degree close-coupled shear-beam system, what are the uncertainties involved in determining the equivalent lateral story stiffnesses and yielding strengths? In addition, can the assumptions underlying the shear-beam model itself be justified?

(II) For a given shear-beam system, the E-P response statistics can be predicted by the modified multi-degree random vibration methodology. The inelastic response characteristics can also be estimated by "multiple" time-history analyses. Are these different response predictions compatible?

(III) The modified MDOF E-P random vibration technique can lead to the

inelastic "story" response prediction. However, the inelastic "local" structural component response is of major engineering interest. How can the two different levels of response measures, i.e., local versus story, be related?

The relationships of these above-mentioned uncertainties are depicted in Fig. 4-1.

Three steel moment-resisting frames are employed in the compatibility studies. They represent real-world low, middle-height and high-rise buildings, i.e., 4-, 10- and 16-story, respectively. A background description of these frames is presented first in this chapter. The artificial strong ground motions and the corresponding power spectral density functions used in this study are briefly presented. This is followed by detailed discussion of the determination of equivalent lateral story stiffnesses and yielding strengths.

Based on the equivalent story shear-spring parameters, the elasto-plastic story response statistics are computed by multiple time-history analyses of an ensemble of synthetic ground motions. The results are compared with the random vibration predictions based on input with compatible PSD functions. Further, the results will be examined versus the time-history predictions of the structural frames.

From the compatibility studies, the validity of the modified multi-degree elasto-plastic random vibration methodology is assessed for the response prediction of actual structural frames. Moreover, the relationship between two different levels of response characteristics, i.e., local versus story, is established. The effects of gravity loads on inelastic response prediction are also explored. Finally, the prediction of maximum story displacement is discussed.

4.2 Description of Building Frames Investigated

Three steel moment-resisting frames, i.e., 4-, 10- and 16-story, are used extensively in the compatibility studies. These frames were originally designed by Piąue [49] according to the 1973 edition of the Uniform Building Code [58]. The zone 3 seismic risk characterization was used. The frames were assumed to have adequate bracing systems to resist out-of-plane motions. Elevations and member sizes (based on the original design) of the three steel frames are shown in Figures 4-2, 4-3 and 4-4, respectively.

In his investigation of the aseismic design procedure for buildings, Lai [39] redesigned these frames using the so-called "inelastic frame design procedure". The procedure is briefly outlined below.

Given the preliminary member sizes, the design ductility ratio of the structure and the design peak ground acceleration, the maximum member forces can be computed by modal analysis using the so-called "Inelastic Acceleration Response Spectrum" (IARS) [46]. Modal responses are combined based on the "square root of the sum of the squares" (SRSS) superposition method. Based on this analysis, the structure is redesigned to provide the required strength in each member.

Based upon the argument that static end moments do not alter the member plastic capacity after its first yield, the required girder moment capacity, M_y^G, can be determined as follows:

$$M_y^G = \text{maximum } \{M_{EQ}^G \text{ or } wL_G^2/8\} \tag{4-1}$$

where M_{EQ}^G is the average of the girder end moments computed by the modal analysis using IARS. The second criterion, $wL_G^2/8$, is to ensure against

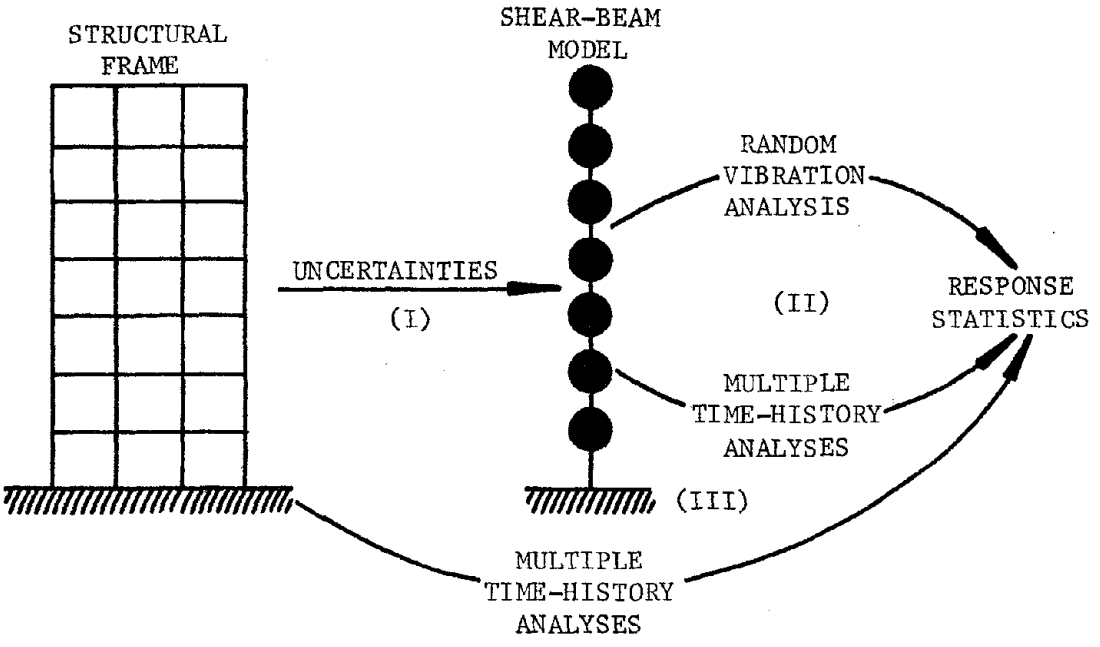

FIG. 4-1 COMPATIBILITY STUDIES INVOLVED IN THIS INVESTIGATION

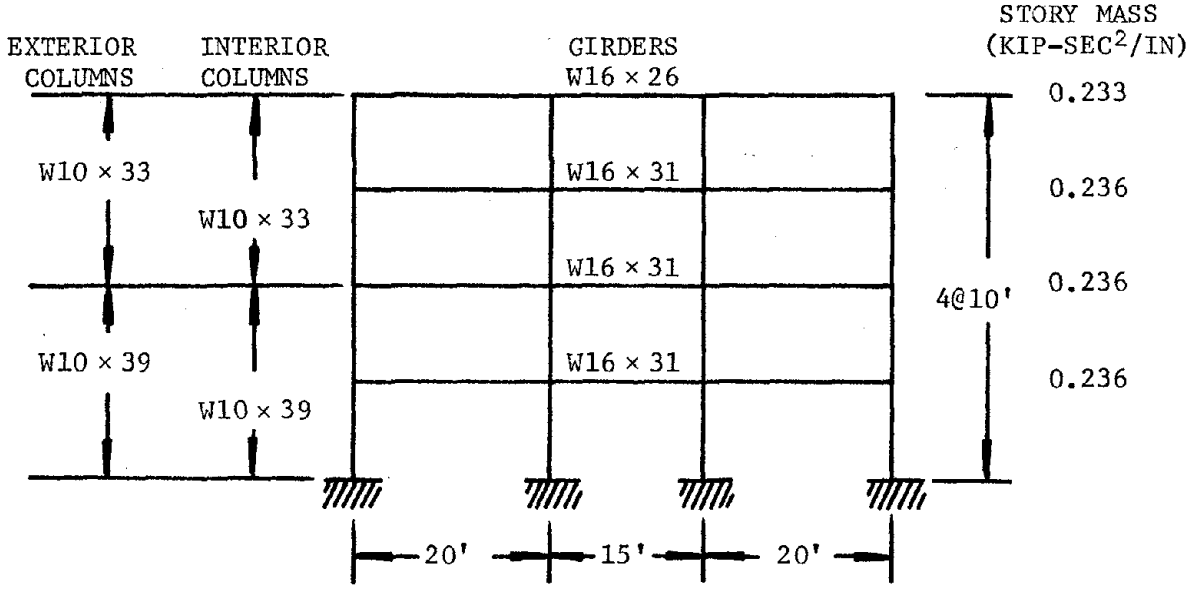

FIG. 4-2 4-STORY STEEL FRAME ELEVATION [PIQUE, 49]

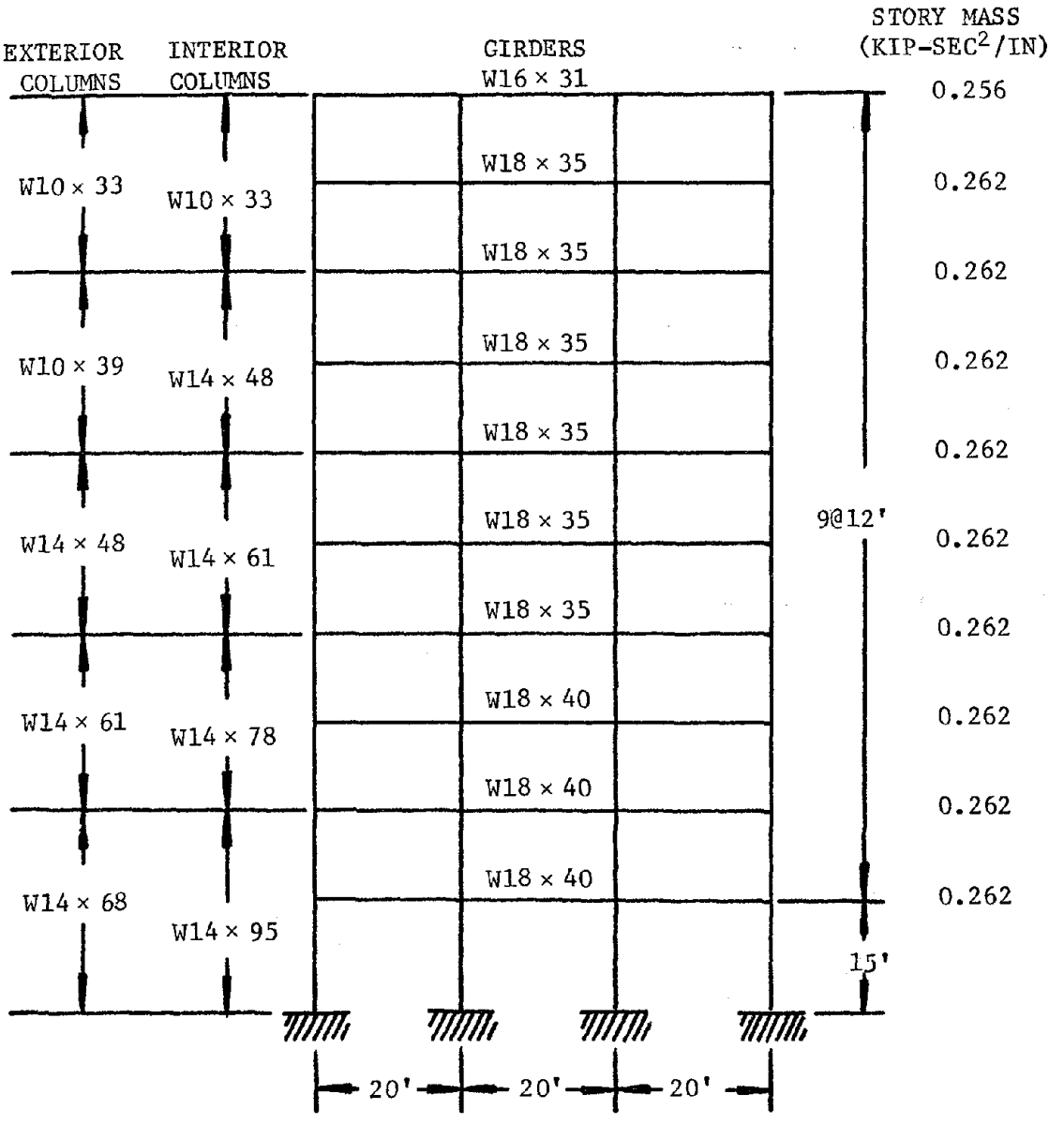

FIG. 4-3 10-STORY STEEL FRAME ELEVATION [PIQUE,49]

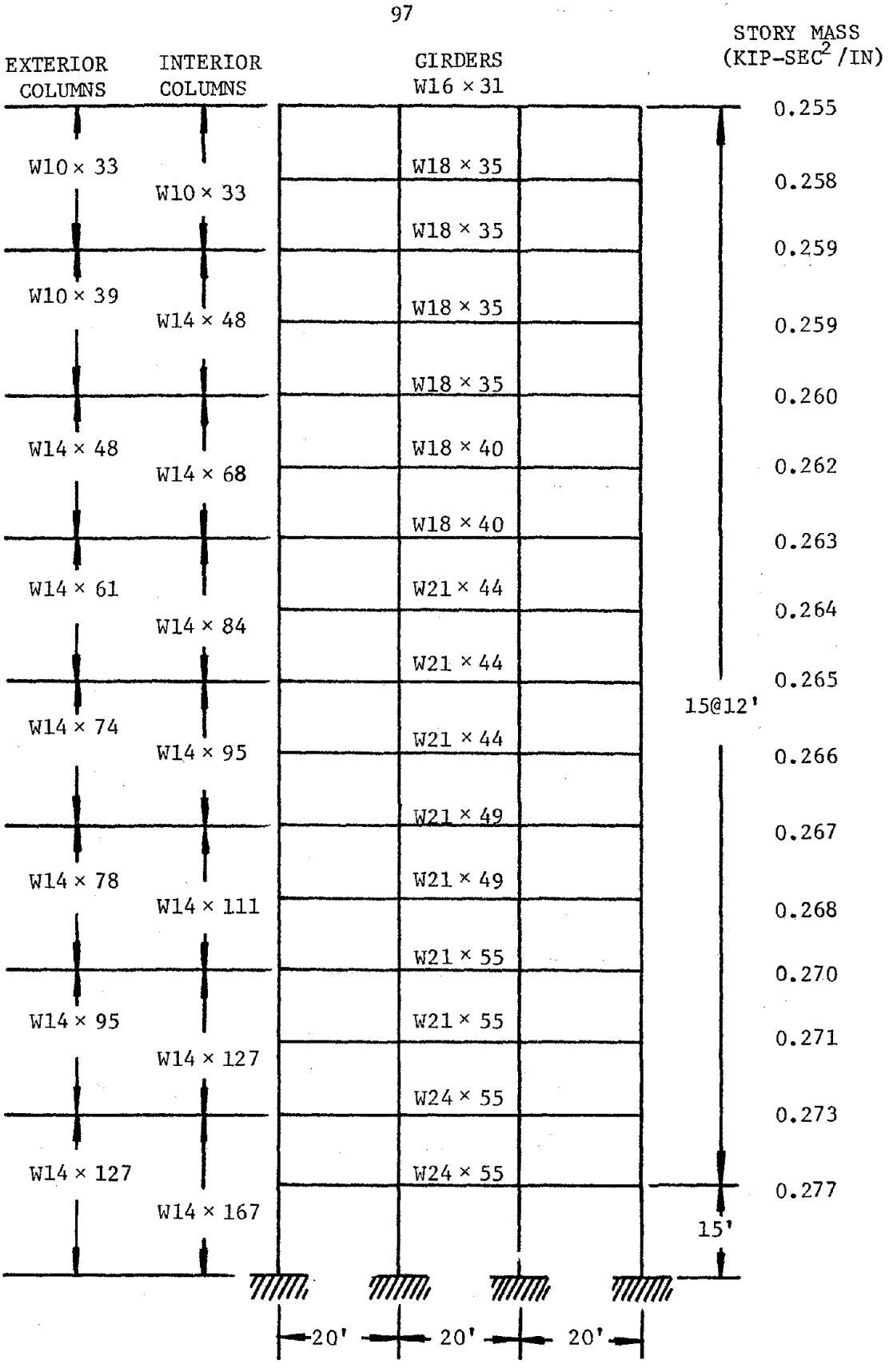

FIG. 4-4 16-STORY STEEL FRAME ELEVATION [PIQUE,49]

the undesirable formation of a plastic hinge at girder midspan due to the uniform gravity load, w. Notice that L_G is the girder span.

Column moment capacity is determined by the AISC axial-flexural interaction formula (Section 2.4-3, 1973):

$$\frac{P^C}{P^C_y} + \frac{M^C}{1.18\ M^C_y} \leq 1.0 \quad ; \quad M^C_y \geq M^C \tag{4-2}$$

where $P^C = P^C_{EQ} + P^C_{GR}$ = maximum axial force in the column due to earthquake and gravity loads. P^C_{EQ} is computed by the modal analysis using IARS. M^C is the column design moment defined as the maximum value of M^C_{EQ} or M^C_{GR}, where M^C_{EQ} and M^C_{GR} are the average of the two column end moments due to earthquake and gravity loads.

Assuming the ratio of the plastic modulus to the cross-sectional area is approximately equal to 6 for column sections of interest, the interaction formula becomes:

$$M^C_y \geq 6\ P^C + M^C/1.18 \quad ; \quad M^C_y \geq M^C \tag{4-3}$$

and

$$P^C_y = M^C_y/6 \tag{4-4}$$

Based on the preliminary member sizes, the three frames were redesigned by the above-mentioned inelastic design procedure using the IARS as proposed by Lai [39]. (Notice that the IARS proposed by Lai predicts a higher response than that of the commonly used Newmark and Hall spectra [46]. Moreover, the difference is more pronounced with increasing ductility ratio.)

Assuming a design ductility ratio of 4, a 5% damping and a peak ground

acceleration of 1/3 g, the required member strengths of the three steel moment-resisting frames were computed. The results are listed in Tables B-1, B-2 and B-3 of Appendix B. The three redesigned steel frames with new member strengths will be incorporated in the compatibility studies.

4.3 Description of Strong Ground Motions Used

For the purpose of compatibility studies, two sets of artificial strong ground motions with durations of 10 and 20 seconds have been generated by using the computer program SIMQKE [21]. Based on the Newmark-Hall elastic design response spectrum of 5% damping [46], the program first computes the corresponding power spectral density function. Then, by randomly generating a set of phase angles, ϕ_i, as expressed in Eq. 2-1, different synthetic strong ground motions can be obtained by sinusoidal superposition.

In this study, five different motions (with common peak ground acceleration equal to 1.0 g) have been generated for each of the two durations. In order to simulate the transient character of actual strong ground shaking, trapezoidal intensity envelope functions were employed [39]. The rise and decay times are both assumed to be equal one-tenth of the total duration.

Fig. 4-5 shows the PSD functions for the motions corresponding to S_o = 10 and 20 seconds. These two PSD functions provide the basic input for the random vibration computations. Two example time histories are shown in Fig. 4-6. These ten accelerograms will be used extensively for the compatibility studies. Notice that the same set of artificial motions was also used in the simulation study of SDOF systems presented in Sec. 3.3.2.

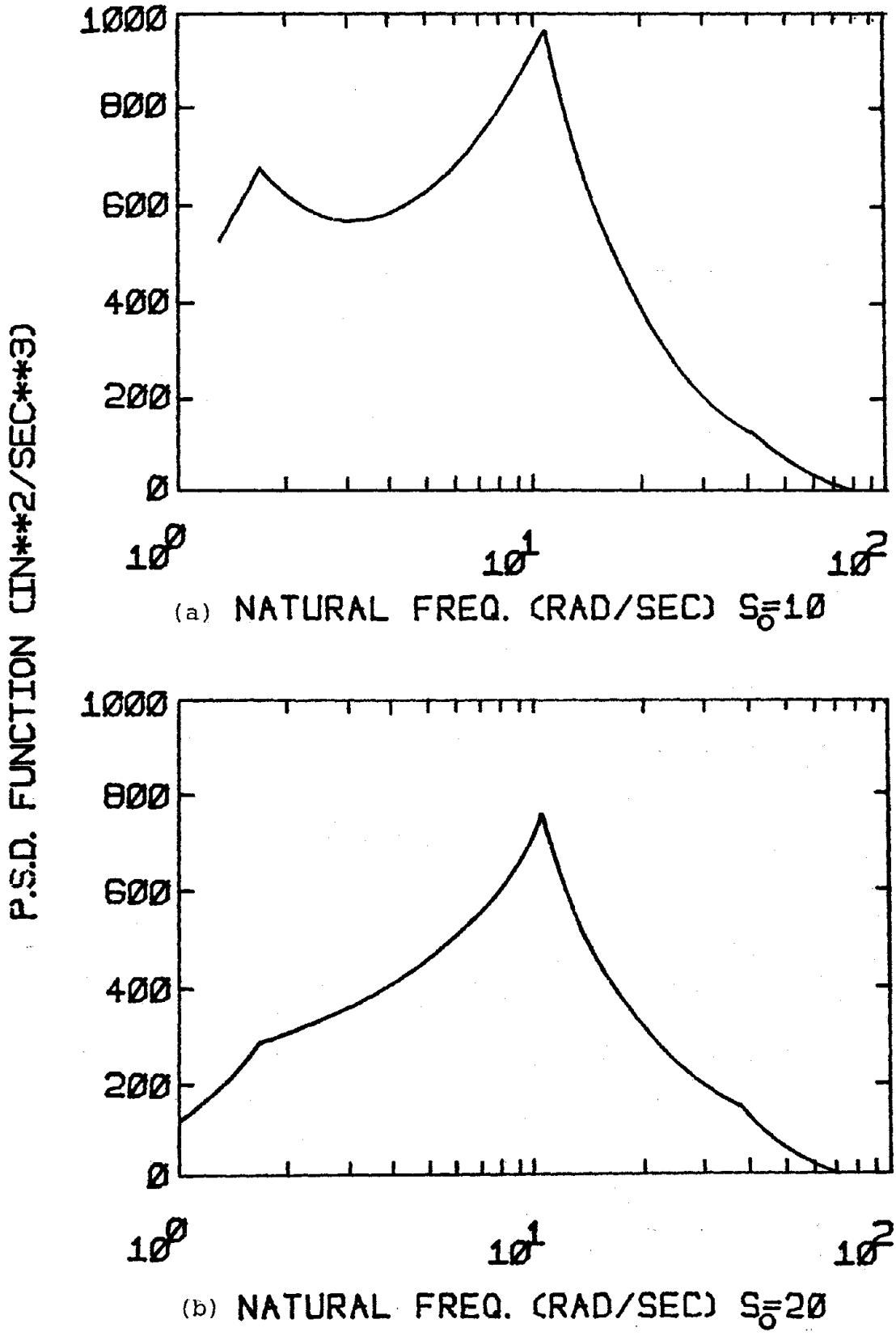

FIG. 4-5 POWER SPECTRAL DENSITY FUNCTIONS FOR DIFFERENT STRONG-MOTION DURATIONS

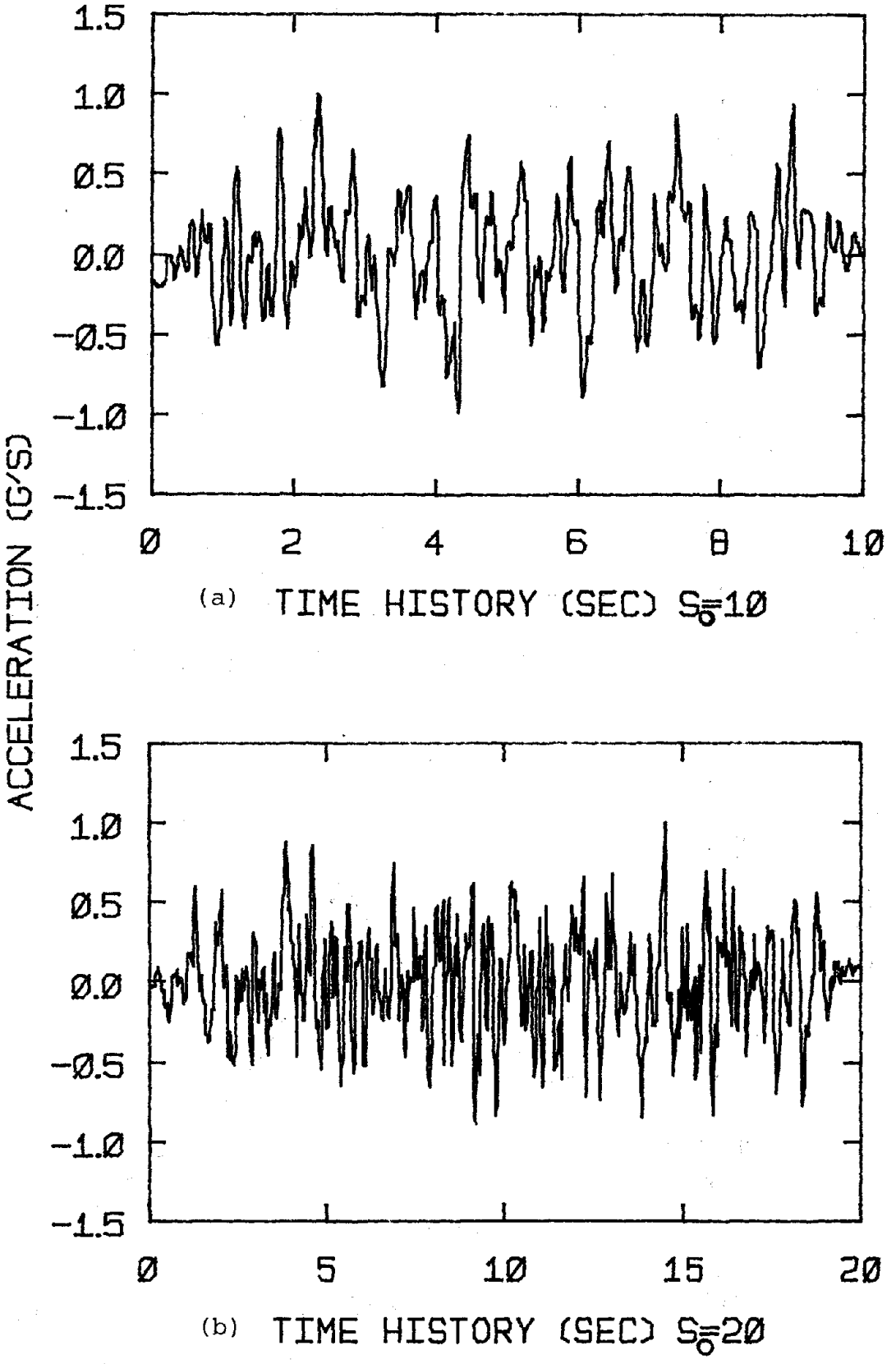

FIG. 4-6 EXAMPLE TIME HISTORIES FOR DIFFERENT STRONG-MOTION DURATIONS

4.4 Determination of Story Shear Spring Parameters

4.4.1 Estimation of Equivalent Story Stiffness

Assuming the steel frame behaves as an elasto-plastic multi-degree close-coupled shear-beam system, two key parameters are needed to characterize each of the story shear springs. They are the equivalent story lateral stiffness and the equivalent story yielding strength. A detailed discussion on the determination of story stiffness is presented below.

Based on the assumptions that: i) column shears above and below a joint are the same, ii) inflection points in columns above and below a joint are located symmetrically with respect to the joint, iii) rotations of all joints in one floor are the same, Biggs suggested the following expression for the lateral story stiffness, K_L, of a multi-story frame [2]:

$$K_L = \frac{24\,E}{L_C^2}\left(\frac{1}{\frac{2}{\sum K^C} + \frac{1}{\sum K_T^G} + \frac{1}{\sum K_B^G}}\right) \tag{4-5}$$

where $E = 29 \times 10^3$ ksi is the Young's modulus for steel, L_C is the story height, K^C is the column member stiffness. K_T^G and K_B^G are the girder member stiffnesses for the adjacent top and bottom floors, respectively.

Given the moments of inertia of all the columns and girders, the equivalent lateral story stiffnesses of the three steel moment-resisting frames can be computed based on Eq. 4-5. The resulting stiffnesses are plotted in Fig. 4-7.

Alternatively, by the "direct stiffness method", one can combine the element stiffnesses so as to generate the system global stiffness matrix. Two degrees-of-freedom per joint, i.e., the vertical displacement and the rotation, can first be condensed out statically. Assuming that all

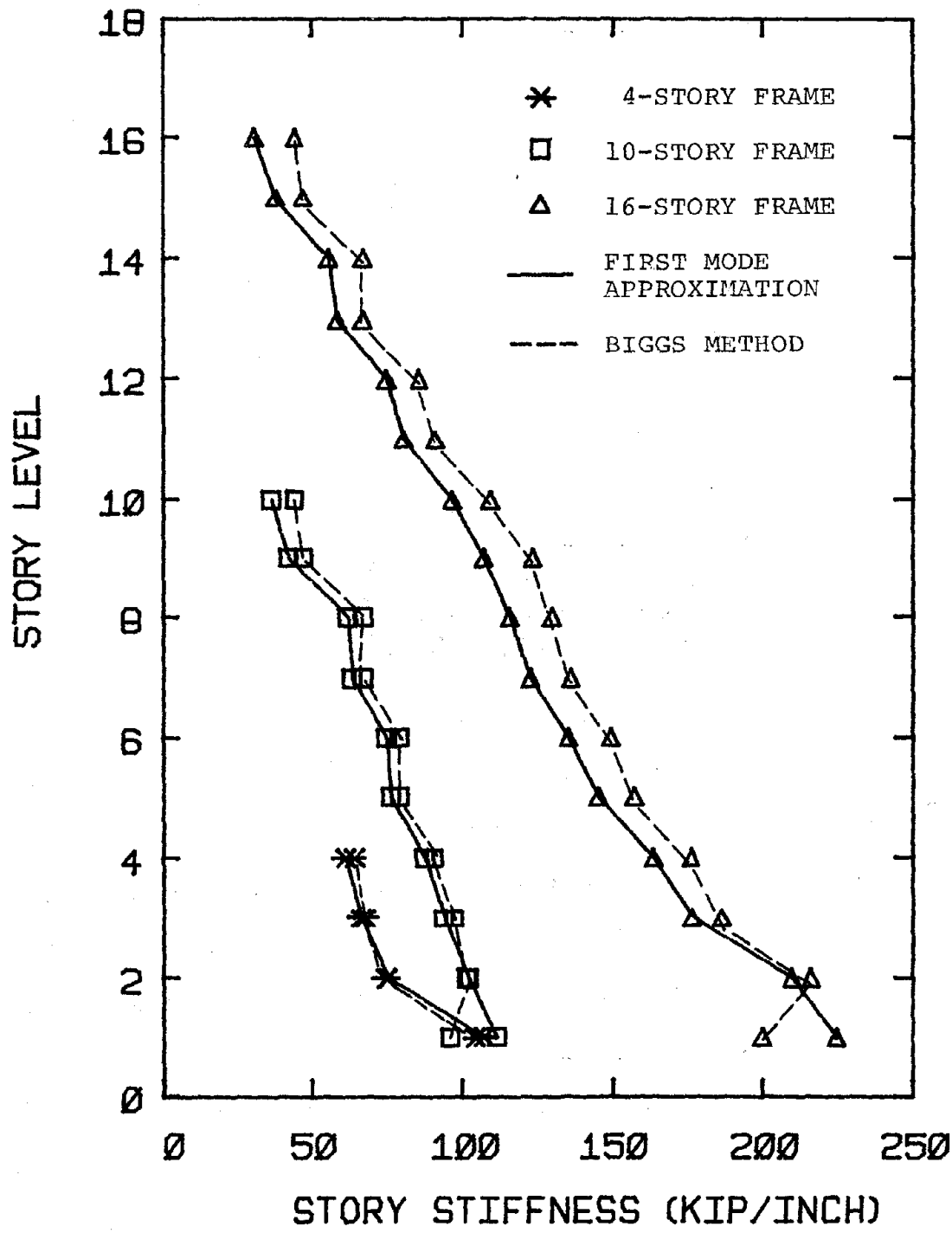

FIG. 4-7 EQUIVALENT STORY STIFFNESSES PREDICTED BY THE FIRST MODE APPROXIMATION METHOD AND THE BIGGS METHOD

joints for a given floor level displace laterally by the same amount, the "far-coupled" lateral stiffness matrix, $\underline{K}$, can be determined by the kinematic condensation. Notice that $\underline{K}$ is usually a fully occupied matrix. In order to obtain the "close-coupled" banded lateral stiffness matrix $\underline{K}_L$ of the shear-beam model, further assumptions are necessary.

Based on modal analysis, the equation of motion of the structural frame can be expressed as follows:

$$[\underline{K} - \omega_n^2 \underline{M}] \underline{\Phi}_n = \underline{0} \tag{4-6}$$

where $\underline{M}$ is the diagonal story mass matrix, ω_n is the natural frequency of the nth mode, and $\underline{\Phi}_n$ is the nth modal shape vector. Assuming that the characteristics of the first mode of the close-coupled shear-beam system are the same as those of the structural frame, Eq. 4-6 becomes:

$$[\underline{K} - \omega_1^2 \underline{M}] \underline{\Phi}_1 = \underline{0} = [\underline{K}_L - \omega_1^2 \underline{M}] \underline{\Phi}_1 \tag{4-7}$$

where $\underline{K}_L$ is the close-coupled lateral stiffness matrix of the shear-beam model.

As an example, consider a 4-story shear-springs system:

$$\underline{K}_L \ \underline{\Phi}_1 = \begin{bmatrix} K_1 + K_2 & -K_2 & 0 & 0 \\ -K_2 & K_2 + K_3 & -K_3 & 0 \\ 0 & -K_3 & K_3 + K_4 & -K_4 \\ 0 & 0 & -K_4 & K_4 \end{bmatrix} \begin{bmatrix} \phi_{11} \\ \phi_{12} \\ \phi_{13} \\ \phi_{14} \end{bmatrix}$$

$$= \begin{bmatrix} \phi_{11} & \phi_{11} - \phi_{12} & 0 & 0 \\ 0 & -\phi_{11} + \phi_{12} & \phi_{12} - \phi_{13} & 0 \\ 0 & 0 & -\phi_{12} + \phi_{13} & \phi_{13} - \phi_{14} \\ 0 & 0 & 0 & -\phi_{13} + \phi_{14} \end{bmatrix} \begin{bmatrix} K_1 \\ K_2 \\ K_3 \\ K_4 \end{bmatrix}$$

$$= \omega_1^2 \underline{M} \underline{\Phi}_1 = \omega_1^2 \begin{bmatrix} m_1 \phi_{11} \\ m_2 \phi_{12} \\ m_3 \phi_{13} \\ m_4 \phi_{14} \end{bmatrix} \tag{4-8}$$

By solving this system of linear equations, the close-coupled equivalent lateral story stiffnesses K_1, K_2, K_3 and K_4 can be conveniently determined. In the above formulation, m_i represents the ith story mass, whereas ϕ_{1i} is the first modal shape.

Based on the above-mentioned "First Mode Approximation" (FMA) method, the equivalent lateral stiffnesses for the three steel moment-resisting frames can be computed. The results are also presented in Fig. 4-7. Note that, except for the first story, the equivalent story stiffnesses computed by this method are generally smaller than those obtained by the Biggs approach.

Using different sets of incremental lateral loads, Piąue [49] statically computed the equivalent story stiffnesses for the three UBC-based steel frames. Except for the differences in member strengths, the member characteristics of those frames are the same as those of the three steel frames used in this study. Hence, their initial lateral stiffnesses should be the same. This is confirmed by our study: the equivalent story stiffnesses computed by the FMA method are indeed the same as those reported by Piąue. This further suggests that the First Mode Approximation method will lead to satisfactory estimates for the equivalent story stiffnesses. Moreover, except for the first story, the Biggs approach will result in slightly conservative prediction of the story stiffness.

The resulting equivalent lateral story stiffnesses for the three steel

moment-resisting frames, i.e., 4-, 10- and 16-story, are listed in Tables B-4, B-5 and B-6, respectively (see Appendix B).

4.4.2 Estimation of Equivalent Story Yielding Strength

Based on the assumption of a story yielding mechanism (i.e., plastic hinges developed in the two ends of all the columns and girders), Anagnostopoulos suggested an upper bound for the equivalent story yielding strength F_y [2]:

$$F_y = \text{minimum} \left\{ \frac{2\sum M_y^C}{L_C} , \frac{2\sum M_y^G}{L_C} \right\} \qquad (4\text{-}9)$$

where ΣM_y^C and ΣM_y^G are the sums of all the column and girder plastic moment capacities in one floor, respectively. L_C is the story height. Owing to its simplicity, Eq. 4-9 is used in this study to provide rough estimates of the equivalent story yielding strengths of the three steel moment-resisting frames.

For an elasto-plastic shear spring, the story yielding strength is equal to the maximum story shear force when yielding occurs. Therefore, the equivalent story yielding strength can be alternatively determined by the nonlinear time-history analysis of the actual frame. In this study, five different artificial ground motions were used to compute the maximum story shears for the three steel frames. The average of the maximum shears has been calculated for each story. The corresponding coefficients of variation are only about 3%. A detailed discussion of the time-history analysis of the frames is presented in Section 4.6.

In order to compare the above-mentioned results with those obtained earlier (by means of Eq. 4-9), the "yielding strength factor", R_y, is introduced. R_y is defined as the ratio of the mean maximum story shear di-

vided by the value F_y obtained from Eq. 4-9. The values of the factor R_y for the three steel moment-resisting frames have been computed and are shown in Fig. 4-8. Notice that the factor generally decreases with increasing story level, and that it exceeds one except for the upper stories. The yielding strength factors for the three UBC steel frames designed by Piúque [49] have also been computed and are plotted in Fig. 4-9. The results display the same trend as those obtained previously for the steel frames designed based on IARS. Therefore, it may be concluded that Eq. 4-9 will generally underpredict the equivalent story yielding strength.

Eq. 4-9 is derived based on the assumption that the column stiffnesses will be approximately equal to the girder stiffnesses for a particular story. But for actual structural frames, the column stiffnesses of the upper stories are usually small compared with the girder stiffnesses. Due to earthquake and wind load requirements, the column stiffnesses of bottom stories are much greater than those of the girders. Therefore, the effect of actual stiffness distribution on the yielding strength factor needs to be investigated.

An important quantity in the investigation is the column/girder stiffness ratio, where the column stiffness is $\Sigma\ I_C/L_C$; the girder stiffness is $\Sigma\ I_G/L_G$. I_C and I_G are the moments of inertia for column and girder, respectively, whereas L_C and L_G are the column height and the girder span, respectively. The column/girder stiffness ratios have been computed for the three steel frames. Fig. 4-10 shows the relationship between the column/girder stiffness ratio versus the yielding strength factor. The story levels are also indicated in the figure.

As depicted in Fig. 4-10, the column/girder stiffness ratio increases

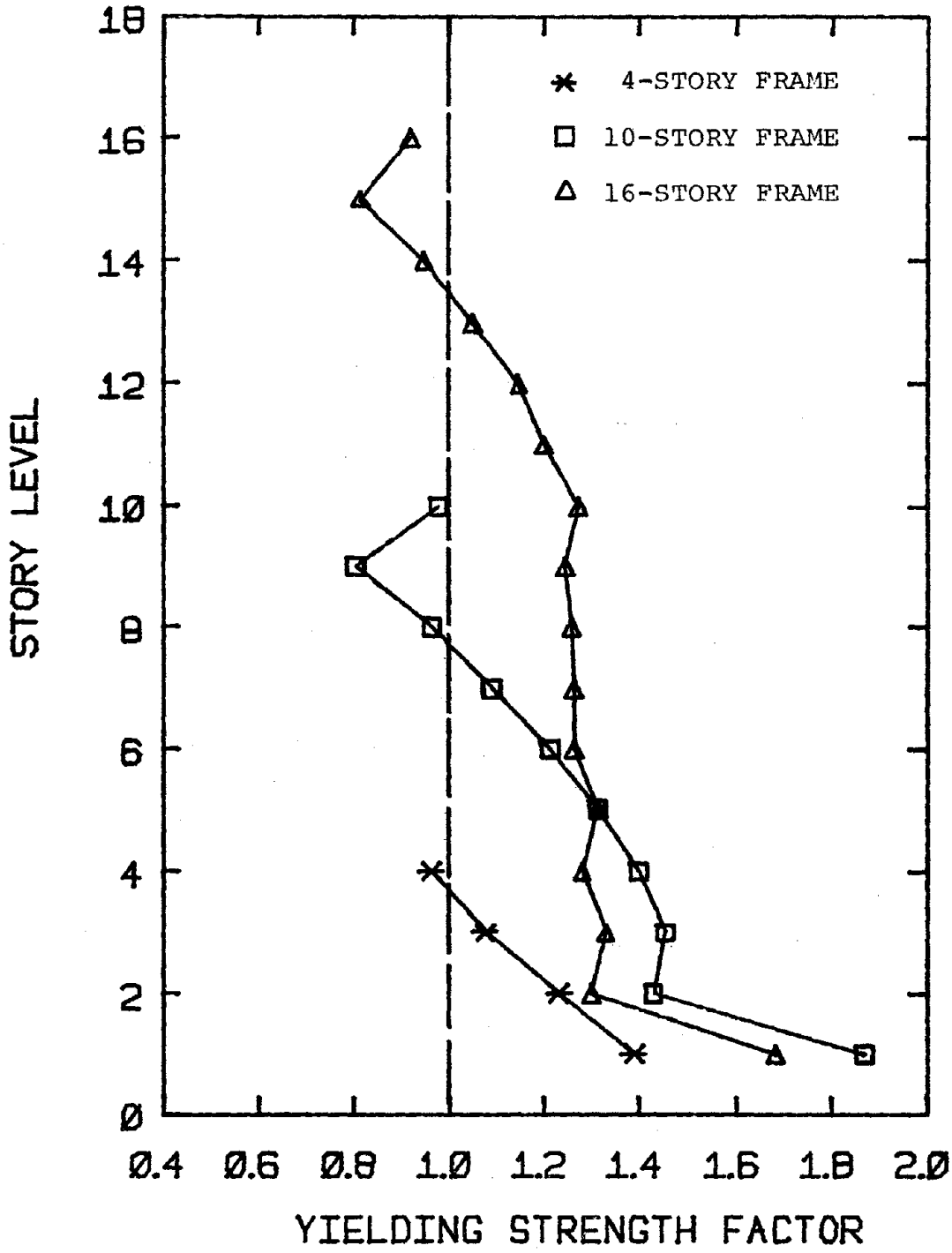

FIG. 4-8 YIELDING STRENGTH FACTORS FOR THREE STEEL MOMENT-RESISTING FRAMES

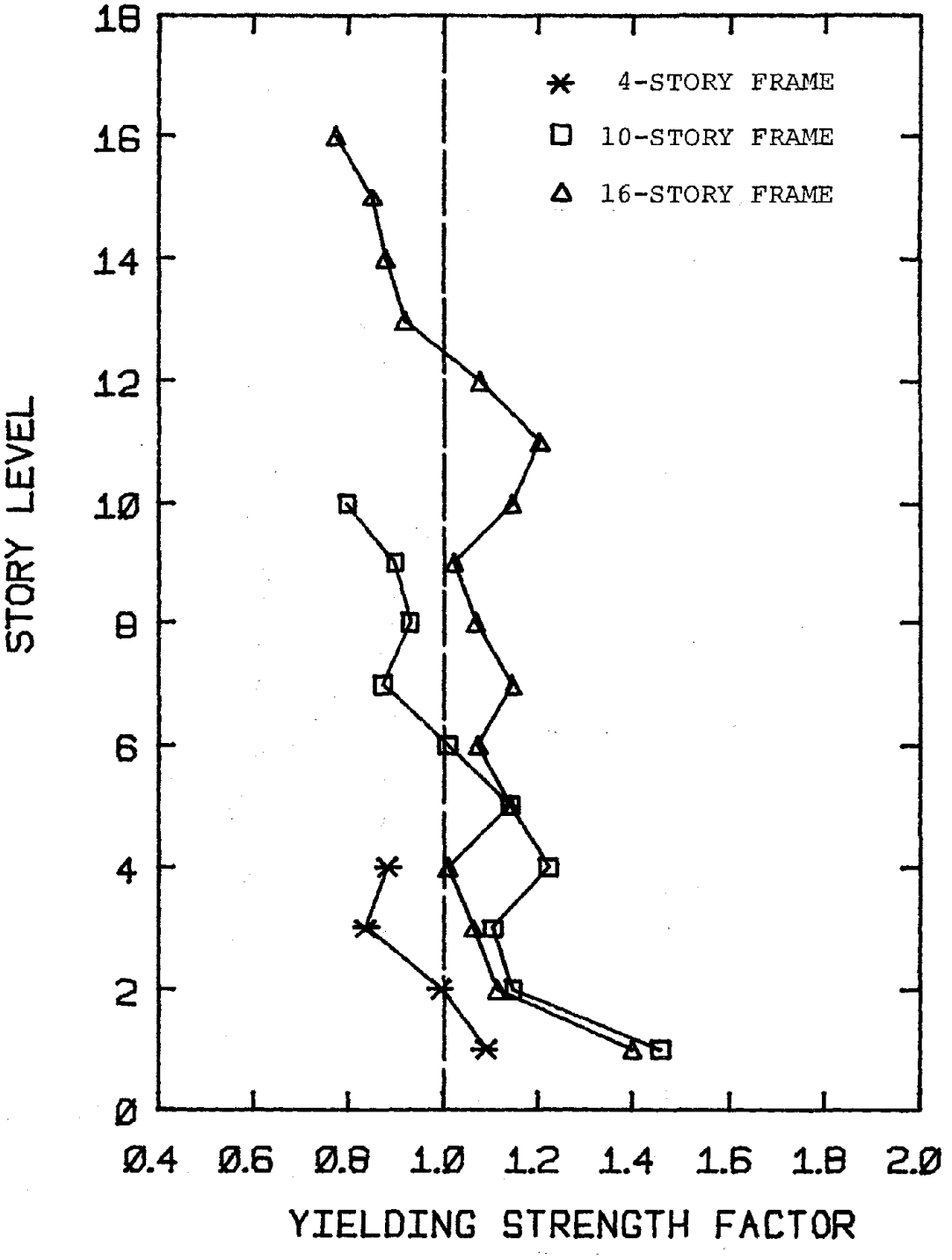

FIG. 4-9 YIELDING STRENGTH FACTORS FOR THE THREE UBC STEEL MOMENT-RESISTING FRAMES DESIGNED BY PIQUE

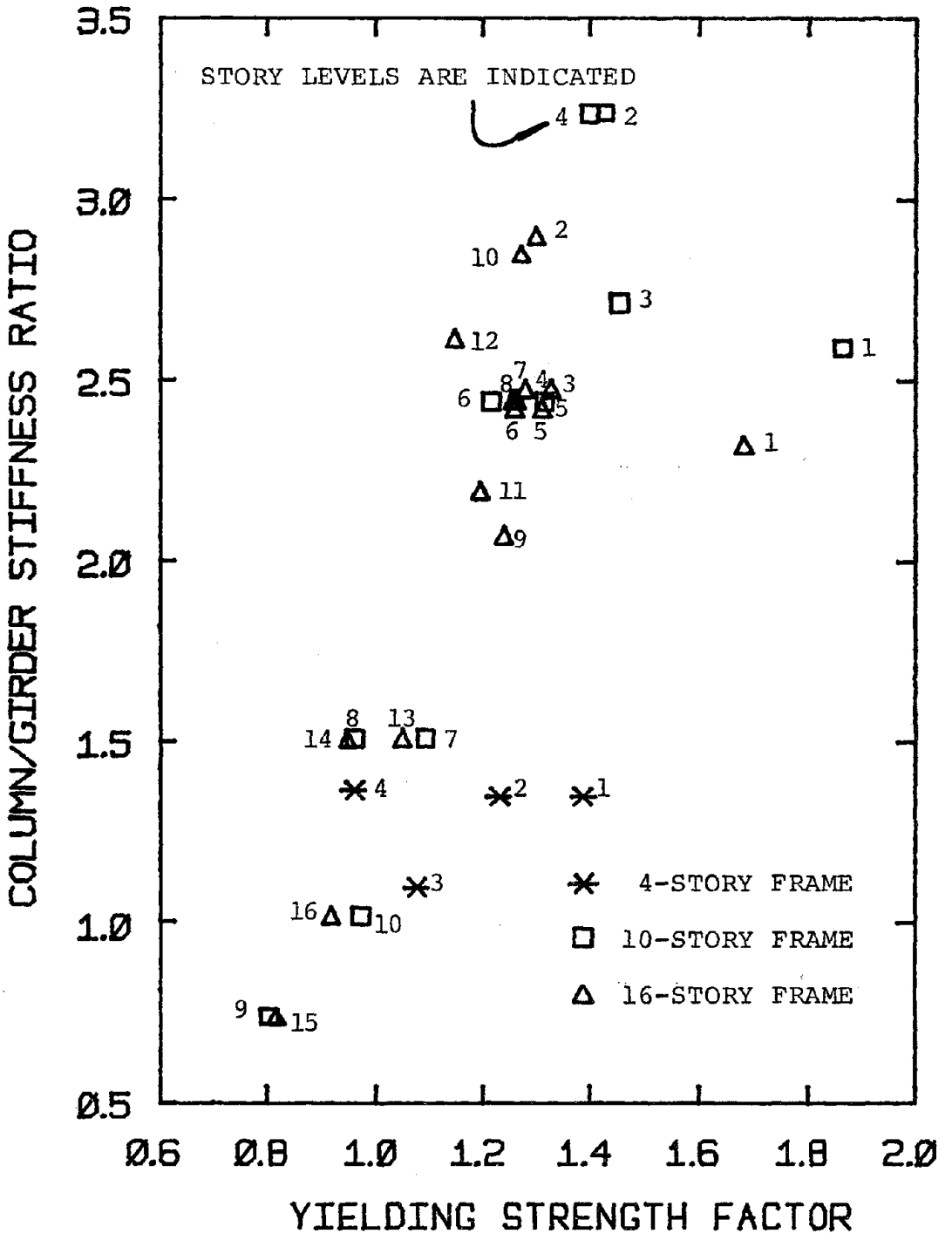

FIG. 4-10 SCATTERGRAM OF COLUMN/GIRDER STIFFNESS RATIO VERSUS YIELDING STRENGTH FACTOR FOR THE THREE STEEL MOMENT-RESISTING FRAMES

approximately linearly with the yielding strength factor. This suggests that the yielding strength factor is dependent on the actual stiffness distribution between columns and girders within one particular story. Moreover, it is reasonable to use the yielding strength factor so as to correct the equivalent story yielding strength predicted by Eq. 4-9.

For the purpose of evaluating seismic safety of buildings, the variability of the equivalent story yielding strength should be investigated. The statistics of the yielding strength factor have been computed based on the results of the three UBC frames and three IARS frames. The mean value of the yielding strength factor is 1.128, the standard deviation is 0.219, and the coefficient of variation is 0.194. The data fit approximately a Lognormal probability density function:

$$f_{R_y}(R_y) = \frac{1}{0.482\ R_y} \exp\{-13.534\ [\ell n\ R_y - 0.102]^2\} \qquad (4\text{-}10)$$

The histogram and the fitted PDF of the yielding strength factor are presented in Fig. 4-11.

The equivalent story yielding strengths of the three steel moment-resisting frames are listed in Tables B-4, B-5 and B-6 of Appendix B. The story yielding strengths of the three UBC frames designed by Piqúe are also listed in the same tables.

4.5 Validity of MDOF Inelastic Random Vibration Response Prediction for Shear-Beam Systems

4.5.1 Time-History Analyses for Shear-Beam Systems

The uncertainties of determining the equivalent lateral story stiffness and yielding strength have been investigated in the preceding sections. The story shear-spring parameters for the three steel moment-re-

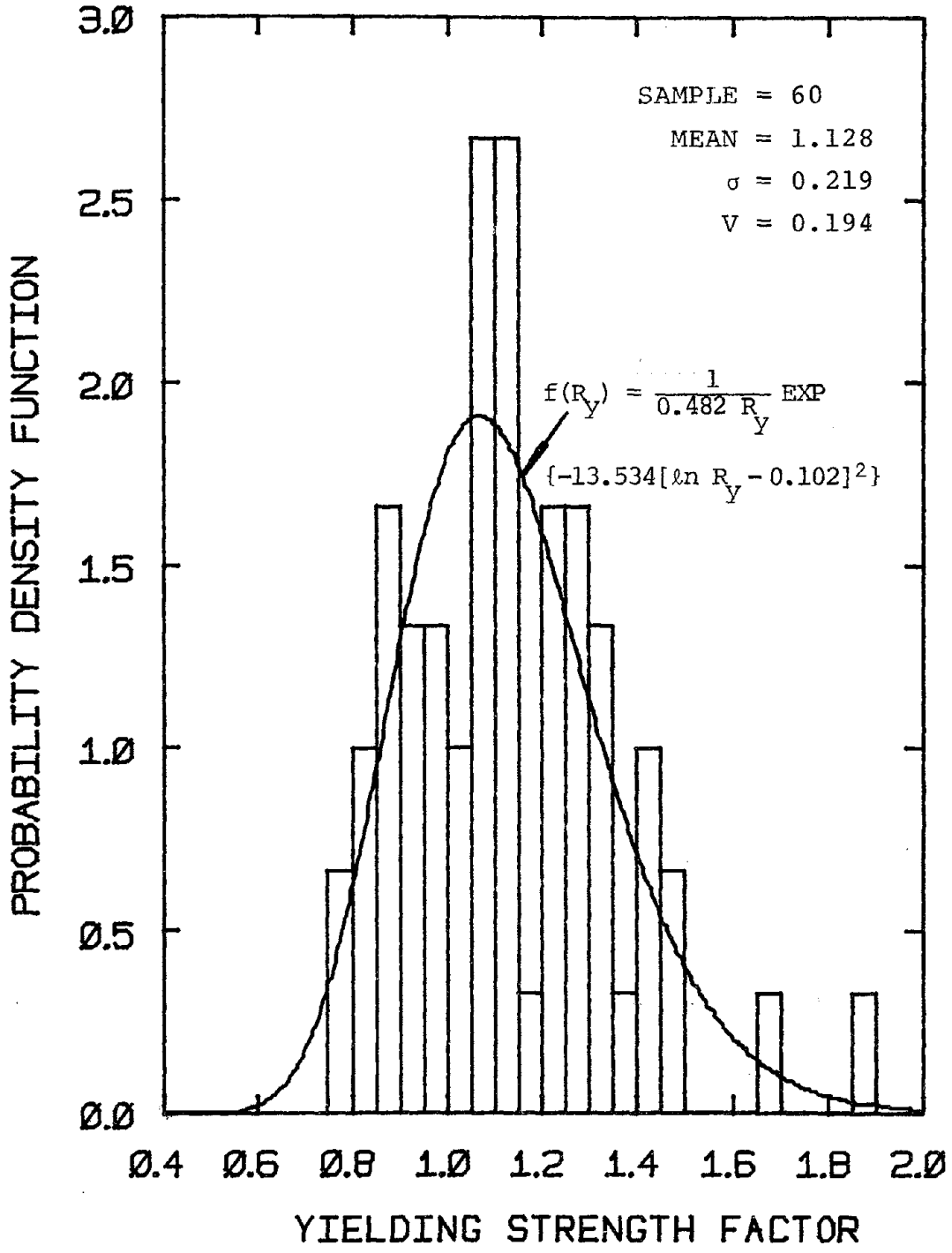

FIG. 4-11 HISTOGRAM OF YIELDING STRENGTH FACTOR

sisting frames have been determined. Using these parameters, the probabilistic inelastic story response can be predicted by the modified multi-degree E-P random vibration methodology when the ground motion spectral density function and duration are specified. The results will be compared with predictions based on time-history analyses of an ensemble of compatible artificial ground motions. Based on these compatibility studies, the validity of the random vibration solution strategy for shear-beam systems can be assessed.

The program STAVROS [2] was used to compute the inelastic time-history responses of the three (4-, 10- and 16-story) equivalent shear-beam systems. 5% damping was assumed for all systems. Since the gravity loads cannot readily be included in a shear-beam model, they have been neglected herein. A detailed discussion of the effects of gravity loads on the inelastic response is presented in Section 4.7.

Five artificial strong ground motions (described in Section 4.3) with duration equal to 10 seconds were used for the time-history analyses of the 4-story system. Five different motions with duration equal to 20 seconds were used for the analyses of the 10-story and 16-story systems. Three different levels of peak ground acceleration, i.e., 1/3 g, 2/3 g and 1.0 g were considered for the 4-story system. Two acceleration levels of 1/3 g and 2/3 g were used for the 10-story system. For the 16-story shear-beam system, based on cost considerations, calculations were made only for the 1/3 g level of peak ground acceleration. Therefore, all together, thirty time-history analyses were performed as part of the compatibility studies.

The elastic dynamic modal characteristics are determined at the start

of the time-history analysis. The first four modal shapes of the three equivalent shear-beam systems, i.e., 4-, 10 and 16- story, are listed in Tables B-7, B-8 and B-9, respectively, in Appendix B. The modal shapes are nomalized with respect to the story masses.

For each level of ground motion intensity, the mean and the standard deviation of the maximum story distortion are computed for each shear-beam system subjected to five different ground motions. The variation with height of the mean and the mean plus (or minus) one standard deviation of the maximum mean story distortions are plotted in Figures 4-12 to 4-17, for the different systems and the different ground motion intensities.

Obviously, the maximum story distortion increases with increasing ground motion intensity. Notice that the effect is more pronounced for the bottom stories. Moreover, there is a tendency for the predicted story distortions to vary in two-story intervals. This may be explained by the fact that the column sections were kept the same for two consecutive stories so as to minimize member size variations. This suggests that the higher of the two stories is relatively stronger than the lower one. Hence, the distortion of the higher story tends to be smaller than that of the lower story of each two-story interval.

4.5.2 Random Vibration Predictions for Shear-Beam Systems

As described in Section 4.3, two PSD functions compatible with the artificial ground motions were employed for the random vibration analyses. The PSD function with duration equal to 10 seconds was used for the 4-story shear-beam system, whereas that corresponding to S_o = 20 seconds was incorporated into the analysis of the 10- and 16-story shear beam systems.

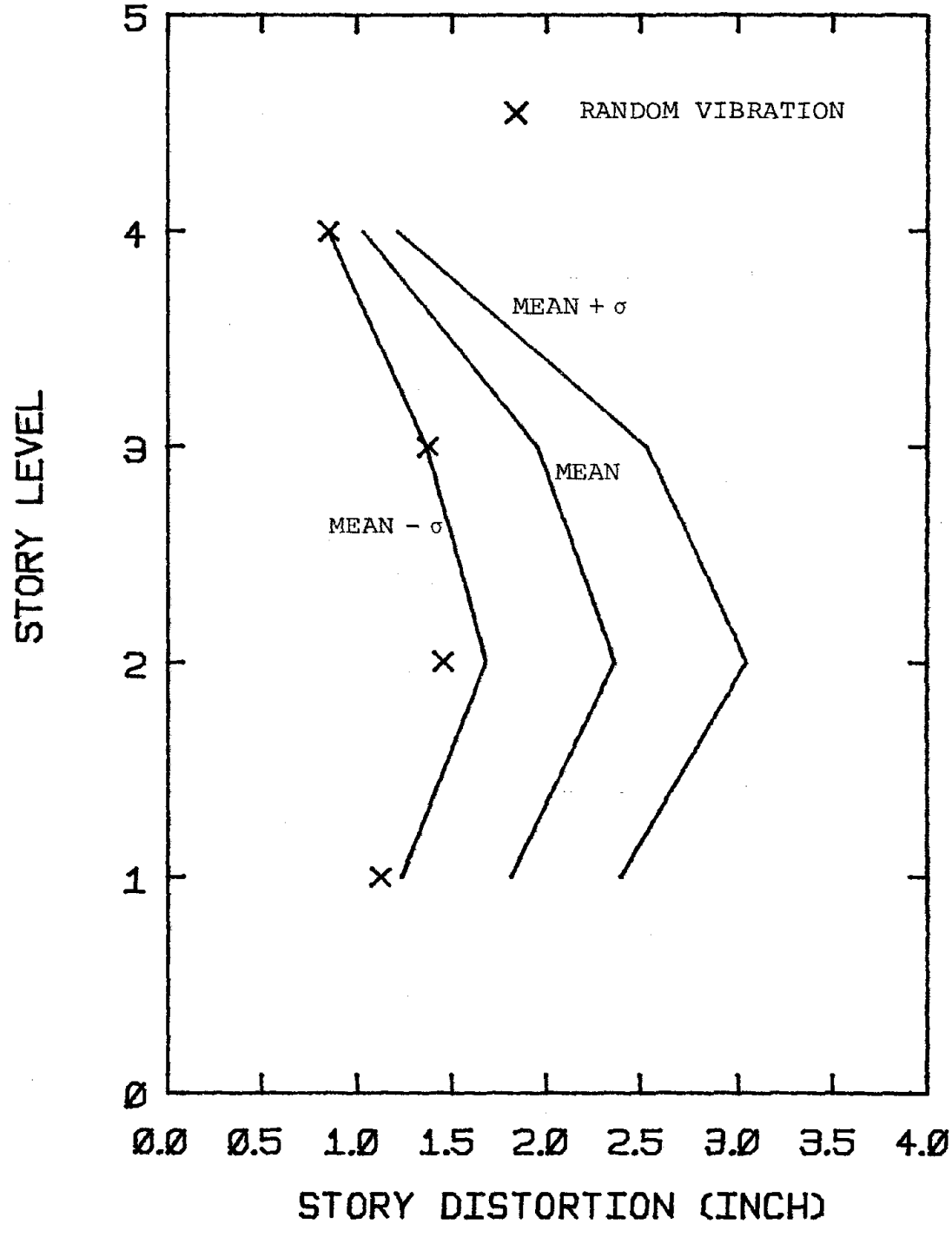

FIG. 4-12 STORY DISTORTIONS PREDICTED BY TIME-HISTORY AND RANDOM VIBRATION ANALYSIS (4-STORY FRAME, a_{max} = 1/3 g)

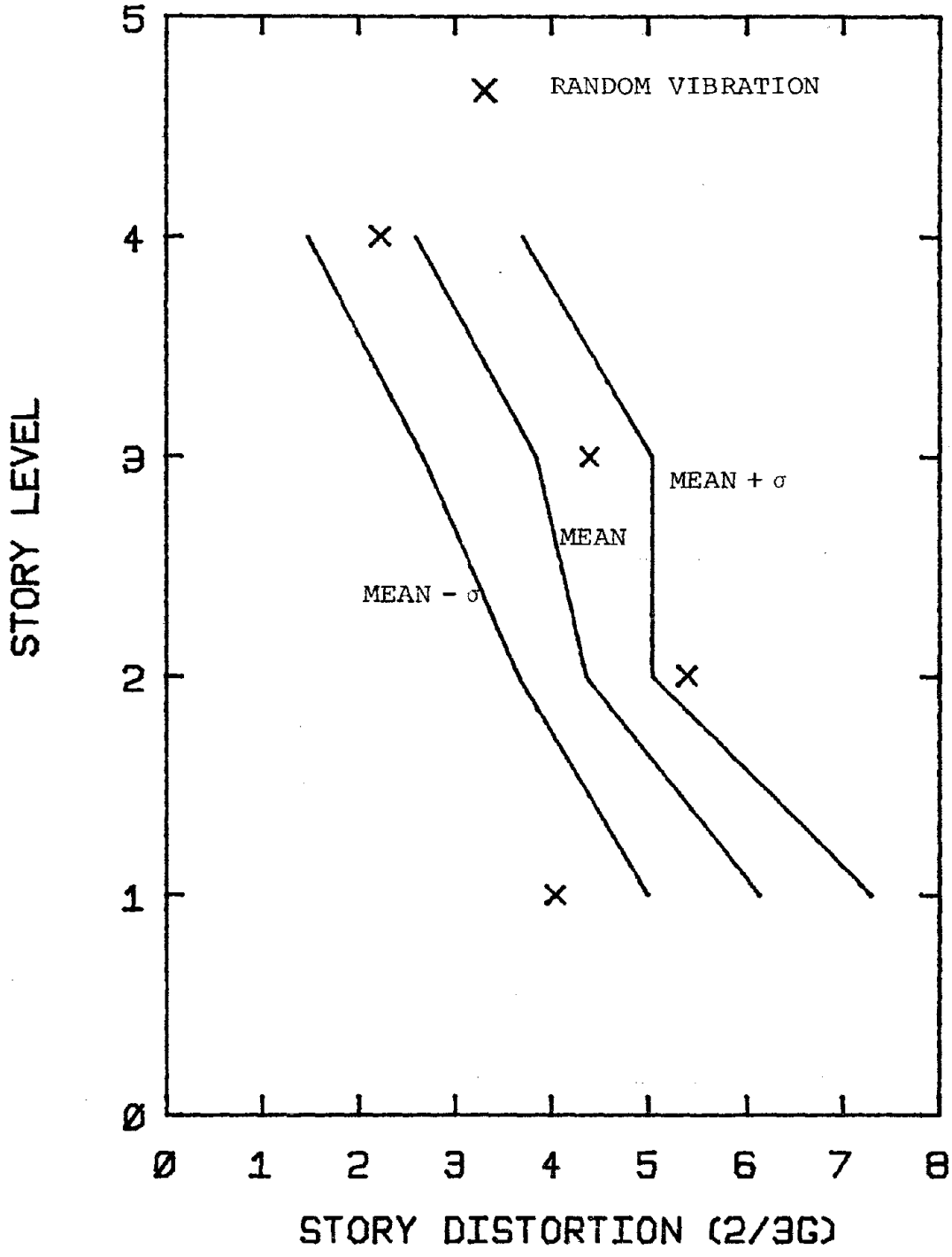

FIG. 4-13 STORY DISTORTIONS PREDICTED BY TIME-HISTORY AND RANDOM VIBRATION ANALYSIS (4-STORY FRAME, a_{max} = 2/3 g)

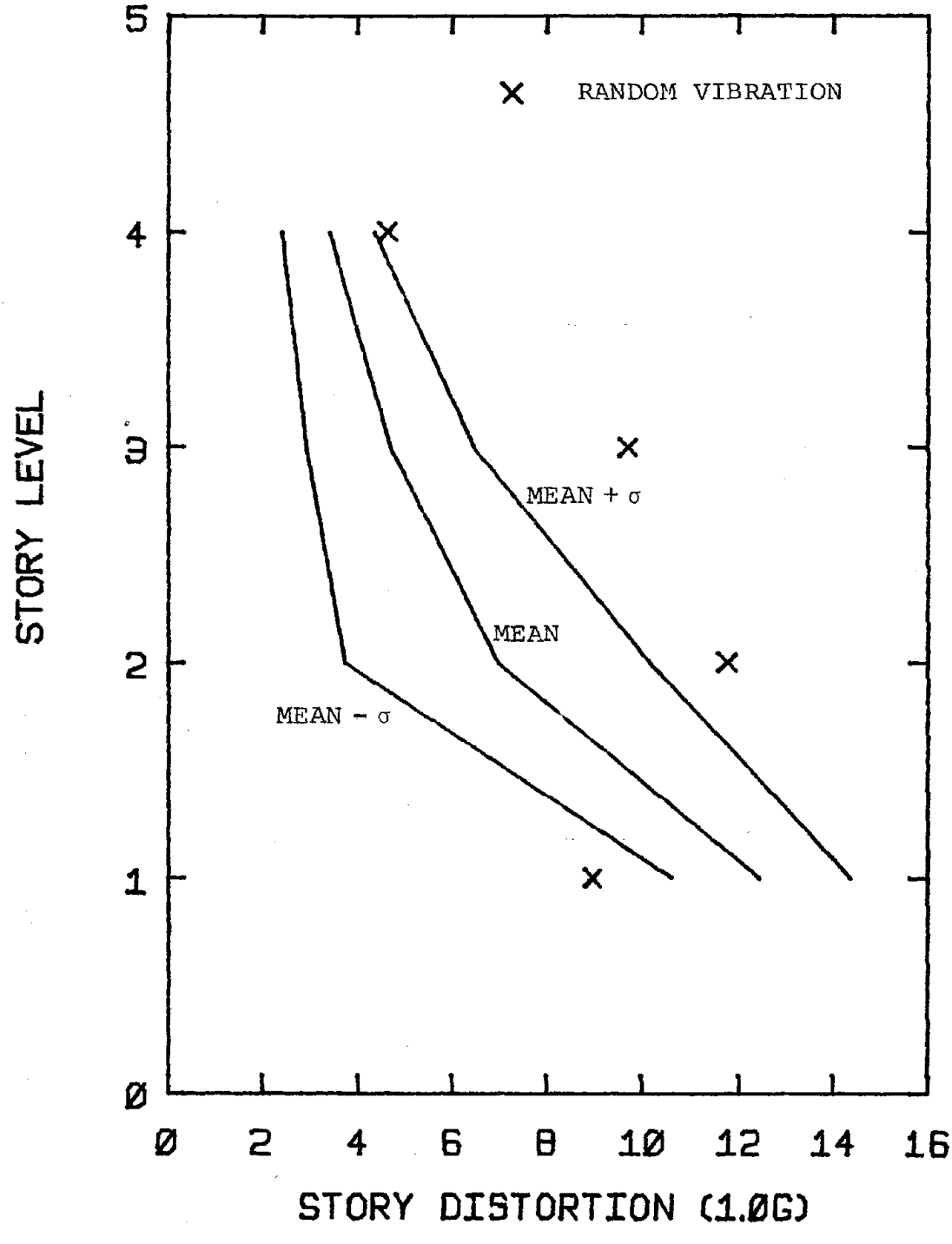

FIG. 4-14 STORY DISTORTIONS PREDICTED BY TIME-HISTORY AND RANDOM VIBRATION ANALYSIS (4-STORY FRAME, a_{max} = 1.0 g)

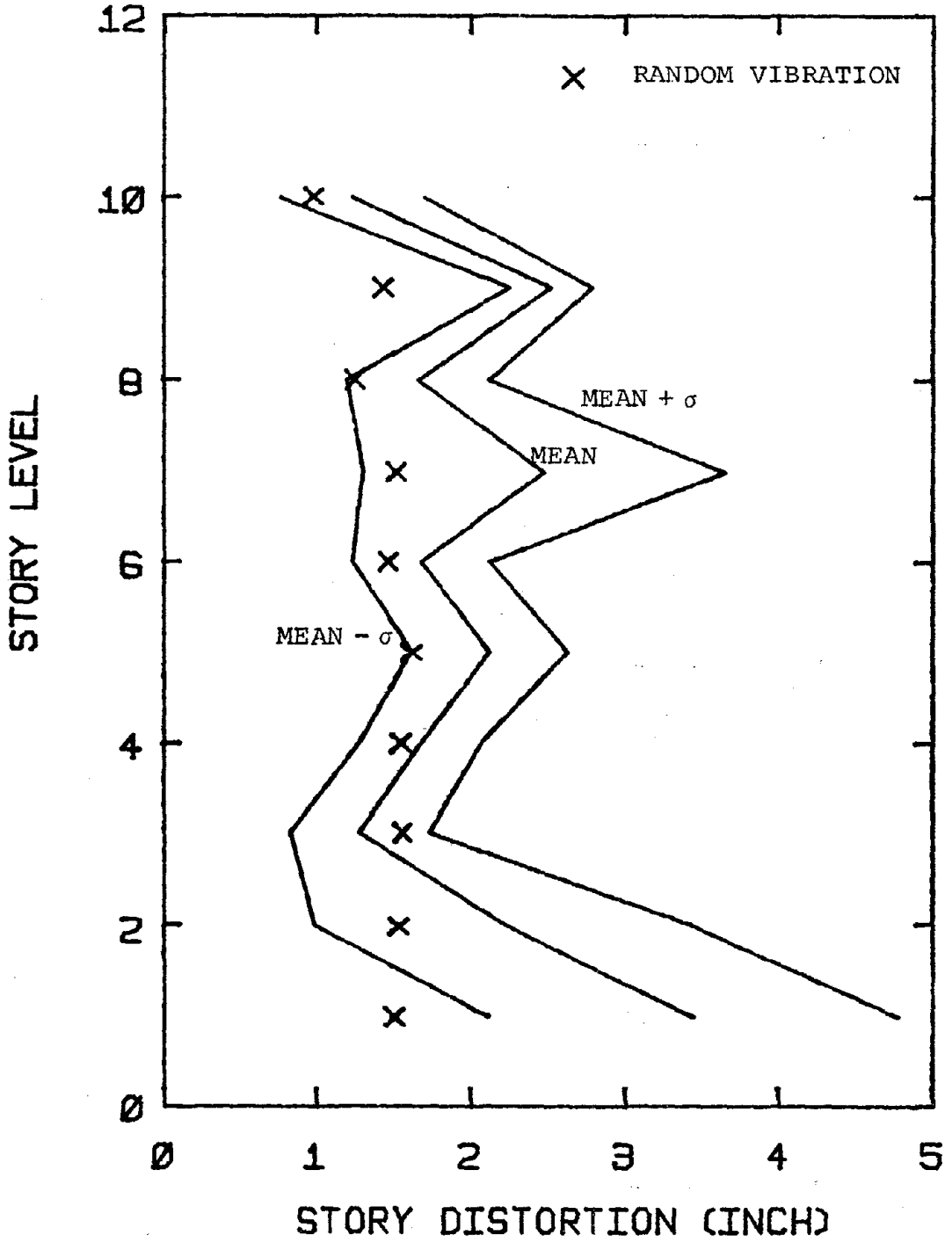

FIG. 4-15 STORY DISTORTIONS PREIDCTED BY TIME-HISTORY AND RANDOM VIBRATION ANALYSIS (10-STORY FRAME, a_{max} = 1/3 g)

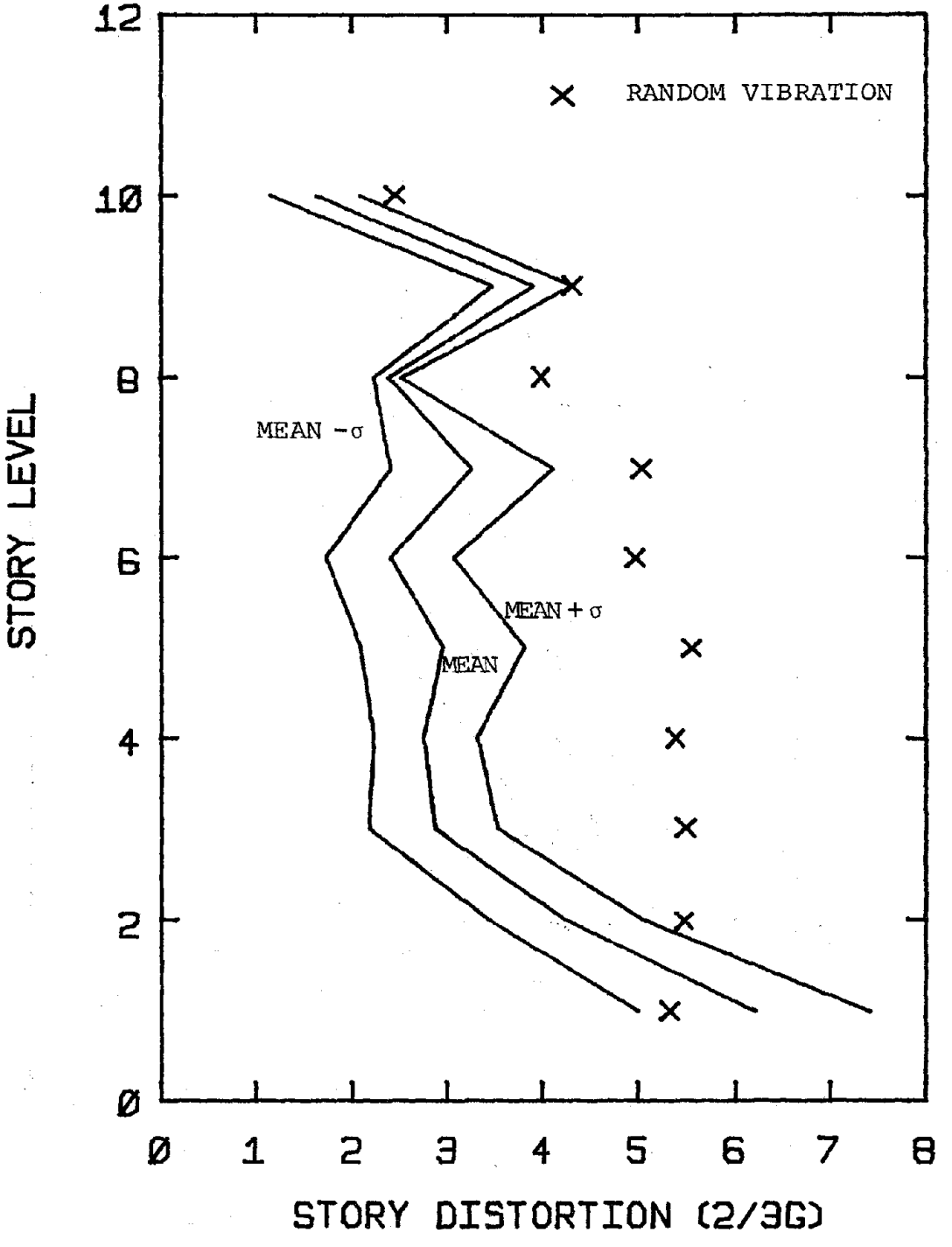

FIG. 4-16 STORY DISTORTIONS PREDICTED BY TIME-HISTORY AND RANDOM VIBRATION ANALYSIS (10-STORY FRAME, a_{max} = 2/3 g)

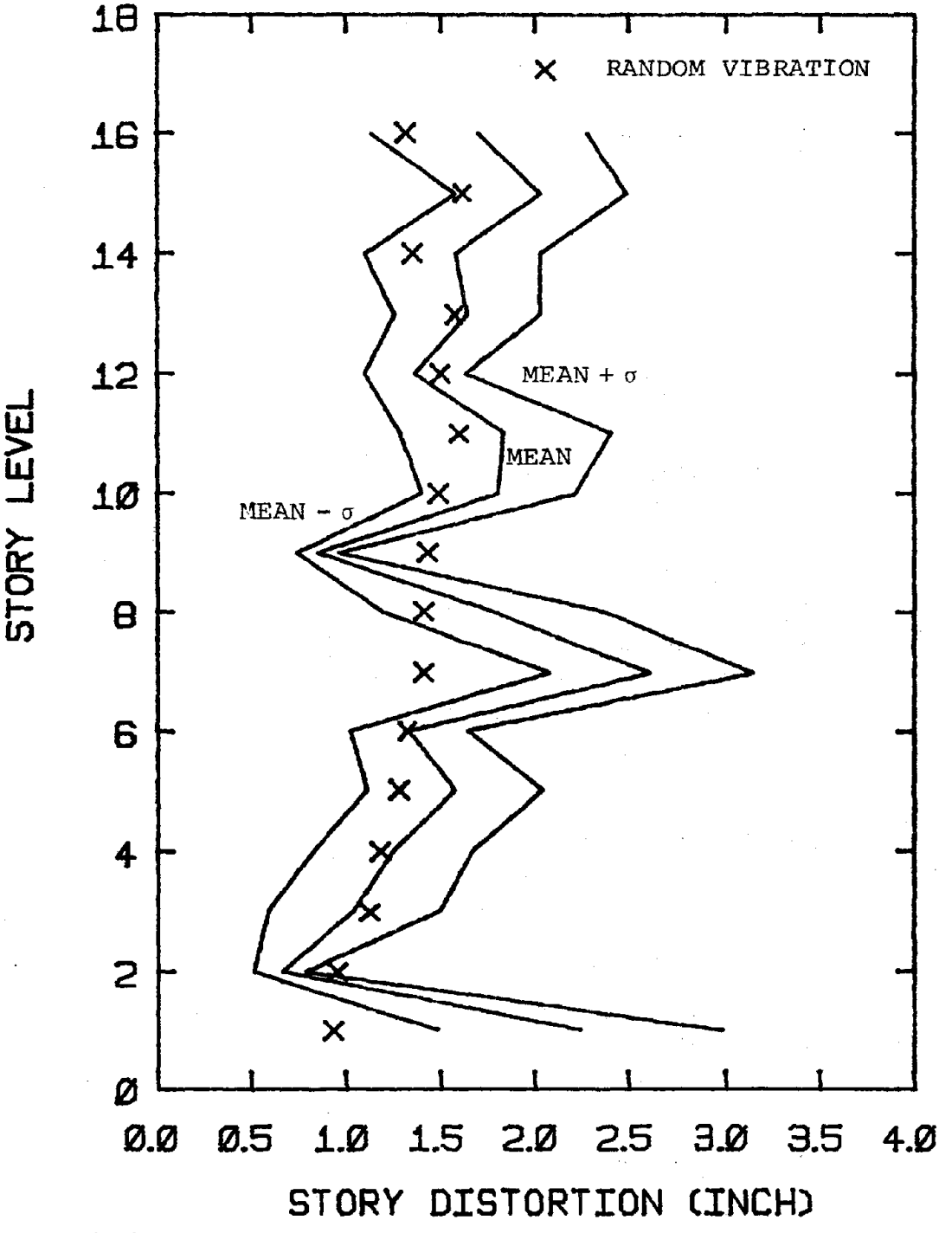

FIG. 4-17 STORY DISTORTIONS PREDICTED BY TIME-HISTORY AND RANDOM VIBRATION ANALYSIS (16-STORY FRAME, a_{max} = 1/3 g)

Since the PSD function is related to the square of the acceleration amplitude (Eq. 2-2), it can be scaled with respect to the peak ground acceleration. As mentioned in the preceding section, three levels of ground motion intensity are considered for the 4-story system, two levels for the 10-story system, and only one for the 16-story system. Hence, in the compatibility studies, six random vibration analyses are required. The random vibration-based predictions of the mean story distortions for the different systems and ground motion intensities are also plotted in Figures 4-12 to 4-17.

The figures show that the story distortions predicted by the modified random vibration methodology are generally quite compatible with those obtained from multiple time-history analyses. However, the random vibration solutions tend to be too conservative when the peak ground acceleration is large. Notice that the random vibration predictions of the first story responses are generally smaller than those of the time-history predictions. As pointed out by Anagnostopoulos [2], this is probably due to the fact that the time-history analysis of a shear-beam model will usually lead to an overpredicted inelastic response of the first story.

Based on the above-mentioned observations, it may be concluded that the modified multi-degree elasto-plastic random vibration methodology will result in satisfactory response prediction for close-coupled shear-spring systems. The inelastic response may be somewhat overestimated when the ground motion is very intense. The applicability of the random vibration solution strategy for seismic response prediction of actual structural frames is discussed in the next section.

4.6 Validity of MDOF Inelastic Random Vibration Response Prediction for Structural Frames

4.6.1 Time-History Analyses for Moment-Resisting Frames

Since the modified MDOF random vibration technique only provides "story" level response statistics, for practical engineering purposes, it is necessary to relate the story responses to the "local" component responses. A series of time-history analyses have been performed for the three steel moment-resisting frames. The resulting inelastic responses expressed in terms of the local component ductility ratios will be compared with the random vibration story response predictions.

The FRIEDA program (Frame Inelastic Earthquake Dynamic Analysis) (Luyties et al., 42] was used to calculate by time-history analysis the inelastic responses of the three steel moment-resisting frames. In performing the analysis, shear deformation, axial deformation in the girders, soil-structural interaction, as well as the P-Δ effect have been neglected. The gravity loads have been included in the computations. In measuring the response, the local "rotational" ductility ratio is used for columns, whereas the local "moment" ductility ratio is used for girders. For detailed discussion of the relative merits of these two different ductility ratios, the reader is referred to Lai [39].

As discussed in Section 4.5.1, three levels of peak ground acceleration, i.e., 1/3 g, 2/3 g and 1.0 g, were employed for the time-history analyses of the 4-story steel frame. Two levels, i.e., 1/3 g and 2/3 g, were used for the 10-story frame, and only one level, 1/3 g, for the 16-story frame. For each level of the peak ground acceleration, five diffe-

rent synthetic strong ground motions were used for the time-history analyses. Hence, all together, thirty time-history analyses have been performed.

The elastic dynamic modal characteristics of the three steel moment-resisting frames have been computed by the time-history analyses. The resulting first four modal shapes of these frames are listed in Tables B-10, B-11 and B-12 of Appendix B. Because of the use of First Mode Approximation method, the first modal shapes of these frames, as expected, are exactly the same as those of the equivalent shear-beam systems as listed in Tables B-7, B-8 and B-9. The 2nd, 3rd and 4th modal shapes of the three moment-resisting frames are also very close to those of the shear-beam systems. This suggests that the dynamic characteristics of the equivalent shear-spring systems are quite compatible with those of the steel moment-resisting frames.

From each time-history analysis, the maximum local ductility ratios can be obtained for all possible plastic hinges in the columns and girders. Since there are two possible plastic hinges for each individual column and girder, 14 plastic hinges per story must be considered for a three-bay steel frame. In addition, five different artificial strong ground motions were used for each frame; therefore, the local component response statistics can be computed from the resulting data base of 70 maximum local ductility ratios.

In this study, the mean and the standard deviation of the local component ductility ratio have been determined for each story of the three steel moment-resisting frames. The resulting mean and the mean plus (or minus) one standard deviation of the local ductility ratios corresponding

to the different frames and motion intensities are presented in Figures 4-18 to 4-23.

As shown in the figures, the local component ductility ratio generally increases with ground motion intensity, and the increase is more pronounced at the bottom stories. This seems to confirm the frequently made observation that major structural damage usually occurs in the bottom stories during strong ground shaking (soft-story concept, [2]). Physically, this may be explained by the fact that a great portion of the excitation energy is dissipated by severe yielding action in the bottom stories. Consequently, smaller inelastic responses are observed in the upper stories.

4.6.2 Local Ductility Ratio Versus Story Ductility Ratio

The maximum story distortions of the three equivalent shear-beam systems have been computed previously by the modified multi-degree elasto-plastic random vibration technique. Since the "story ductility" is defined as the ratio of the maximum inelastic story distortion divided by the story yield displacement, it can readily be determined. The story ductility ratios of the three shear-beam systems have been calculated for varying ground motion intensities. These results are also plotted in Figures 4-18 to 4-23.

As shown in the figures, the mean story ductility ratios determined by the random vibration method are quite compatible with the time-history predictions of the mean local ductility ratios for low ground motion intensities. For high motion intensities (e.g., 2/3 g), the mean story ductility ratios are generally larger than the mean local ductility ratios. Another useful way of presenting the results is to plot the scattergram of the mean story ductility ratio versus the mean local ductility ratio.

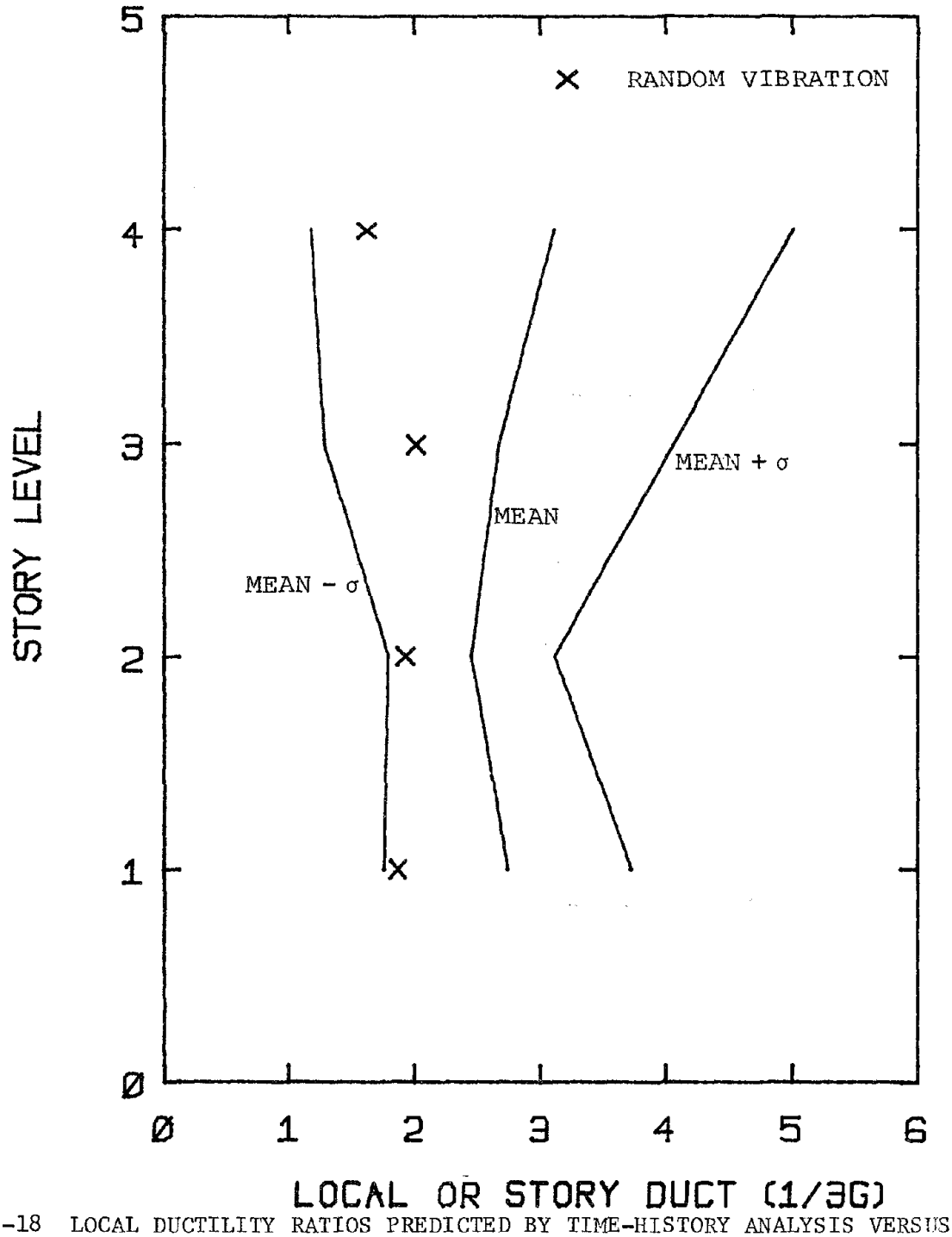

FIG. 4-18 LOCAL DUCTILITY RATIOS PREDICTED BY TIME-HISTORY ANALYSIS VERSUS STORY DUCTILITY RATIOS BY RANDOM VIBRATION (4-STORY FRAME, a_{max} = 1/3 g)

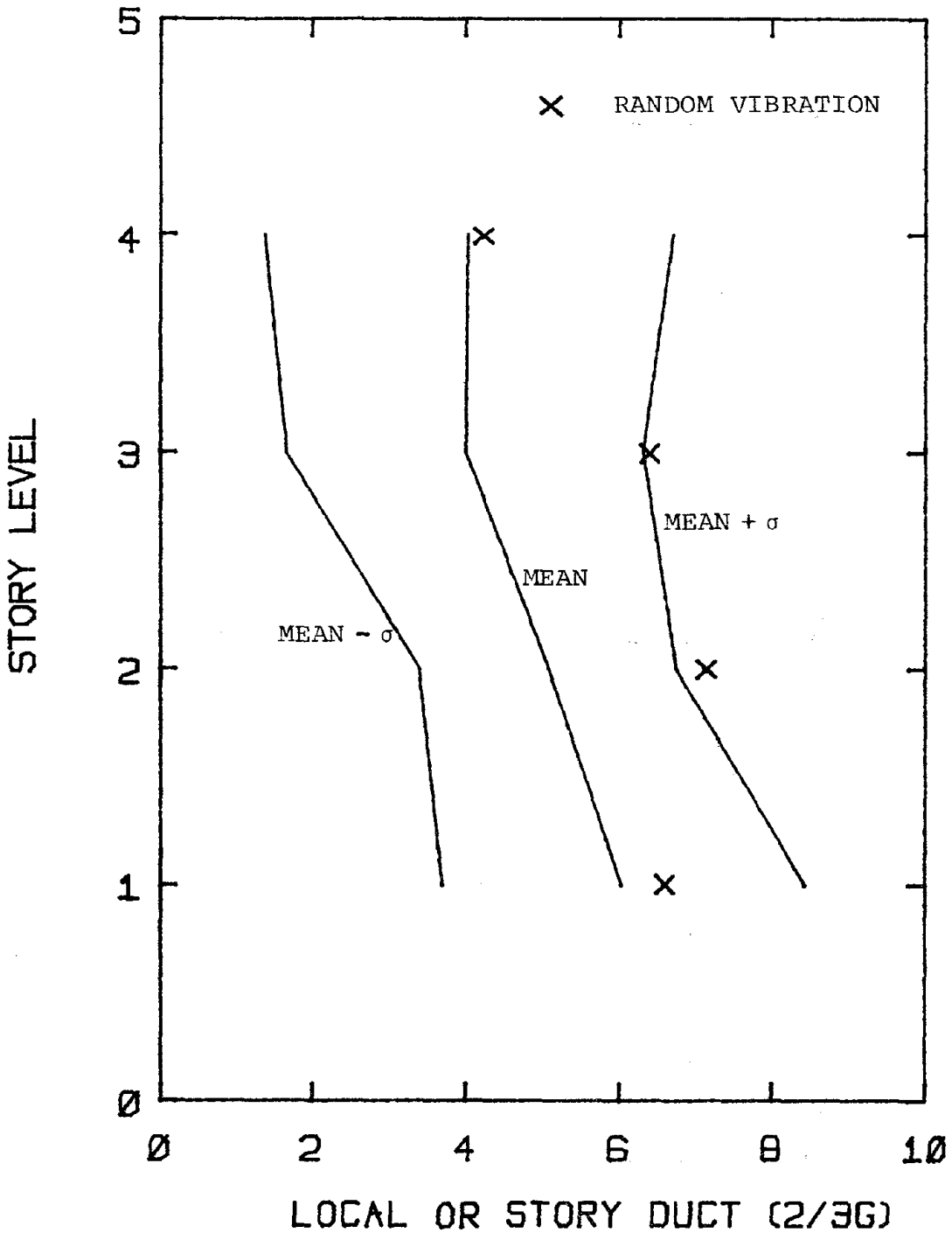

FIG. 4-19 LOCAL DUCTILITY RATIOS PREDICTED BY TIME-HISTORY ANALYSIS VERSUS STORY DUCTILITY RATIOS BY RANDOM VIBRATION (4-STORY FRAME, a_{max} = 2/3 g)

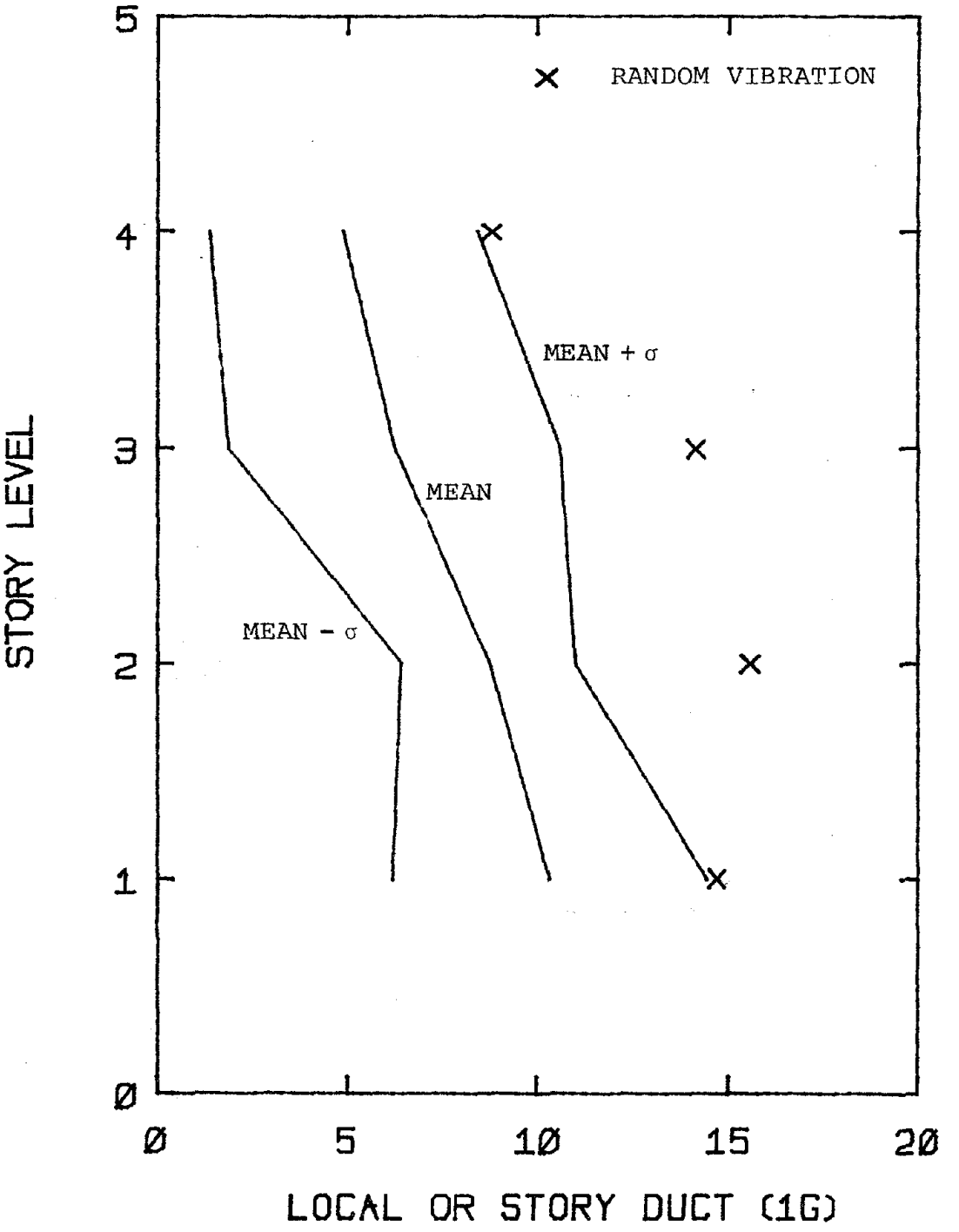

FIG. 4-20 LOCAL DUCTILITY RATIOS PREDICTED BY TIME-HISTORY ANALYSIS VERSUS STORY DUCTILITY RATIOS BY RANDOM VIBRATION (4-STORY FRAME, a_{max} = 1.0 g)

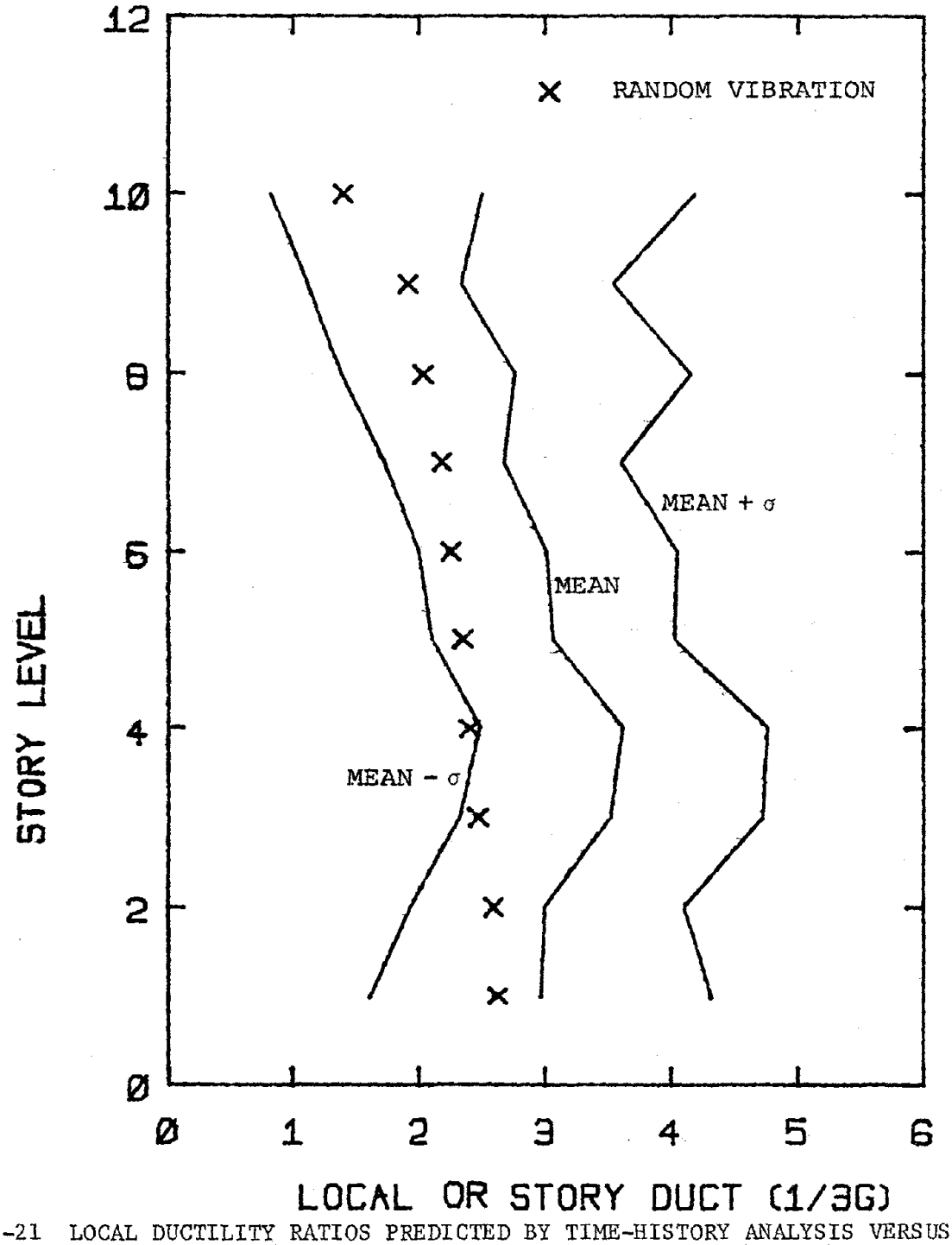

FIG. 4-21 LOCAL DUCTILITY RATIOS PREDICTED BY TIME-HISTORY ANALYSIS VERSUS STORY DUCTILITY RATIOS BY RANDOM VIBRATION (10-STORY FRAME, a_{max} = 1/3 g)

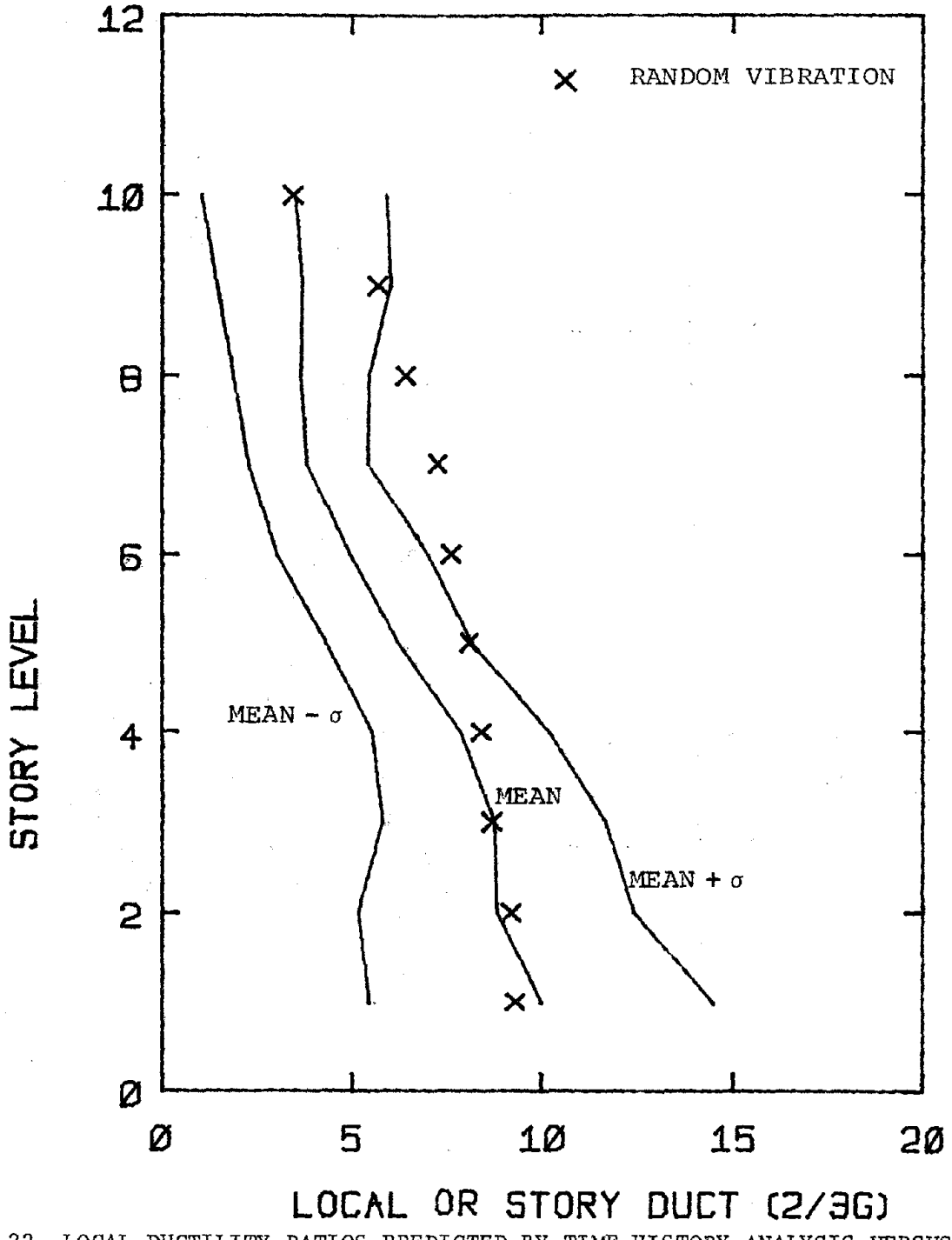

FIG. 4-22 LOCAL DUCTILITY RATIOS PREDICTED BY TIME-HISTORY ANALYSIS VERSUS STORY DUCTILITY RATIOS BY RANDOM VIBRATION (10-STORY FRAME, a_{max} = 2/3 g)

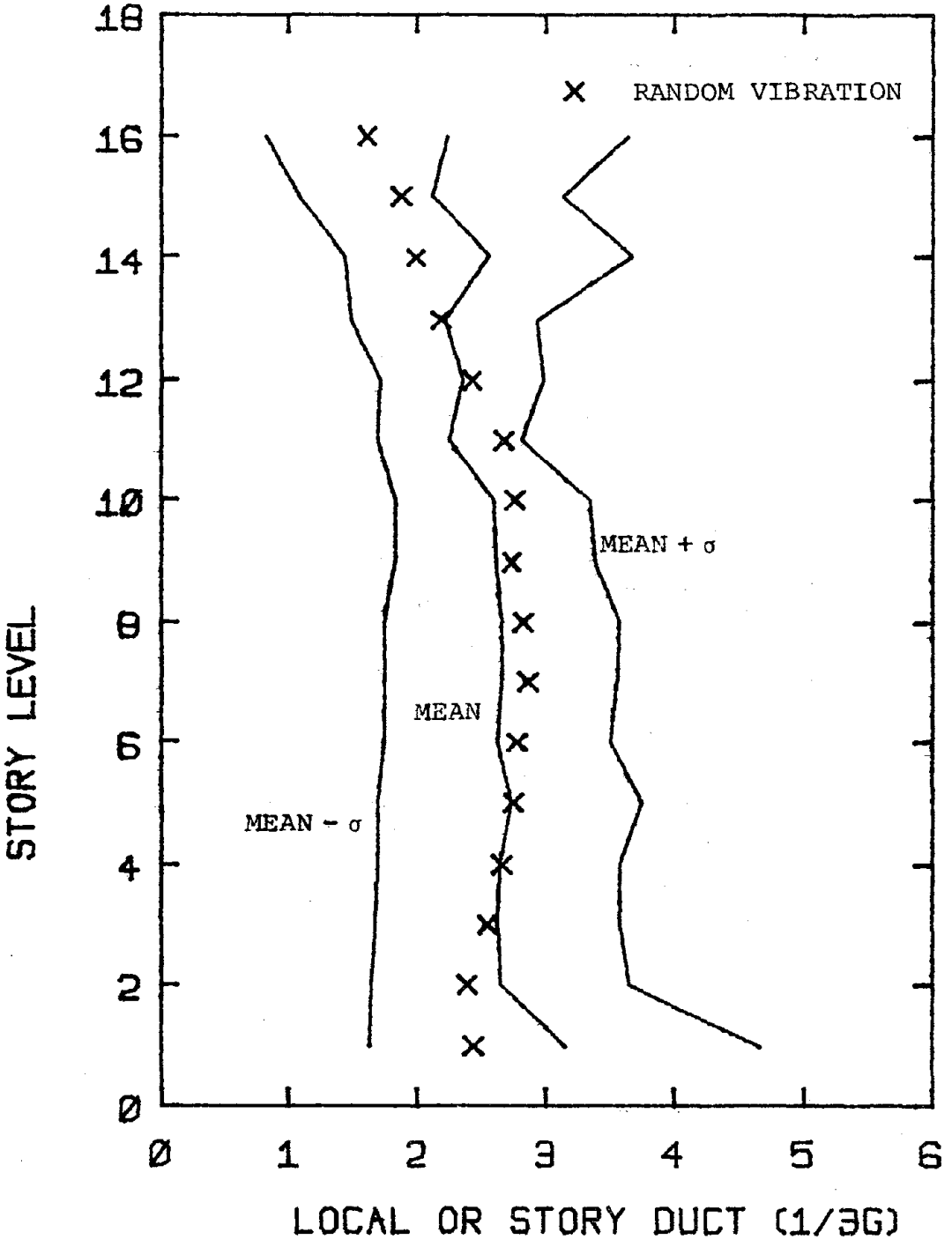

FIG. 4-23 LOCAL DUCTILITY RATIOS PREDICTED BY TIME-HISTORY ANALYSIS VERSUS STORY DUCTILITY RATIOS BY RANDOM VIBRATION (16-STORY FRAME, a_{max} = 1/3 g)

This is shown in Figure 4-24.

As depicted in the figure, the mean story ductility ratio computed by the random vibration methodology is almost linearly related to the mean local ductility ratio obtained by time-history analysis. In order to correlate the two different ductility ratios, the "local ductility correction factor", R_L, is introduced. It is defined as follows:

$$R_L = \frac{\text{local component ductility ratio}}{\text{mean story ductility ratio}} \tag{4-11}$$

For a given power spectral density function, the story ductility ratio can first be predicted by the modified MDOF elasto-plastic random vibration model. Using the correction factor R_L, the response statistics in terms of the local component ductility ratio can then be determined.

The local ductility correction factors of the three steel moment-resisting frames have been computed for different ground motion intensities. Based on a sample of 3360 values of R_L, the mean is equal to 1.038, and the other statistics are: $\sigma = 0.586$, $V = 0.565$, $\gamma_1 = 1.355$, $\gamma_2 = 6.272$. The Gamma probability density function appears to fit the histogram quite well:

$$f_{R_L}(R_L) = 14.06\ R_L^{2.134}\ \exp(-3.02\ R_L) \tag{4-12}$$

The histogram as well as the corresponding probability density function of the local ductility correction factor are plotted in Fig. 4-25.

Using Eq. 4-12, the variability in the prediction of the local component inelastic response can readily be incorporated in the evaluation of overall seismic safety for buildings.

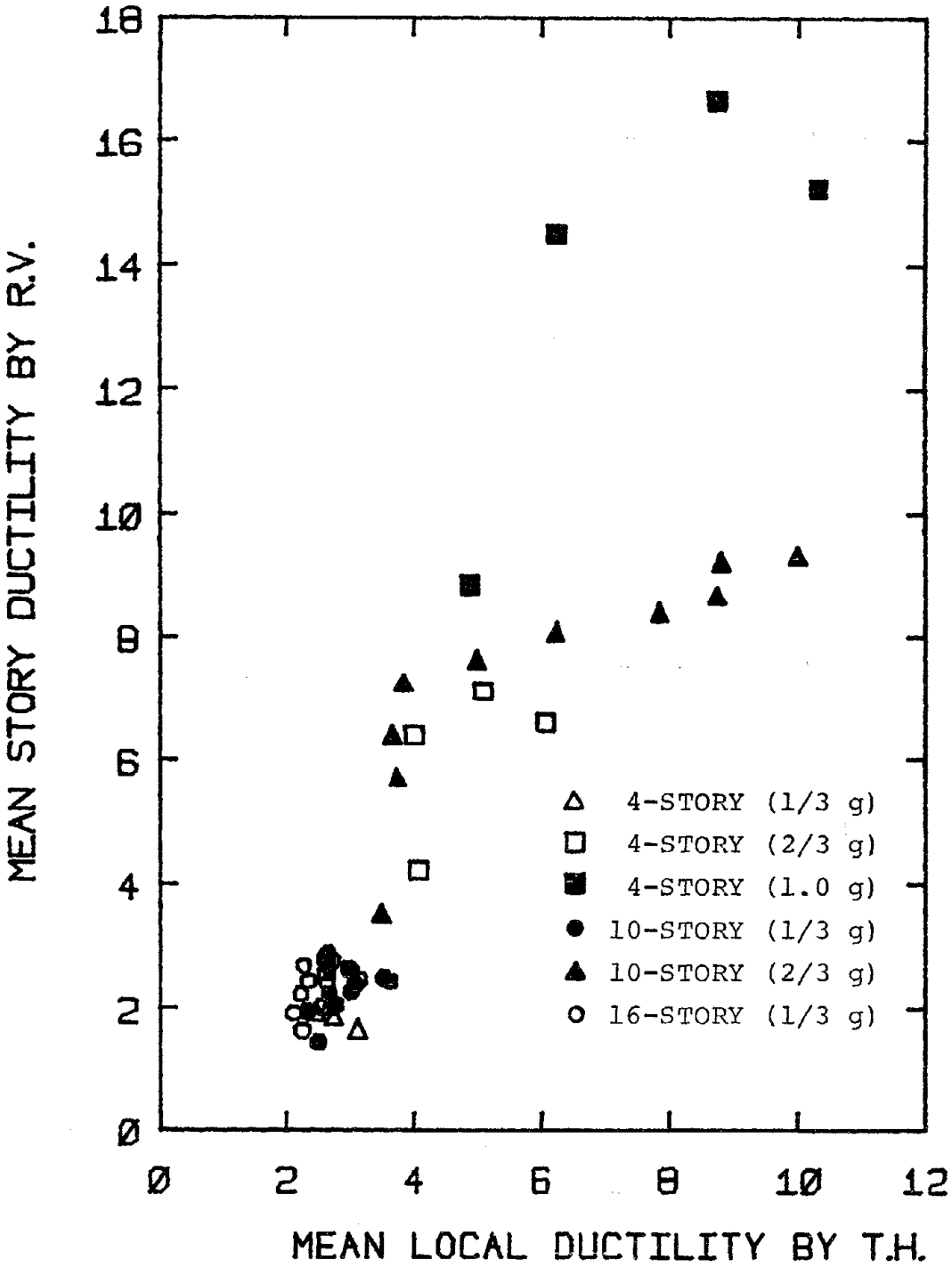

FIG. 4-24 SCATTERGRAM OF STORY DUCTILITY RATIO PREDICTED BY RANDOM VIBRATION VERSUS LOCAL DUCTILITY RATIO BY TIME-HISTORY ANALYSIS

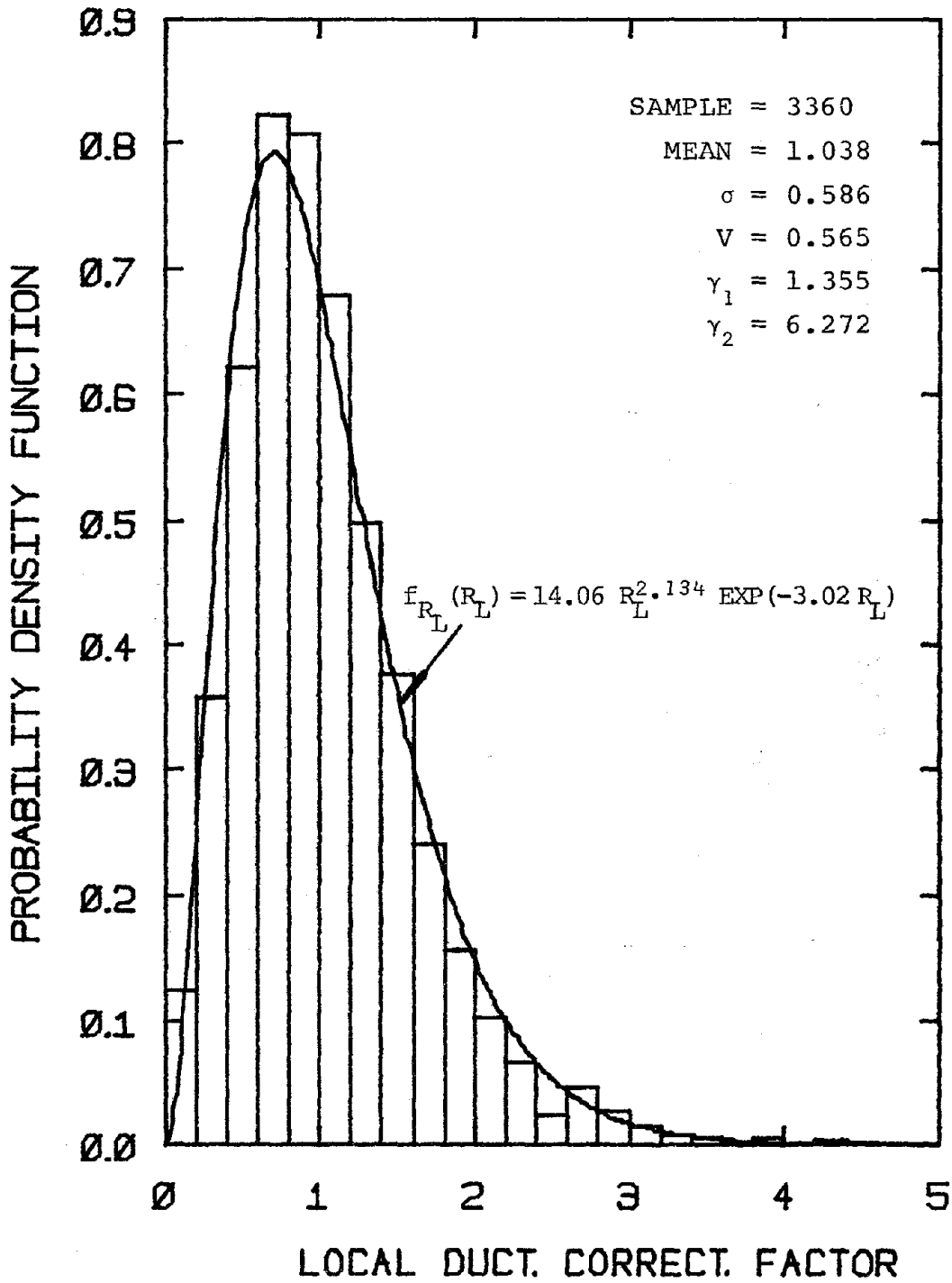

FIG. 4-25 HISTOGRAM OF LOCAL DUCTILITY CORRECTION FACTOR (ALL FRAMES TOGETHER)

4.7 Effects of Gravity Loads on Inelastic Response

As mentioned earlier, gravity loads have been neglected in the response prediction of the three equivalent shear-beam systems. However, the axial forces in the columns due to gravity loads will lead to reductions of the column moment capacities according to the column interaction formula (Eq. 4-2). Depending on the story level, the ratio of P^C/P_y^C under gravity loads is about 20% to 50%. This corresponds to a reduction in the column moment capacity by about 20% to 50%. Consequently, the equivalent story yielding strengths as estimated by Eq. 4-9 should be modified accordingly.

Nevertheless, the results reported earlier in Section 4.4.2 indicate that except for the upper few stories, the equivalent story yielding strengths of the three steel frames are primarily controlled by the girder moment capacities. Hence, the effects of gravity loads on the column moment capacities are not critical for determining the story yielding strengths and can be neglected.

For girders, the axial forces due to gravity loads are very small, and they can be ignored. But the bending moments due to gravity loads are quite high, e.g., up to 60% of the plastic capacities in some cases. It appears that the girder moment capacity needs to be corrected. However, during an earthquake excitation, the girder moment changes its sign frequently. This suggests that the existing moment due to gravity loads is equally likely to decrease as increase the girder moment capacity. Hence, the effects of gravity loads on the girder response cannot be readily accounted for.

Based on the results of a series of progressive static analyses using the incremental lateral loads, Piqué [49] suggested that the change of the equivalent lateral yielding strength due to gravity loads, usually only 5%,

could be neglected. He further argued that the only major difference in the presence of gravity loads would be the lowering of the first yield point, which should not affect the characteristics of overall inelastic response. This is quite consistent with the findings of this study.

Since the gravity loads have already been incorporated in the time-history analyses of the actual steel moment-resisting frames, their effects have implicitly been accounted for in the computations of the local ductility correction factor.

4.8 Predictions of Maximum Lateral Story Displacement

Thus far in this chapter, discussions have been limited to the prediction of nonlinear response in terms of the maximum story distortion, the story ductility ratio, and the local component ductility ratio. The response prediction of the maximum story displacement is investigated below.

From time-history analyses of the 4-, 10- and 16-story steel moment-resisting frames, the "average" maximum story lateral displacements can be computed for the five synthetic ground motions considered. Alternatively, using the equivalent story stiffnesses and yielding strengths (Section 4.4), the average maximum story displacements can be determined by the time-history analyses of the equivalent shear-beam systems.

Since random vibration methodology leads to the probabilistic predictions of maximum lateral story distortion, the maximum story displacement can then be estimated by either of the following approximate methods of computation: i) simple summation of the maximum story distortions in absolute values, or ii) combining the maximum story distortions by the SRSS method (square root of the sum of the squares). The maximum story dis-

placements of the three steel frames have been computed by the four different approaches mentioned above. The results are presented in Figures 4-26 to 4-31.

The figures show that the story displacements predicted by the frame time-history analyses (FRIEDA) are quite compatible with those obtained by the equivalent shear-beam time-history analyses (STAVROS). This is mostly true except for the 10-story frame with 2/3 g ground motion intensity. The shear-beam model generally overpredicts the maximum displacements of the lower stories, especially for the first story. This observation is consistent with the findings reported by other authors, e.g., Anagnostopoulos [2].

The story displacements computed by the simple summation of the maximum story distortions obtained by random vibration are too conservative. The conservatism increases with increasing ground motion intensity. One possible explanation is that the maximum lateral displacements for each story do not necessarily occur at the same time. Hence summing the maximum story distortions directly results in a conservative prediction of the story displacement. On the other hand, the SRSS method of combining the maximum story distortions tends to underestimate the maximum story displacement. The degree of underestimation decreases with increasing ground motion intensity. Moreover, the two methods combined (SRSS and sum of the absolute maxima) appear to give approximate lower and upper bounds on the maximum story displacement.

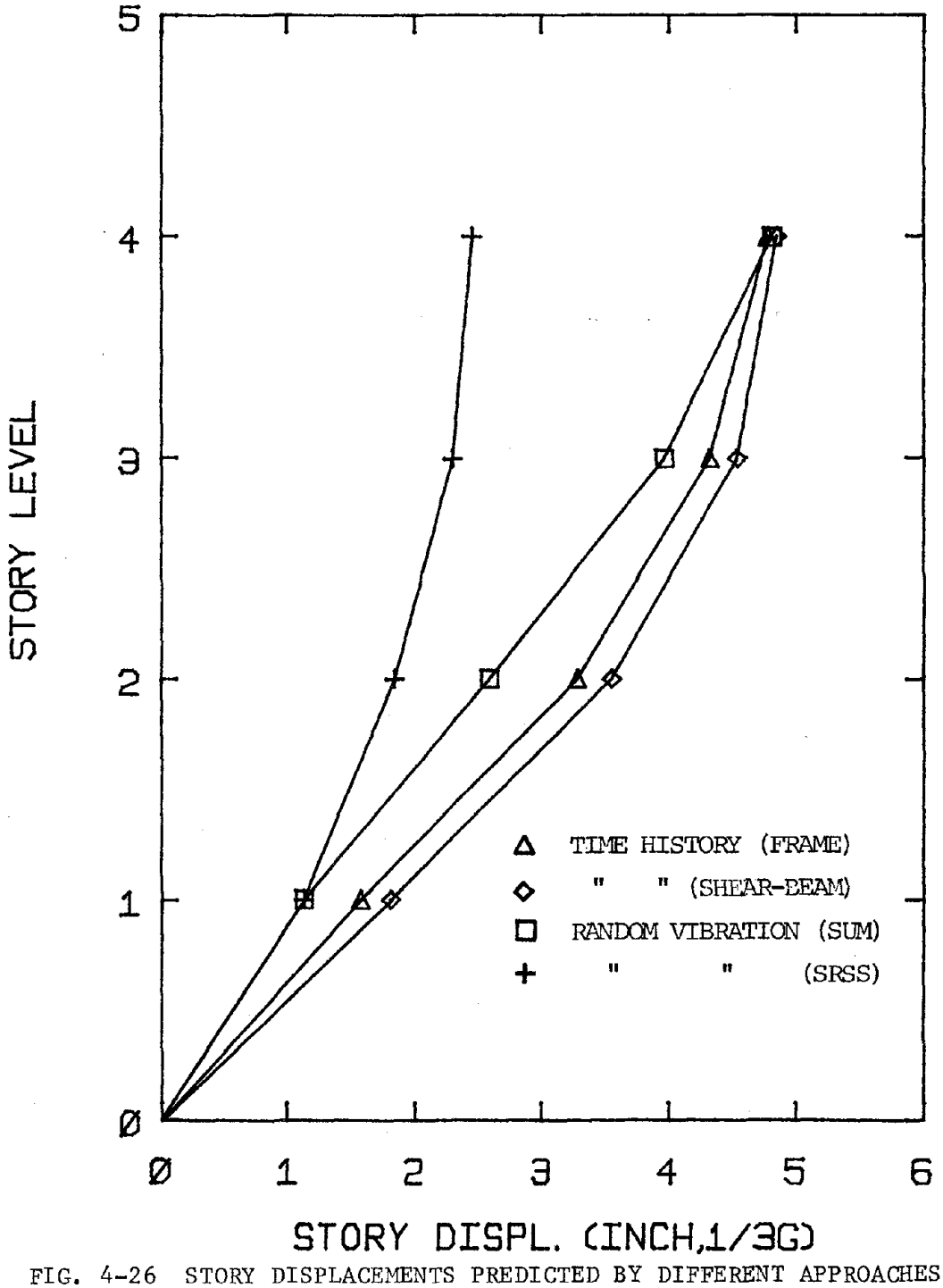

FIG. 4-26 STORY DISPLACEMENTS PREDICTED BY DIFFERENT APPROACHES (4-STORY FRAME, a_{max} = 1/3 g)

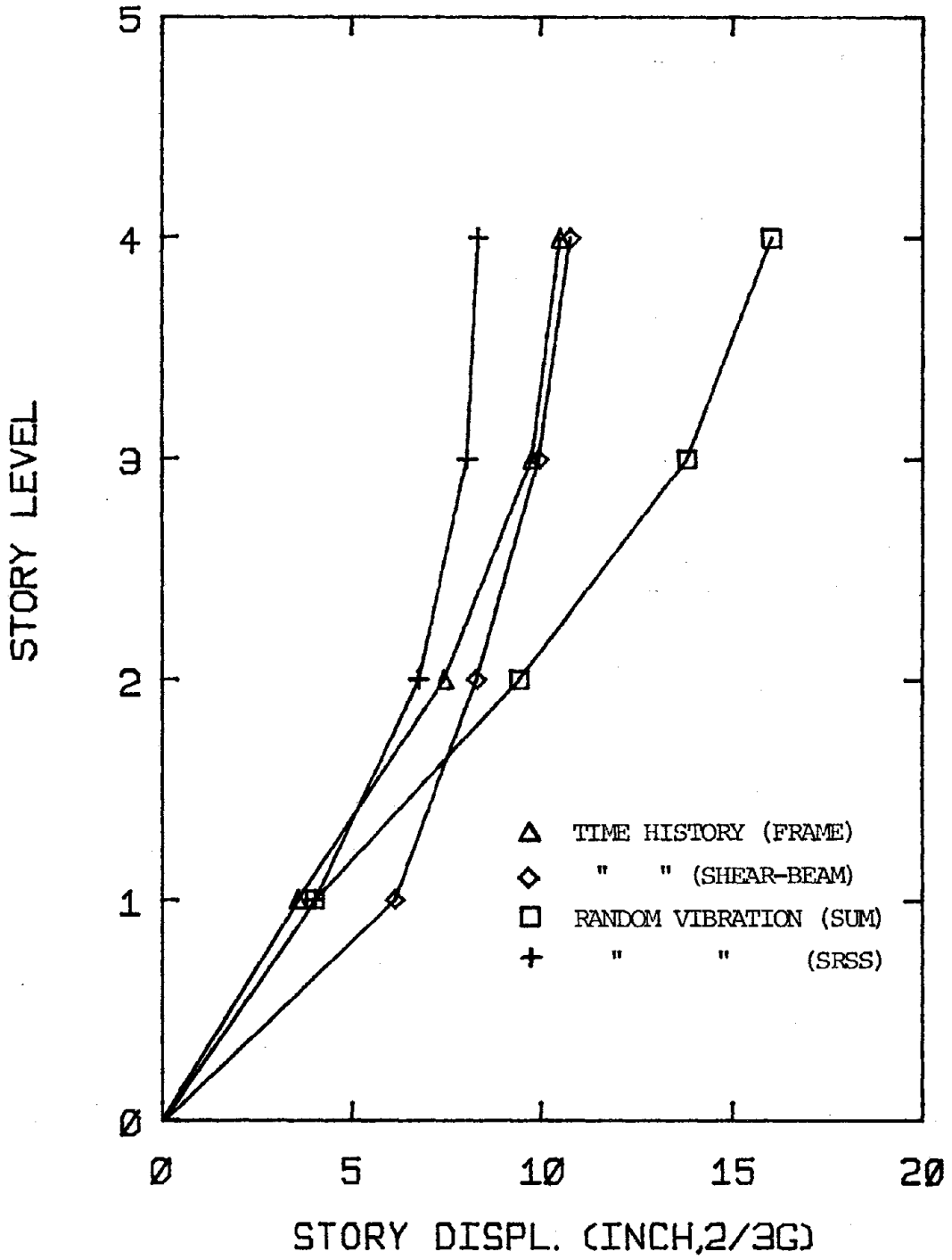

FIG. 4-27 STORY DISPLACEMENTS PREDICTED BY DIFFERENT APPROACHES (4-STORY FRAME, a_{max} = 2/3 g)

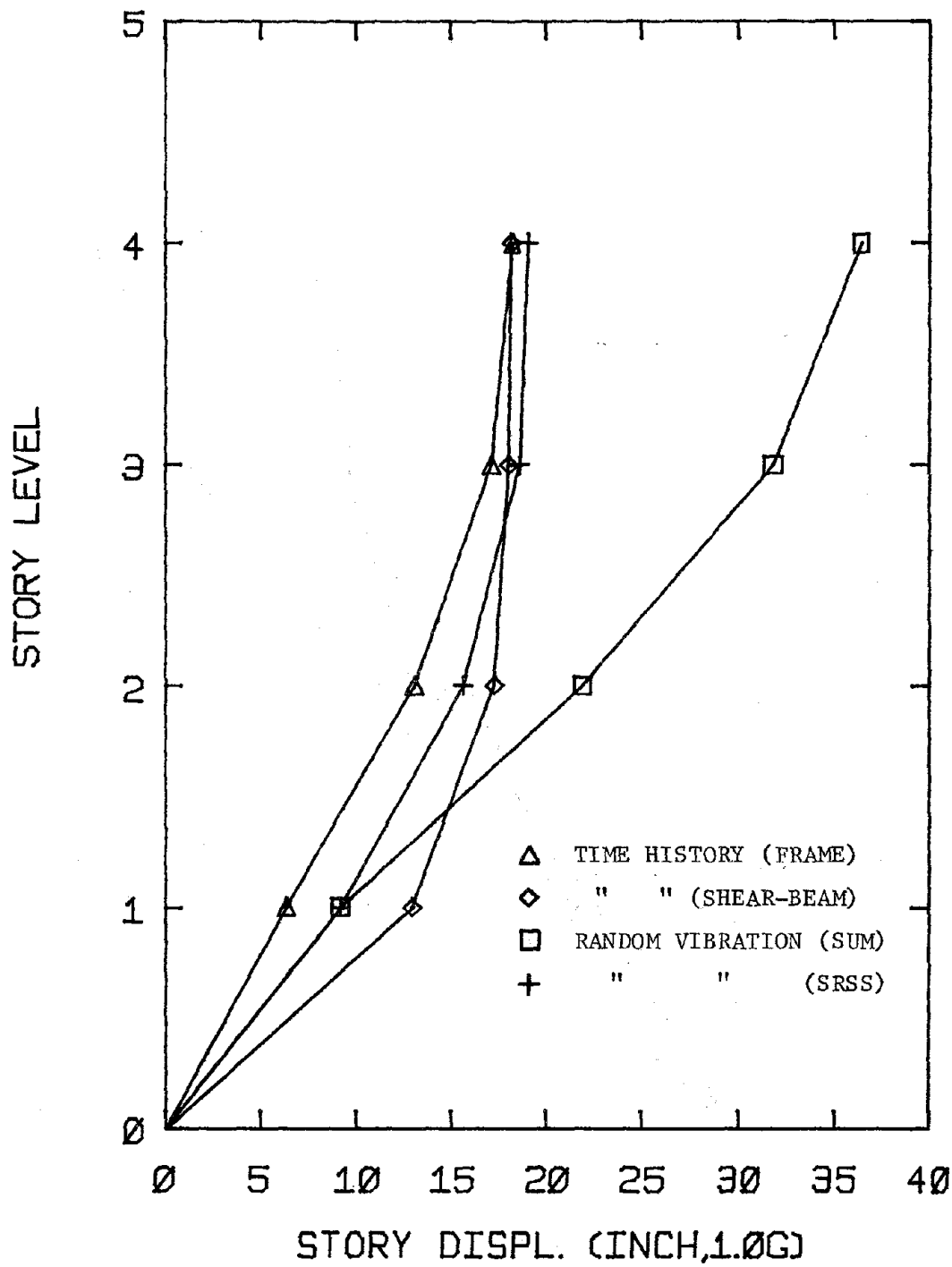

FIG. 4-28 STORY DISPLACEMENTS PREDICTED BY DIFFERENT APPROACHES (4-STORY FRAME, a_{max} = 1.0 g)

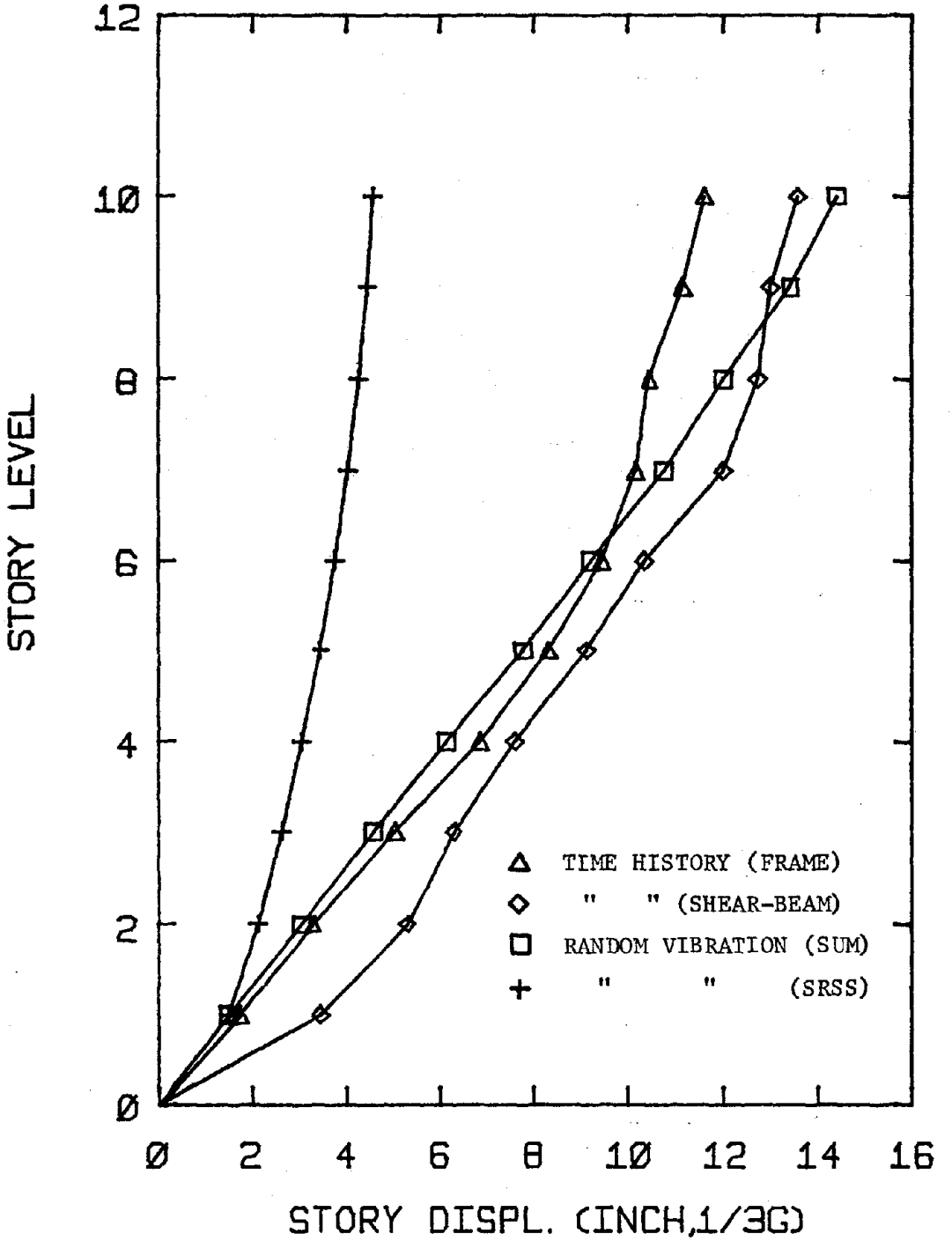

FIG. 4-29 STORY DISPLACEMENTS PREDICTED BY DIFFERENT APPROACHES (10-STORY FRAME, a_{max} = 1/3 g)

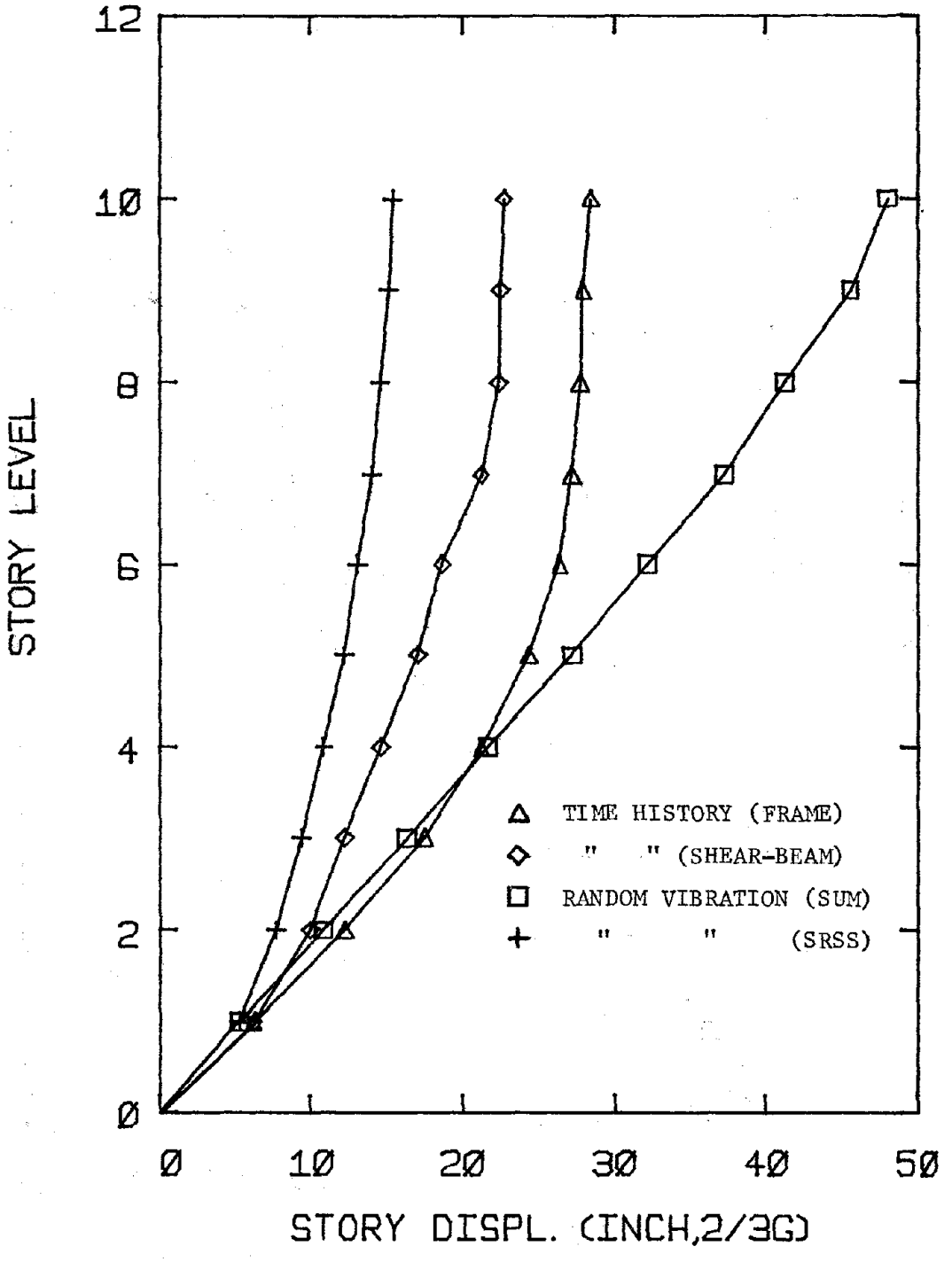

FIG. 4-30 STORY DISPLACEMENTS PREDICTED BY DIFFERENT APPROACHES (10-STORY FRAME, a_{max} = 2/3 g)

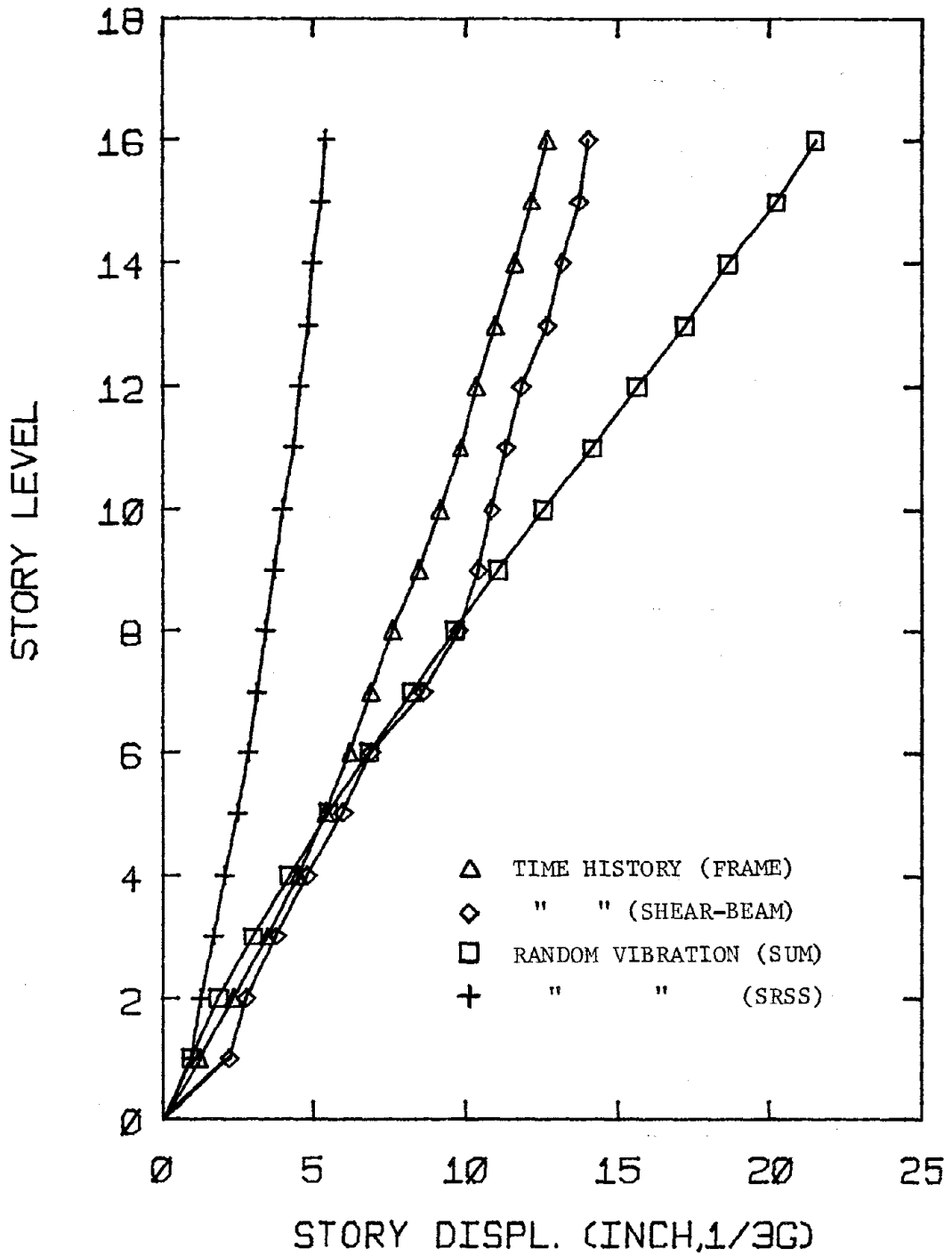

FIG. 4-31 STORY DISPLACEMENTS PREDICTED BY DIFFERENT APPROACHES (16-STORY FRAME, a_{max} = 1/3 g)

4.9 Summary

Three steel moment-resisting frames which represent real world low, middle-height and high-rise buildings, i.e., 4-, 10- and 16-story, respectively, have been employed for the compatibility studies. The applicability of the modified multi-degree elasto-plastic random vibration methodology towards the seismic response prediction of structural frames have been investigated herein. Major conclusions can be summarized as follows:

(1) The equivalent story stiffness of the shear-beam system corresponding to a structural frame can be satisfactorily determined by the "First Mode Approximation" method. The straightforward "Biggs method" will generally lead to an unconservative estimate of the first story stiffness and conservative lateral stiffnesses for the other stories.

(2) The equivalent story yielding strength computed by the upper bound approximation as suggested by Anagnostopoulos is generally too low. The "yielding strength factor" is introduced so as to correct the underestimation of the story yielding strength. For a given story, the yielding strength factor is found to be dependent on the actual stiffness distribution between columns and girders.

(3) For a close-coupled shear-springs system, the response statistics predicted by the modified multi-degree elasto-plastic random vibration analysis are quite compatible with those computed by the multiple time-history analyses. The inelastic response predicted by the random vibration methodology may be somewhat overestimated when the ground motion is very intense.

(4) Using the "local ductility correction factor", the "local" component

response characteristics of a structural frame can be satisfactorily related to the random vibration prediction of the "story" response statistics for the equivalent shear-beam system.

(5) The effects of gravity loads on the equivalent story stiffness and yielding strength are negligible. The local ductility correction factor implicitly accounts for the effects of gravity loads on the local component inelastic response.

(6) The average maximum story displacements computed by the multiple time-history analyses of the structural frame and the equivalent shear-beam system are quite compatible. The story displacement determined by the simple summation of maximum story distortions obtained by random vibration analysis is too conservative, whereas the SRSS method of combining maximum story distortions is unconservative. The two methods together provide useful approximate bounds on the maximum story displacement.

CHAPTER 5

FORMULATION OF OVERALL SEISMIC SAFETY ANALYSIS FOR BUILDINGS

5.1 INTRODUCTION

Given the amplitude, frequency content, and duration of a strong ground motion, as well as the dynamic properties of a structural frame (i.e., viscous damping, equivalent story stiffness, and yielding strength), the conditional probability distribution of inelastic "story" responses can be computed by the random vibration methodology described in the preceding chapters. By means of the local ductility correction factor introduced in Section 4.6.2, the "local" component inelastic response statistics can be approximately determined for the structural frame.

The probability of exceeding a given local response threshold can then be evaluated by combining the uncertainties in ground motion characterization and in dynamic modeling of the structure. This exceedance probability is commonly expressed as "conditional" on a chosen seismic parameter, say, peak ground acceleration [10,22]. Finally, to quantify the "overall seismic safety" of a particular structure at a specific site, it is necessary to incorporate the information about the seismic risk at the site (i.e., the relationship between the peak ground acceleration and the mean return period for the site).

The main objective of this chapter is to formulate the overall safety analysis of earthquake-resistant buildings. The major uncertainties involved in the seismic safety analysis are briefly discussed first. This is followed by the formulation of component response prediction for given earthquake peak ground acceleration. This methodology is used to investigate the sensitivity of the predicted component response with respect to the following sources of uncertainty: i) the ground motion parameters, ii) the structural dynamic properties, iii) the correlation between strong-motion duration and the peak ground acceleration, and iv) the local ductility correction factor. The effect of ground motion intensity is also explored.

5.2 Uncertainties Involved in Seismic Safety Assessment of Buildings

5.2.1 Ground Motion Representation

There are three major sources of uncertainty involved in seismic safety assessment of buildings: i) representation of earthquake environment, ii) structural dynamic properties, and iii) method of dynamic analysis. The first source of uncertainty is discussed below, whereas the latter two are discussed in Sections 5.2.2 and 5.2.3, respectively.

The details of the ground motion representation in terms of the Kanai-Tajimi PSD function have already been discussed in Chapter 2. The statistics of the strong-motion duration, the K-T frequency and damping were computed for a set of 140 real ground motion records, and the probability density functions were suggested for these three pertinent seismic parameters. These results constitute the basis of characterizing seismic input for the sensitivity studies reported in this chapter.

For given Kanai-Tajimi frequency and damping, the central frequency ω_c of the excitation can be determined by calculating the K-T spectral moments (Eq. 2-6). Alternatively, the central frequency can be approximately related to the K-T frequency as expressed in Eq. 2-17. Since the predominant period T_o is equal to $2\pi/\omega_c$, the r.m.s. strong motion acceleration σ_o can be estimated from Eq. 2-13 if the peak ground acceleration is given. The corresponding white noise bedrock excitation intensity can then be obtained using Eq. 2-5.

As an example, assuming that the peak ground acceleration is 1/3 g, the corresponding strong-motion duration is estimated as equal to 3.27 sec by Eq. 2-17. If one further assumes a K-T frequency of 20.3 rad/sec, and a K-T damping of 0.32, the central frequency is found to be equal to 22.65 rad/sec. This corresponds to the excitation variance σ_o^2 of 2623.2 in^2/sec^4, and the white noise bedrock excitation intensity of 38.67 in^2/sec^3. Hence, the PSD function is fully described and is plotted in Fig. 5-1.

As illustrated in the example, only four ground motion parameters are needed in the statistical characterization of strong ground motions: i) peak ground acceleration, ii) strong-motion duration, iii) Kanai-Tajimi frequency, and iv) Kanai-Tajimi damping. Notice that in this particular study, the strong-motion duration and the peak ground acceleration are assumed to be negatively correlated (in accordance with Eq. 2-18). Under this assumption, the ground motion is defined by only three independent parameters.

5.2.2 Structural Dynamic Properties

The structural dynamic properties constitute the second major source

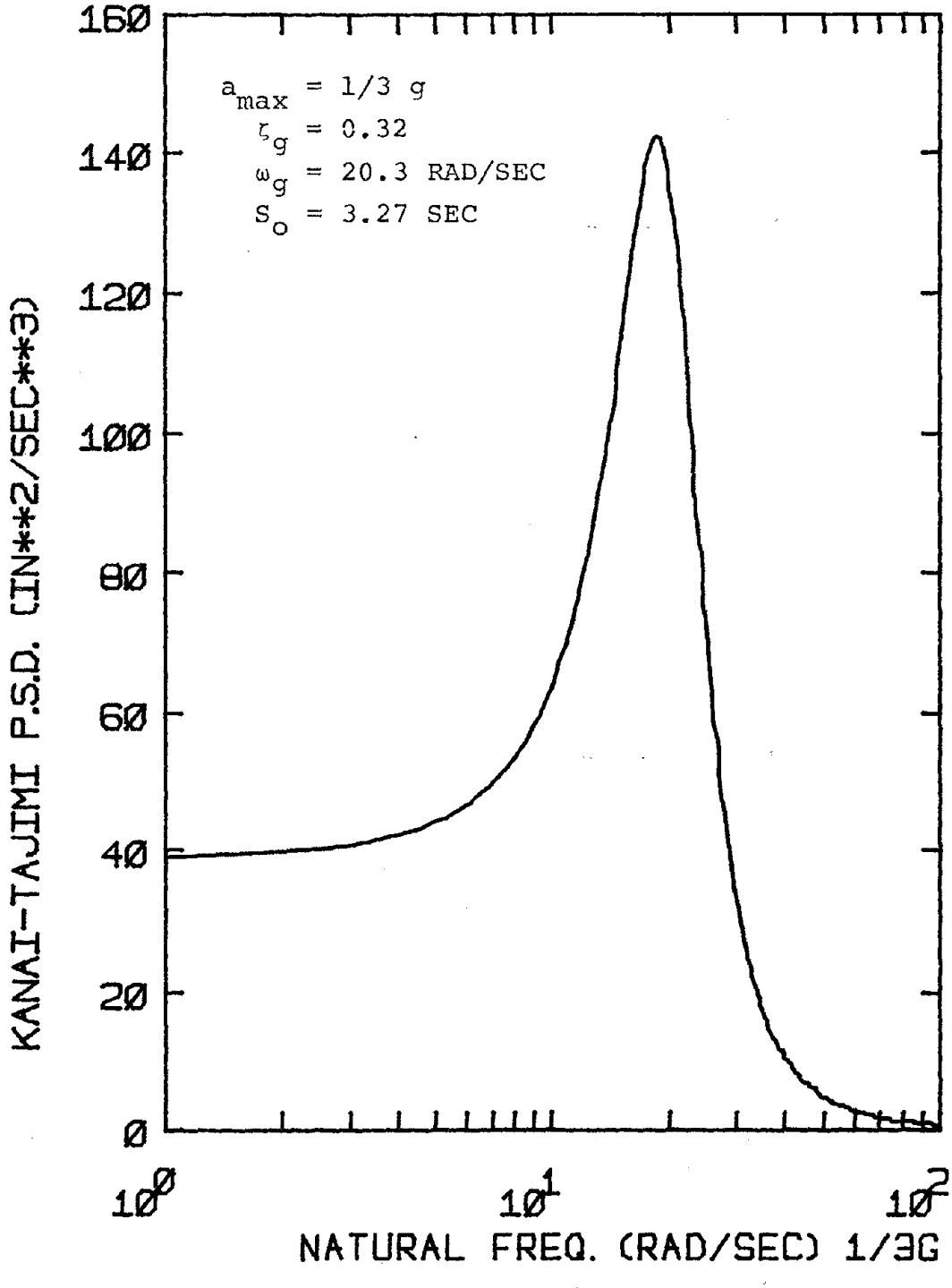

FIG. 5-1 KANAI-TAJIMI POWER SPECTRAL DENSITY FUNCTION FOR THE DETERMINISTIC ANALYSIS

of uncertainty affecting the overall seismic safety of buildings. The uncertainty is attributable to numerous factors, e.g., material imperfections, non-structural partitions and panels, interaction of translational and torsional modes and actual energy-dissipating mechanisms. In Chapter 4, the uncertainties involved in determining the equivalent lateral story stiffness and yielding strength have already been discussed. In this section, the variability of the damping and natural period of the structure undergoing strong ground excitation are assessed.

The actual dynamic properties of several tall buildings shaken during the 1971 San Fernando earthquake has been reported by Wood [69], Benfer and Coffman [7], and Hart et al. [28,29]. Tanaka et al. [56] investigated the implied dynamic parameters of several buildings shaken by the 1968 Tokyo earthquake in Japan. Based on these data, Haviland [30] computed statistics for the structural damping coefficient and what he called the "natural period ratio". The natural period ratio R_T is defined as the ratio between the "observed" fundamental natural period and the "predicted" natural period (by modal analysis). The results reported by Haviland are used herein to characterize the variability of the damping and the natural period of the structure.

Based on the data from 22 real tall buildings, Haviland [30] reported the following statistics for the natural period ratio: the mean value is equal to 1.15, the standard deviation (σ) is 0.344, and the coefficient of variation (V) is 0.3. The Lognormal probability density function appears to fit the data quite well:

$$f_{R_T}(R_T) = \frac{1}{0.734\ R_T} \exp\{-5.834\ [\ln R_T - 0.097]^2\} \qquad (5\text{-}1)$$

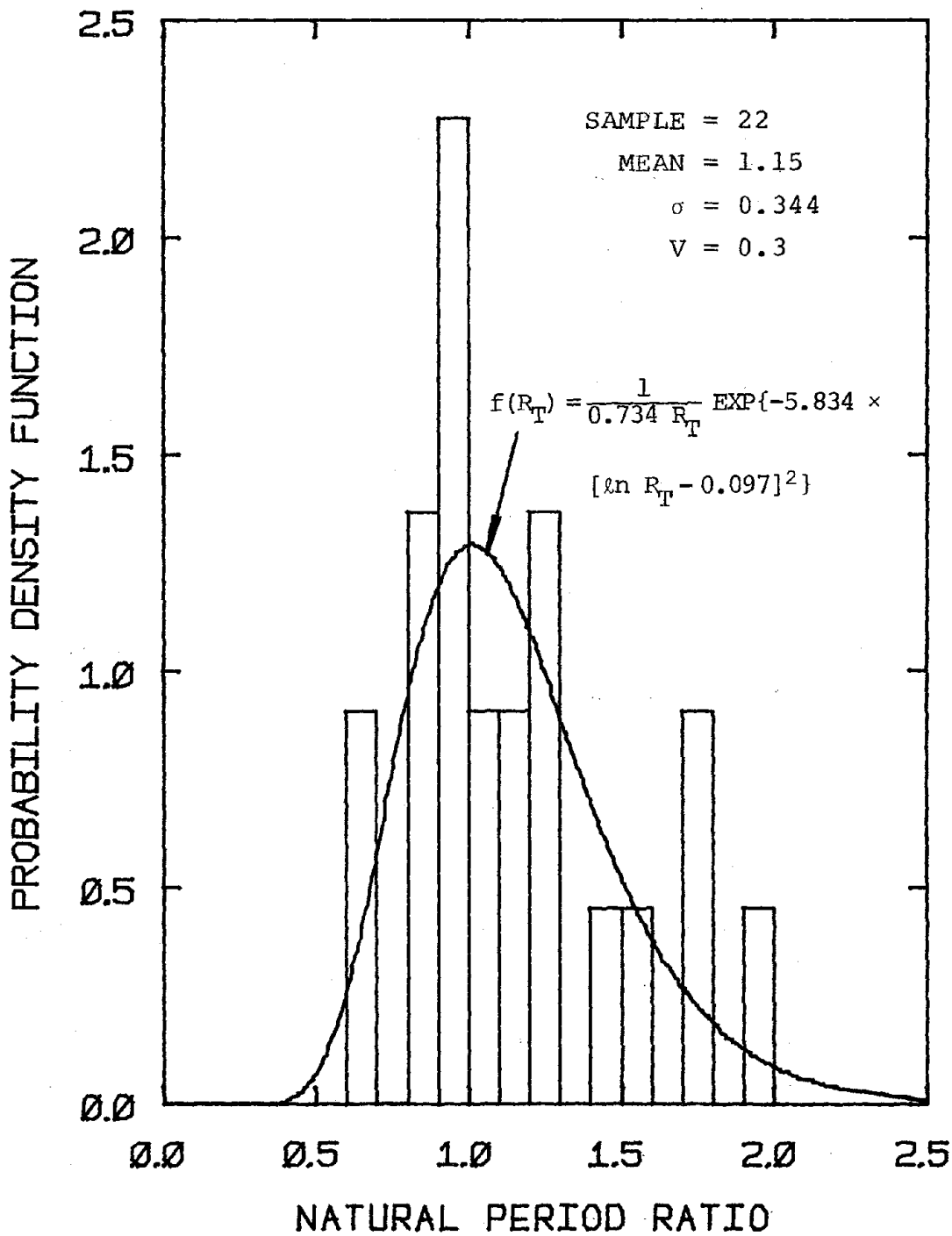

FIG. 5-2 HISTOGRAM OF NATURAL PERIOD RATIO

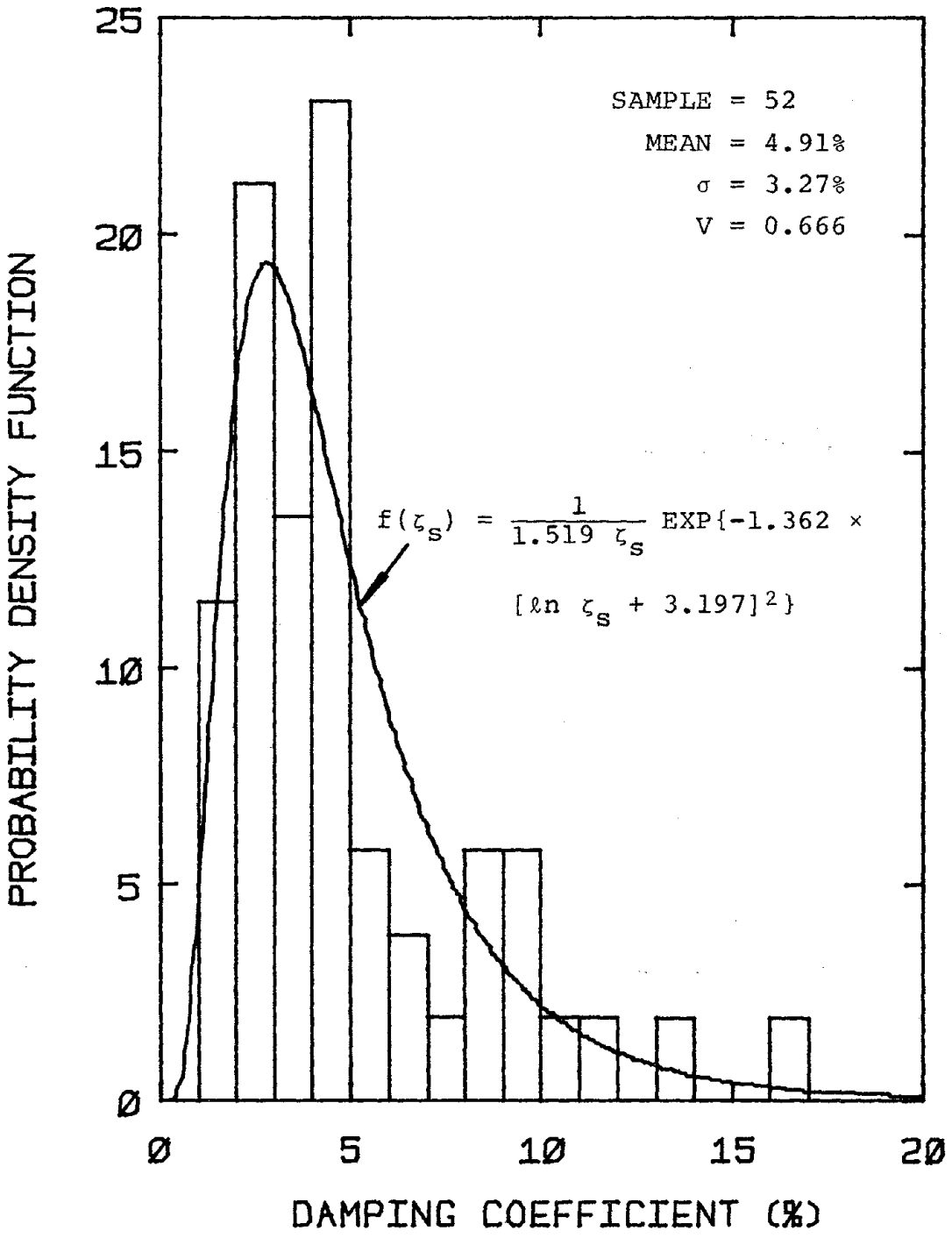

FIG. 5-3 HISTOGRAM OF STRUCTURAL DAMPING COEFFICIENT

The histogram as well as the fitted PDF are plotted in Fig. 5-2.

Based on the data from 52 actual buildings, Haviland suggested the following statistics for the structural viscous damping coefficient ζ_s: the mean value is equal to 4.91%, σ = 3.27 %, and V = 0.666. The histogram and the fitted analytical PDF of structural damping are presented in Fig. 5-3. A Lognormal PDF appears to fit the histogram well:

$$f_{\zeta_s}(\zeta_s) = \frac{1}{1.519\ \zeta_s} \exp\{-1.362\ [\ell n\ \zeta_s + 3.197]^2\} \qquad (5\text{-}2)$$

The above two probability distributions will be used to characterize the variability of the natural period and the damping of the structure. In addition, the uncertainties of equivalent lateral story stiffness and yielding strength are also incorporated in the overall seismic safety assessment of buildings.

5.2.3 Method of Dynamic Analysis

Assuming the steel moment-resisting frame behaves as a close-coupled shear-beam system, the story response characteristics can be satisfactorily computed by the modified multi-degree elasto-plastic random vibration methodology. Based on multiple time-history analyses of an ensemble of strong ground motions, the inelastic response statistics of local components can be estimated. The two different types of inelastic response measures, i.e, "story" response and "local" response, are related by the "local ductility correction factor" R_L (see Section 4.6.2).

In essence then, the uncertainty in local inelastic response prediction due to the method of dynamic analysis is captured by the local ductility correction factor. The variability of the local ductility correction factor has been extensively investigated in the preceding chapter.

The probability distribution given by Eq. 4-12 will be used in the sensitivity studies.

5.3 Local Response Prediction Conditional on Peak Ground Acceleration

In the preceding sections, eight random variables have been identified as potentially significant in their effect on component response to earthquake shaking: i) peak ground acceleration (a_{max}), ii) strong-motion duration (S_o), iii) Kanai-Tajimi frequency (ω_g), iv) Kanai-Tajimi damping (ζ_g), v) natural period ratio (R_T), vi) structural damping (ζ_s), vii) yielding strength factor (R_y), and viii) local ductility correction factor (R_L). Probability density functions have been proposed for the last seven random variables.

Using the modified elasto-plastic random vibration methodology, local response characteristics of a structural frame can be computed for any particular combination of the above-mentioned random variables. It is useful to define the probability of occurrence of the event C, i.e., the combination of pertinent parameters S_o^i, ω_g^j, ζ_g^k, R_T^l, ζ_s^m, R_y^n, and R_L^o, conditional on the level of peak ground acceleration a_{max}^i:

$$P[C|a_{max}^i] = P[C \cap a_{max}^i]/P[a_{max}^i] = P[S_o^i \cap \omega_g^j \cap \zeta_g^k \cap R_T^l \cap \zeta_s^m \cap R_y^n \cap R_L^o \cap a_{max}^i]/P[a_{max}^i] \quad (5\text{-}3)$$

where $P[a_{max}^i]$ is the site-dependent probability distribution of the peak ground acceleration as discussed in Chapter 6.

Based on the assumptions that the strong-motion duration is negatively correlated with the peak ground acceleration, and that the other six pertinent random variables are statistically independent, Eq. 5-3 becomes:

$$
\begin{aligned}
P[C|a^i_{max}] &= P[\omega_g^j] \cdot P[\zeta_g^k] \cdot P[R_T^l] \cdot P[\zeta_s^m] \cdot P[R_y^n] \cdot P[R_L^o] \\
&\quad \cdot P[S_o^i \cap a^i_{max}]/P[a^i_{max}] \\
&= P[\omega_g^j] \cdot P[\zeta_g^k] \cdot P[R_T^l] \cdot P[\zeta_s^m] \cdot P[R_y^n] \cdot P[R_L^o] \\
&\quad \cdot P[S_o^i|a^i_{max}]
\end{aligned}
\tag{5-4}
$$

The local response characteristics of a structural frame can be computed for each combination of discrete variables by the modified multi-degree elasto-plastic random vibration methodology. The probability of exceeding a given local response threshold, say, a local ductility ratio μ^*, can then be expressed as follows:

$$
P[\mu > \mu^*] = \sum_{C \cap a^i_{max}} P[\mu > \mu^*|C \cap a^i_{max}] \cdot P[C \cap a^i_{max}] \tag{5-5}
$$

There are several methods available to compute the above-mentioned overall response characteristics, e.g., the Monte Carlo simulation technique, the method of enumeration [8], and the First-Order Second-Moment methods [15,51]. Detailed discussions are presented in Section 6.2.

Assuming the enumeration method applies, if five values are used to discretize the probability distribution of each of the seven random variables in Eq. 5-4, the total number of multi-degree random vibration computations needed would be $5^7 = 78125$. This is obviously too time consuming and costly to be practical. In an attempt to cut down the necessary computational effort, a series of sensitivity studies have been performed to investigate the relative importance of the different random variables to the predicted seismic response. A detailed discussion of these sensitivity studies is presented in the next five sections.

5.4 Sensitivity Studies of Uncertainties Associated with Local Response Prediction

5.4.1 Background

Seven random variables affecting the prediction of local structural response conditional on peak ground acceleration have been identified as expressed by Eq. 5-4. Sensitivity analyses have been performed for each of the random variables. In addition, the sensitivity of the predicted component response has been investigated with respect to the correlation between the strong-motion duration and the peak ground acceleration.

Since the three steel moment-resisting frames were designed for a peak ground acceleration of 1/3 g, this intensity level is assumed in the sensitivity studies. Five discrete values are used to characterize the probability distribution of the Kanai-Tajimi damping, whereas ten values are employed for the other parameters, (i.e., the K-T frequency, the strong-motion duration, the natural period ratio, the structural damping, the yielding strength factor, and the local ductility correction factor). The probability mass function (PMF) of the random variables are listed in Table 5-1.

The results of the sensitivity studies of the three (4-, 10- and 16-story) steel moment-resisting frames are presented in terms of the mean and the coefficient of variation of inelastic local ductility ratio.

5.4.2 Sensitivity of Ground Motion Parameters

Three ground motion parameters are considered herein: i) strong-motion duration, (conditional on the peak ground acceleration), ii) Kanai-Tajimi frequency, and iii) Kanai-Tajimi damping. If the peak ground acceleration equals 1/3 g, the mean strong-motion duration is estimated to be 3.27 sec (Eq. 2-18). Assuming the conditional coefficient of variation

TABLE 5-1 DISCRETE PROBABILITY MASS FUNCTIONS OF KEY PARAMETERS

ζ_g	$P[\zeta_g]$	ω_g	$P[\omega_g]$	$S_o \mid a_{max}$	$P[S_o \mid a_{max} = 1/3\ g]$	R_T	$P[R_T]$
0.06	0.0139	2	0.0004	0.2	0.0266	0.7	0.0951
0.19	0.3381	3	0.0041	0.5	0.0756	0.8	0.0943
0.32	0.3934	6	0.0264	1	0.1748	0.9	0.1191
0.45	0.1754	8	0.0379	2	0.1996	1.0	0.1279
0.58	0.0792	10	0.1262	3	0.1561	1.1	0.1192
--	--	15	0.241	4	0.1141	1.2	0.1107
--	--	20	0.2237	5	0.1163	1.3	0.0885
--	--	25	0.1506	7	0.0737	1.4	0.0982
--	--	30	0.1256	9	0.0368	1.6	0.0775
--	--	40	0.0641	12	0.0264	1.8	0.0695
ζ_s	$P[\zeta_s]$	R_y	$P[R_y]$	R_L	$P[R_L]$	S_o	$P[S_o]$
0.01	0.0495	0.6	0.0087	0.2	0.057	0.5	0.0503
0.02	0.1595	0.8	0.0767	0.4	0.12	1	0.0702
0.03	0.1923	0.9	0.1294	0.6	0.1538	2	0.0847
0.04	0.1583	1.0	0.1788	0.8	0.1546	3	0.1231
0.05	0.1283	1.1	0.1818	1.0	0.1358	5	0.1305
0.06	0.0884	1.2	0.1603	1.2	0.1094	7	0.1255
0.07	0.065	1.3	0.1128	1.4	0.083	10	0.1491
0.08	0.0436	1.4	0.0933	1.6	0.0603	15	0.1134
0.09	0.0328	1.6	0.045	1.8	0.0424	20	0.0642
0.10	0.0823	1.8	0.0132	2.0	0.0837	25	0.089

$V_{S_o|a_{max}} = 0.804$ (see Section 2.4.2), then the probability density function of the strong-motion duration has the following form:

$$f_{S_o|a_{max}}(S_o|a_{max} = 1/3\ g) = 0.353\ S_o^{0.547} \exp(-0.473\ S_o) \qquad (5\text{-}6)$$

This PDF is plotted in Fig. 5-21.

For the deterministic case, the random variables are replaced by their mean values: $\zeta_g = 0.32$, $\omega_g = 20.3$ rad/sec, $S_o = 3.27$ sec, $R_T = 1.0$, $\zeta_s = 0.05$, $R_y = 1.0$, and $R_L = 1.038$. Notice that both the natural period ratio and the yielding strength factor are assumed to be equal to one. This stems from the fact that the corrected values of the equivalent story stiffnesses and yielding strengths are used for the three steel frames.

The results of the deterministic analyses and the sensitivity analyses concerning the three ground motion parameters are presented in Figures 5-4 to 5-9. Also shown in the figures are the results of the analysis of sensitivity with respect to the local ductility correction factor, to be discussed in Section 5.4.5. The figures show that the mean and the coefficient of variation of the local ductility ratio are generally not very sensitive to variations in the strong-motion duration and the K-T damping, but they are rather sensitive to the K-T frequency. This suggests that the Kanai-Tajimi damping may be assumed deterministic in the overall seismic safety assessment of buildings.

The dependence of the local ductility ratio on the K-T frequency is further investigated through the "inelastic local response spectrum", i.e., a plot of the mean local ductility ratio versus the corresponding K-T frequency. The inelastic first- and top-story "local response spectra" of the three steel moment-resisting frames, i.e., 4-, 10- and 16-story,

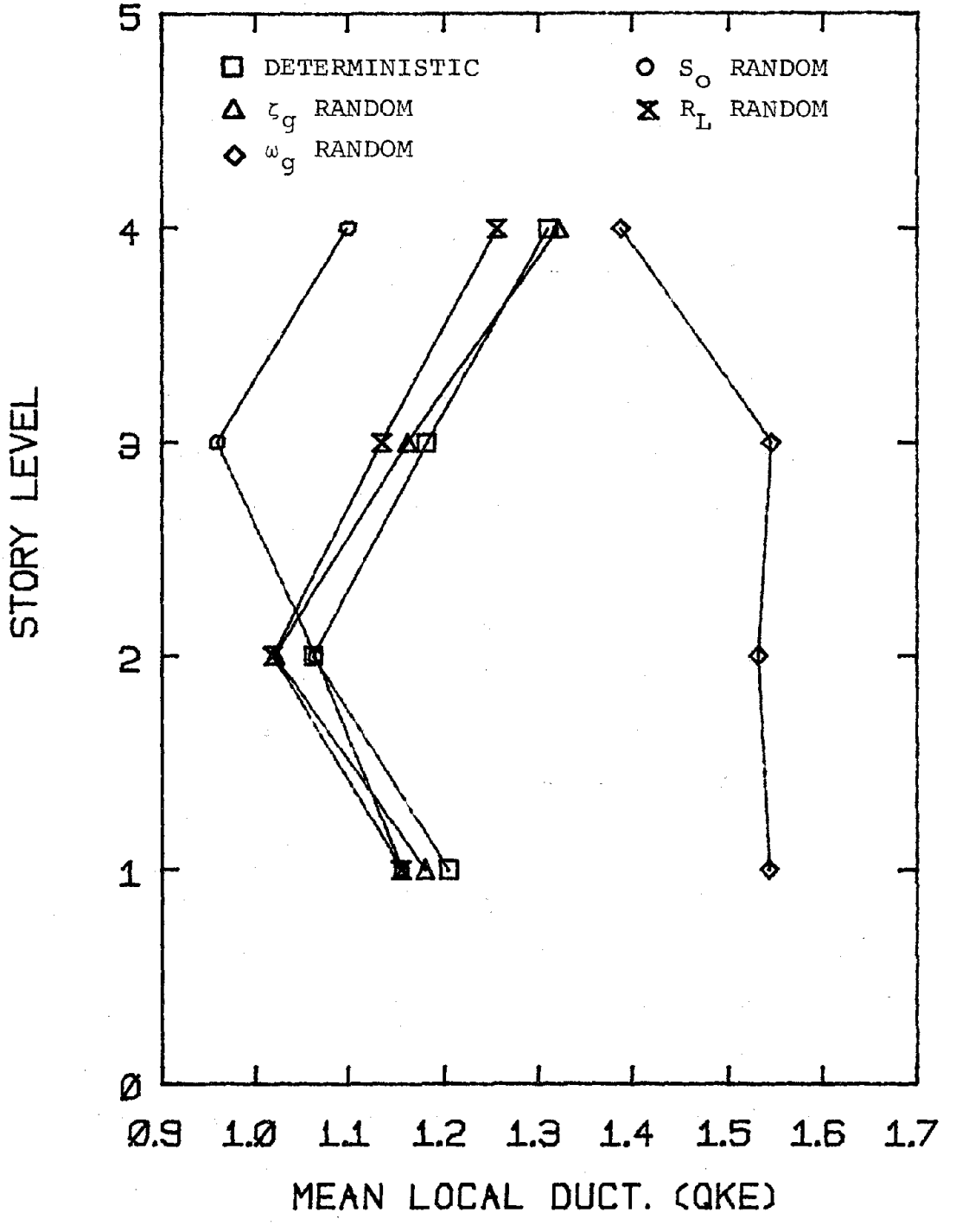

FIG. 5-4 SENSITIVITY OF LOCAL RESPONSE ON GROUND MOTION PARAMETERS AND LOCAL DUCTILITY CORRECTION FACTOR (4-STORY FRAME)

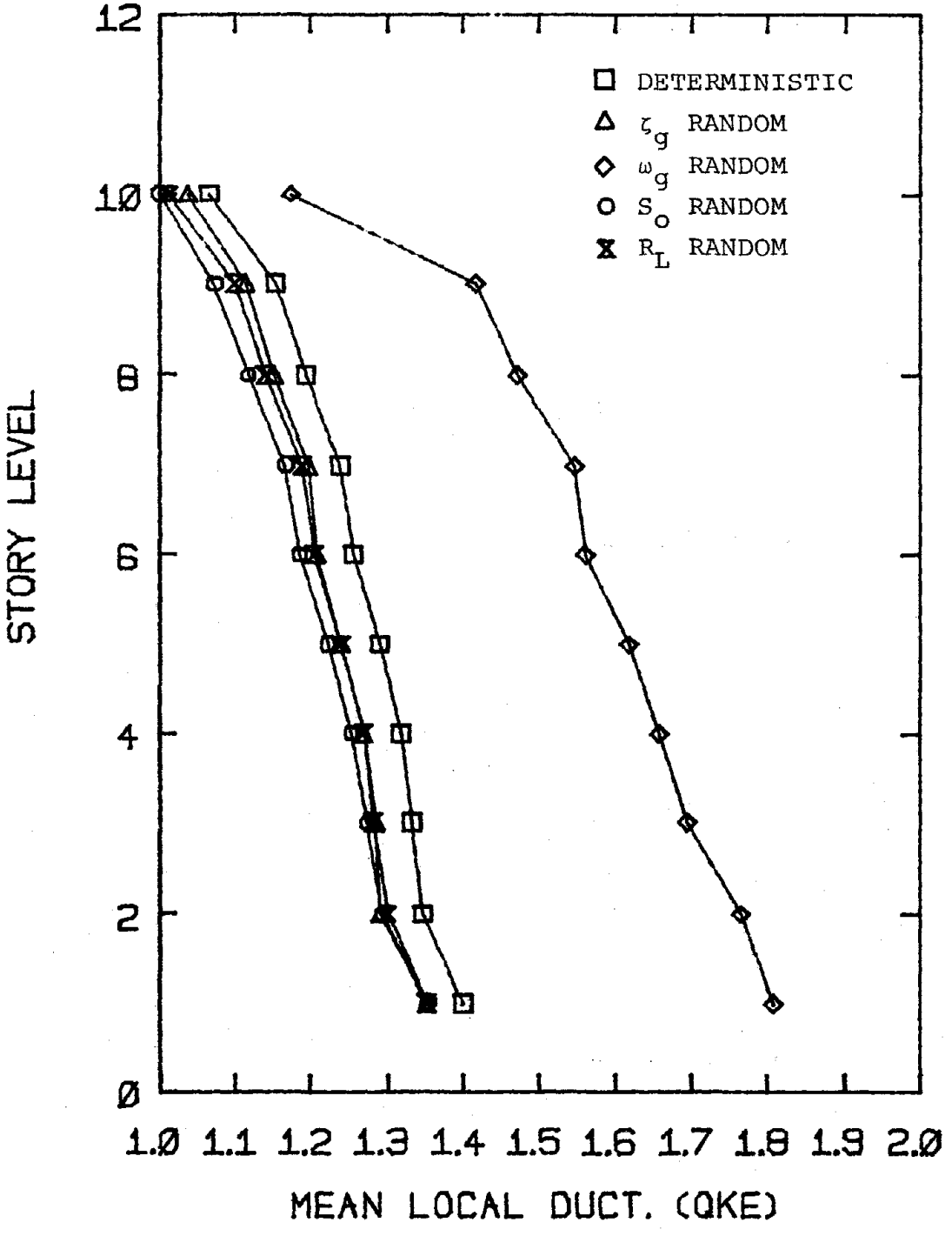

FIG. 5-5 SENSITIVITY OF LOCAL RESPONSE ON GROUND MOTION PARAMETERS AND LOCAL DUCTILITY CORRECTION FACTOR (10-STORY FRAME)

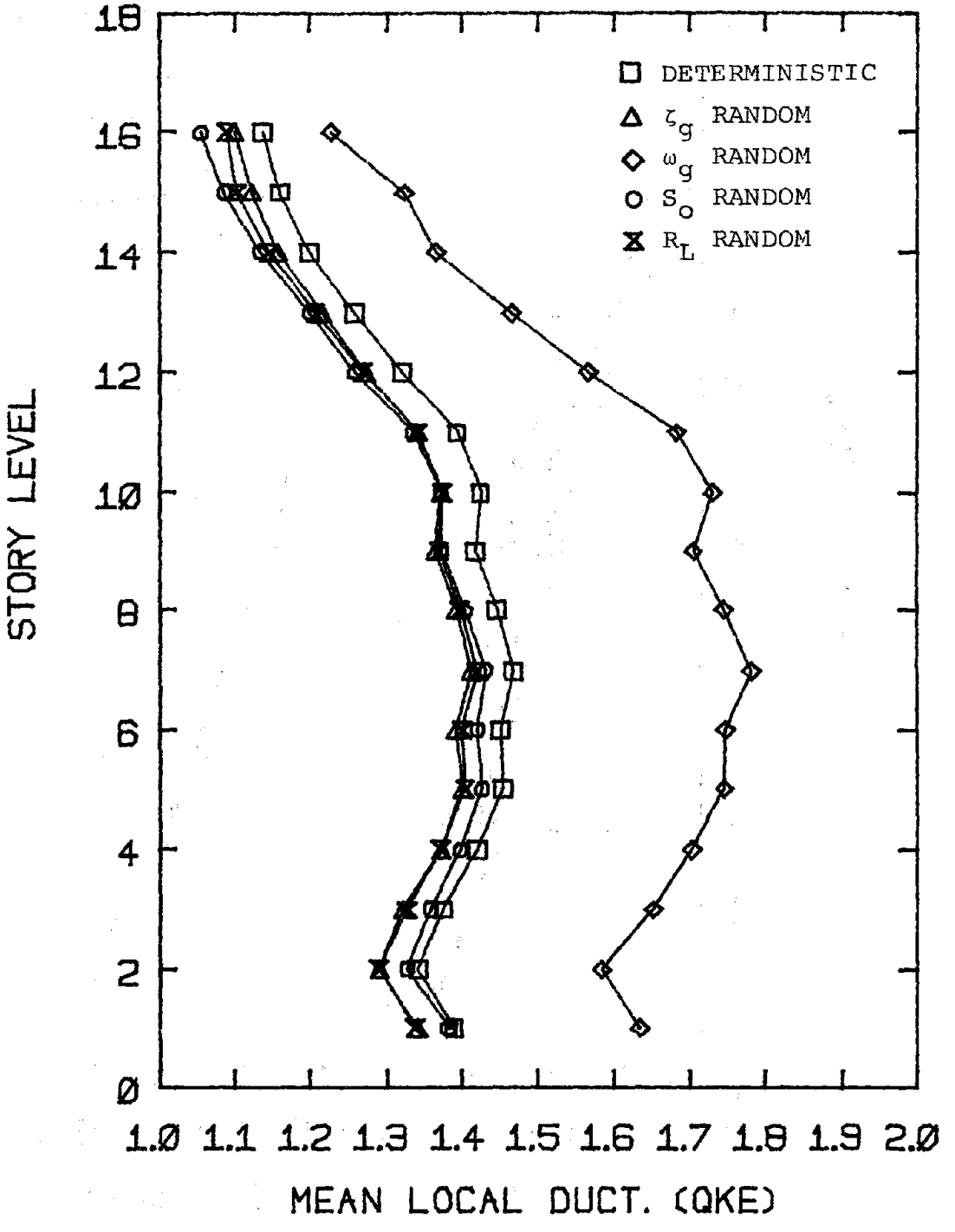

FIG. 5-6 SENSITIVITY OF LOCAL RESPONSE ON GROUND MOTION PARAMETERS AND LOCAL DUCTILITY CORRECTION FACTOR (16-STORY FRAME)

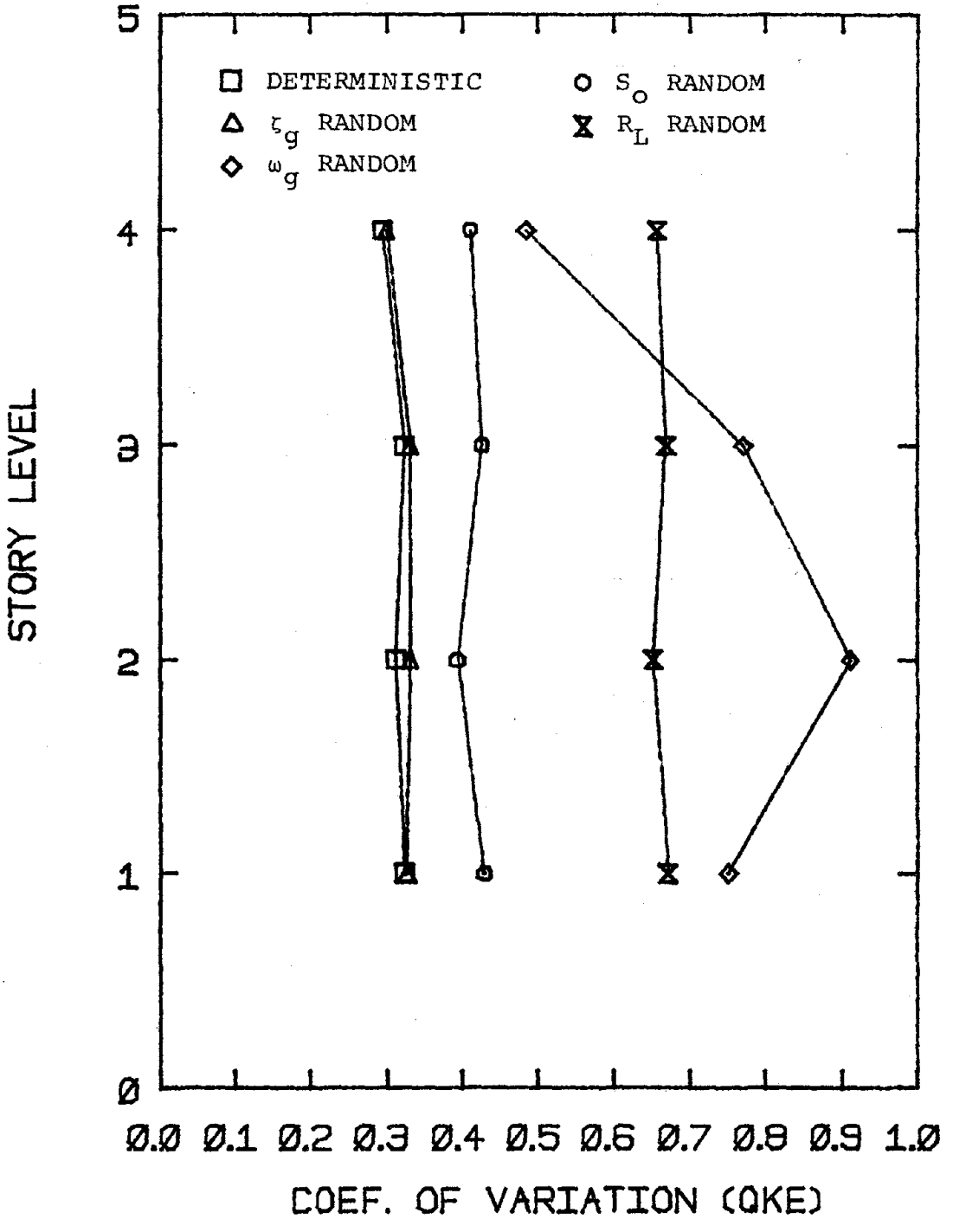

FIG. 5-7 SENSITIVITY OF C.O.V. OF LOCAL RESPONSE ON GROUND MOTION PARAMETERS AND LOCAL DUCTILITY CORRECTION FACTOR (4-STORY FRAME)

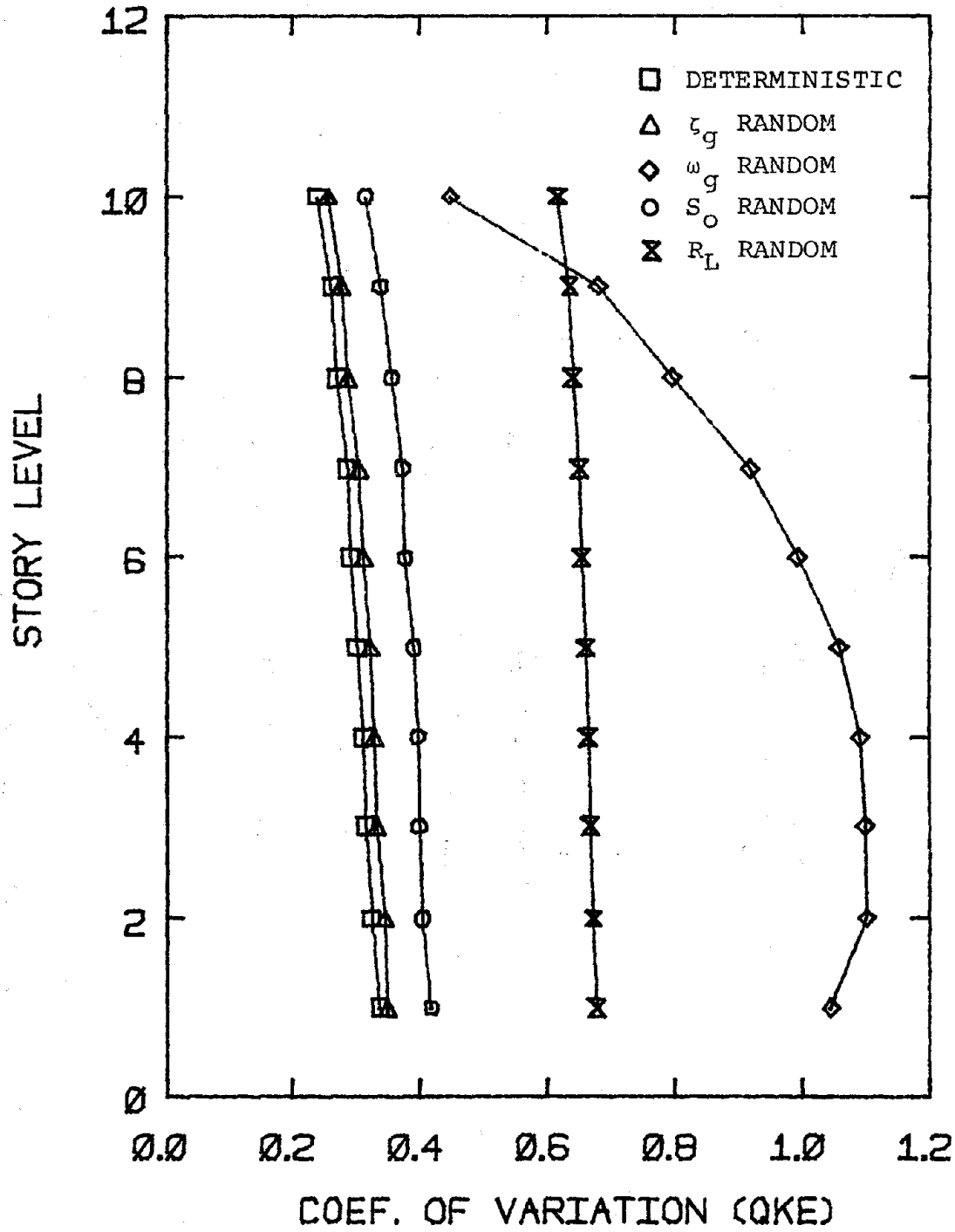

FIG. 5-8 SENSITIVITY OF C.O.V. OF LOCAL RESPONSE ON GROUND MOTION PARAMETERS AND LOCAL DUCTILITY CORRECTION FACTOR (10-STORY FRAME)

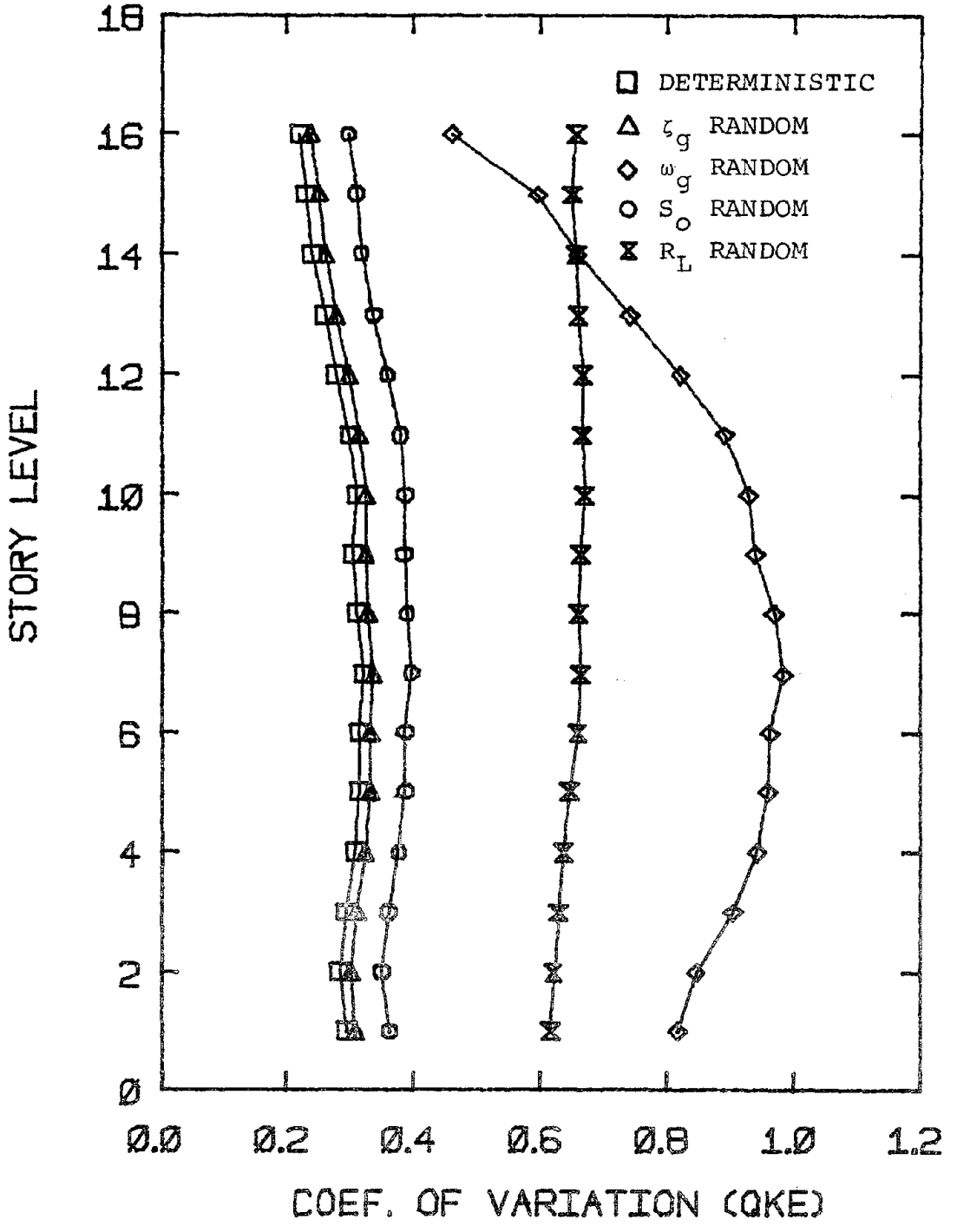

FIG. 5-9 SENSITIVITY OF C.O.V. OF LOCAL RESPONSE ON GROUND MOTION PARAMETERS AND LOCAL DUCTILITY CORRECTION FACTOR (16-STORY FRAME)

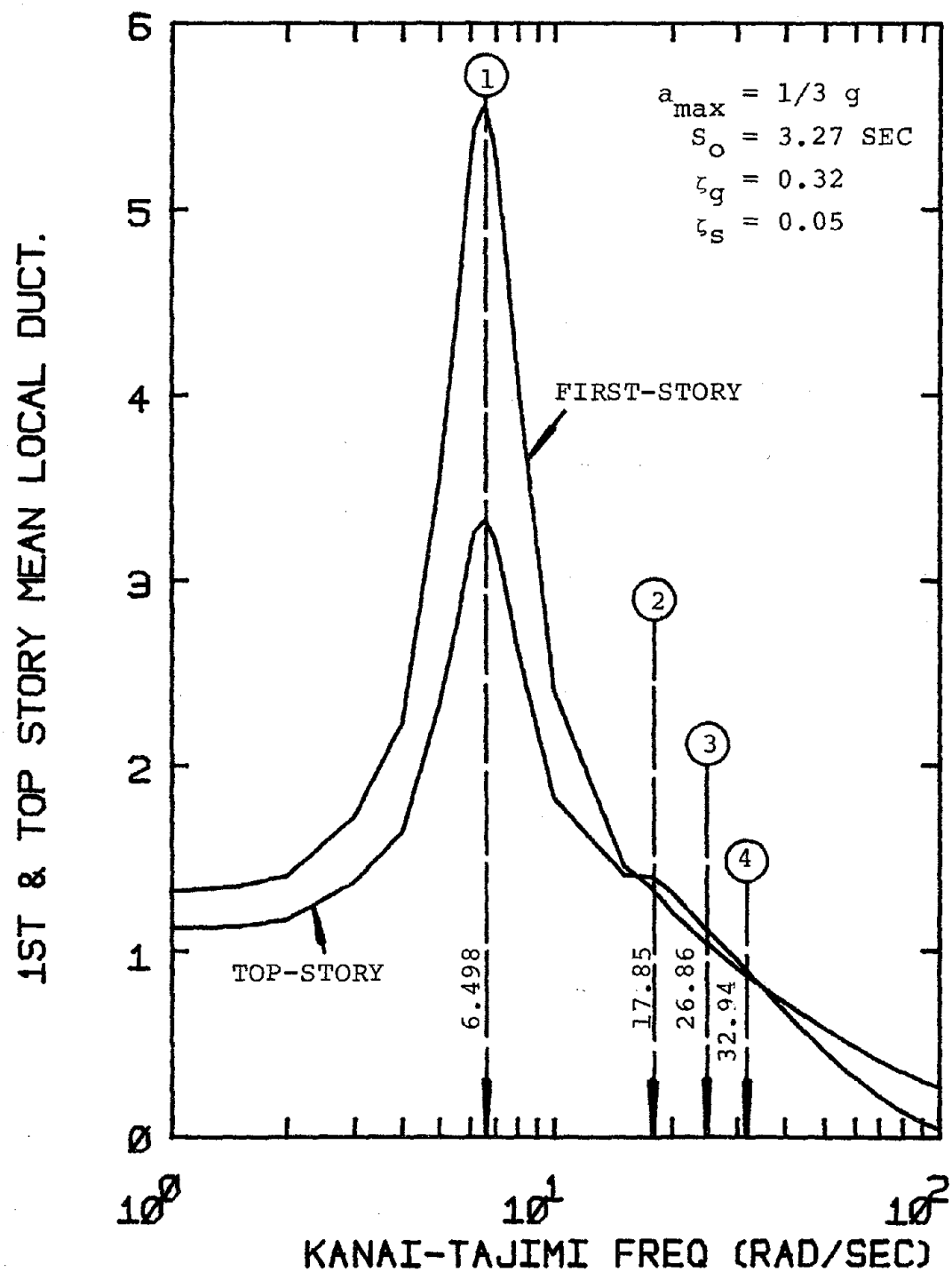

FIG. 5-10 1ST- AND TOP-STORY MEAN LOCAL DUCTILITY RATIOS VERSUS KANAI-TAJIMI FREQUENCY (4-STORY FRAME)

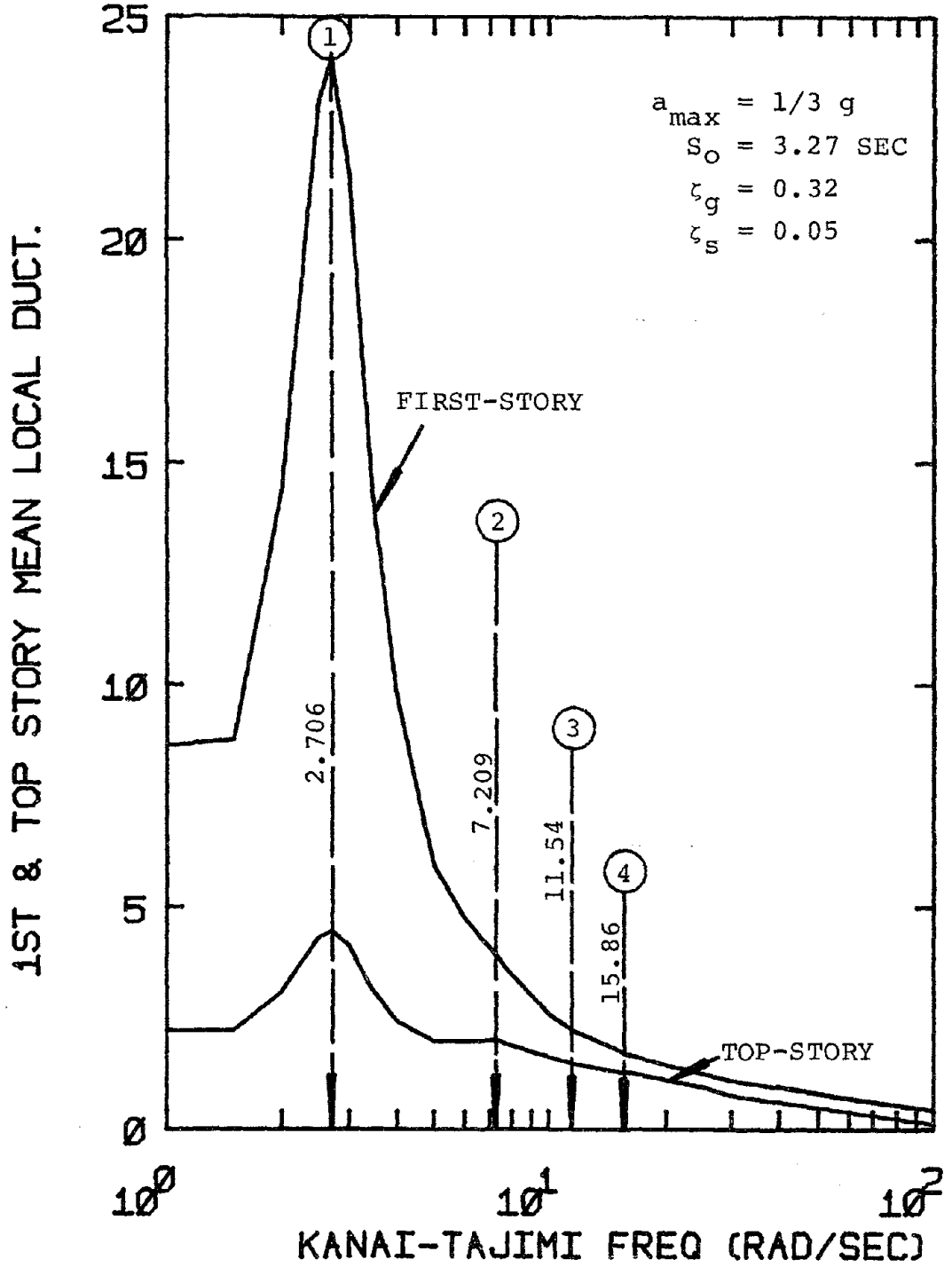

FIG. 5-11 1ST- AND TOP-STORY MEAN LOCAL DUCTILITY RATIOS VERSUS KANAI-TAJIMI FREQUENCY (10-STORY FRAME)

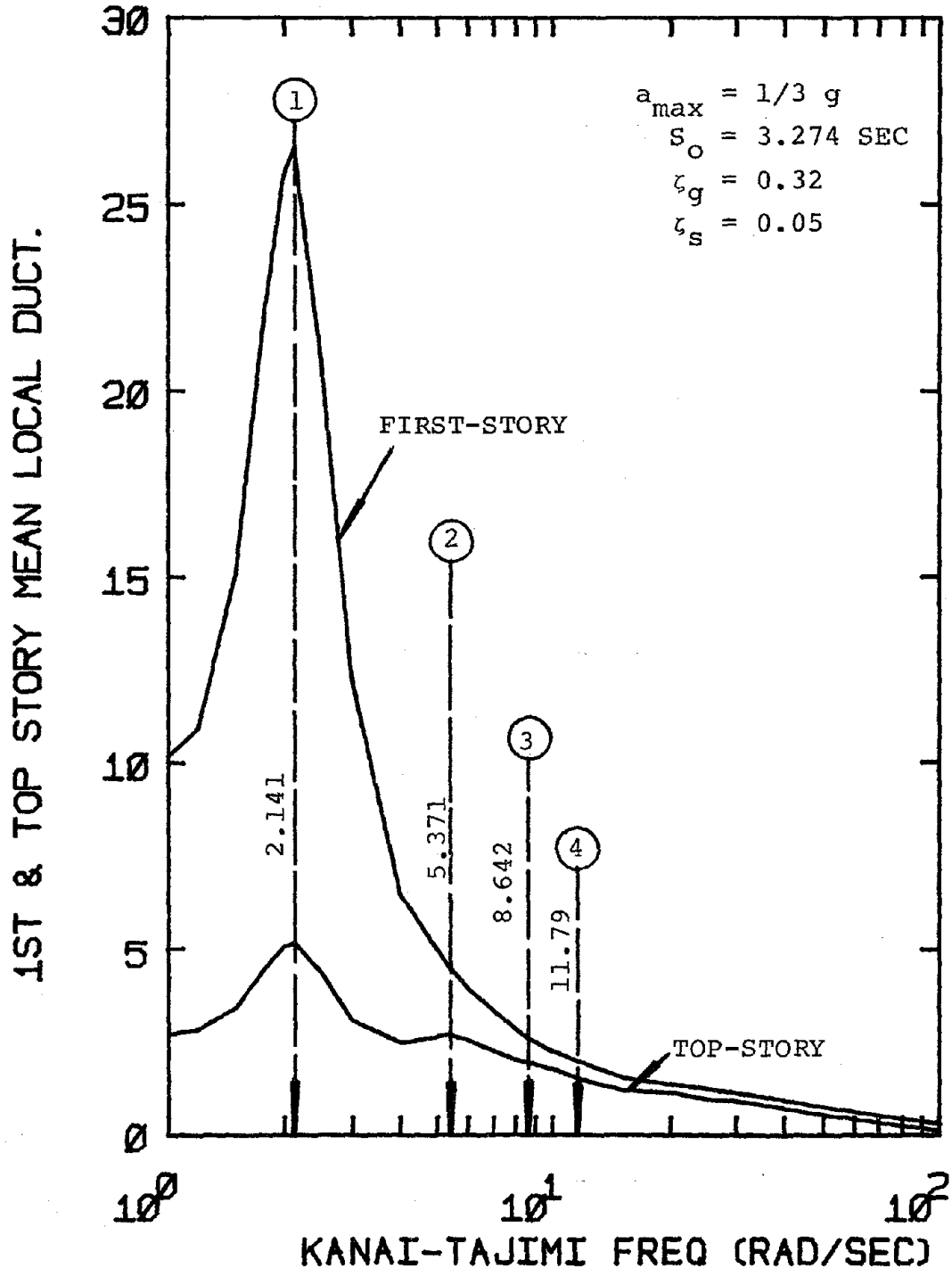

FIG. 5-12 1ST- AND TOP-STORY MEAN LOCAL DUCTILITY RATIOS VERSUS KANAI-TAJIMI FREQUENCY (16-STORY FRAME)

are plotted in Figures 5-10, 5-11 and 5-12, respectively. The natural frequencies of the first four modes are also indicated in the figures.

Notice that the local response characteristics of the three steel frames depend significantly on the Kanai-Tajimi frequency. In particular, the first-story mean local ductility ratio reaches its peak when the K-T frequency coincides with the fundamental natural frequency of the structural frame. The effects of higher modes are relatively unimportant. For the top-story, the local inelastic response is still dominated by the fundamental mode; however, the effects of the second mode are more pronounced. From the results, it may be concluded that the Kanai-Tajimi frequency is a most important ground motion parameter with respect to the local inelastic response of structural frames.

5.4.3 Sensitivity of Structural Dynamic Properties

Three structural dynamic properties are considered in the sensitivity studies: i) natural period ratio, ii) structural damping, and iii) yielding strength factor. Table 5-1 lists the discretized probability mass function of each of the three structural dynamic properties. For the three steel frames, the results of the analyses of sensitivity with respect to the structural dynamic properties are plotted in Figures 5-13 through 5-18.

As mentioned in the preceding section, the local inelastic response is significantly related to the fundamental natural frequency of the structure. Since the natural period ratio R_T will change the fundamental frequency, the local inelastic response may be expected to be strongly dependent on the natural period ratio. This is confirmed by the results shown in the figures.

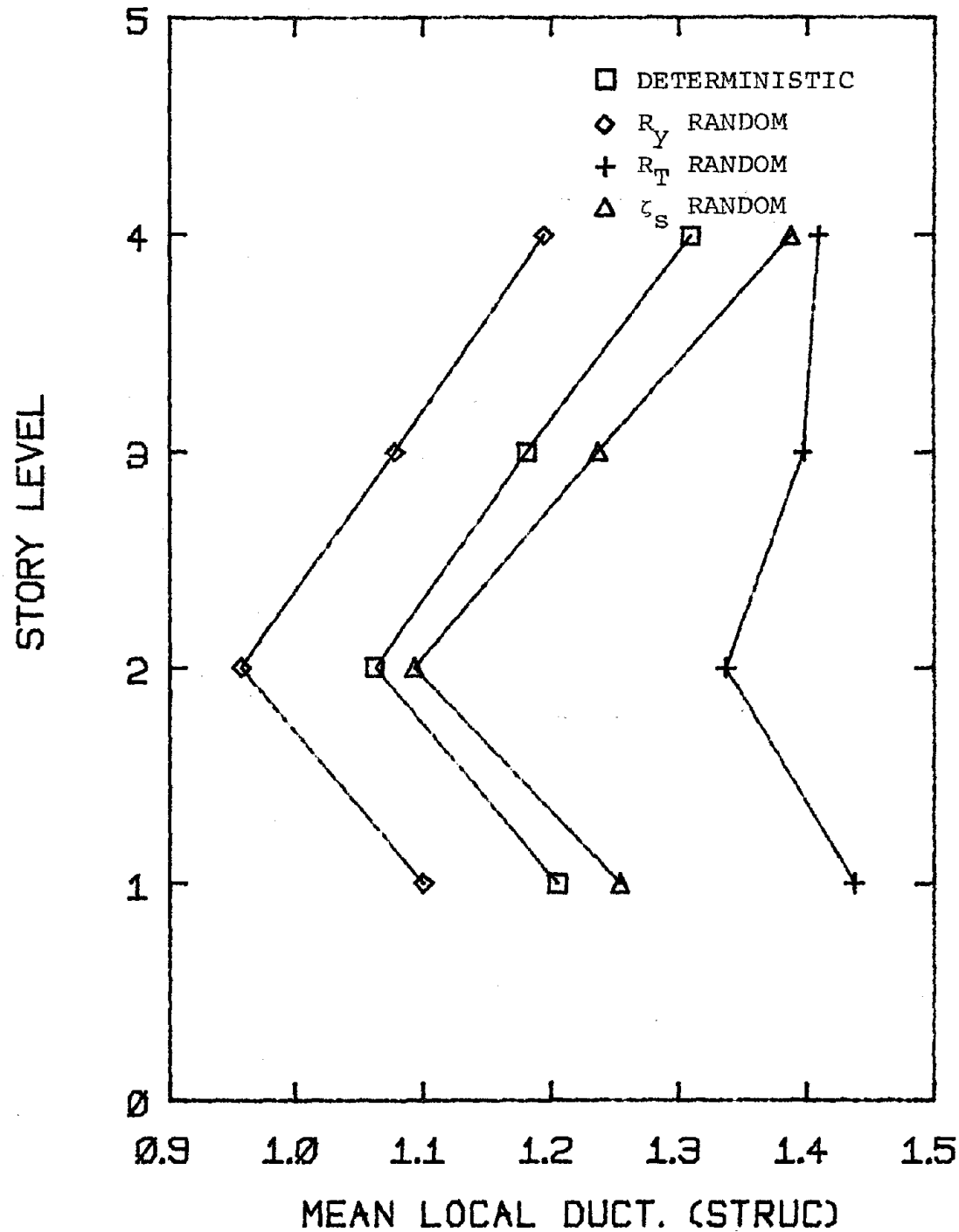

FIG. 5-13 SENSITIVITY OF LOCAL RESPONSE ON STRUCTURAL DYNAMIC PROPERTIES (4-STORY FRAME)

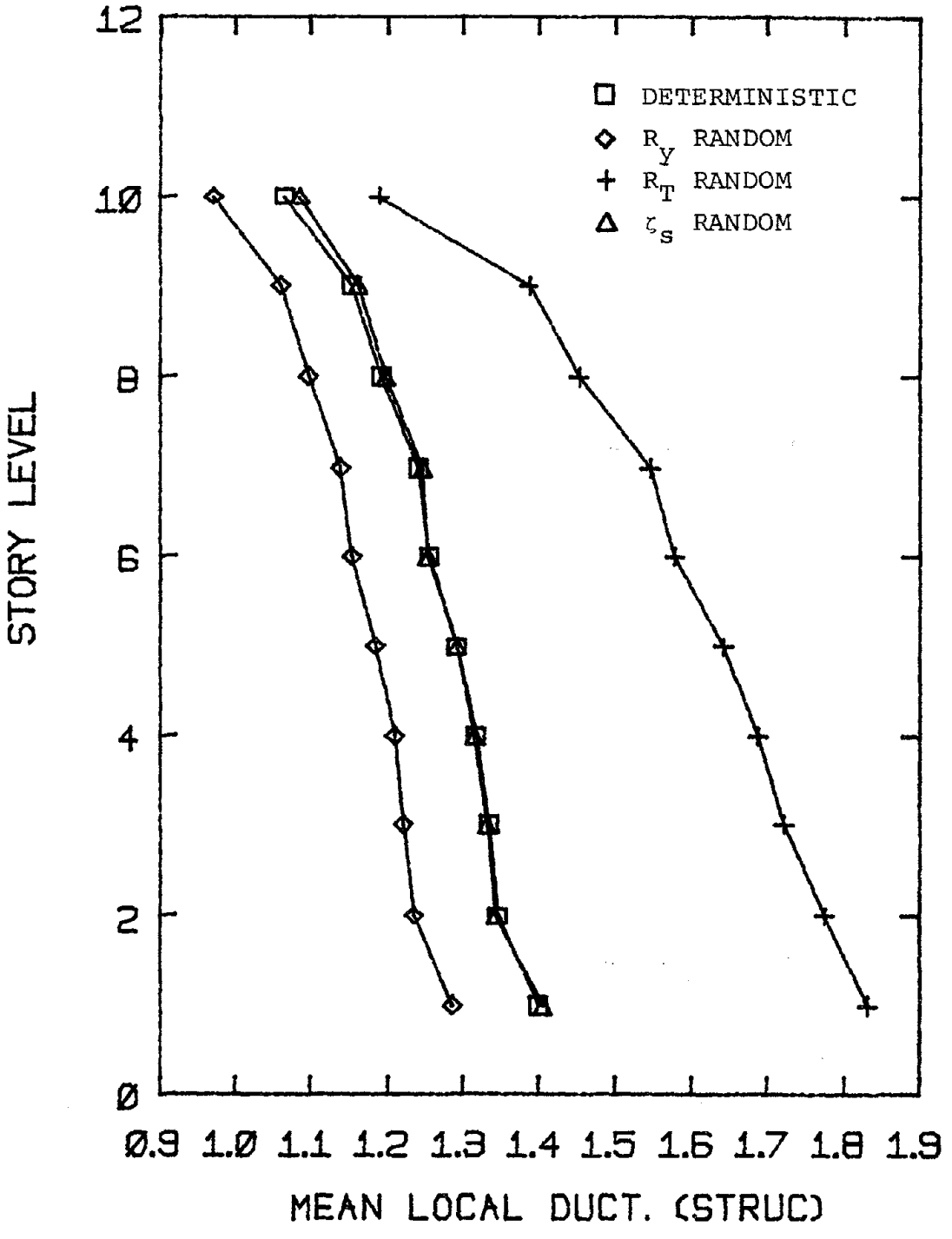

FIG. 5-14 SENSITIVITY OF LOCAL RESPONSE ON STRUCTURAL DYNAMIC PROPERTIES (10-STORY FRAME)

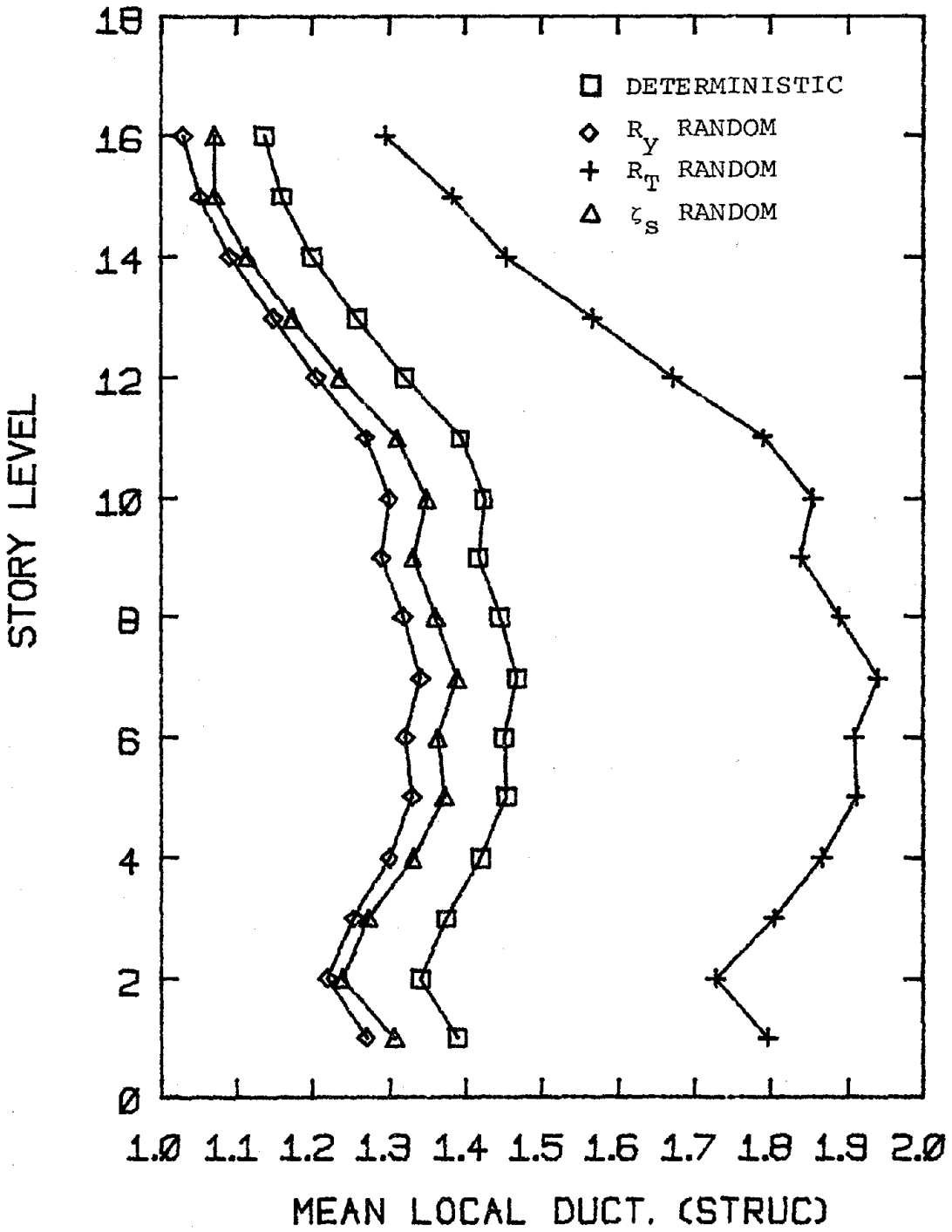

FIG. 5-15 SENSITIVITY OF LOCAL RESPONSE ON STRUCTURAL DYNAMIC PROPERTIES (16-STORY FRAME)

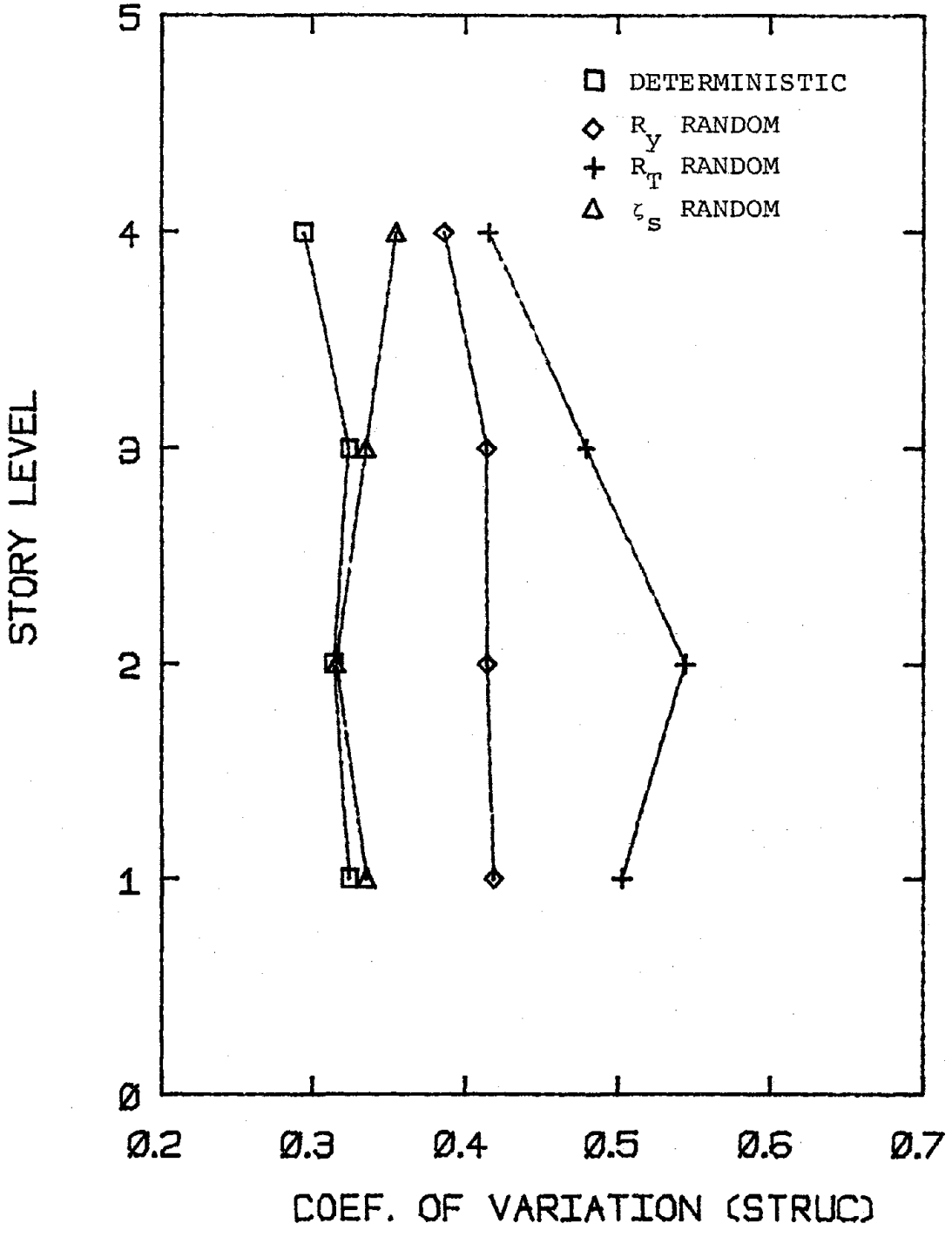

FIG. 5-16 SENSITIVITY OF C.O.V. OF LOCAL RESPONSE ON STRUCTURAL DYNAMIC PROPERTIES (4-STORY FRAME)

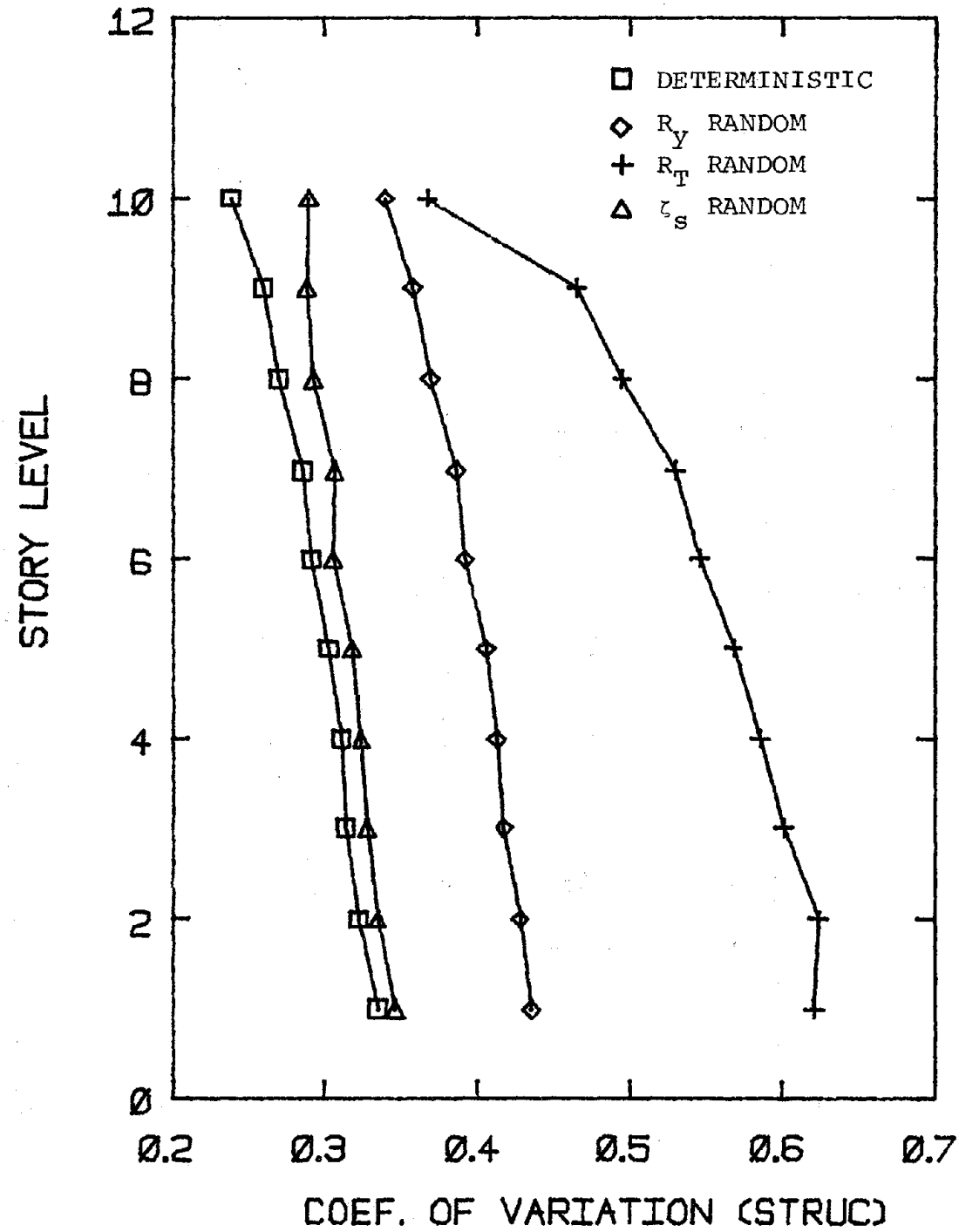

FIG. 5-17 SENSITIVITY OF C.O.V. OF LOCAL RESPONSE ON STRUCTURAL DYNAMIC PROPERTIES (10-STORY FRAME)

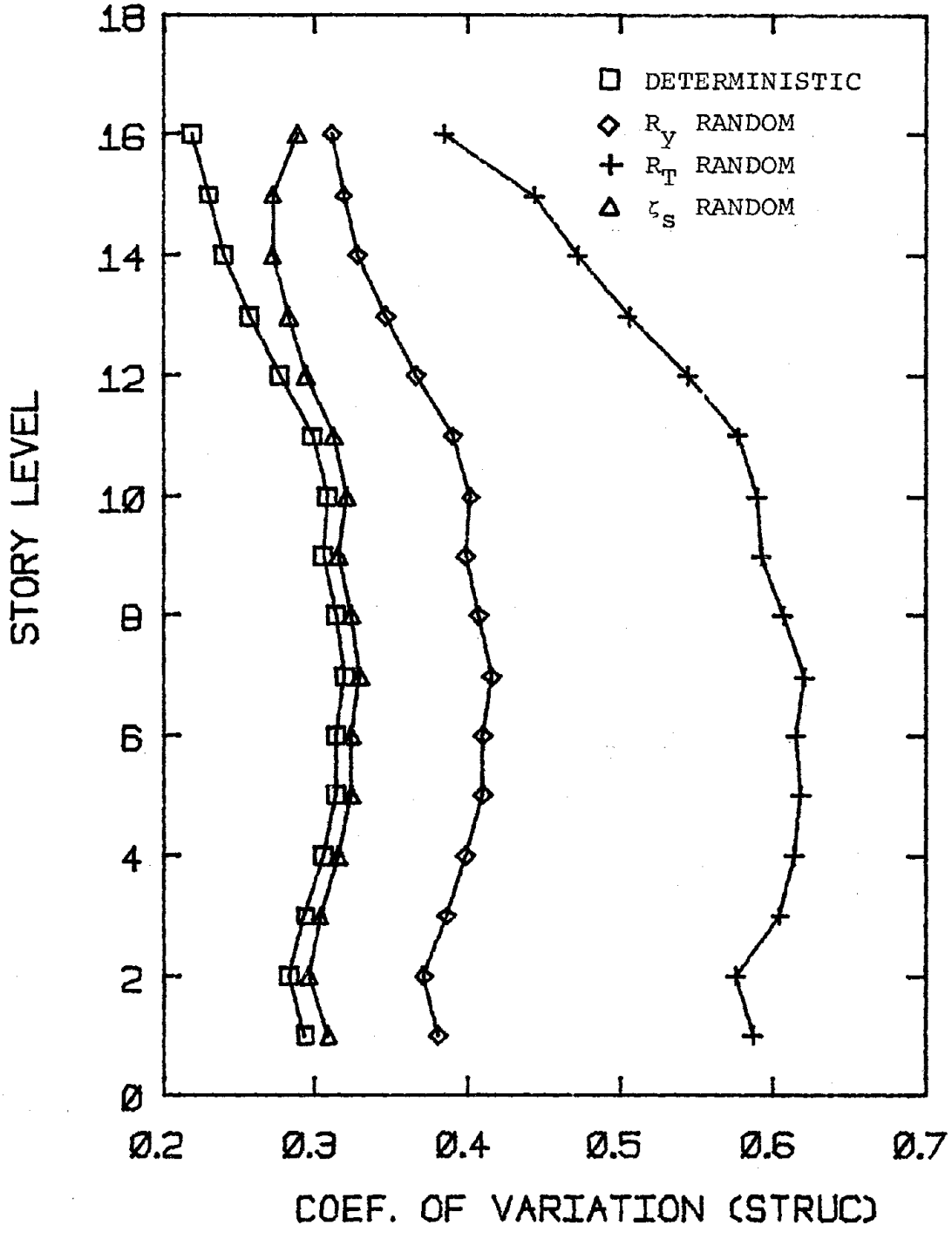

FIG. 5-18 SENSITIVITY OF C.O.V. OF LOCAL RESPONSE ON STRUCTURAL DYNAMIC PROPERTIES (16-STORY FRAME)

When the yielding strength factor is random, the mean local ductility ratio is generally smaller than it is in the deterministic case. This is mainly attributable to the fact that the mean value for the yielding strength factor is equal to 1.128, whereas the value of one is assumed in the deterministic analysis.

Notice that the local inelastic response is surprisingly insensitive to variation of the structural damping. This is further illustrated by plotting the first- and top-story mean local ductility ratios versus structural damping for the three steel frames in Fig. 5-19. Theoretically, the inelastic response should increase with decreasing structural damping, but only the results of the 4-story frame conform to this trend. For the 10- and 16-story frames, the mean local ductility ratio does not necessarily increase with decreasing structural damping.

Based on elastic random vibration theory, when the system damping is small, the response will usually take a long time to reach "stationarity" [24]. For example, a suddenly excited linear-elastic 5% damped system requires about five response cycles to achieve approximate stationarity. The fundamental natural period of the 10-story steel frame is equal to 2.32 sec, hence the excitation duration required to attain stationarity is about 12 sec. However, the strong-motion duration used in the sensitivity studies is only 3.27 sec, obviously not long enough to reach the stationary response.

For comparison, an additional sensitivity analysis of the 10-story frame was performed based on a strong-motion duration of 10 sec. The resulting first- and top-story mean local ductility ratios are plotted in Fig. 5-20. The original results corresponding to the 3.27 sec duration

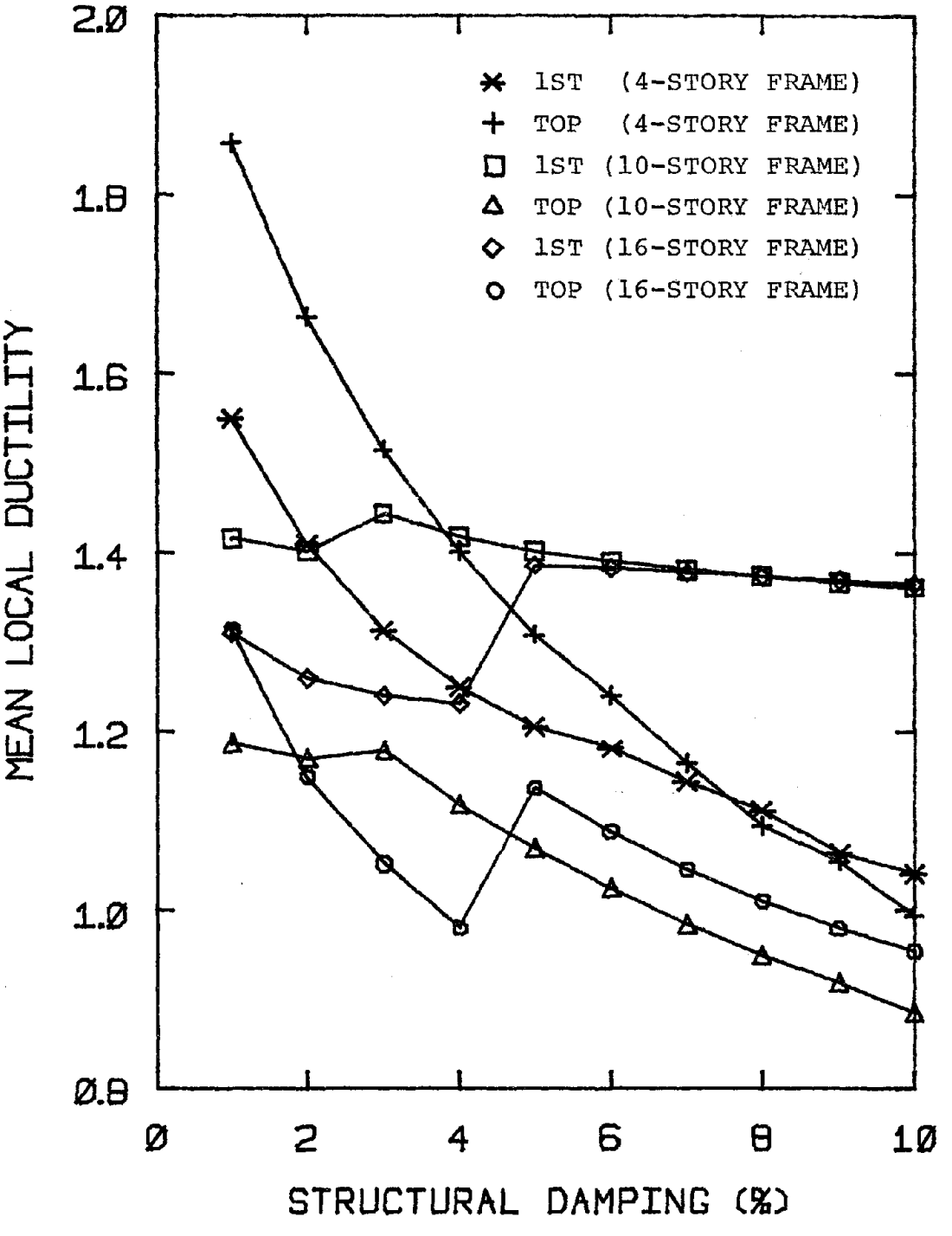

FIG. 5-19 SENSITIVITY OF 1ST- AND TOP-STORY MEAN LOCAL DUCTILITY RATIOS ON STRUCTURAL DAMPING

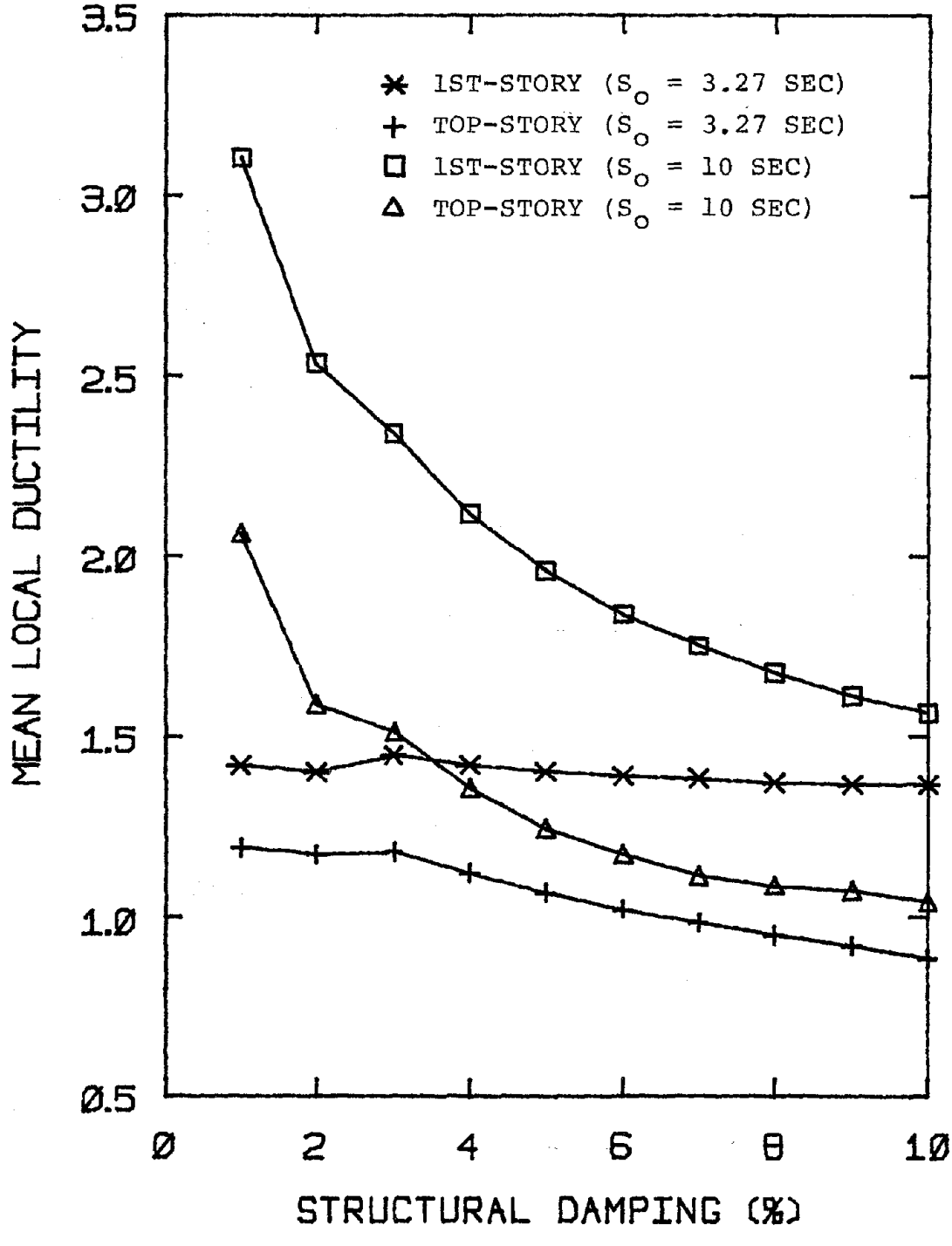

FIG. 5-20 SENSITIVITY OF 1ST- AND TOP-STORY MEAN LOCAL DUCTILITY RATIOS ON STRUCTURAL DAMPING (FOR DIFFERENT STRONG-MOTION DURATIONS, 10-STORY FRAME)

are also presented in the figure. Notice that the mean local ductility ratio now increases with decreasing structural damping. Hence, it may be concluded that the local inelastic response depends in a fairly complicated manner on the strong-motion duration and the structural damping. Nevertheless, the structural damping can be assumed deterministic for the purpose of overall safety evaluation of earthquake-resistant buildings.

5.4.4 Conditionality of Strong-Motion Duration on Peak Ground Acceleration

Thus far in the sensitivity studies, the strong-motion duration has been assumed "conditional" on the peak ground acceleration, and the negative correlation suggested in Eq. 2-18 has been employed. The effect of this assumption has been examined through a series of sensitivity analyses using the "unconditional" (or marginal) strong-motion duration. The results are presented below.

For a given peak ground acceleration of 1/3 g, the conditional probability density function of strong-motion duration (Eq. 5-6) is plotted in Fig. 5-21. Also shown in this figure is the marginal PDF of the strong-motion duration as expressed by Eq. 2-14. The discrete probability mass function for the unconditional strong-motion duration is also listed in Table 5-1.

For the three moment-resisting steel frames, the results of the analyses of sensitivity to the conditionality of duration on peak acceleration are presented in Figures 5-22 to 5-27. The results of the deterministic analyses are also plotted in the figures.

Notice that the mean local ductility ratio generally increases with the strong-motion duration. The mean local ductility ratio corresponding

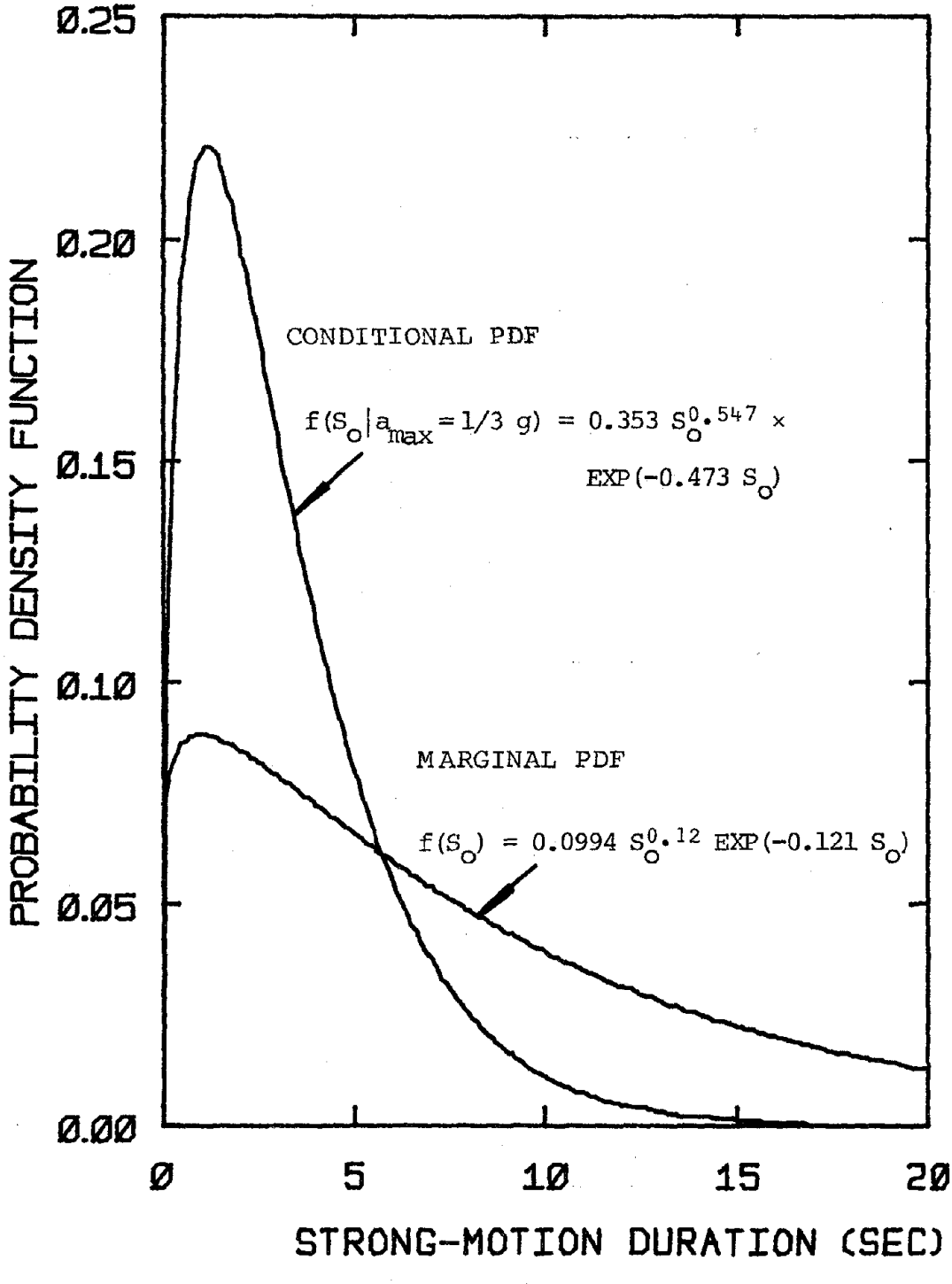

FIG. 5-21 CONDITIONAL AND MARGINAL PROBABILITY DENSITY FUNCTIONS OF STRONG-MOTION DURATION

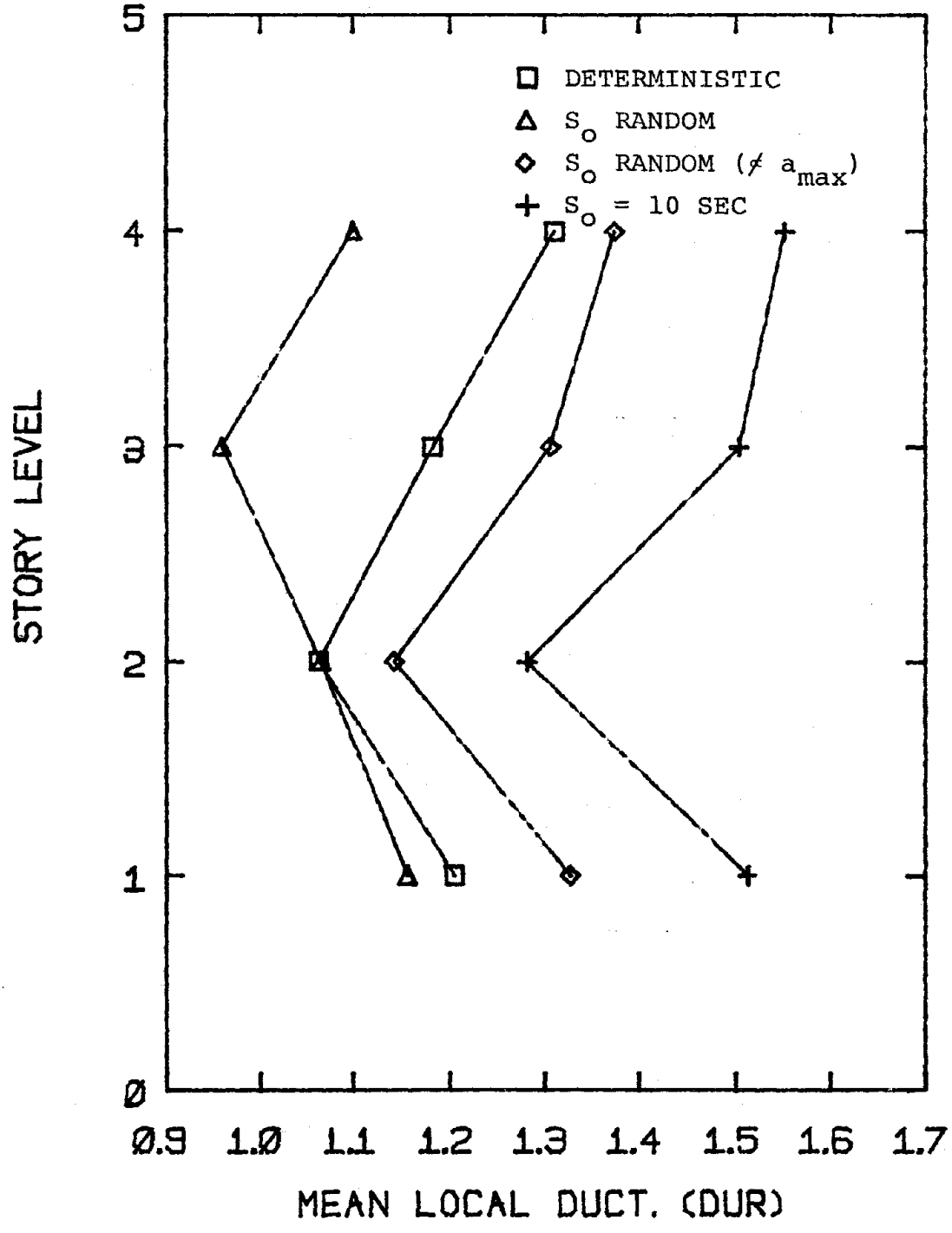

FIG. 5-22 SENSITIVITY OF LOCAL RESPONSE ON CONDITIONALITY OF STRONG-MOTION DURATION (4-STORY FRAME)

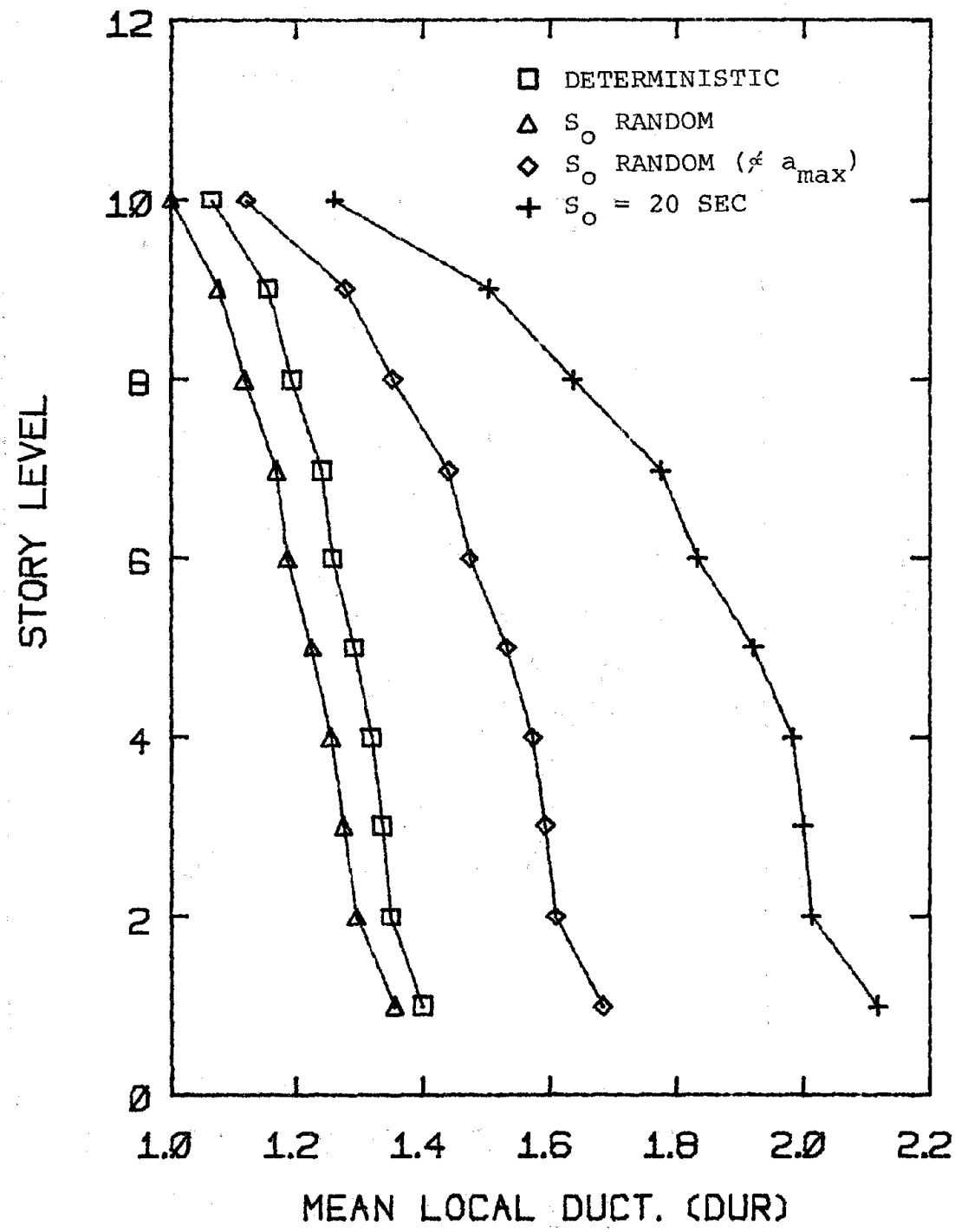

FIG. 5-23 SENSITIVITY OF LOCAL RESPONSE ON CONDITIONALITY OF STRONG-MOTION DURATION (10-STORY FRAME)

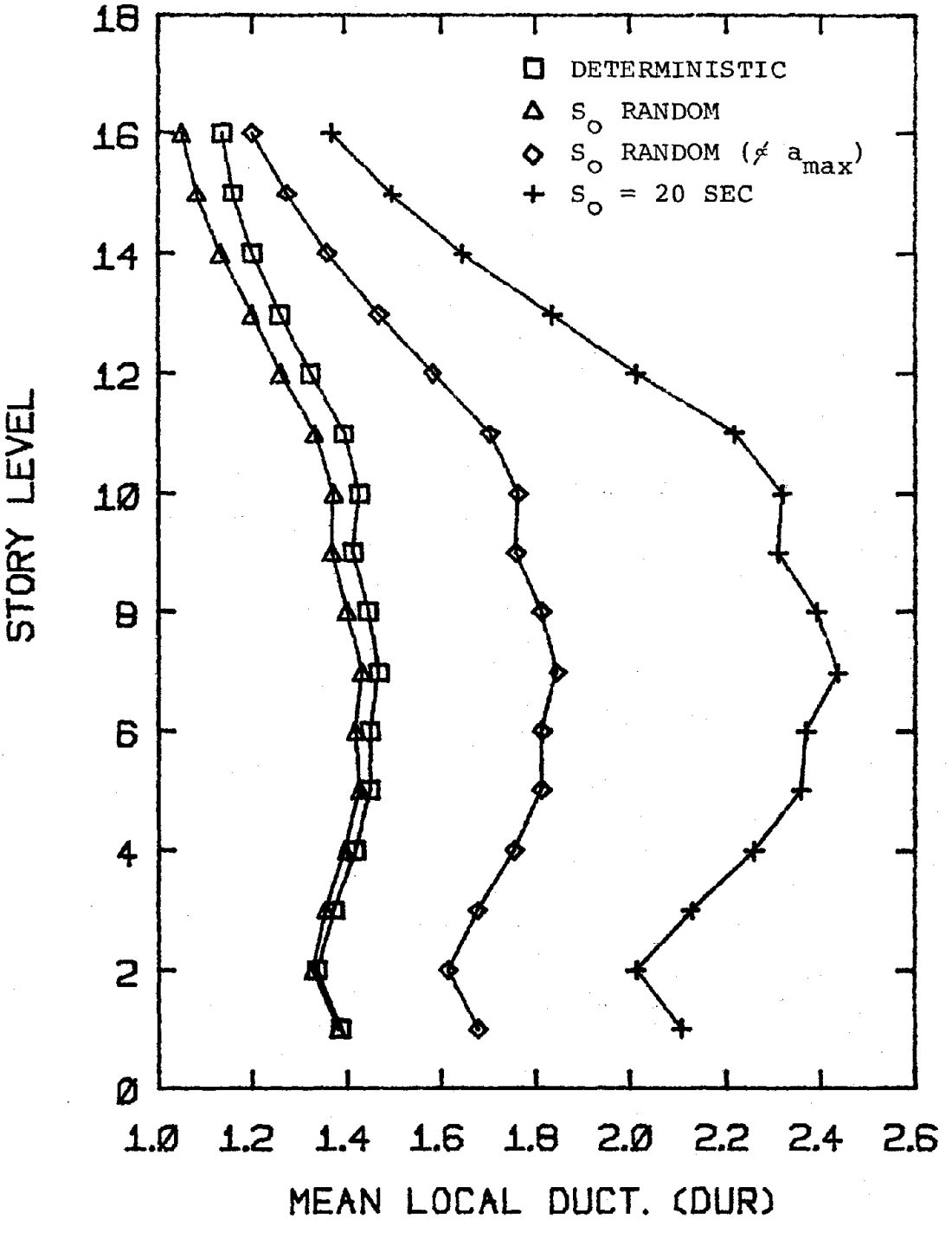

FIG. 5-24 SENSITIVITY OF LOCAL RESPONSE ON CONDITIONALITY OF STRONG-MOTION DURATION (16-STORY FRAME)

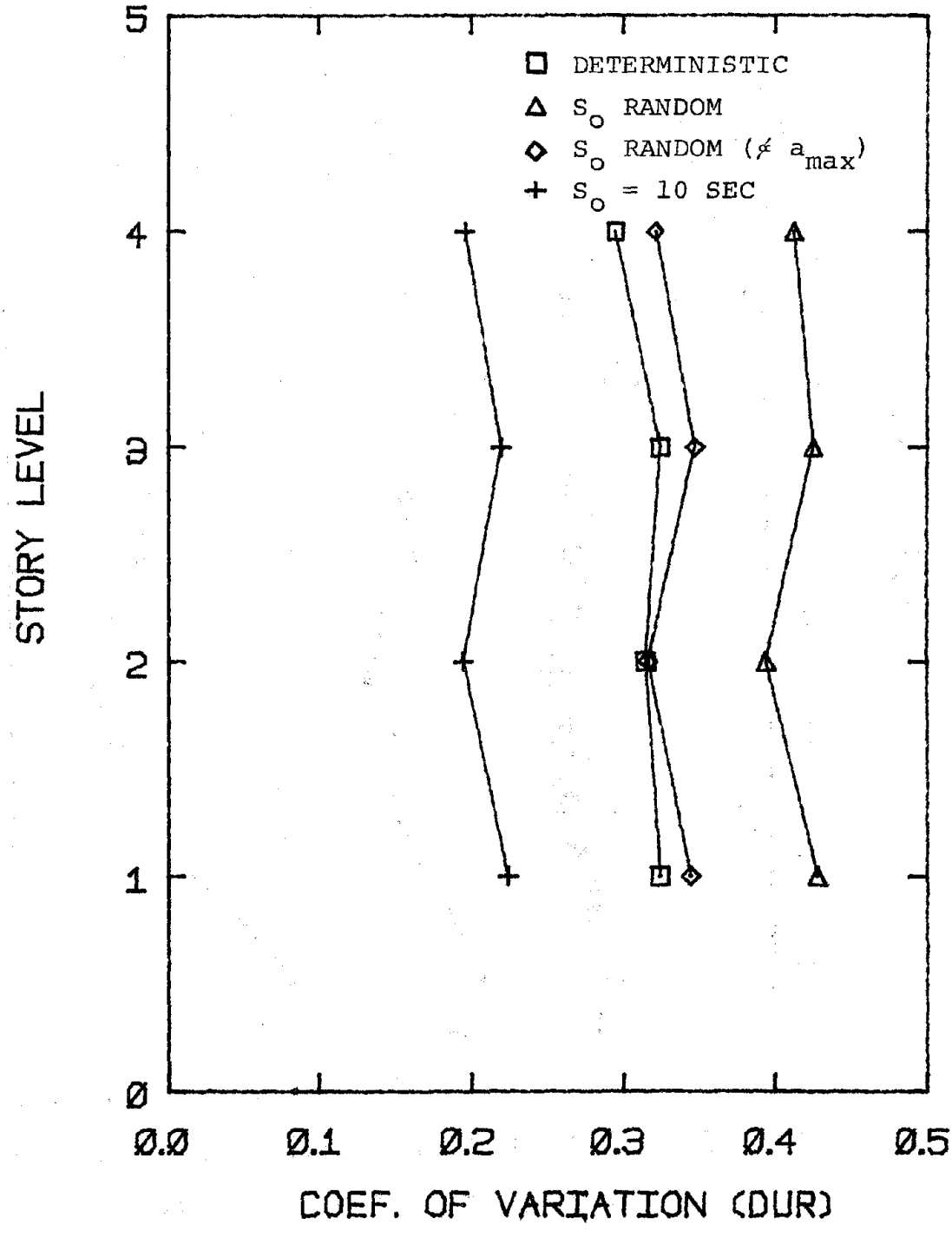

FIG. 5-25 SENSITIVITY OF C.O.V. OF LOCAL RESPONSE ON CONDITIONALITY OF STRONG-MOTION DURATION (4-STORY FRAME)

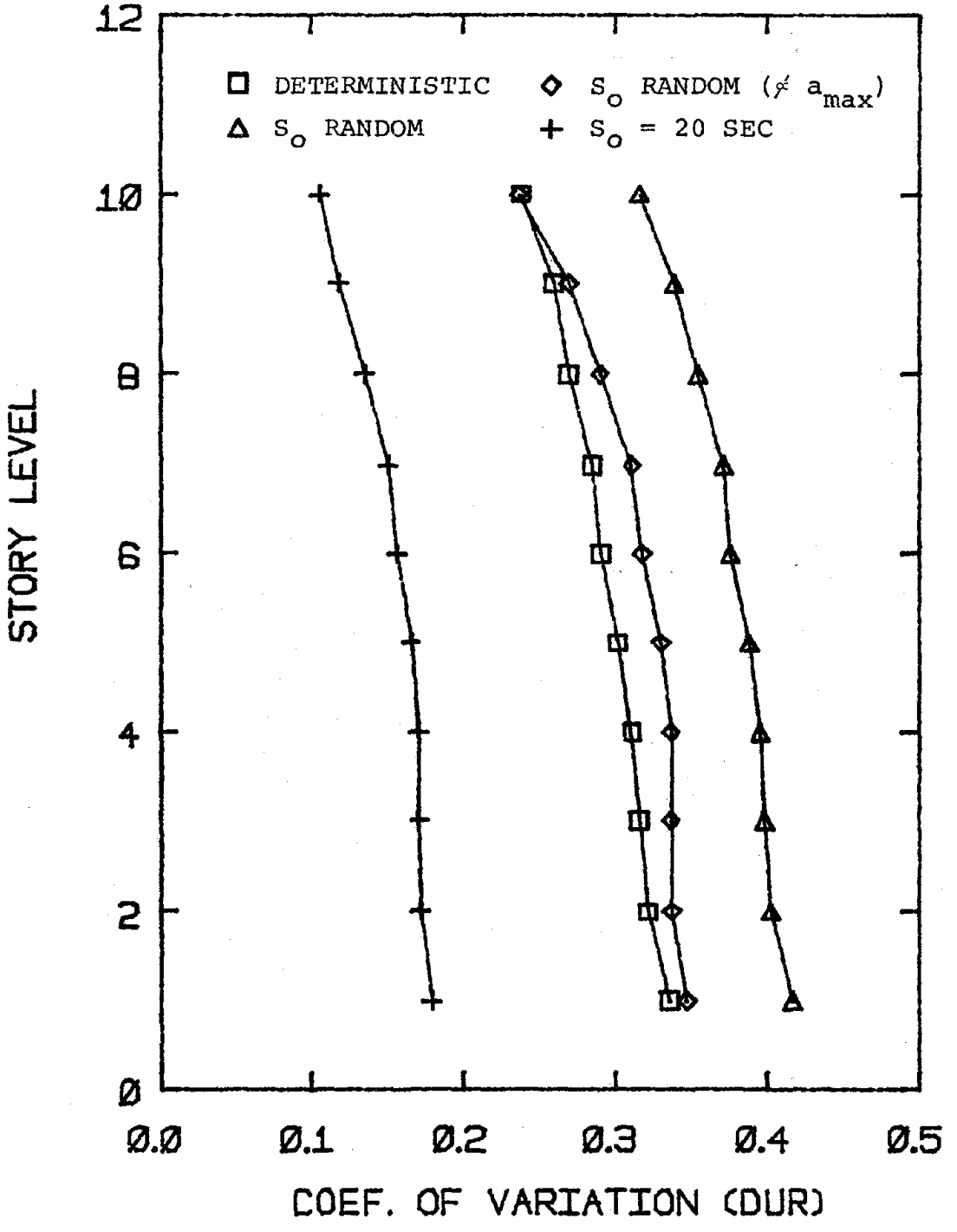

FIG. 5-26 SENSITIVITY OF C.O.V. OF LOCAL RESPONSE ON CONDITIONALITY OF STRONG-MOTION DURATION (10-STORY FRAME)

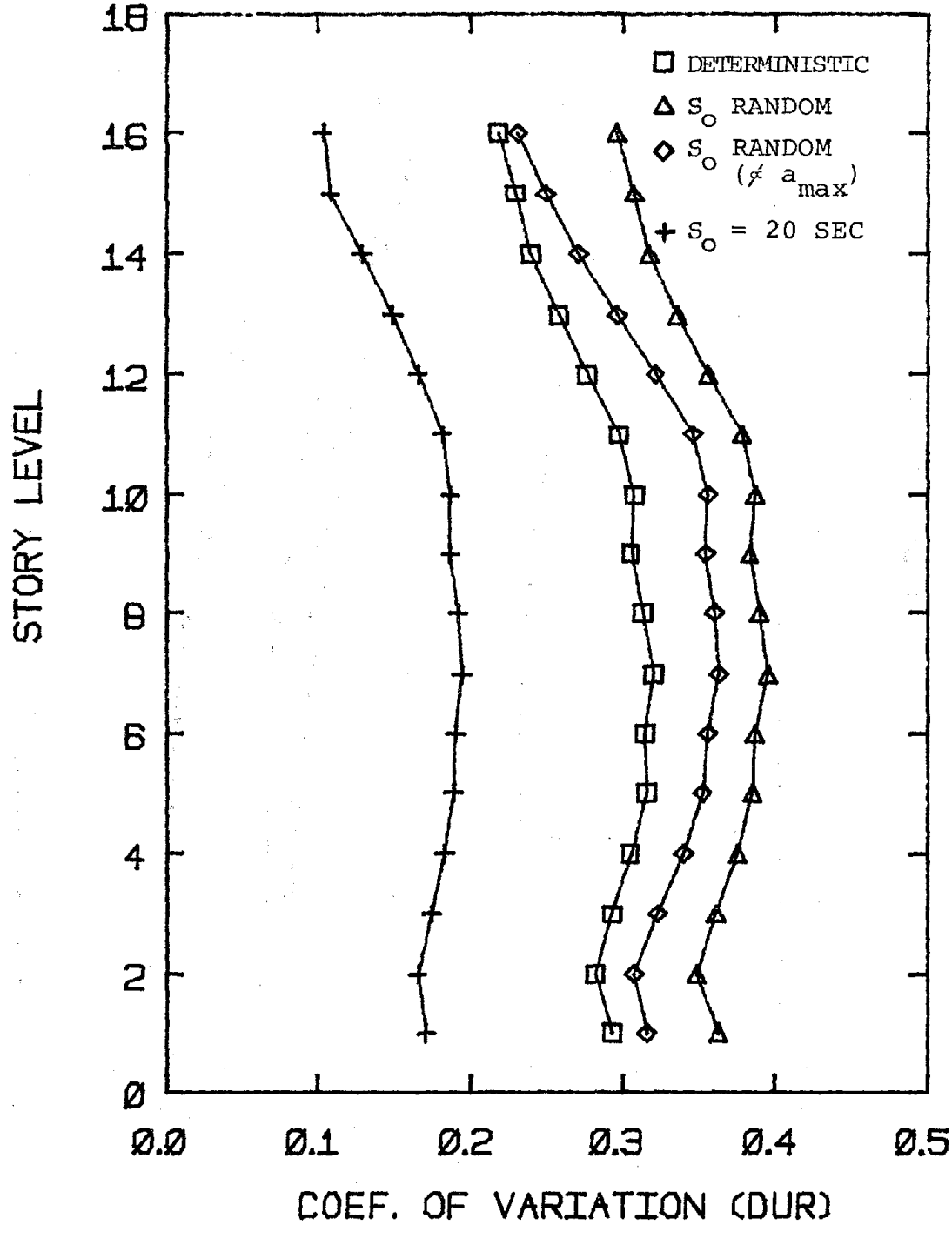

FIG. 5-27 SENSITIVITY OF C.O.V. OF LOCAL RESPONSE ON CONDITIONALITY OF STRONG-MOTION DURATION (16-STORY FRAME)

to the "conditional" strong-motion duration is always smaller than that associated with the "unconditional" strong-motion duration. This may be explained by the fact that the mean value of the conditional strong-motion duration is 3.27 sec, which is smaller than the marginal mean value of 9.27 sec.

By comparison to the sensitivity w.r.t. the Kanai-Tajimi frequency, the variability of the local response due to the "conditionality" of strong-motion duration is insignificant.

5.4.5 Sensitivity of Local Ductility Correction Factor

The local ductility correction factor has been introduced to relate the two different types of response measures, i.e, story response versus local component response. The sensitivity of the local inelastic response w.r.t. the local ductility correction factor has been investigated for the three steel moment-resisting frames. The discrete probability mass function used herein is listed in Table 5-1. The results are presented in Figures 5-4 through 5-9.

The figures show that the mean local ductility is insensitive to variation of the local ductility correction factor. However, the coefficient of variation of the local ductility ratio appears to be quite sensitive. This suggests that the variability of the local ductility correction factor is important for the overall seismic safety assessment of buildings.

5.4.6 Effects of Peak Ground Acceleration

The sensitivity studies of the local inelastic response of structural frames have been based on a peak ground acceleration of 1/3 g. In order to investigate the effect of the peak ground acceleration on the local response prediction, other levels of ground motion intensity are also ex-

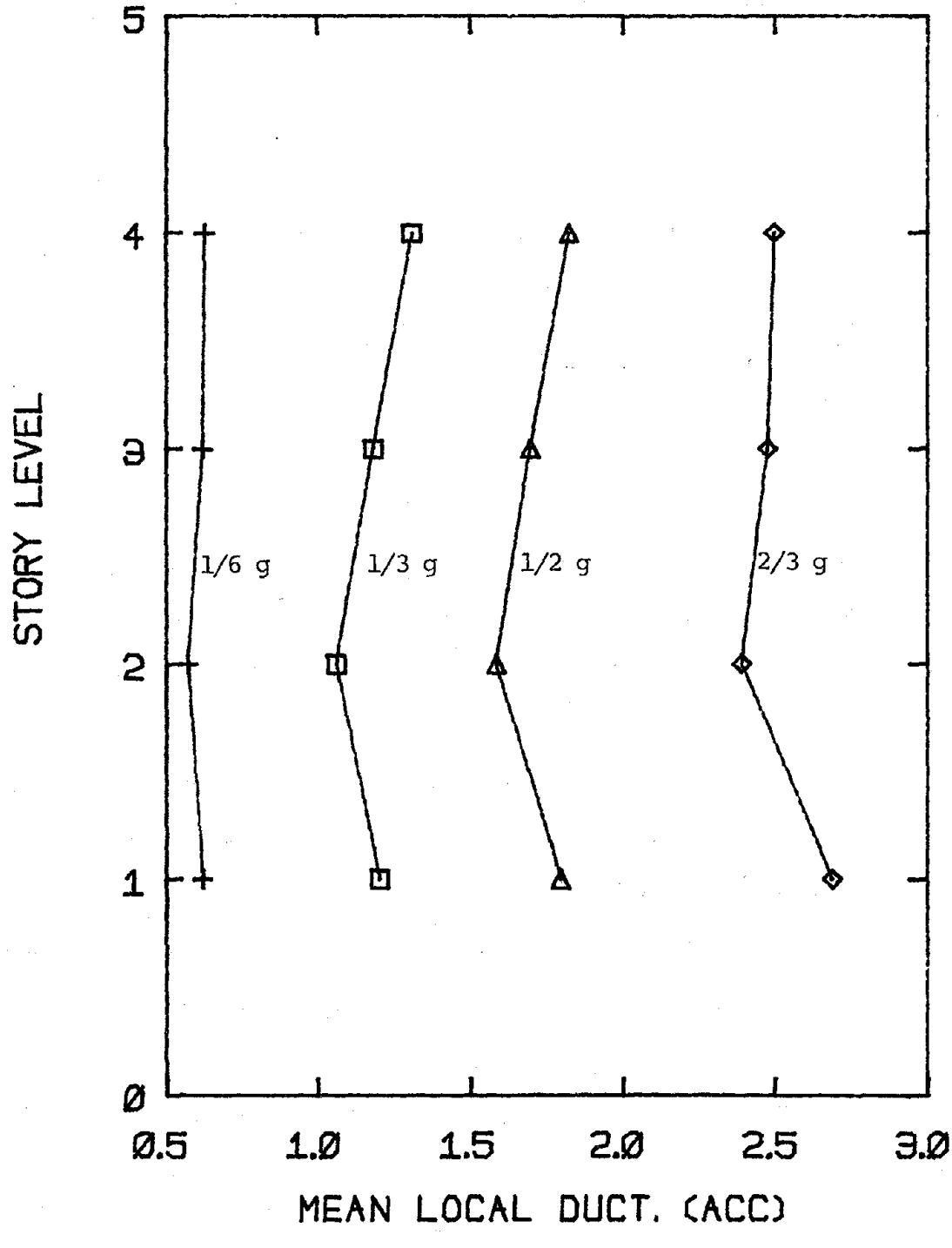

FIG. 5-28 MEAN LOCAL DUCTILITY RATIOS FOR DIFFERENT PEAK GROUND ACCELERATIONS (4-STORY FRAME)

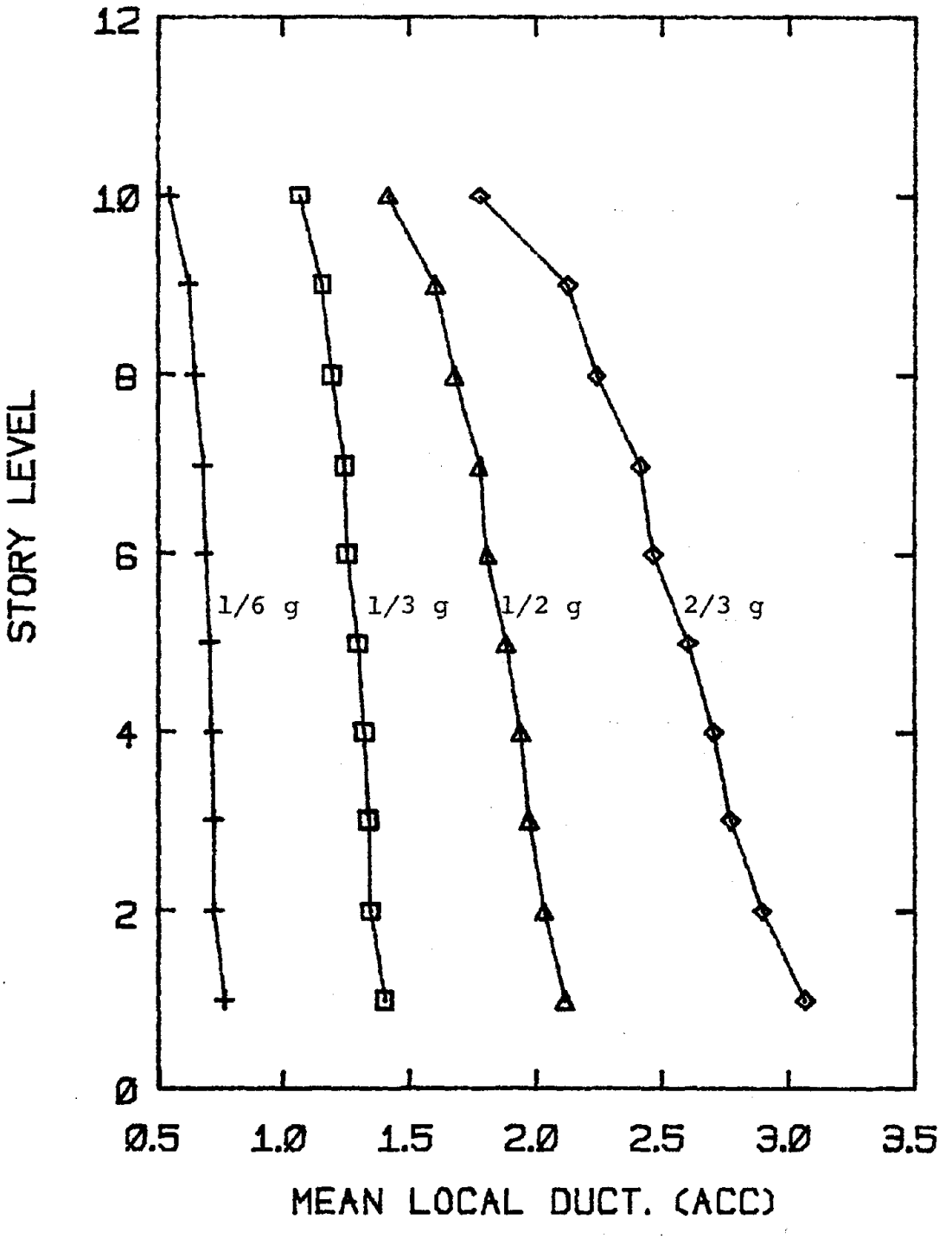

FIG. 5-29 MEAN LOCAL DUCTILITY RATIOS FOR DIFFERENT PEAK GROUND ACCELERATIONS (10-STORY FRAME)

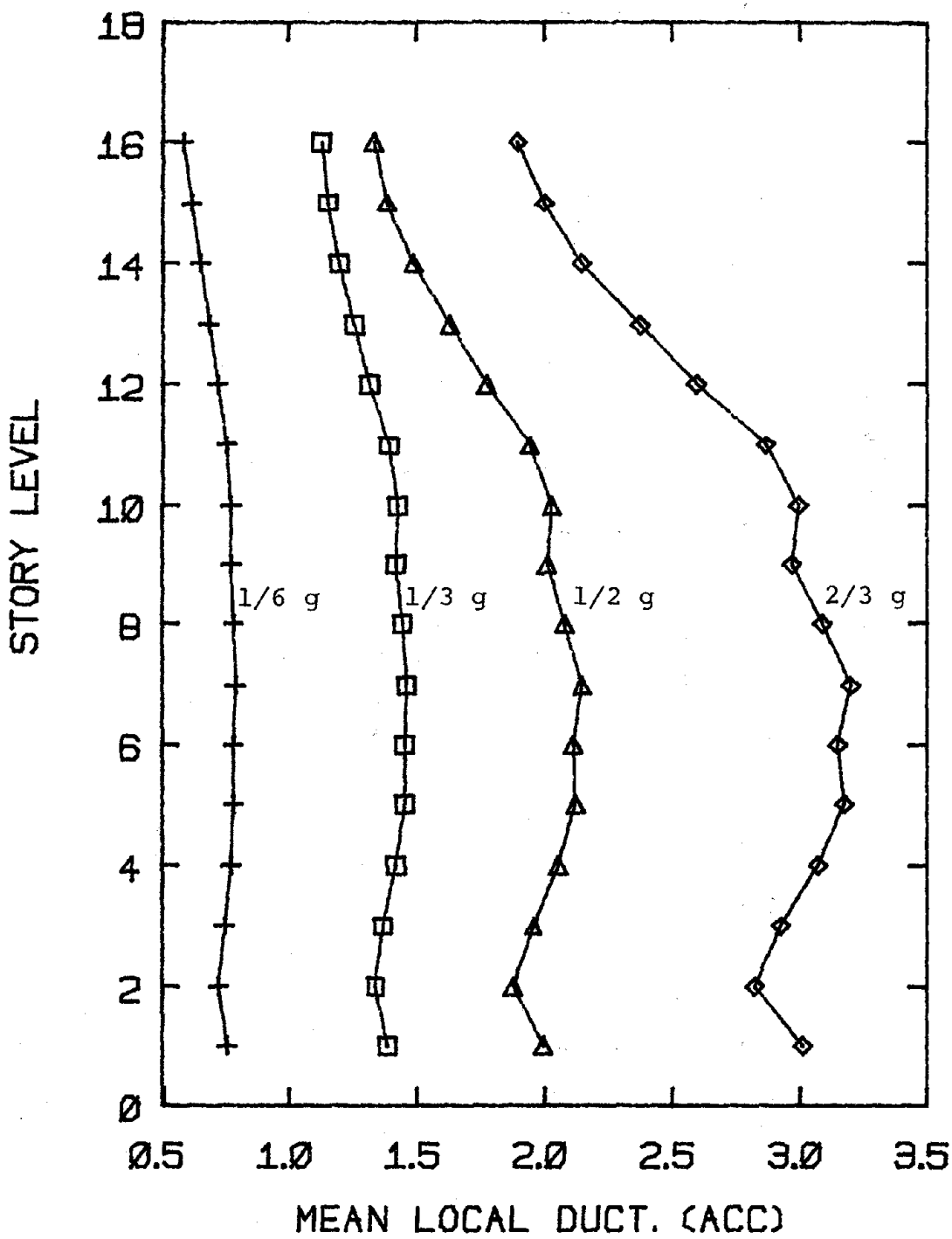

FIG. 5-30 MEAN LOCAL DUCTILITY RATIOS FOR DIFFERENT PEAK GROUND ACCELERATIONS (16-STORY FRAME)

TABLE 5-2 STRONG-MOTION DURATIONS AND EXCITATION VARIANCES FOR DIFFERENT GROUND ACCELERATIONS

SEISMIC PARAMETERS	PEAK GROUND ACCELERATION (a_{max})			
	1/6 g	1/3 g	1/2 g	2/3 g
S_o (sec)	5.28	3.27	2.34	1.78
σ_o (in^2/sec^4)	569.4	2623.2	6609.7	12,992

amined, namely, 1/6 g, 1/2 g, and 2/3 g. The corresponding conditional mean values of the strong-motion duration and the excitation variances are listed in Table 5-2. The resulting mean local ductility ratios for the three (4-, 10- and 16-story) steel frames are plotted in Figures 5-28, 5-29 and 5-30, respectively.

Notice that the mean local ductility ratio increases with the peak ground acceleration as expected, and the increase is more pronounced at the bottom stories. As discussed in Section 4.6.1, this may be attributable to the fact that a great portion of the excitation energy is dissipated by severe plastic action in the bottom stories, resulting in smaller inelastic response at the upper stories (soft-story concept, [2]).

5.5 Summary

The relative importance to inelastic response prediction of uncertainties due to the ground motion representation, the structural dynamic properties, and the method of dynamic analysis has been assessed. The results may be summarized as follows:

(1) The local inelastic response in terms of the local ductility ratio is insensitive to the variation of the Kanai-Tajimi damping; therefore, the K-T damping may be assumed deterministic in the overall seis-

mic safety assessment of buildings.

(2) The local response is quite sensitive to the variability of the Kanai-Tajimi frequency. It is also significantly related to the fundamental natural frequency of the structural frame, and therefore, to the natural period ratio.

(3) When the structural damping is small, the response takes a relatively long time to approach "stationarity". Since the duration of a strong ground motion is relatively short compared to the lower-mode natural periods of the structure, the local inelastic response does not necessarily increase with decreasing structural damping.

(4) When duration and peak acceleration are taken to be negatively correlated, the mean local ductility is generally smaller than when no correlation is assumed between duration and peak acceleration. The effect is not very pronounced, however.

(5) Since the variability of the local ductility correction factor contributes significantly to the uncertainty of local inelastic response, it is important for the seismic safety evaluation of buildings.

(6) The mean local ductility ratio increases with peak ground acceleration, and the increase is more pronounced at the bottom stories. This is quite consistent with the "soft-story" concept.

CHAPTER 6

OVERALL SEISMIC SAFETY OF MULTISTORY STEEL BUILDINGS PROVIDED BY CODE-BASED DESIGN METHOD VERSUS INELASTIC DESIGN METHOD

6.1 Introduction

The main objective of this research endeavor is to quantify the degree of protection provided by the seismic design of a structural frame. Specifically, the degree of seismic safety is compared for buildings designed by different methods, i.e., the conventional code-based design method versus more complicated inelastic design methods. The comparison will be based on the investigation of three steel moment-resisting frames which represent real world low (4-story), middle-height (10-story) and high-rise (16-story) buildings.

Consider first the three steel frames designed by Piąue [49] in accordance with the 1973 edition of the Uniform Building Code [58]. As discussed in Section 4.4, the equivalent story stiffnesses and yielding strengths of these frames have been obtained and are listed in Tables B-4, B-5 and B-6 of Appendix B. As briefly outlined in Section 4.2, these three UBC frames were redesigned by Lai based on the "Inelastic Acceleration Response Spectrum" (IARS) method of design [39]. The corresponding story

stiffnesses and yielding strengths of the three IARS-designed frames are also listed in Tables B-4, B-5 and B-6.

Since the member sizes of the three IARS steel frames are kept the same as those of the three UBC frames, their equivalent story stiffnesses are identical. But their equivalent story yielding strengths are different. As shown in Fig. 6-1, the story yielding strengths of the three steel frames designed by the UBC specifications are much greater than those of the three IARS-designed frames. This implies that under the same intense earthquake load, more inelastic action is expected in the IARS frames than in the UBC frames. This point is discussed in greater detail in Section 6.3.

As mentioned in the preceding chapter, uncertainties in the ground motion representation, the structural dynamic properties and the method of dynamic analysis can be combined to evaluate local seismic response statistics conditional on peak ground acceleration. In combining the uncertainties, two different approaches, i.e., "First-Order Second-Moment" analysis and the method of enumeration, will be discussed. Given that an earthquake with specified peak ground acceleration occurs, the two methods permit computation of the conditional probabilities of local response exceeding a particular value of the local ductility ratio. These probabilities are computed for the six different steel frames under study.

Based on this "conditional reliability" information, the overall seismic safety of the steel frames can then be assessed by introducing the site-specific seismic risk, i.e., the relationship between average return period and peak ground acceleration. For illustrative purposes, a "weighted" seismic risk curve of the Boston area has been obtained following the

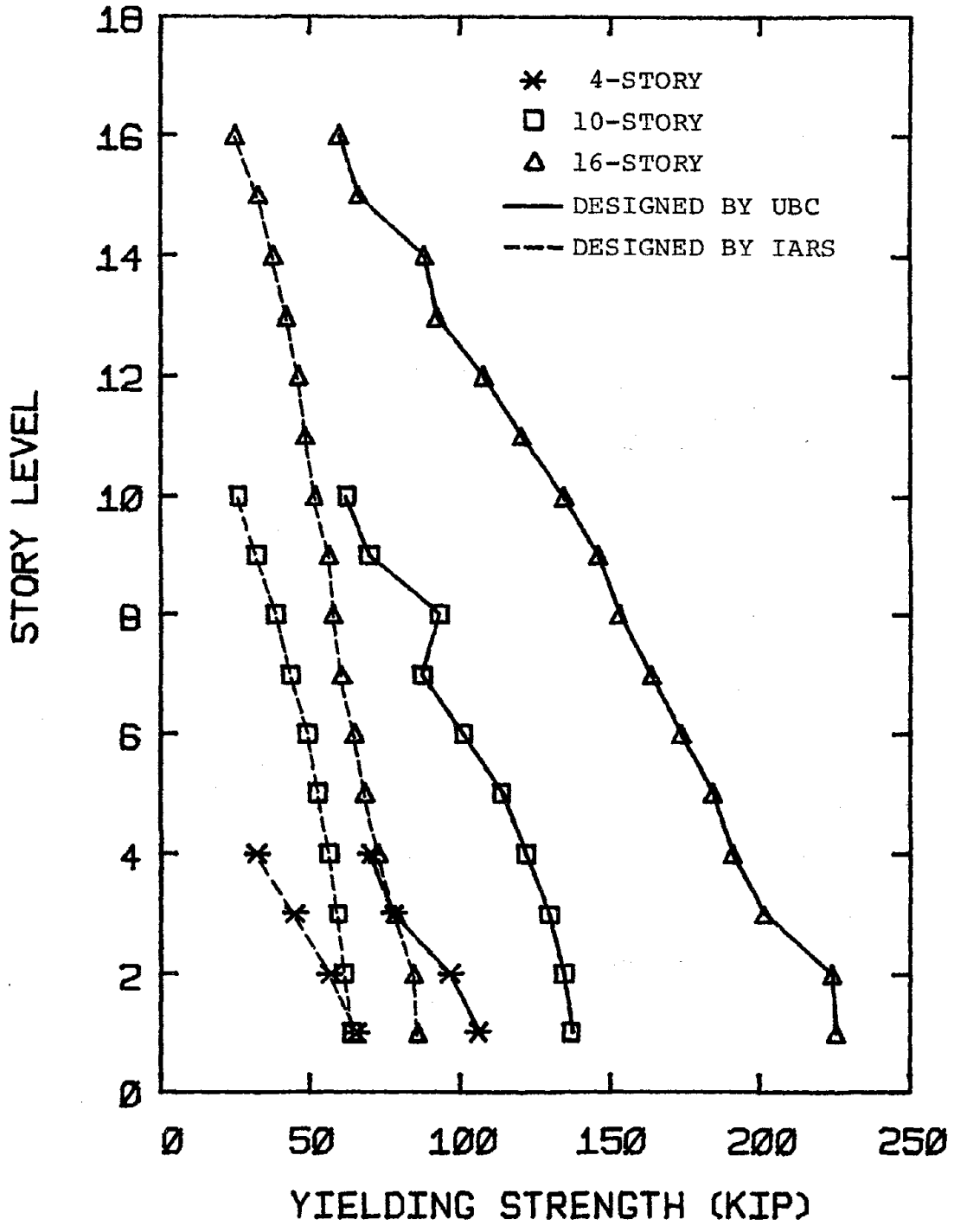

FIG. 6-1 EQUIVALENT STORY YIELDING STRENGTHS FOR FRAMES DESIGNED BY DIFFERENT METHODS

procedure suggested by Cornell and Merz [17]. It is used herein for the seismic safety assessment of steel buildings. In addition, a straight line approximation to the risk curve is employed so as to investigate the sensitivity of overall seismic safety of steel frames with respect to the variation of local seismic risk. The output of the analysis is the annual probability of exceeding various elastic or inelastic response thresholds at different story levels in each frame.

By using empirical relationships between structural (and nonstructural) damage and local ductility ratios, it becomes possible to consider explicitly the balance between initial cost and expected losses due to future earthquakes for each of the steel frames. These results then provide the basis for quantifying the effectiveness of alternate design procedures for steel buildings in reducing the risk of damage and failure under earthquake loads.

6.2 Methods to Combine Discrete Response Characteristics for Overall Response Statistics

Through sensitivity studies presented in the preceding chapter, the local inelastic response (in terms of local ductility ratio) was found to be relatively insensitive to the variations of the Kanai-Tajimi damping and the structural damping. It was concluded that in predicting local response characteristics, conditional on the occurrence of an earthquake with given peak ground acceleration, the following five quantities need to be considered as random: i) strong-motion duration (assumed negatively correlated with the peak ground acceleration), ii) Kanai-Tajimi frequency, iii) natural period ratio, iv) yielding strength factor, and v) local ductility correction factor.

As mentioned in Section 5.3, several methods are available to compute the overall seismic response statistics, e.g., Monte Carlo simulation (the method of last resort), the method of enumeration [8], "mean value" First-Order Second-Moment (FOSM) methods [15], and advanced FOSM methods [51].

The enumeration method involves discretization of each random variable upon which the local response depends. The probability distribution of the response can then be estimated by considering all possible combinations of discrete values of the random variables. Assume that five values are used to discretize the probability distribution of each of the five random variables. The corresponding probability mass functions are listed in Table 6-1. Therefore, the total number of (multi-degree elasto-plastic) random vibration computations involved is $5^5 = 3125$. As an example, consider the 4-story IARS-designed steel frame; the computations required a CPU time of about seven minutes on the Digital VAX-11/780 system at the M.I.T. Joint Computer Facility.

For the 4-story frame subjected to an earthquake with peak ground acceleration of 1/3 g, the resulting cumulative probability distributions of the first story and the top story local ductility ratios are plotted in Figures 6-2 and 6-3, respectively. Notice that the probability of having at least some local yielding (i.e., $\mu > 1$) at the first story is about 44.4%, compared to 42.4% for the top story. Using probability paper, both probability distributions are found to be approximately Lognormal-distributed. The fitted Lognormal distributions are also plotted in the figures.

Alternatively, one may use the mean value "First-Order Second-Moment" method [15,51] to estimate the inelastic response statistics of structural frames. The FOSM method is briefly outlined below.

TABLE 6-1 DISCRETE PROBABILITY MASS FUNCTIONS OF PERTINENT PARAMETERS FOR 4-STORY STEEL FRAME

PARAMETERS	1	2	3	4	5
ζ_g	0.32	-	-	-	-
ω_g	6.5	10	15	20	30
$P[\omega_g]$	0.0541	0.1409	0.2410	0.3069	0.2571
S_o	0.5	1.0	3	5	9
$P[S_o \mid a_{max} = 1/3\ g]$*	0.0917	0.2782	0.2998	0.2161	0.1142
R_T	0.7	0.9	1.1	1.3	1.6
$P[R_T]$	0.1379	0.2328	0.2434	0.2097	0.1762
ζ_s	0.0491	-	-	-	-
R_y	0.8	0.95	1.1	1.25	1.5
$P[R_y]$	0.1113	0.2333	0.2733	0.2507	0.1314
R_L	0.3	0.6	1.0	1.4	1.8
$P[R_L]$	0.1358	0.2738	0.2697	0.167	0.1537

* The discretized $P[S_o \mid a_{max}]$ varies w.r.t. peak ground acceleration

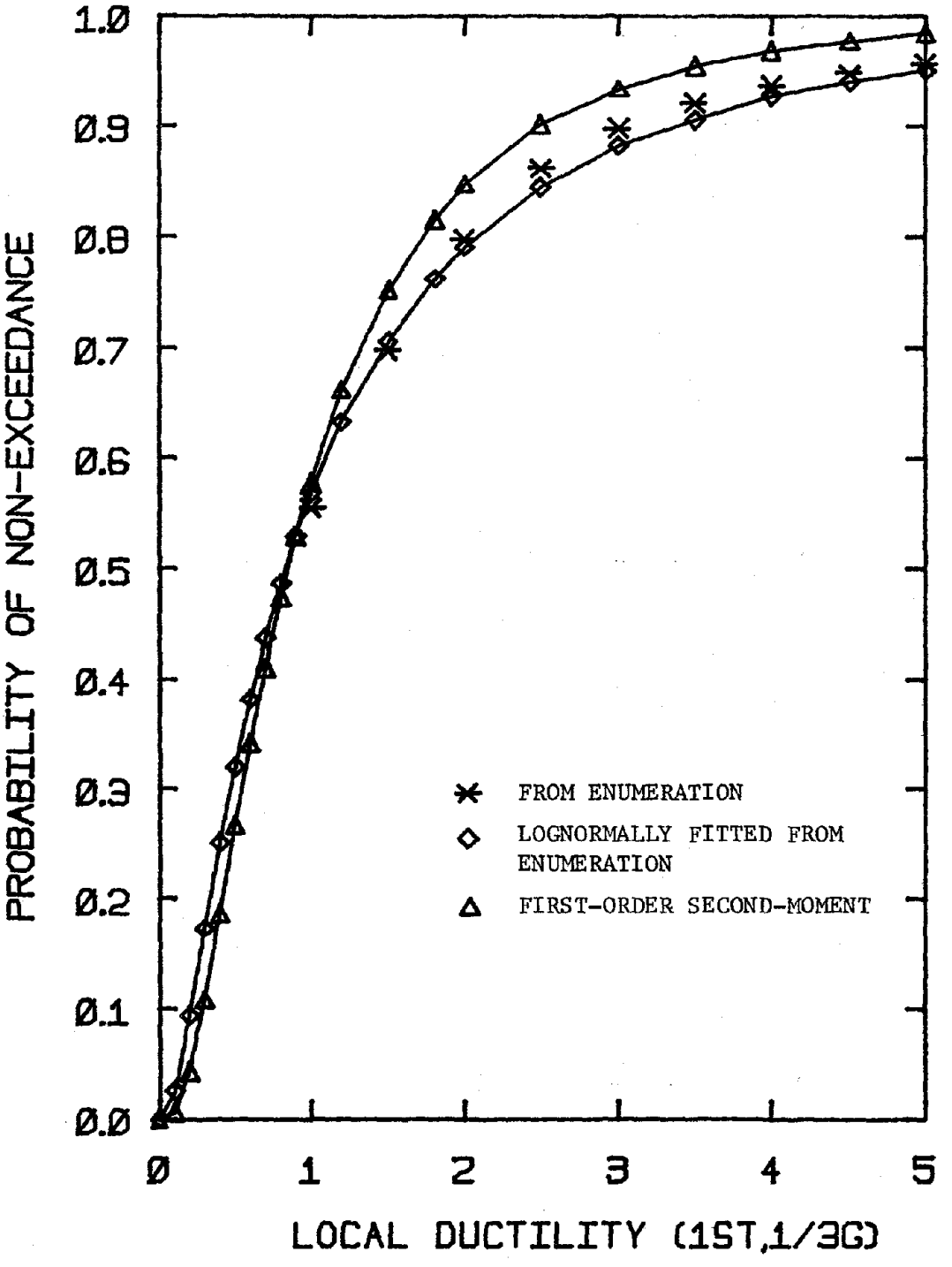

FIG. 6-2 NON-EXCEEDANCE PROBABILITIES OF 1st-STORY LOCAL DUCTILITY PREDICTED BY DIFFERENT METHODS (4-STORY IARS FRAME)

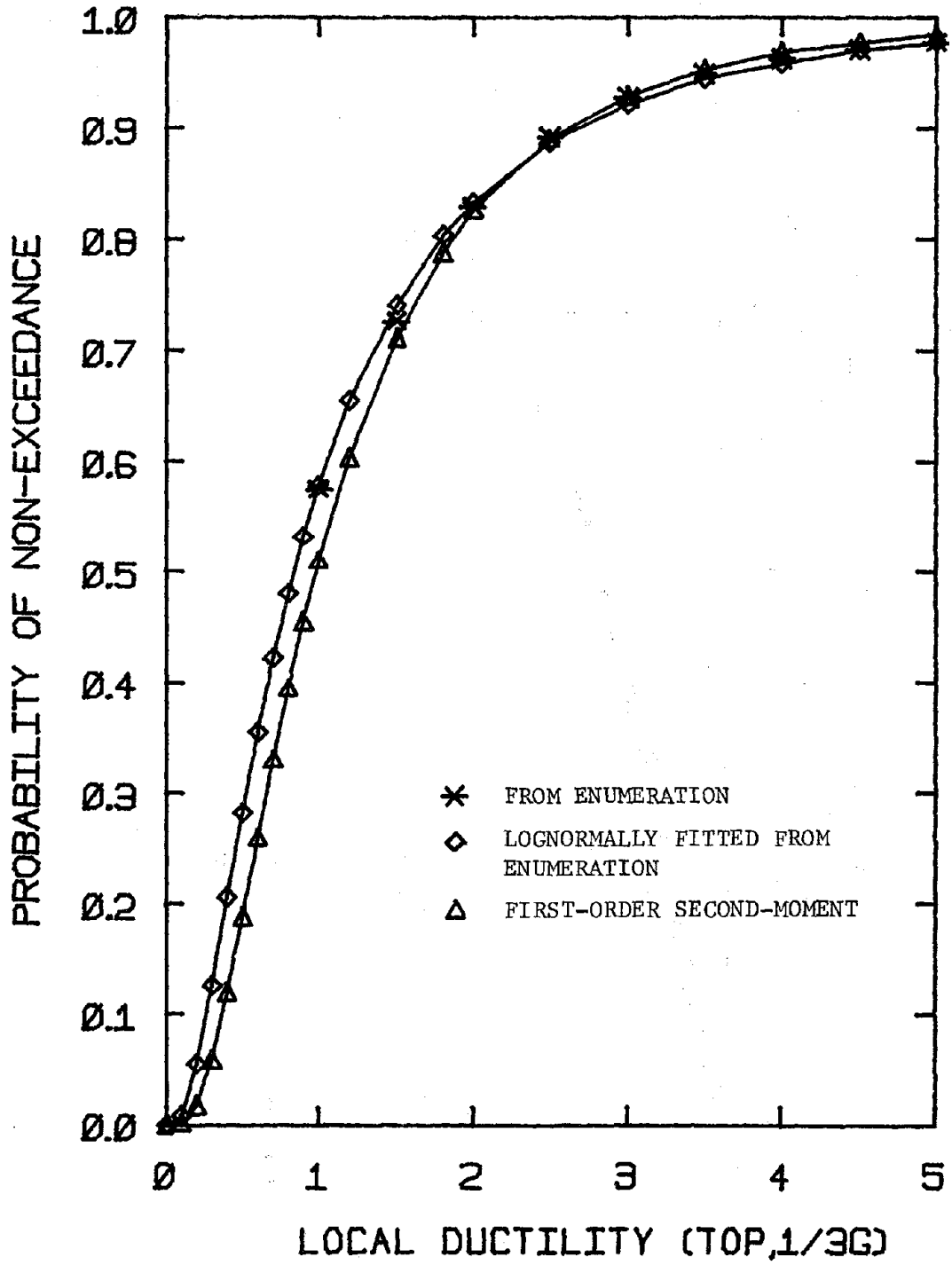

FIG. 6-3 NON-EXCEEDANCE PROBABILITIES OF TOP-STORY LOCAL DUCTILITY PREDICTED BY DIFFERENT METHODS (4-STORY IARS FRAME)

Assume that the random variable Y can be related to a series of random variables X_i by the nonlinear function g:

$$Y = g(X_1, X_2, \ldots, X_n) \tag{6-1}$$

A linear approximation can be obtained by the truncated Taylor's expansion about any given point $(X_1^*, X_2^*, \ldots X_n^*)$ as follows:

$$Y \simeq g(X_1^*, X_2^*, \ldots X_n^*) + \sum_{i=1}^{n} (X_i - X_i^*)\, g_i'(X^*) \tag{6-2}$$

where $g_i'(X^*) = \partial g / \partial X_i$, evaluated at the point $X^* = (X_1^*, X_2^*, \ldots X_n^*)$. Assume that the point X^* corresponds to a vector of mean values of each of the random variables, i.e., $\bar{X}_i$; then the expected value of Y can be approximated as follows:

$$E[Y] \simeq g(\bar{X}) = g(\bar{X}_1, \bar{X}_2, \ldots, \bar{X}_n) \tag{6-3}$$

Assuming that the random variables X_i are mutually independent, the variance of Y can therefore be expressed as a linear combination of the variances $\sigma_{X_i}^2$:

$$\sigma_Y^2 \simeq \sum_{i=1}^{n} [g_i'(\bar{X})]^2\, \sigma_{X_i}^2 \tag{6-4}$$

where the quantity $g_i'(\bar{X})$ is the partial derivative of Y w.r.t. X_i evaluated at the mean value $\bar{X}_i$.

Based on Eq. 6-3, the mean local ductility ratio can be approximated by the result of random vibration analysis when all pertinent variables are replaced by their respective mean values (i.e., $\bar{S}_o$, $\bar{\omega}_g$, $\bar{\zeta}_g$, $\bar{R}_T$, $\bar{\zeta}_s$, $\bar{R}_y$ and $\bar{R}_L$). The variance of the local ductility ratio can be approximately

expressed as follows:

$$\sigma_\mu^2 \simeq \sigma_*^2 + \sum_{i=1}^{7} [g_i'(\bar{X})]^2 \, \sigma_{X_i}^2 \tag{6-5}$$

where

$$g_i'(\bar{X}) = \left.\frac{\partial(\text{Response})}{\partial X_i}\right|_{X_i = \bar{X}_i} \tag{6-6}$$

The first term σ_*^2 represents the variability in the response due to the random phasing of sinusoids, i.e., the uncertainty inherent in classical random vibration analysis. The other terms relate to each of the seven random variables mentioned previously. The quantity $g_i'(\bar{X})$ can be estimated numerically by sensitivity studies as discussed in the preceding chapter.

Using the FOSM method, the mean and the standard deviation of the first story and the top story local ductility ratios (for a_{max} = 1/3 g) have been computed for the 4-story steel frame. Again assuming Lognormal distributions, the cumulative probability distributions of the first- and top-story local ductility ratios are also plotted in Figures 6-2 and 6-3, respectively.

Notice that the probability distributions estimated by the method of enumeration and the FOSM method are quite compatible for the top-story local ductility ratio. For example, based on the FOSM method, the probability of having some local yielding (i.e., $\mu > 1$) at the top story is about 48.9%, compared to 42.4% obtained by the method of enumeration. However, for the first-story local ductility ratio, the two methods lead to quite different results especially for ductility larger than two. This is probably due to the fact that the inelastic local response is sensitive to the extremes of some pertinent random variables considered, e.g., the Kanai-Tajimi frequency. Hence, the local response statistics predicted by the mean value

FOSM method (evaluated at the mean values of all the random variables) may not be adequate.

Improved FOSM techniques have been suggested by several authors [15, 51]. In the remainder of this chapter, the method of enumeration is used to predict the overall local response statistics of steel buildings.

6.3 Conditional Probability Distribution of Local Ductility Ratio Given Peak Ground Acceleration

6.3.1 4-Story Frames

Using the enumeration method and the discrete probability mass functions for the random variables listed in Table 6-1, the conditional probability distribution of the local ductility has been computed for five different levels of peak ground acceleration (i.e., 0.1 g, 0.2 g, 0.3 g, 0.4 g and 0.5 g) for the 4-story IARS-designed steel frame. The results of the first-story local ductility ratio are plotted in Fig. 6-4.

Recall that the IARS design of this 4-story steel frame is based on a local ductility of 4 under a 1/3 g earthquake peak acceleration as discussed in Section 4.2. It is interesting to note that the probability of exceedance of the design local ductility ratio ($\mu = 4$) under the design level earthquake is about 6.3%.

Another useful way of presenting data is to plot the non-exceedance probability of local ductility versus peak ground acceleration. The results for the first story and the top story are plotted in Fig. 6-5. At the design peak ground acceleration of 1/3 g, the probability of having at least some local yielding (i.e., $\mu > 1$) in the first story is estimated

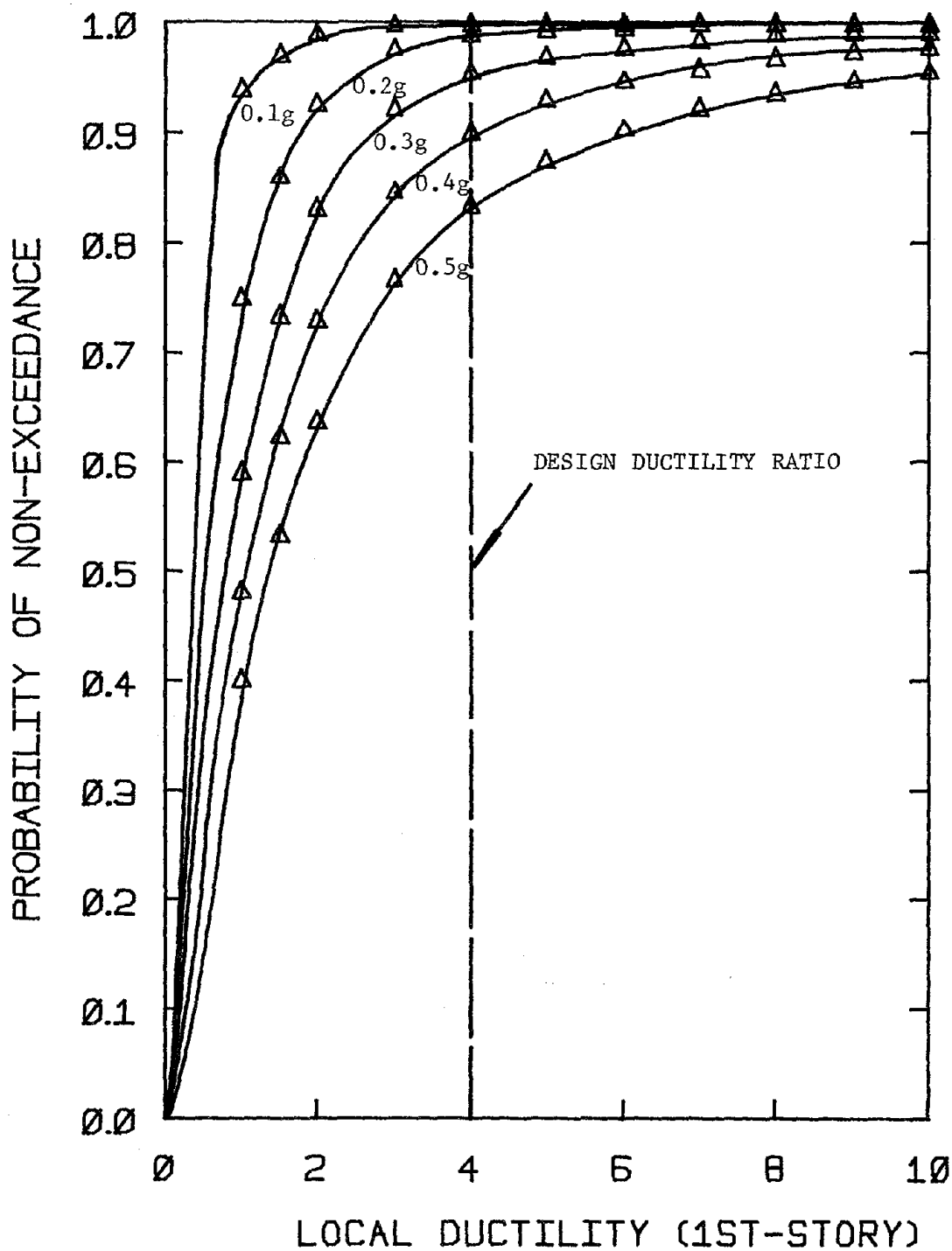

FIG. 6-4 NON-EXCEEDANCE PROBABILITIES OF 1st-STORY LOCAL DUCTILITY FOR DIFFERENT PEAK GROUND ACCELERATIONS (4-STORY IARS FRAME)

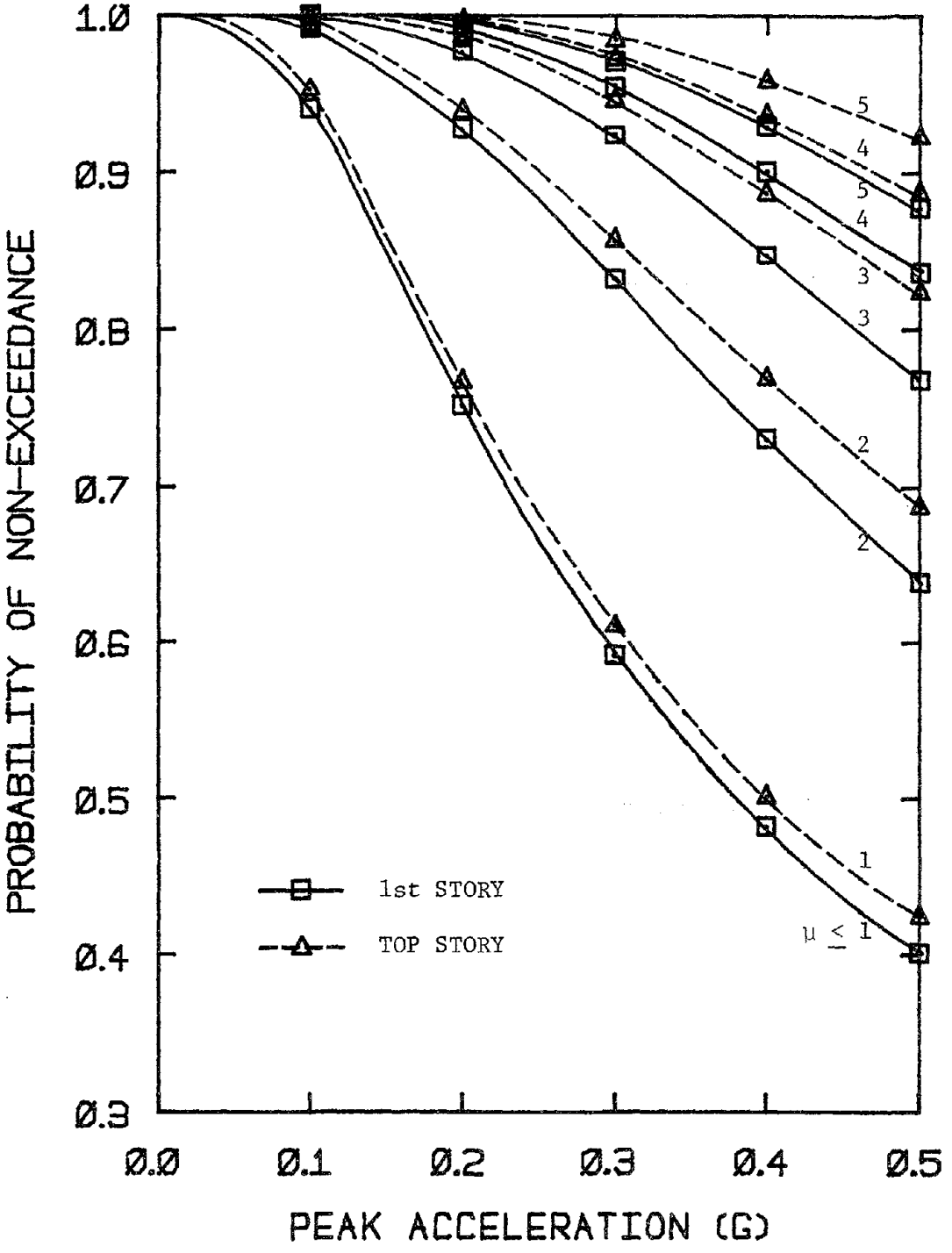

FIG. 6-5 NON-EXCEEDANCE PROBABILITIES OF 1st- AND TOP-STORY LOCAL DUCTILITY CONDITIONAL ON PEAK GROUND ACCELERATION (4-STORY IARS FRAME)

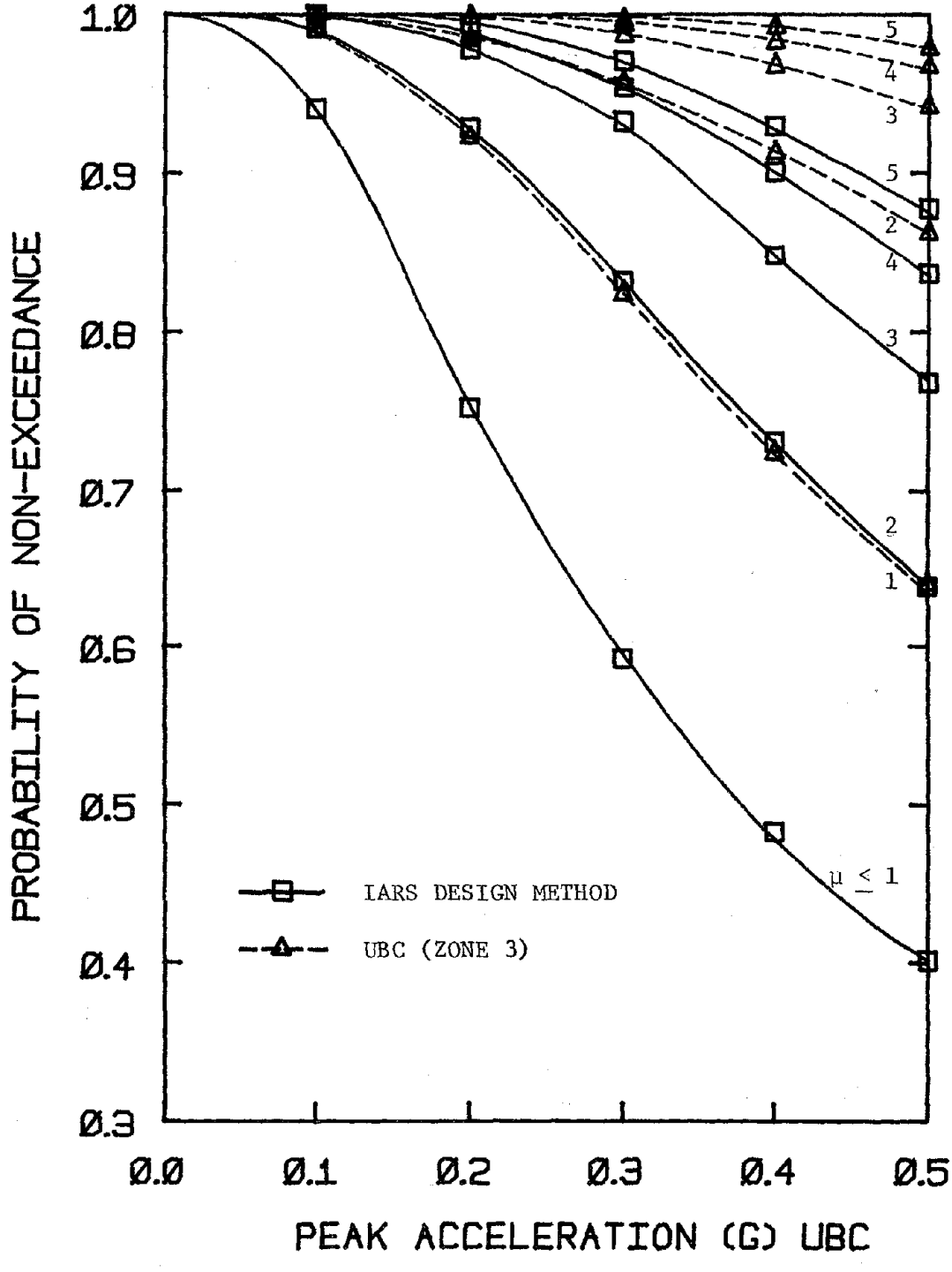

FIG. 6-6 NON-EXCEEDANCE PROBABILITIES OF 1st-STORY LOCAL DUCTILITY CONDITIONAL ON PEAK GROUND ACCELERATION (4-STORY IARS AND UBC FRAMES)

at 44.4%; it is 42.4% for the top story. Note also that there exists a finite probability, estimated at 5.9%, that there will be some yielding in the first story when the peak ground acceleration equals 0.1 g. There is a 4.6% probability that the top story will experience local yielding.

Using the same probability mass functions for the variables, the enumeration method has also been applied to the 4-story UBC steel frame designed by Piqué [49]. The results for the bottom story are presented in Fig. 6-6. Under a 1/3 g peak acceleration ground motion, the probability that the first story of the UBC steel frame will remain elastic is about 79% compared to the 55.6% for the steel frame designed by IARS. The difference is attributable to the fact that the yielding strengths of the UBC-designed frame are much greater than those of the IARS-designed frame as depicted in Fig. 6-1.

6.3.2 10-Story Frame

A parallel set of results has been obtained for the 10-story frames based on the enumeration method. The probability mass function listed in Table 6-2 is used to represent the variability of Kanai-Tajimi frequency,

TABLE 6-2 DISCRETE PROBABILITY MASS FUNCTION OF KANAI-TAJIMI FREQUENCY FOR 10-STORY STEEL FRAME

PARAMETERS	1	2	3	4	5	6
ω_g	3	6	10	15	20	30
$P[\omega_g]$	0.0045	0.0431	0.1474	0.2410	0.3069	0.2571

whereas the PMF's listed in Table 6-1 are used for the other random variables. The resulting cumulative probability distribution of the local duc-

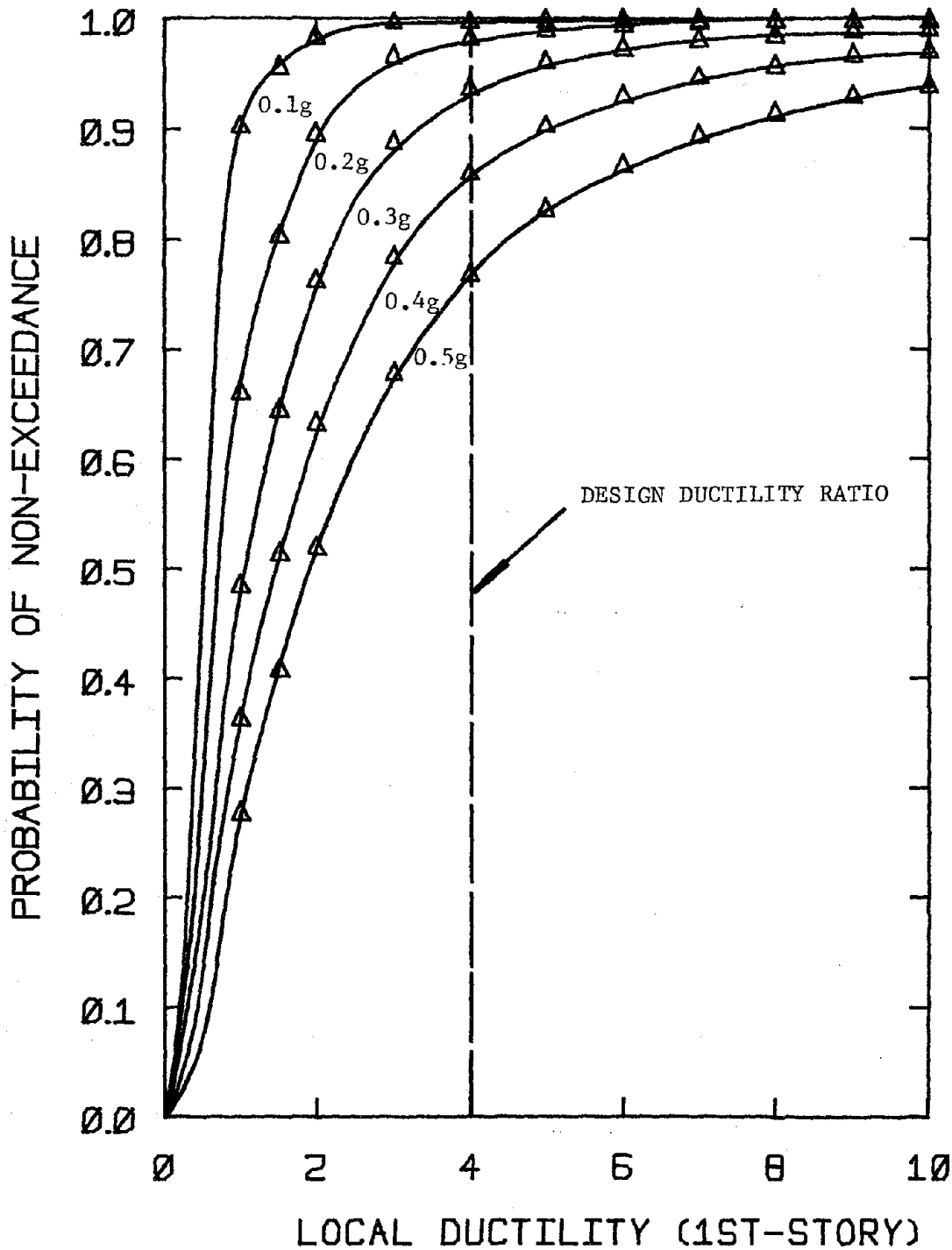

FIG. 6-7 NON-EXCEEDANCE PROBABILITIES OF 1st-STORY LOCAL DUCTILITY FOR DIFFERENT PEAK GROUND ACCELERATIONS (10-STORY IARS FRAME)

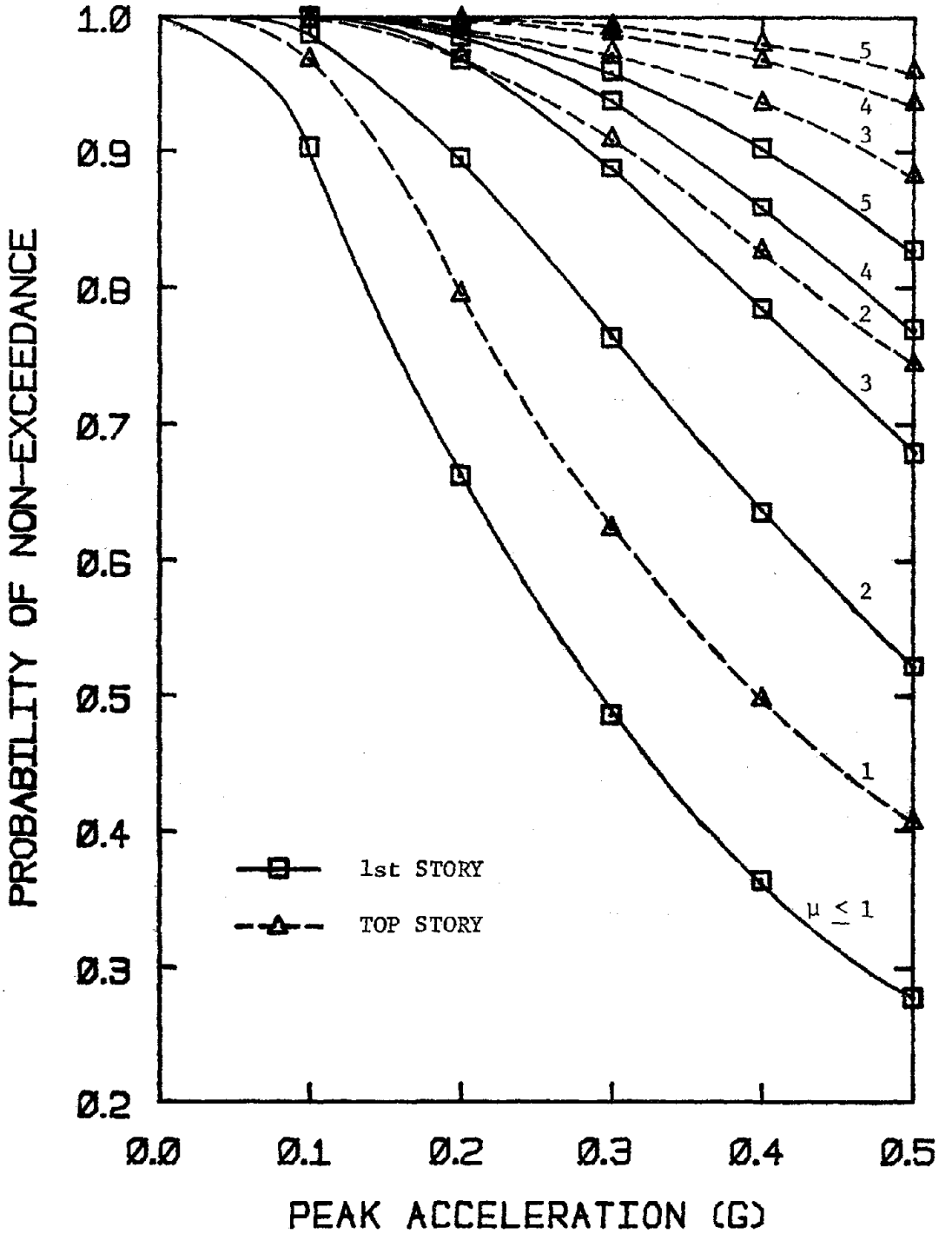

FIG. 6-8 NON-EXCEEDANCE PROBABILITIES OF 1st- AND TOP-STORY LOCAL DUCTILITY CONDITIONAL ON PEAK GROUND ACCELERATION (10-STORY IARS FRAME)

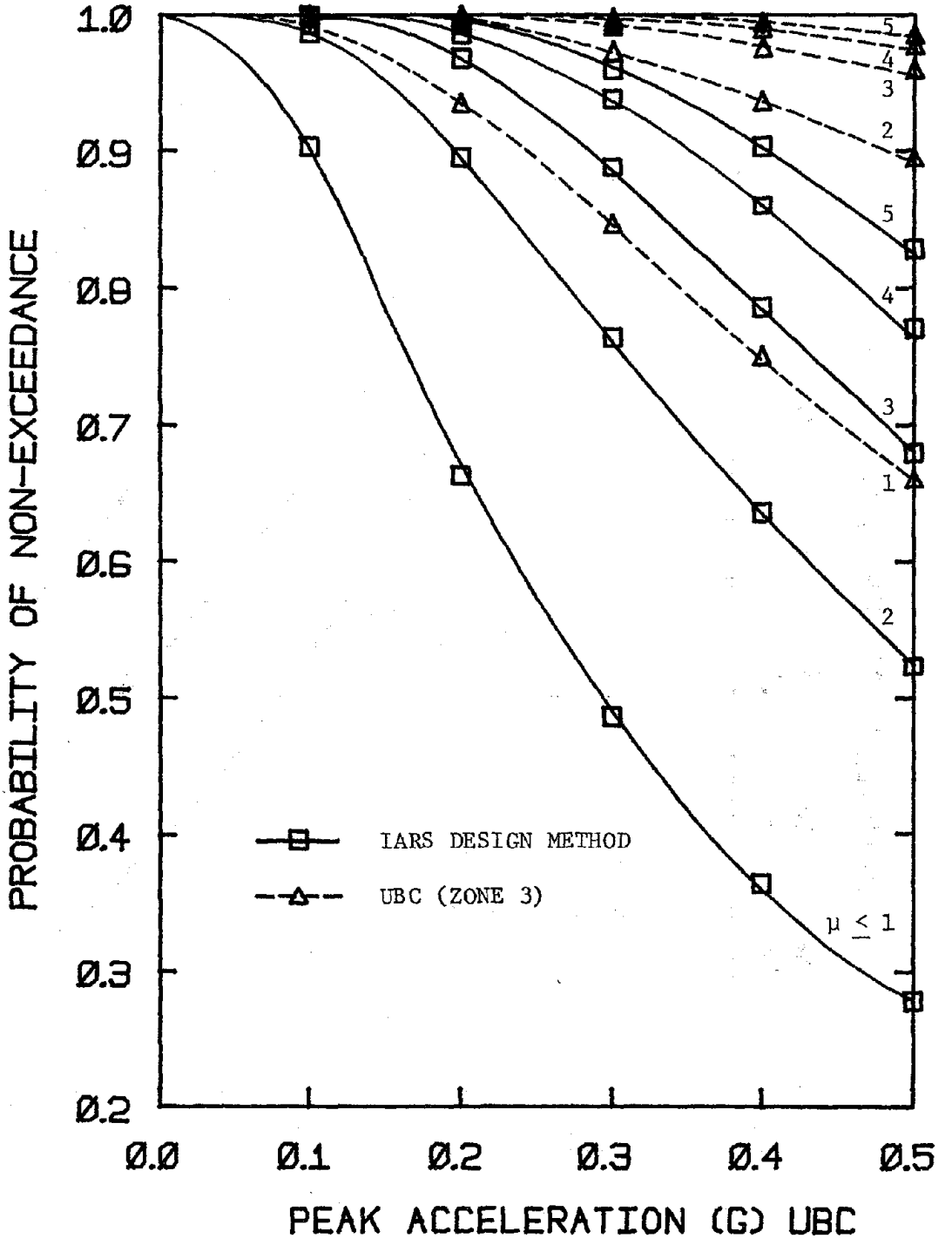

FIG. 6-9 NON-EXCEEDANCE PROBABILITIES OF 1st-STORY LOCAL DUCTILITY CONDITIONAL ON PEAK GROUND ACCELERATION (10-STORY IARS AND UBC FRAMES)

tility ratio in the bottom story of the 10-story IARS steel frame is plotted in Fig. 6-7 for different levels of peak ground acceleration. At the design peak ground acceleration of 1/3 g, the probability that the first-story local ductility will exceed the design value of 4 is about 8.5%.

Fig. 6-8 shows the results for the first story and the top story non-exceedance probability versus peak ground acceleration. Given an earthquake with the design peak acceleration of 1/3 g, it is estimated that the probability of the first story having at least some local yielding is 55.9%; in the top story, it is about 42%.

Using the same input PMF's, the probability distribution of local ductility ratio has also been computed by the enumeration method for the 10-story UBC steel frame. The results for the bottom story are plotted in Fig. 6-9. Again, the non-exceedance probabilities are larger than those of the IARS steel frame. For example, for a peak ground acceleration of 1/3 g, the probability that the bottom story will remain elastic is approximately 81% for the UBC-designed frame, whereas it is only about 44.1% for the IARS-designed frame.

6.3.3 16-Story Frames

The results for the 16-story IARS-designed steel frame are plotted in Figures 6-10 and 6-11. At the design peak ground acceleration of 1/3 g, the probability of exceeding the design local ductility ratio ($\mu = 4$) in the first story is approximately 7.8%. The probability of having at least some local yielding in the first story during a 1/3 g peak acceleration earthquake is estimated at 57.1%; it is about 44.5% for the top story.

Fig. 6-12 shows the results of the bottom-story local ductility for the 16-story UBC-designed steel frame. Under an earthquake of 1/3 g peak acceleration, the bottom story will remain elastic with 88% probability

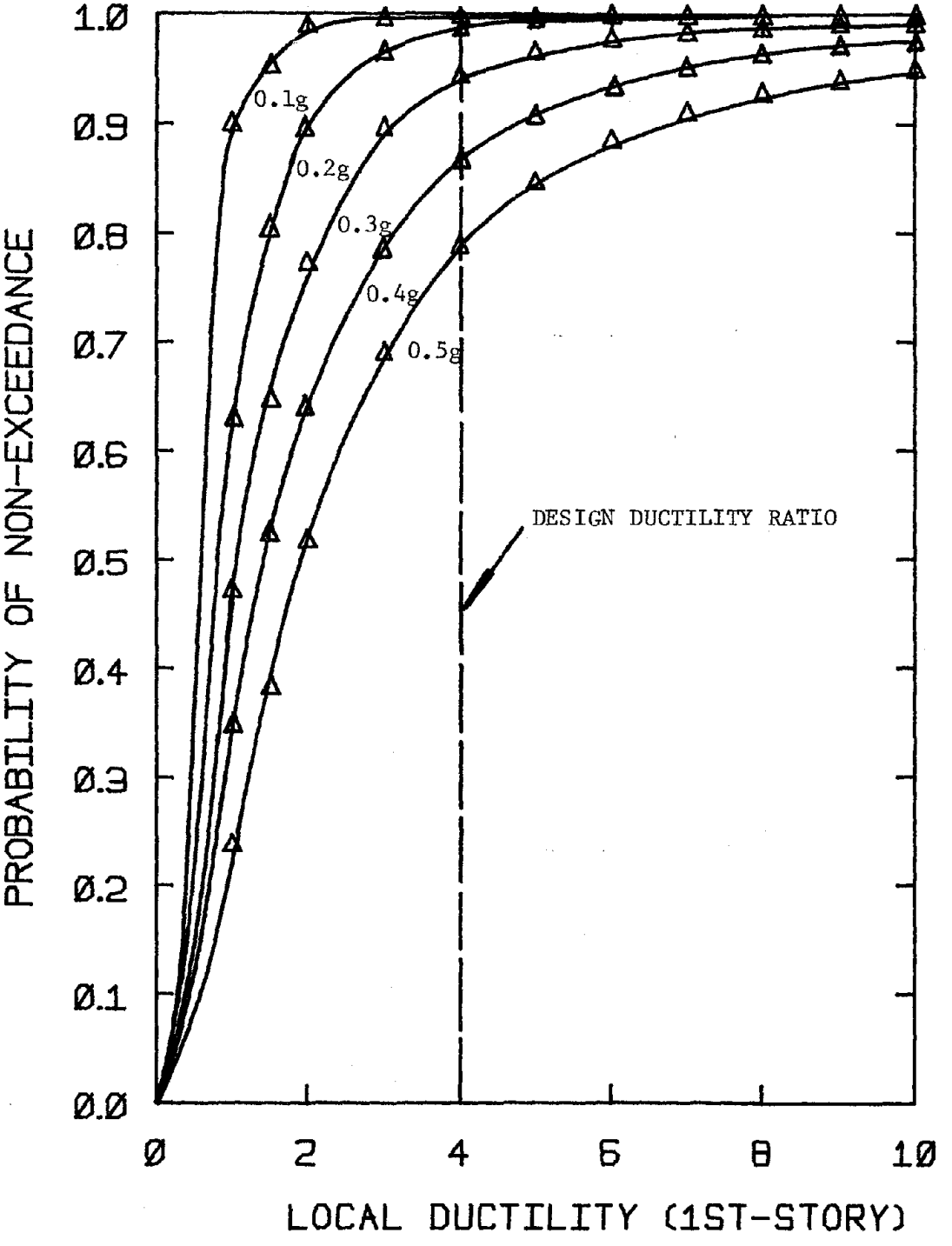

FIG. 6-10 NON-EXCEEDANCE PROBABILITIES OF 1st-STORY LOCAL DUCTILITY FOR DIFFERENT PEAK GROUND ACCELERATIONS (16-STORY IARS FRAME)

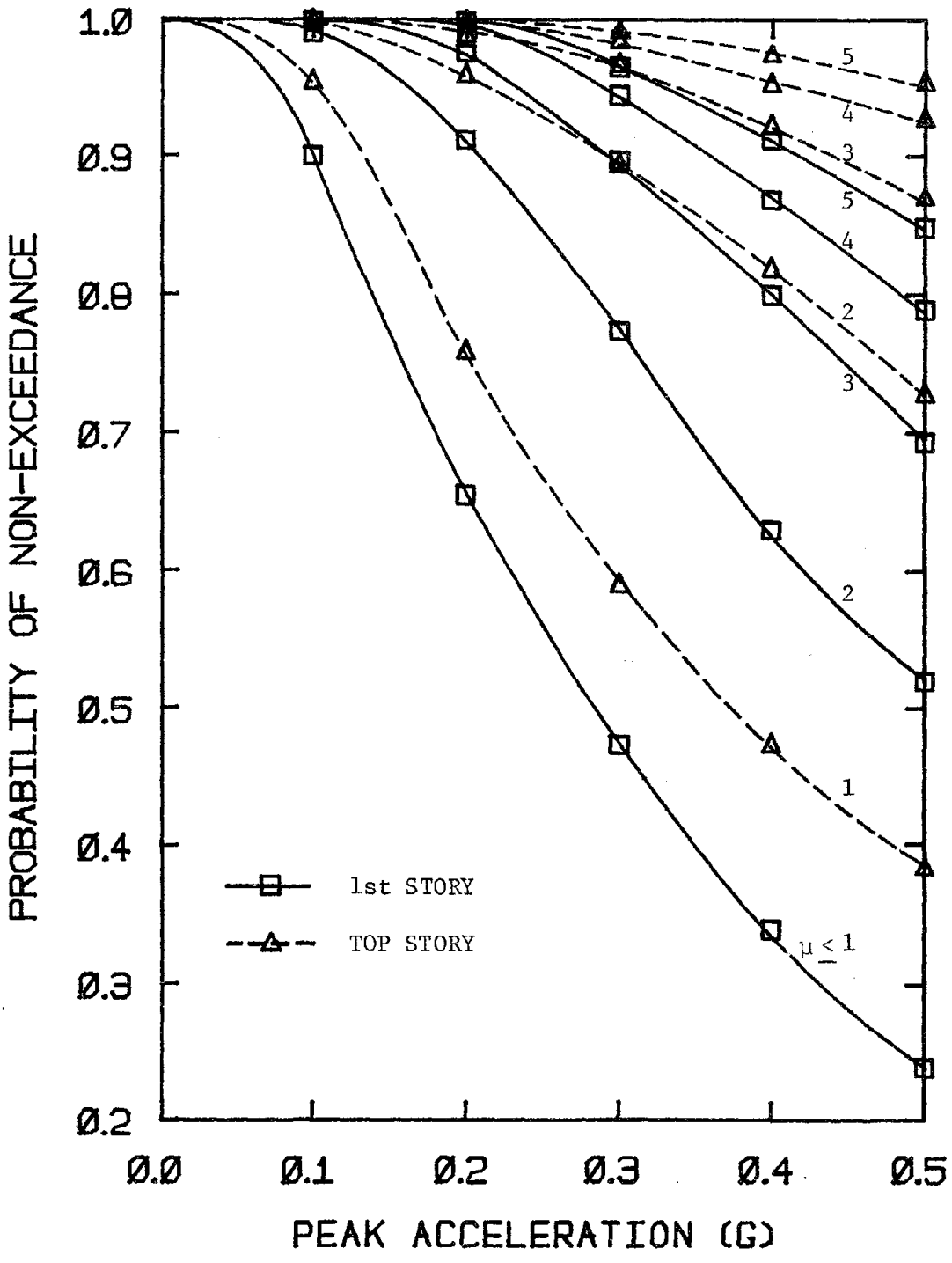

FIG. 6-11 NON-EXCEEDANCE PROBABILITIES OF 1st- AND TOP-STORY LOCAL DUCTILITY CONDITIONAL ON PEAK GROUND ACCELERATION (16-STORY IARS FRAME)

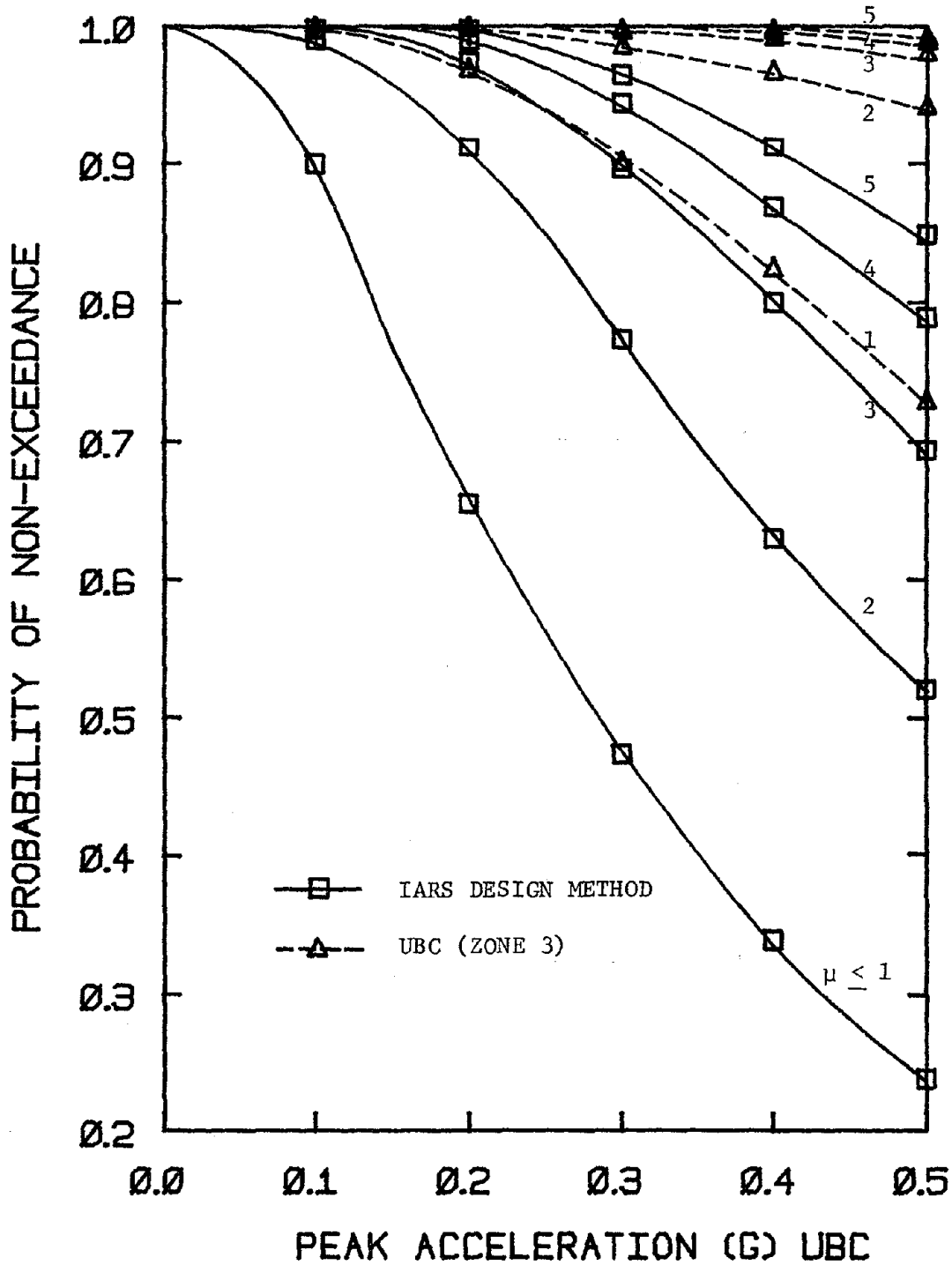

FIG. 6-12 NON-EXCEEDANCE PROBABILITIES OF 1st-STORY LOCAL DUCTILITY CONDITIONAL ON PEAK GROUND ACCELERATION (16-STORY IARS AND UBC FRAMES)

for the UBC-designed steel frame, whereas it is only 42.9% probability for the 16-story IARS-designed steel frame.

6.4 Description of Local Seismic Risk (Boston Case Study)

In order to quantify the overall seismic safety of a building at a specific site, it is necessary to incorporate information about the local seismic risk at the site. For illustrative purposes, consider a hypothetical site in Boston for which a "weighted" seismic risk curve is provided by Tong et al. [57]. To investigate the sensitivity of the overall seismic safety w.r.t. the assumed seismic risk, a straight-line approximation to the "weighted" seismic risk curve is also used. The seismic risk analysis is briefly described below.

In developing the seismic hazard maps for Massachusetts, Tong et al. [57] identified three major seismic source zones (i.e., zones a, b and c) and a background source zone (d), all shown in Fig. 6-13. The associated earthquake occurrence rate and the assumed maximum epicentral intensity are listed in Table 6-3 for each of the seismic source zones. A common minimum intensity of V (five) was assumed for all zones. For detailed description of the model, the reader is referred to Tong et al. [57].

Based on the procedure of seismic risk analysis suggested by Cornell and Merz [17], Tong et al. [57] established the relationship between average return period and modified Mercalli intensity for the Boston site. Using the correlation between site intensity and peak ground acceleration, the seismic risk curve, i.e, the relationship between average return period and peak ground acceleration can be obtained. In this study, the correlation proposed by Gutenberg and Richter is used [27]:

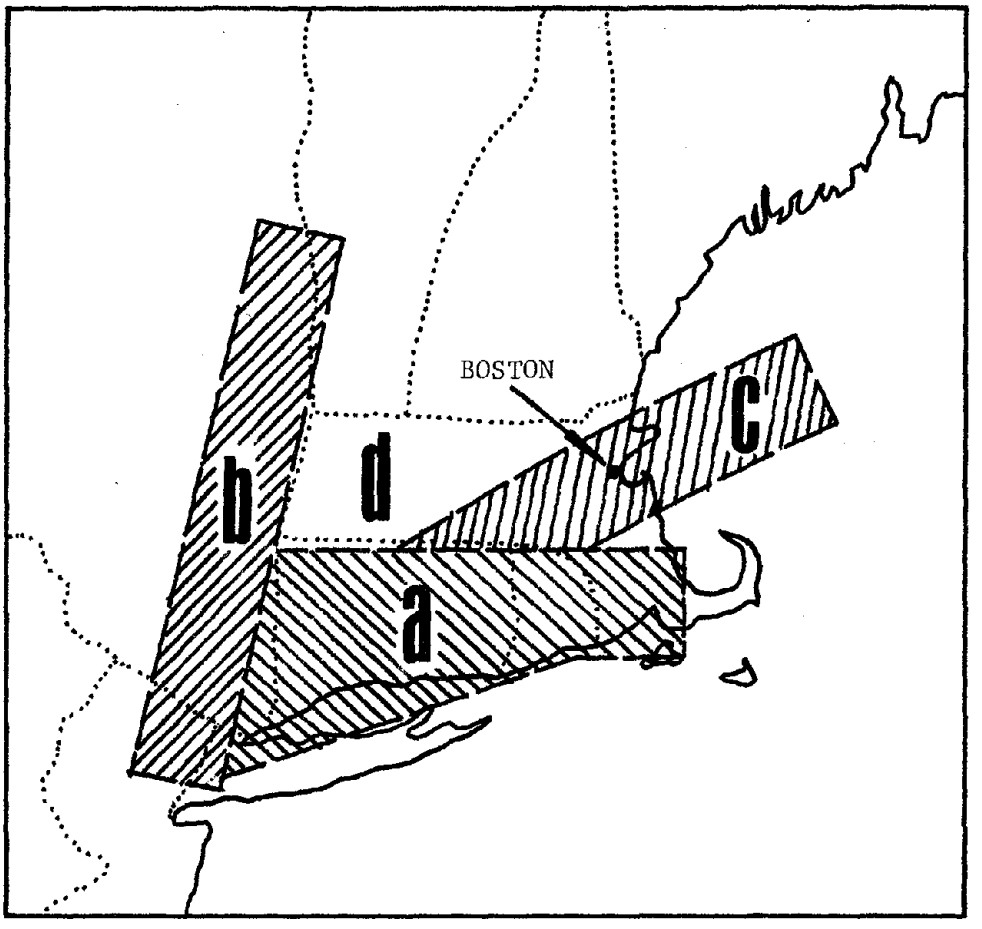

FIG. 6-13 SEISMIC SOURCE ZONES FOR BOSTON SITE [TONG ET AL., 57]

TABLE 6-3 PERTINENT PARAMETERS OF DIFFERENT SEISMIC SOURCE ZONES FOR BOSTON SITE [TONG ET AL., 57]

SOURCE ZONE	EVENTS/YEAR	MAX. EPICENTRAL INTENSITY
a	15/250	VIII. 3
b	6/250	VIII. 3
c	18/250	VIII. 7
d (BACKGROUND)	8×10^{-7}/MILE^2	VI. 3

$$\text{Log}_{10}(a_{max}) = \frac{I_s}{3} - \frac{1}{2} \qquad (6\text{-}7)$$

where a_{max} is in cm/sec^2, and I_s is the firm ground modified Mercalli intensity at the site.

Originally, three different versions of seismic source zone "c" were used by Tong et al., each based on a different assumption about the zone's seismicity. The third version, which gives the most conservative seismic risk, is incorporated herein. The resulting relationship between annual exceedance probability and peak ground acceleration (i.e., the "nominal" risk curve) is plotted in Fig. 6-14.

As pointed out by Cornell and Merz [17], for a given site intensity I_s, the peak ground acceleration may be scattered above or below the "nominal" value given by Eq. 6-7. To account for this uncertainty, they suggested a weighted method of computation: 50% probability is assigned to the nominal value and 25% probability to values of peak ground acceleration corresponding to one intensity level above and below the nominal value (i.e., $I_s + 1$ and $I_s - 1$). This approach yields the "weighted" seismic risk curve for the Boston site as plotted in Fig. 6-14. For comparison, the "Bayesian" seismic risk curve proposed by Cornell and Merz [17] is also plotted in the figure.

The Applied Technology Council [4] suggested that the "effective peak acceleration" (EPA) for the Boston area should be about 0.1 g with 90% probability of not being exceeded in 50 years. This corresponds to an average return period of about 475 years, or an annual exceedance probability of 2.105×10^{-3}. For the "weighted" seismic risk curve obtained herein, it is estimated at 1.09×10^{-3}.

To investigate the sensitivity of local response statistics with re-

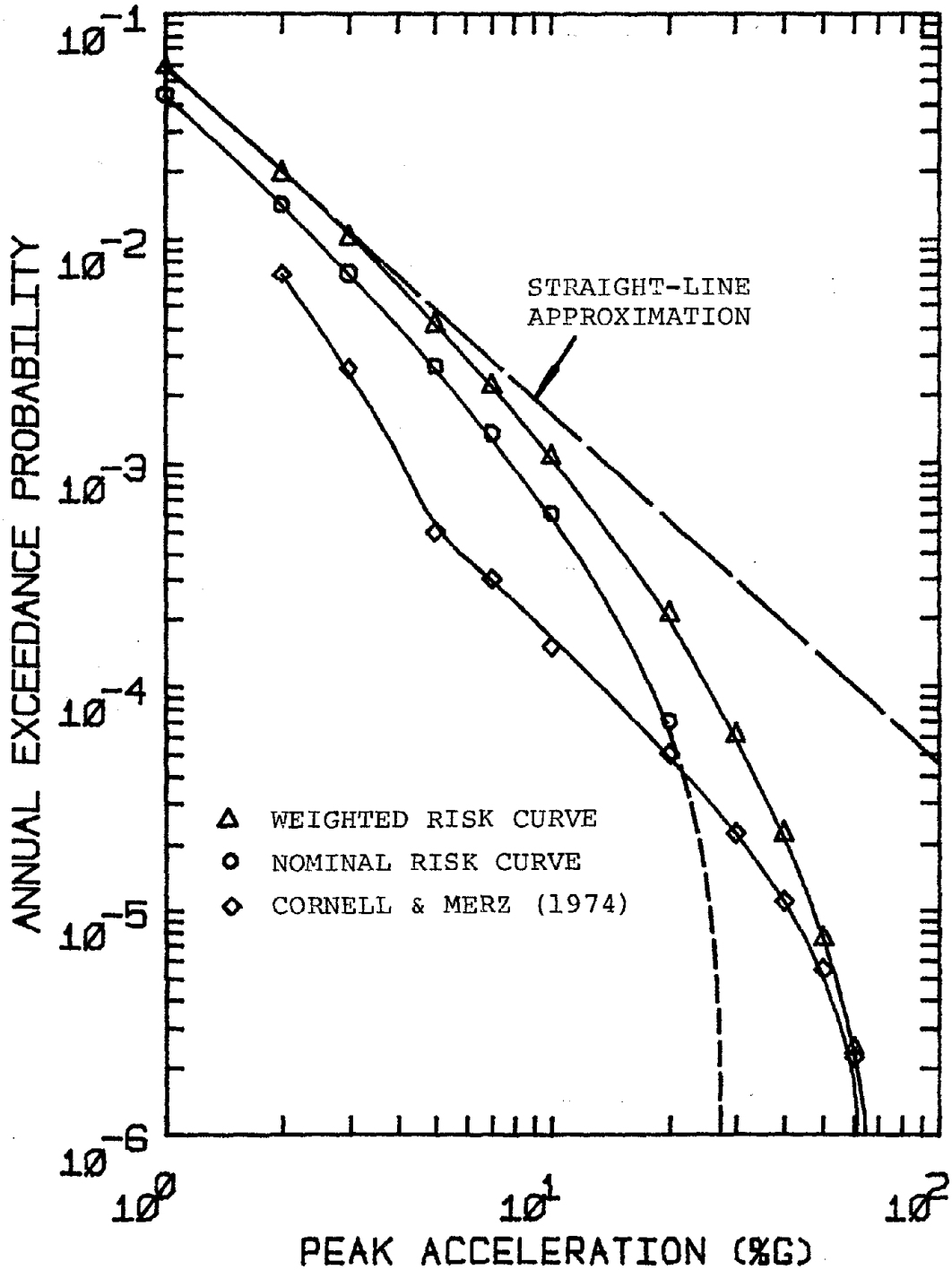

FIG. 6-14 ALTERNATE SEISMIC RISK CURVES FOR BOSTON SITE

spect to variations in the local seismic risk curve, a straight-line approximation (on a log-log plot) to the weighted seismic risk curve has also been incorporated. The linear approximation of the seismic risk curve is also plotted in Fig. 6-14.

6.5 Overall Seismic Safety of IARS- and UBC-Designed Frames

6.5.1 Incorporating Local Seismic Risk

By combining the local seismic risk information described in the preceding section with the results of conditional reliability analysis, the overall seismic safety can be assessed for the three UBC-designed steel frames as well as the three IARS-designed frames. Based on Eq. 5-5, the annual probability that the local inelastic response will exceed a given threshold, say, a local ductility factor μ^*, can be determined as follows:

$$P[\mu > \mu^*] = \sum_{C \cap a^i_{max}} P[\mu > \mu^* | C \cap a^i_{max}] \cdot P[C | a^i_{max}] \cdot P[a^i_{max}]$$

$$\simeq \sum_{a^i_{max}} \left(\sum_{C | a^i_{max}} P[\mu > \mu^* | C \cap a^i_{max}] \cdot P[C | a^i_{max}] \right) \cdot P[a^i_{max}] \tag{6-8}$$

where $P[C|a^i_{max}]$ is expressed by Eq. 5-4 and $P[a^i_{max}]$ is computed from the local seismic risk curve as follows:

$$P[a^i_{max}] = P[a_{max} \geq (a^i_{max} - \Delta a_{max})] - P[a_{max} \geq (a^i_{max} + \Delta a_{max})] \tag{6-9}$$

where Δa_{max} is the discretization interval of the annual exceedance probability of peak ground acceleration.

Due to the fact that a minimum epicentral intensity is often assumed for each seismic source zone, the range of peak accelerations considered

will have a lower bound, and the numerical summation expressed in Eq. 6-8 must be truncated. Denote by a_o the lower bound peak acceleration; Eq. 6-8 can then be normalized with respect to the exceedance probability $P[a_{max} \geq a_o]$ as follows:

$$P[\mu > \mu^*]/P[a_{max} \geq a_o] = \sum_{a^i_{max}} \left(\sum_{C|a^i_{max}} P[\mu > \mu^* | C \cap a^i_{max}] \cdot P[C|a^i_{max}] \right) \cdot (P[a^i_{max}]/P[a_{max} \geq a_o]) \quad (6\text{-}10)$$

where

$$\sum_{a^i_{max}} P[a^i_{max}] = P[a_{max} \geq a_o] \quad (6\text{-}11)$$

and

$$\sum_{a^i_{max}} (P[a^i_{max}]/P[a_{max} \geq a_o]) = 1 \quad (6\text{-}12)$$

The ratio may be interpreted as the probability of occurrence of the peak ground acceleration a^i_{max} given that an earthquake with peak acceleration larger than or equal to a_o occurs.

The advantage of using this "normalized" probability approach is that it permits estimation of the probability $P[\mu > \mu^*]$ for any given value of $P[a_{max} \geq a_o]$. Furthermore, the contributions to the summation expressed in Eq. 6-10 can be compared for different levels of peak ground acceleration.

As mentioned earlier, a minimum epicentral intensity of five (V) was assumed for all seismic source zones of the Boston site. This corresponds approximately to $a_o \simeq 0.01$ g. As shown in Fig. 6-14, the annual exceedance

probability $P[a_{max} \geq 0.01\ g]$ is estimated at 6.013×10^{-2}.

6.5.2 Results of IARS-Designed Steel Frames

Based on Eq. 6-10, the overall seismic safety has been assessed for the three (4-, 10- and 16-story) IARS-designed steel moment-resisting frames. Fifteen values are used to discretize the seismic risk curve. Except at small peak accelerations, the discretization interval Δa_{max} is taken to be 0.05 g. The resulting "normalized" contributions to the annual exceedance probabilities of first-story local ductility ratios are plotted in Figures 6-15, 6-16 and 6-17 for the three steel frames.

Notice that the annual probability of having at least some local yielding in the first story (i.e., $P[\mu > 1]$) has significant contributions due to low levels of peak ground acceleration. For the annual probability of exceeding relatively high local ductility ratio, the contributions are more pronounced in the intermediate ground acceleration range.

In his investigation of the overall seismic safety of a 4-story steel frame, Gasparini [22] reported that the maximum contribution to the overall exceedance probability of a prescribed interstory distortion occurs when the peak ground acceleration is about 1.2 times the design acceleration (which is 1/3 g for the IARS-designed steel frames). The results obtained herein do not support this observation.

By summing individual contributions (Eq. 6-10), the "normalized" annual exceedance probabilities of the local ductility ratios are determined for the three steel frames. The results of the first-story local ductility ratio are listed in Tables C-1, C-2 and C-3 of Appendix C. The annual risk of having a particular value of local ductility ratio exceeded can then be computed by multiplying with the probability $P[a_{max} \geq a_o]$. The

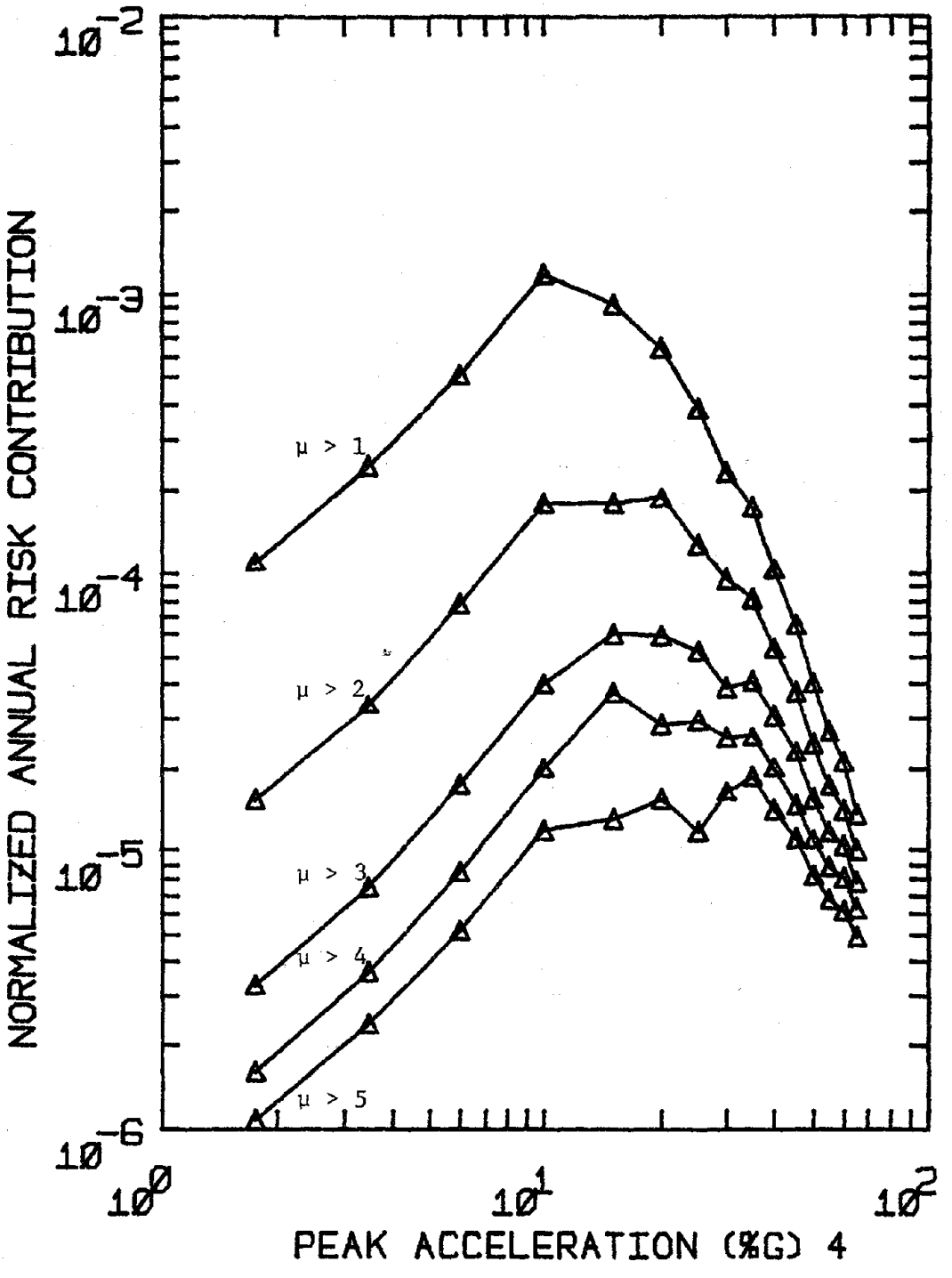

FIG. 6-15 NORMALIZED CONTRIBUTIONS TO ANNUAL EXCEEDANCE PROBABILITY OF 1st-STORY LOCAL DUCTILITY RATIO DUE TO DIFFERENT LEVELS OF PEAK ACCELERATION (4-STORY IARS FRAME)

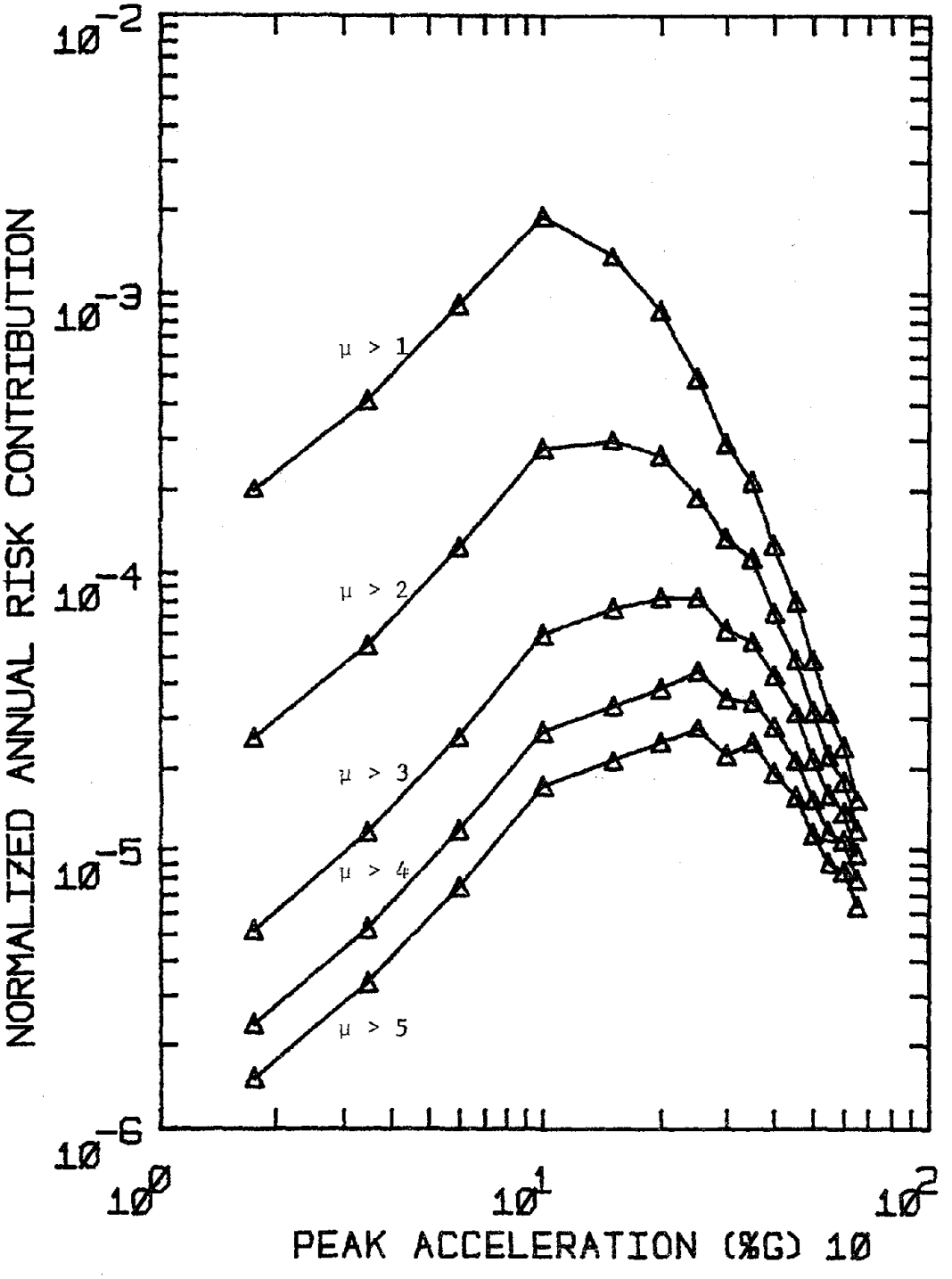

FIG. 6-16 NORMALIZED CONTRIBUTIONS TO ANNUAL EXCEEDANCE PROBABILITY OF 1st-STORY LOCAL DUCTILITY RATIO DUE TO DIFFERENT LEVELS OF PEAK ACCELERATION (10-STORY IARS FRAME)

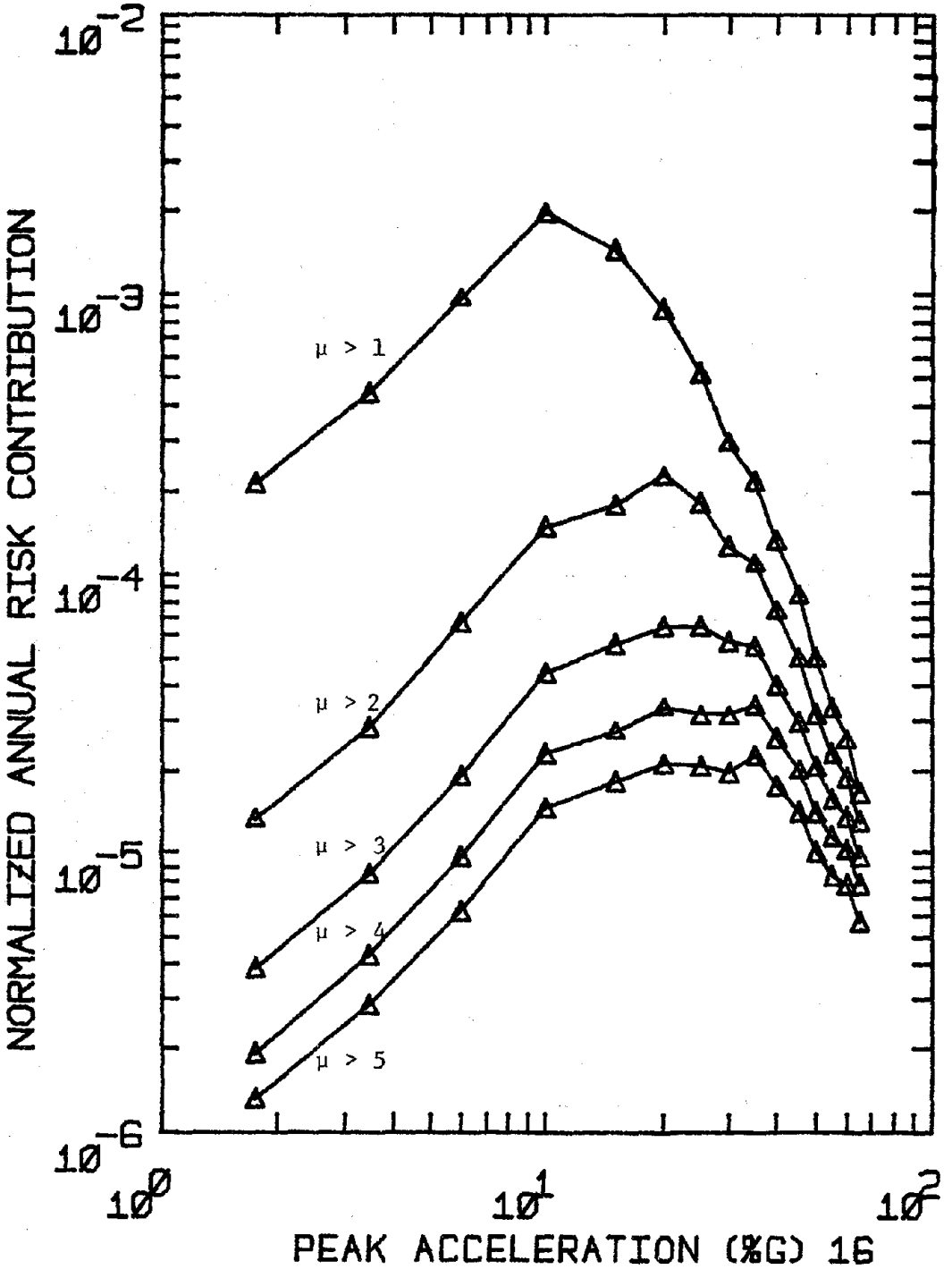

FIG. 6-17 NORMALIZED CONTRIBUTIONS TO ANNUAL EXCEEDANCE PROBABILITY OF 1st-STORY LOCAL DUCTILITY RATIO DUE TO DIFFERENT LEVELS OF PEAK ACCELERATION (16-STORY IARS FRAME)

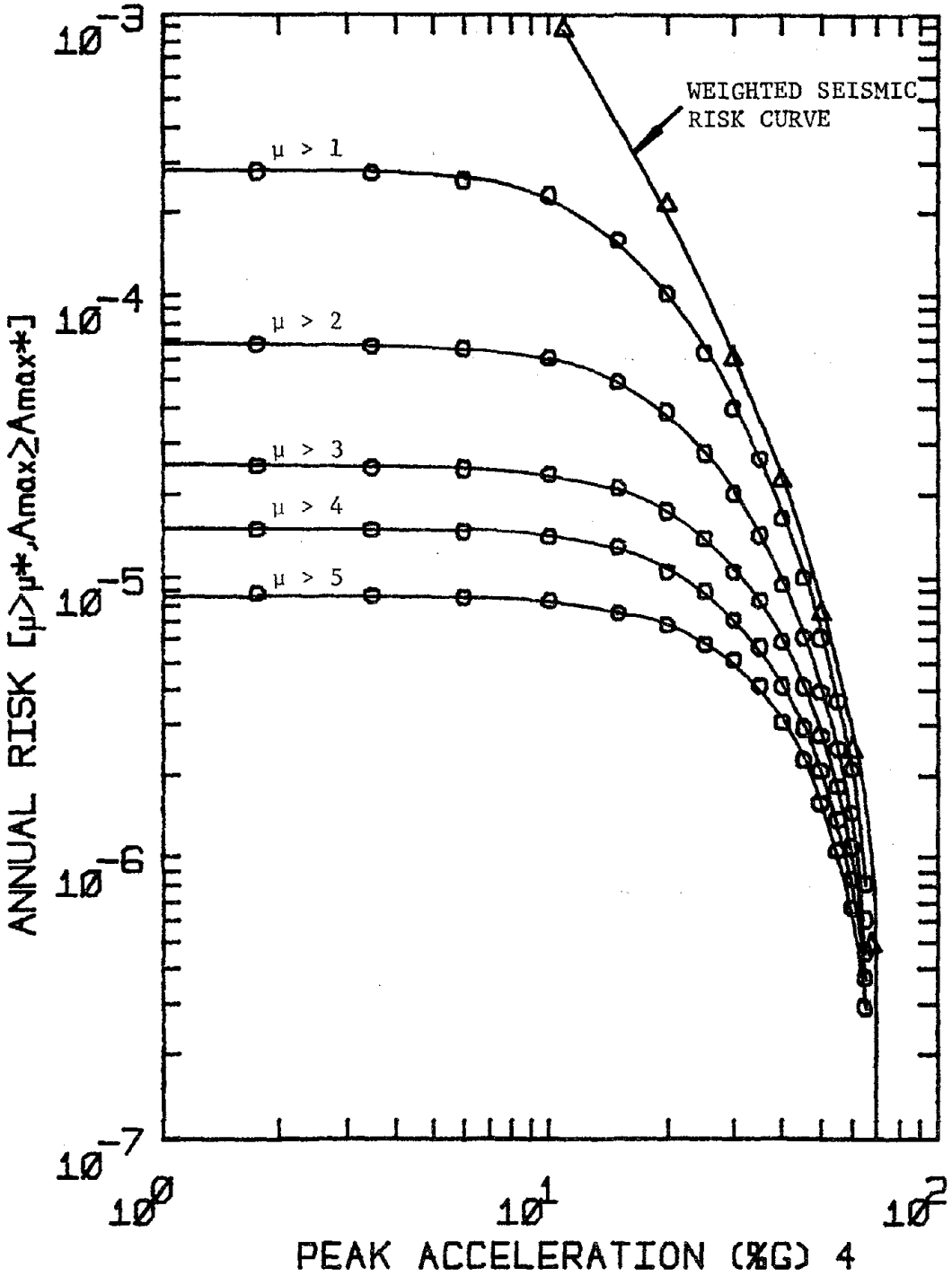

FIG. 6-18 ANNUAL EXCEEDANCE PROBABILITY OF 1st-STORY LOCAL DUCTILITY RATIO (4-STORY IARS FRAME)

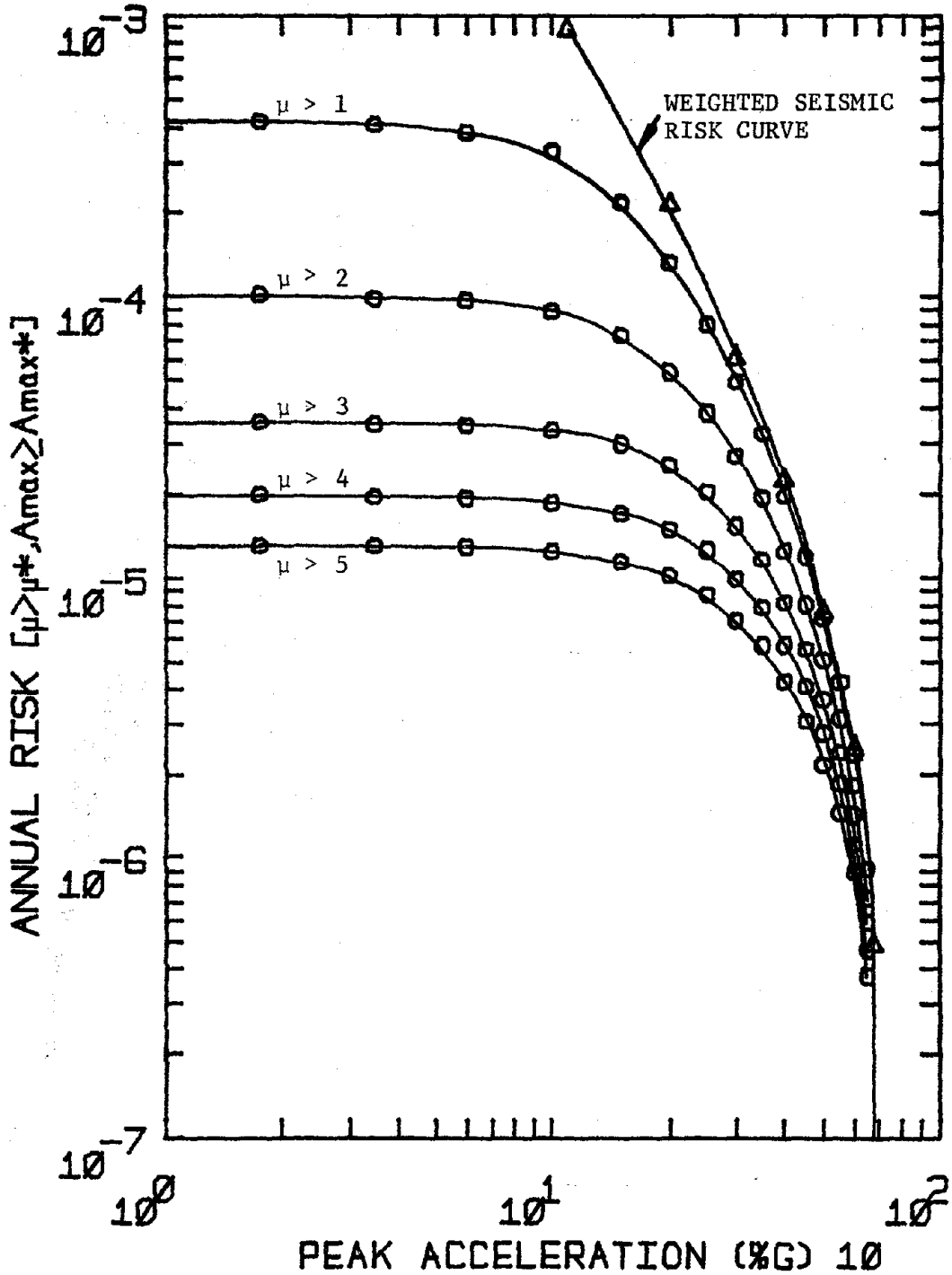

FIG. 6-19 ANNUAL EXCEEDANCE PROBABILITY OF 1st-STORY LOCAL DUCTILITY RATIO (10-STORY IARS FRAME)

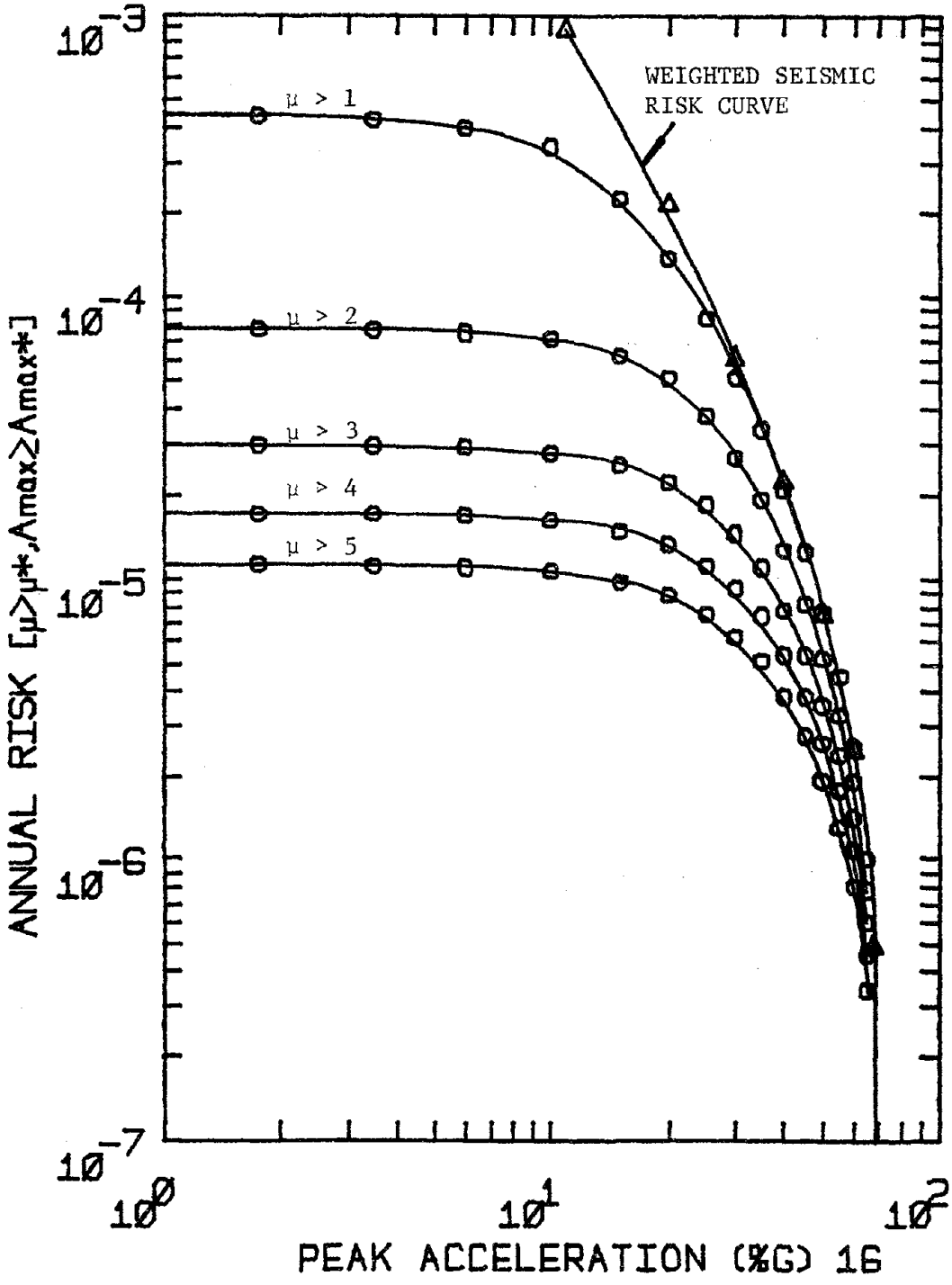

FIG. 6-20 ANNUAL EXCEEDANCE PROBABILITY OF 1st-STORY LOCAL DUCTILITY RATIO (16-STORY IARS FRAME)

results for the three (4-, 10- and 16-story) IARS-designed steel frames are plotted in Figures 6-18, 6-19 and 6-20, respectively. The results for the overall annual risk of exceeding various levels of local ductility ratio are listed in Table 6-4.

The figures show that the annual exceedance probability of the local ductility ratio is asymptotic to the weighted risk curve at high levels of peak ground acceleration; it tends to level off when the peak acceleration is relatively small. For the 4-story steel frame, the annual probability of having at least some local yielding in the first story is estimated at 2.81×10^{-4}, compared to 4.21×10^{-4} and 4.4×10^{-4}, respectively for the 10- and 16-story steel frames. The annual probabilities of exceeding the design local ductility ratio ($\mu = 4$) in the first story are estimated at 1.49×10^{-5}, 1.97×10^{-5} and 1.72×10^{-5}, respectively, for the 4-, 10- and 16-story IARS-designed frames.

Another useful way of presenting data is in terms of a plot of annual exceedance probability versus local ductility threshold. The results for the three frames are presented in Figures 6-21, 6-22 and 6-23. The figures show that the annual exceedance probability generally decreases with increasing local ductility threshold as expected. For peak ground acceleration greater than the design level of 1/3 g, the annual probability that the first-story local ductility ratio will exceed the design value ($\mu = 4$) is estimated at 6.15×10^{-6} for the 4-story frame. It is approximately 8.48×10^{-6} and 8.04×10^{-6} for the 10- and 16-story frames respectively.

6.5.3 Results of UBC-Designed Steel Frames

Using the "weighted" seismic risk curve for the Boston site, the overall seismic safety has also been evaluated for the three steel frames designed according to UBC specifications. The resulting "normalized" an-

TABLE 6-4 ANNUAL EXCEEDANCE PROBABILITIES OF 1st-STORY LOCAL DUCTILITY RATIO FOR DIFFERENT FRAMES

LOCAL DUCTILITY		4-STORY FRAME	10-STORY FRAME	16-STORY FRAME
LARS DESIGN METHOD	$\mu > 1$	2.81×10^{-4}	4.21×10^{-4}	4.40×10^{-4}
	$\mu > 2$	6.80×10^{-5}	1.01×10^{-4}	7.78×10^{-5}
	$\mu > 3$	2.51×10^{-5}	3.58×10^{-5}	3.02×10^{-5}
	$\mu > 4$	1.49×10^{-5}	1.97×10^{-5}	1.72×10^{-5}
	$\mu > 5$	8.80×10^{-6}	1.32×10^{-5}	1.13×10^{-5}
UBC DESIGN METHOD	$\mu > 1$	6.80×10^{-5}	6.70×10^{-5}	3.72×10^{-5}
	$\mu > 2$	1.86×10^{-5}	1.08×10^{-5}	5.28×10^{-6}
	$\mu > 3$	4.15×10^{-6}	3.60×10^{-6}	1.53×10^{-6}
	$\mu > 4$	1.62×10^{-6}	1.61×10^{-6}	9.89×10^{-7}
	$\mu > 5$	5.91×10^{-7}	1.14×10^{-6}	5.91×10^{-7}

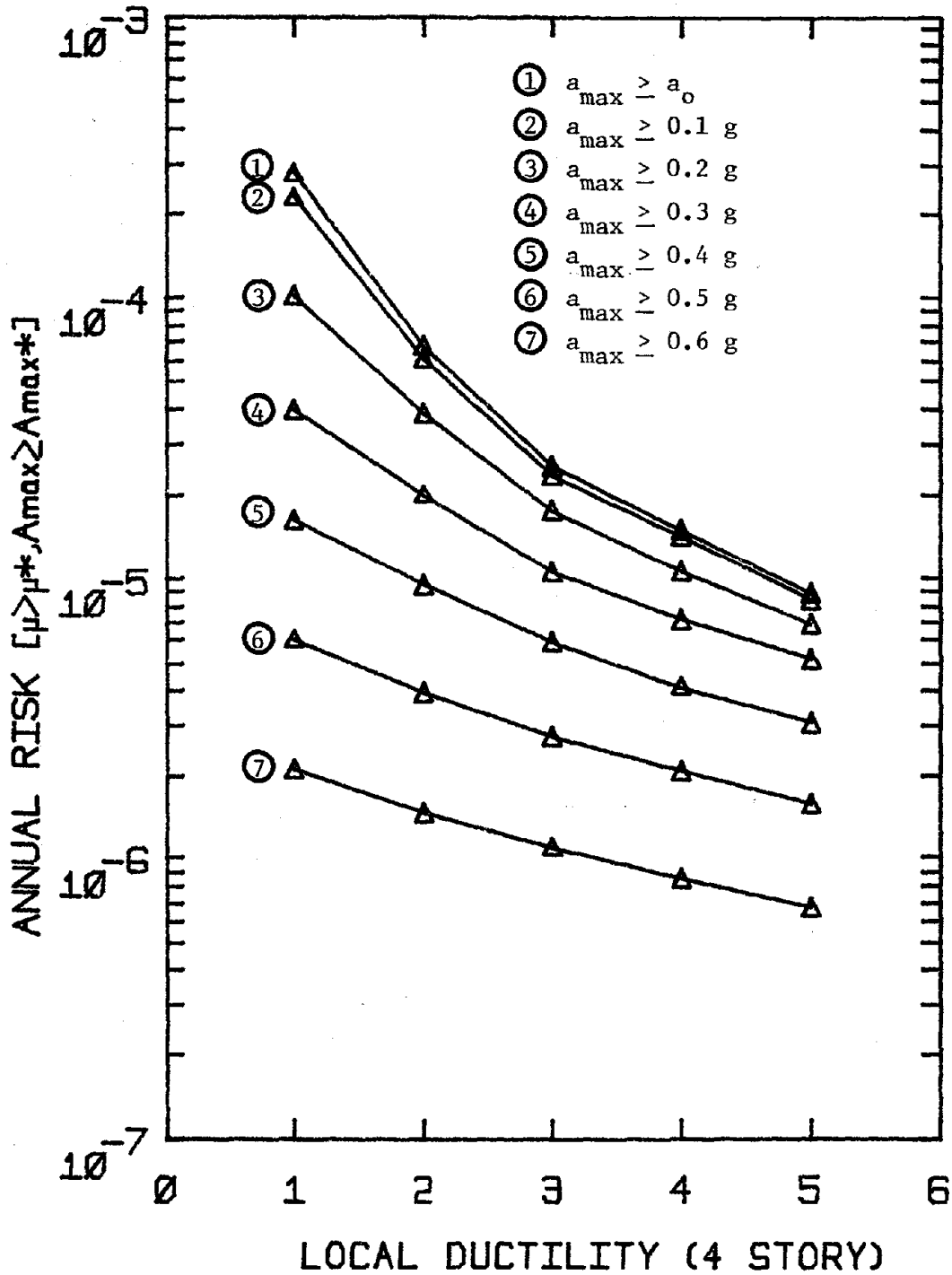

FIG. 6-21 ANNUAL EXCEEDANCE PROBABILITY OF 1st-STORY LOCAL DUCTILITY RATIO FOR DIFFERENT PEAK ACCELERATION THRESHOLDS (4-STORY IARS FRAME)

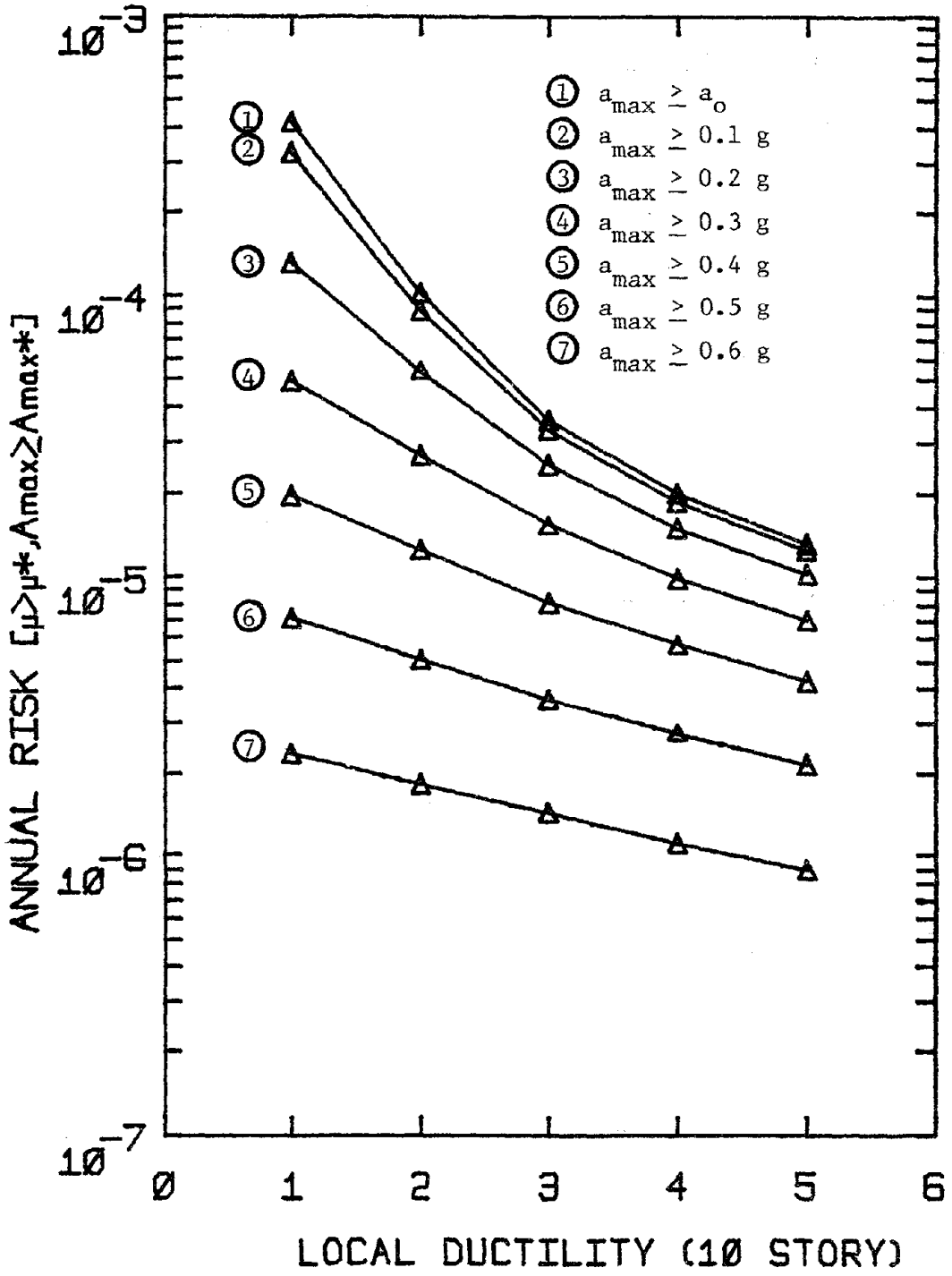

FIG. 6-22 ANNUAL EXCEEDANCE PROBABILITY OF 1st-STORY LOCAL DUCTILITY RATIO FOR DIFFERENT PEAK ACCELERATION THRESHOLDS (10-STORY IARS FRAME)

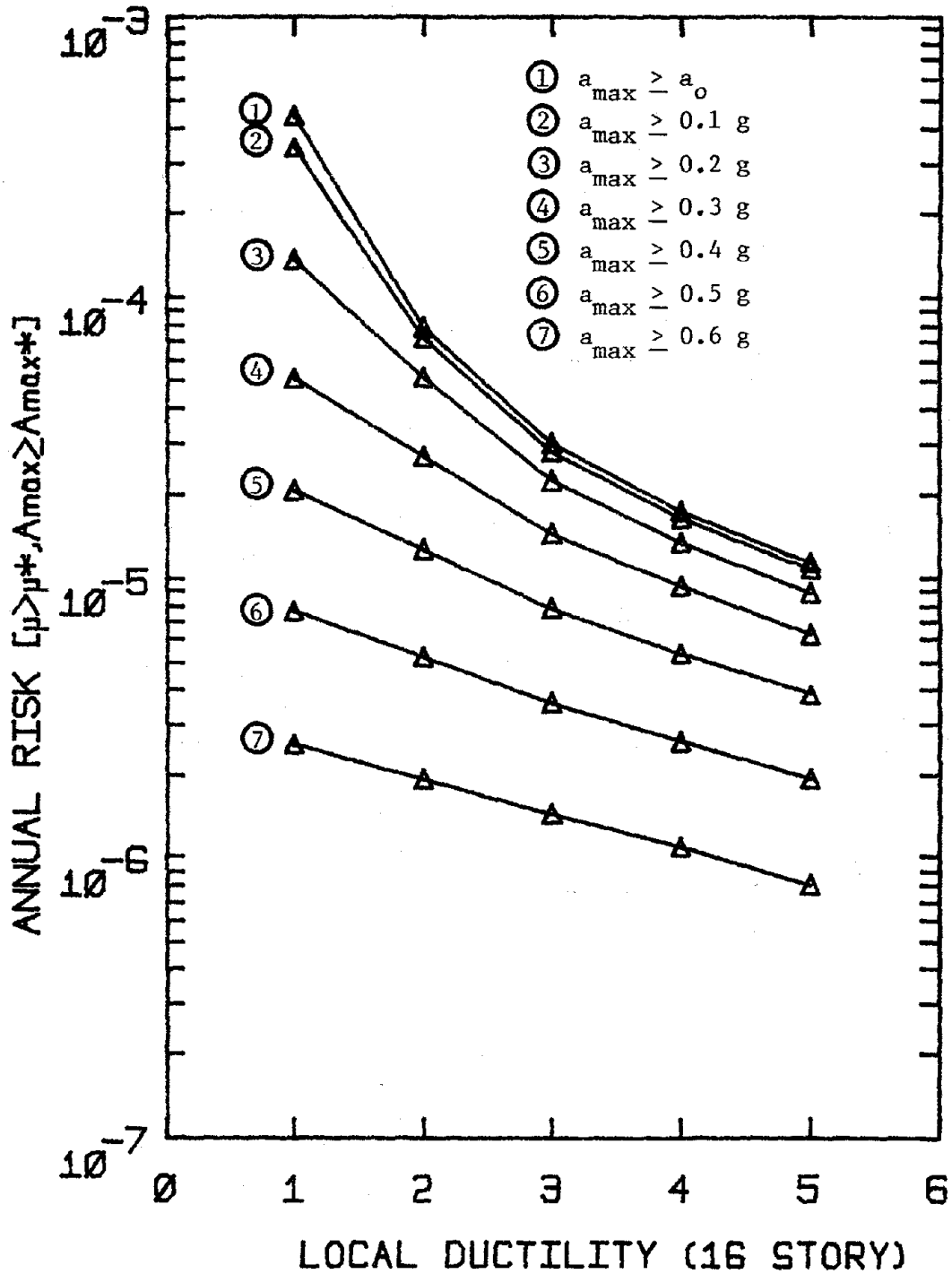

FIG. 6-23 ANNUAL EXCEEDANCE PROBABILITY OF 1st-STORY LOCAL DUCTILITY RATIO FOR DIFFERENT PEAK ACCELERATION THRESHOLDS (16-STORY IARS FRAME)

nual exceedance probabilities for the local ductility ratio are listed in Tables C-4, C-5 and C-6 of Appendix C. The annual risk of exceeding various levels of the local ductility ratio is plotted in Figures 6-24, 6-25 and 6-26 for the three steel frames. The results for the overall annual risk of exceeding different levels of the local ductility ratio are listed in Table 6-4.

As shown in the figures, the annual probability of having at least some yielding (i.e., $\mu > 1$) in the first story is estimated at 6.8×10^{-5} for the 4-story frame. It is approximately 6.7×10^{-5} and 3.72×10^{-5} for the 10- and 16-story steel frames. Notice that these annual exceedance probabilities are smaller than those of the IARS-designed steel frames. This is attributable to the fact that the equivalent story yielding strengths of the UBC-designed frames are greater than those of the IARS-designed steel frames, as depicted in Fig. 6-1.

Figures 6-27, 6-28 and 6-29 show the annual exceedance probability plotted versus the local ductility ratio for the 4-, 10- and 16-story UBC-designed frames. As observed in the preceding section, the annual exceedance probability decreases with increasing local ductility threshold.

6.5.4 Sensitivity w.r.t. Local Seismic Risk

Thus far, local response exceedance probabilities have been computed based on the "weighted" seismic risk curve for the Boston site. An alternative straight-line approximation to the risk curve is employed herein so as to investigate the sensitivity of overall response statistics with respect to assumptions about seismic risk. The linear relationship (on a log-log plot of average return period versus peak ground acceleration) is plotted in Fig. 6-14.

Based on Eq. 6-10, the normalized contributions to the annual exceed-

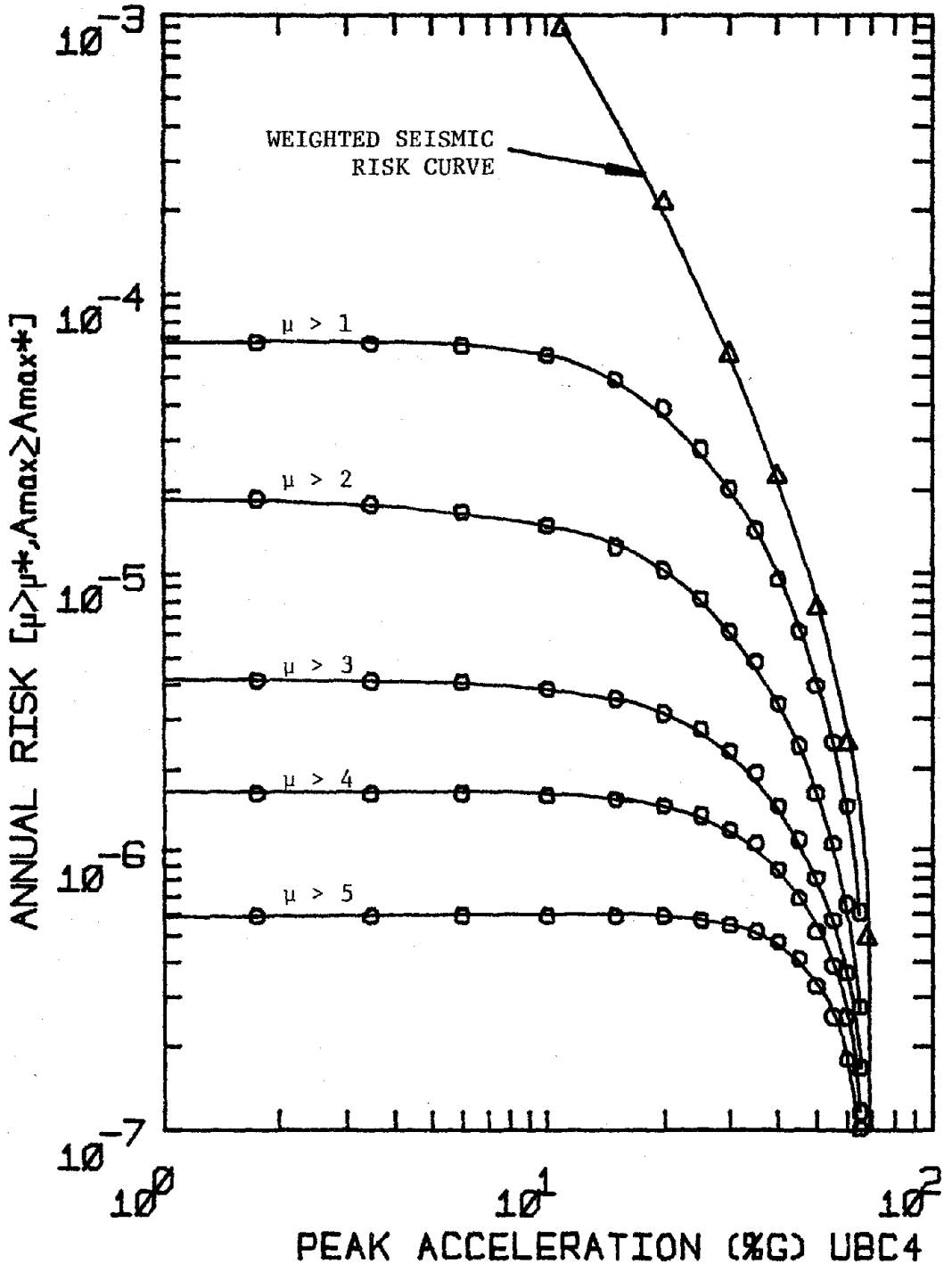

FIG. 6-24 ANNUAL EXCEEDANCE PROBABILITY OF 1st-STORY LOCAL DUCTILITY RATIO (4-STORY UBC FRAME)

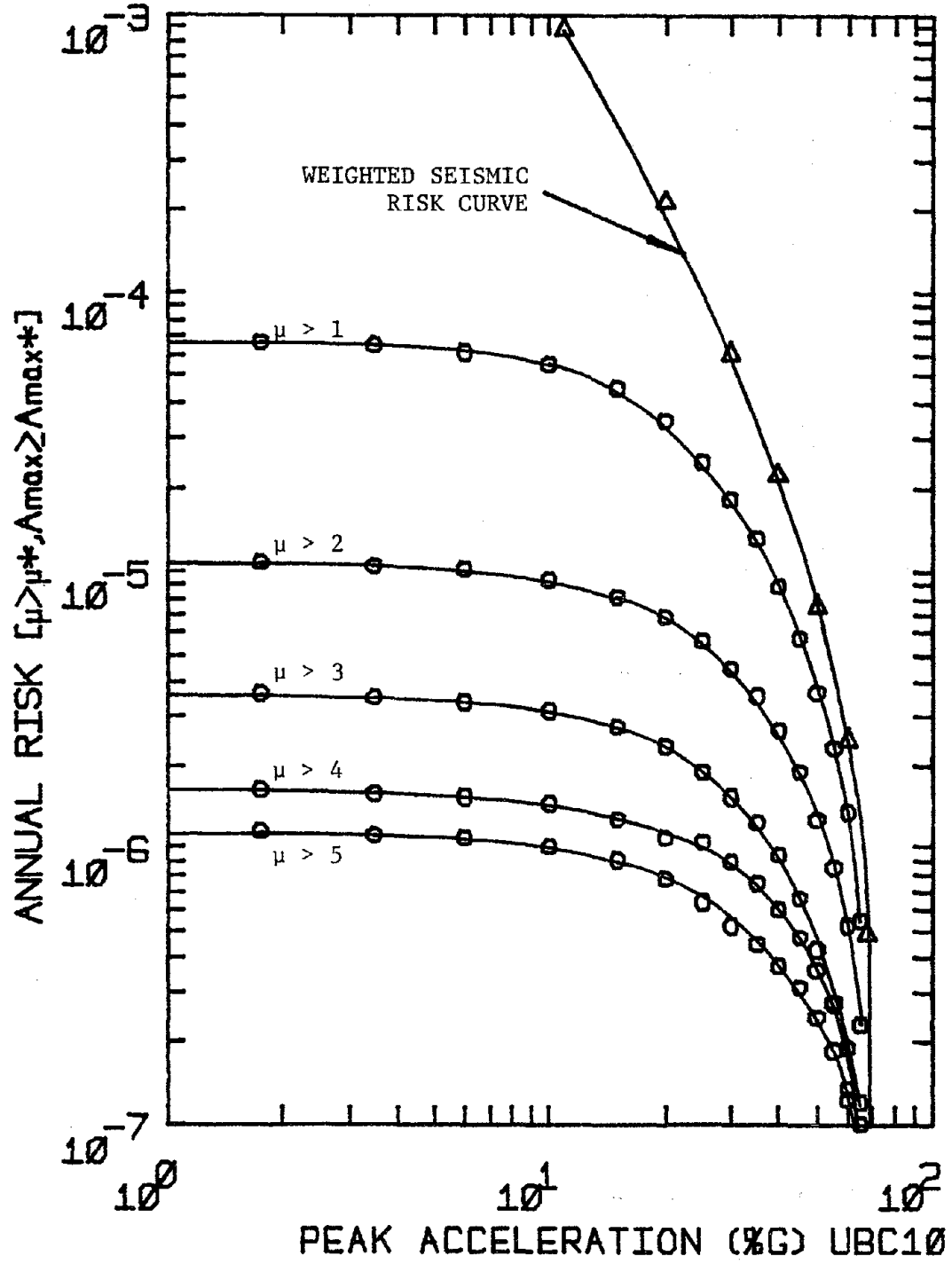

FIG. 6-25 ANNUAL EXCEEDANCE PROBABILITY OF 1st-STORY LOCAL DUCTILITY RATIO (10-STORY UBC FRAME)

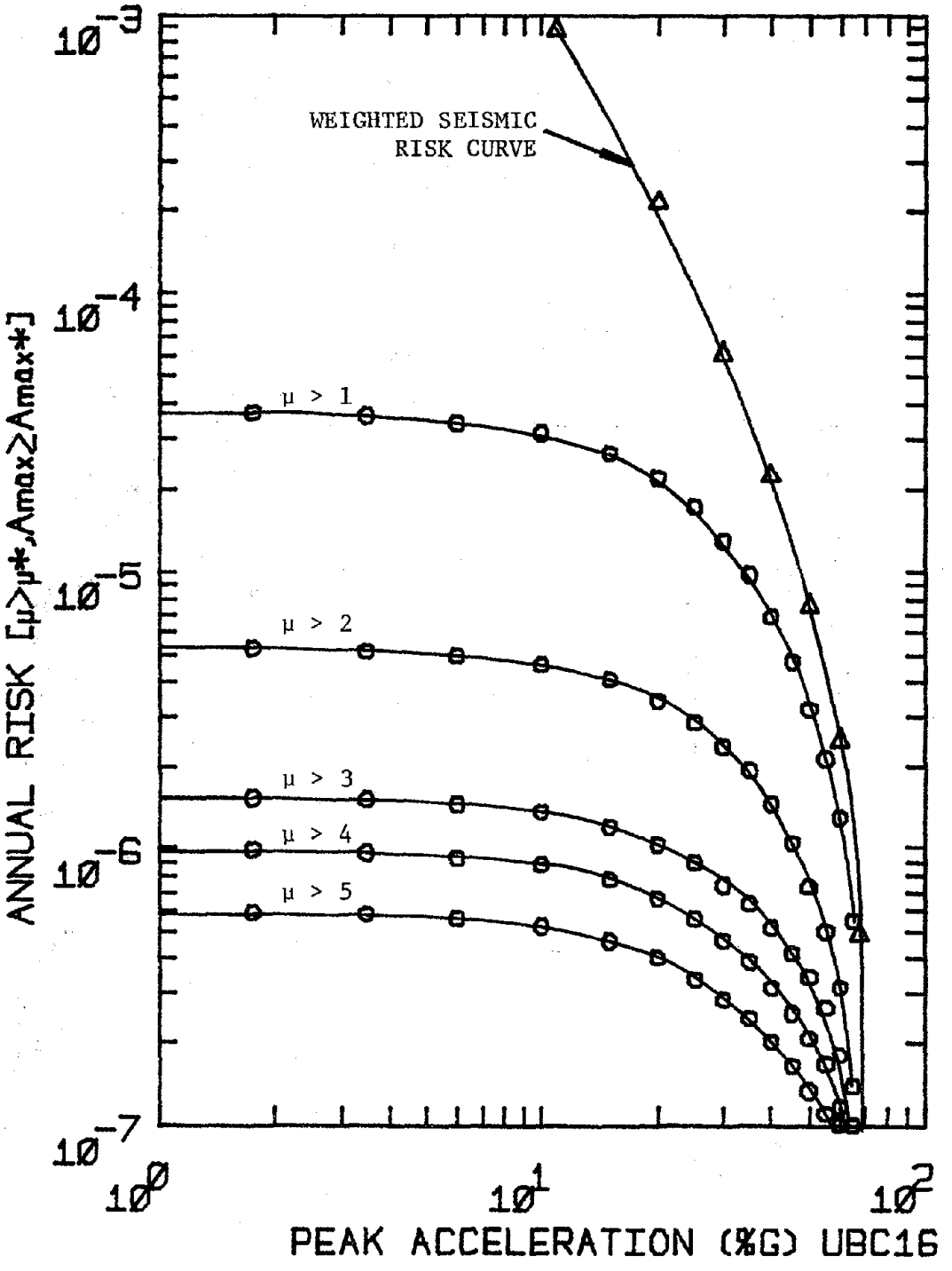

FIG. 6-26 ANNUAL EXCEEDANCE PROBABILITY OF 1st-STORY LOCAL DUCTILITY RATIO (16-STORY UBC FRAME)

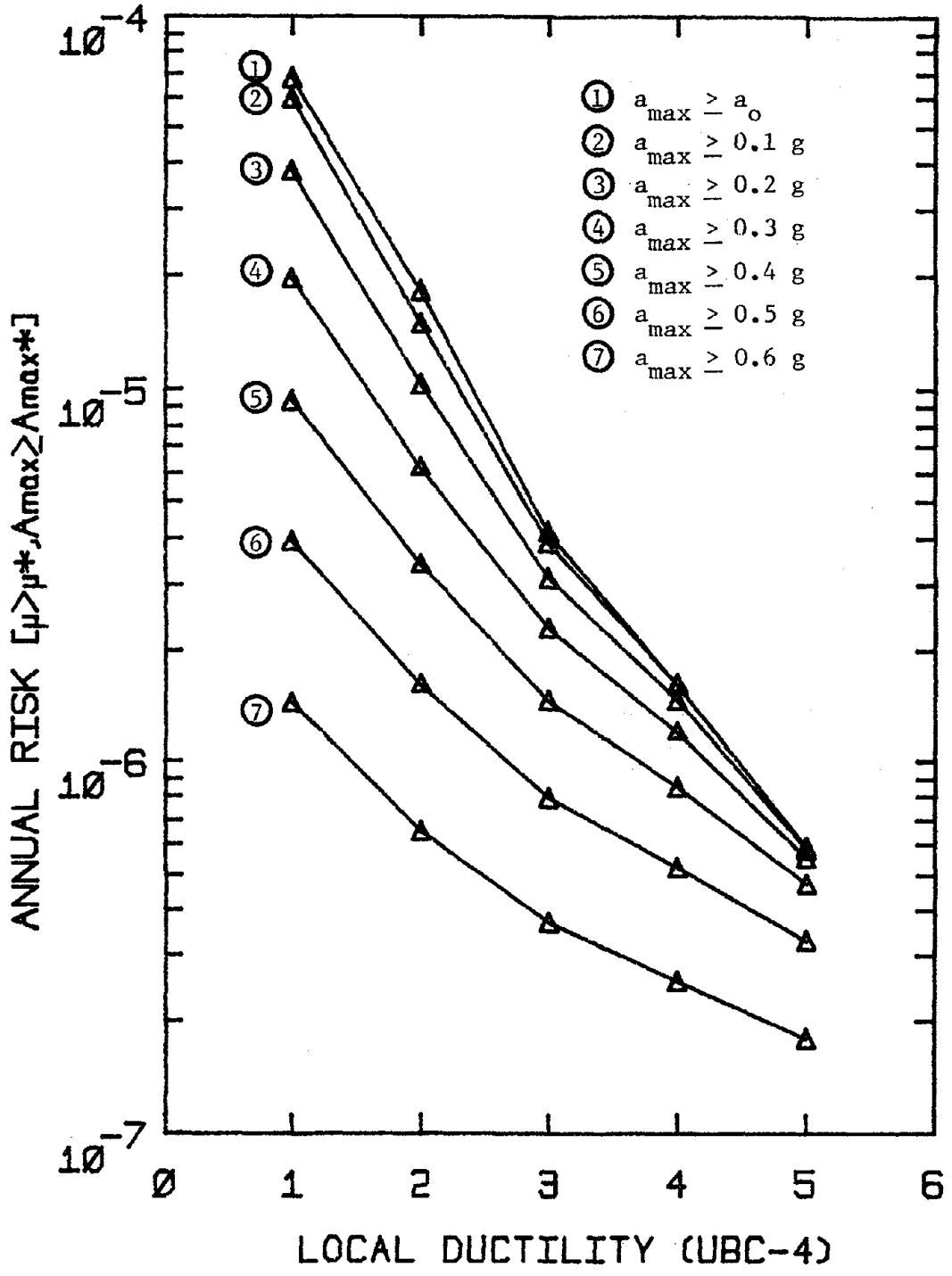

FIG. 6-27 ANNUAL EXCEEDANCE PROBABILITY OF 1st-STORY LOCAL DUCTILITY RATIO FOR DIFFERENT PEAK ACCELERATION THRESHOLDS (4-STORY UBC FRAME)

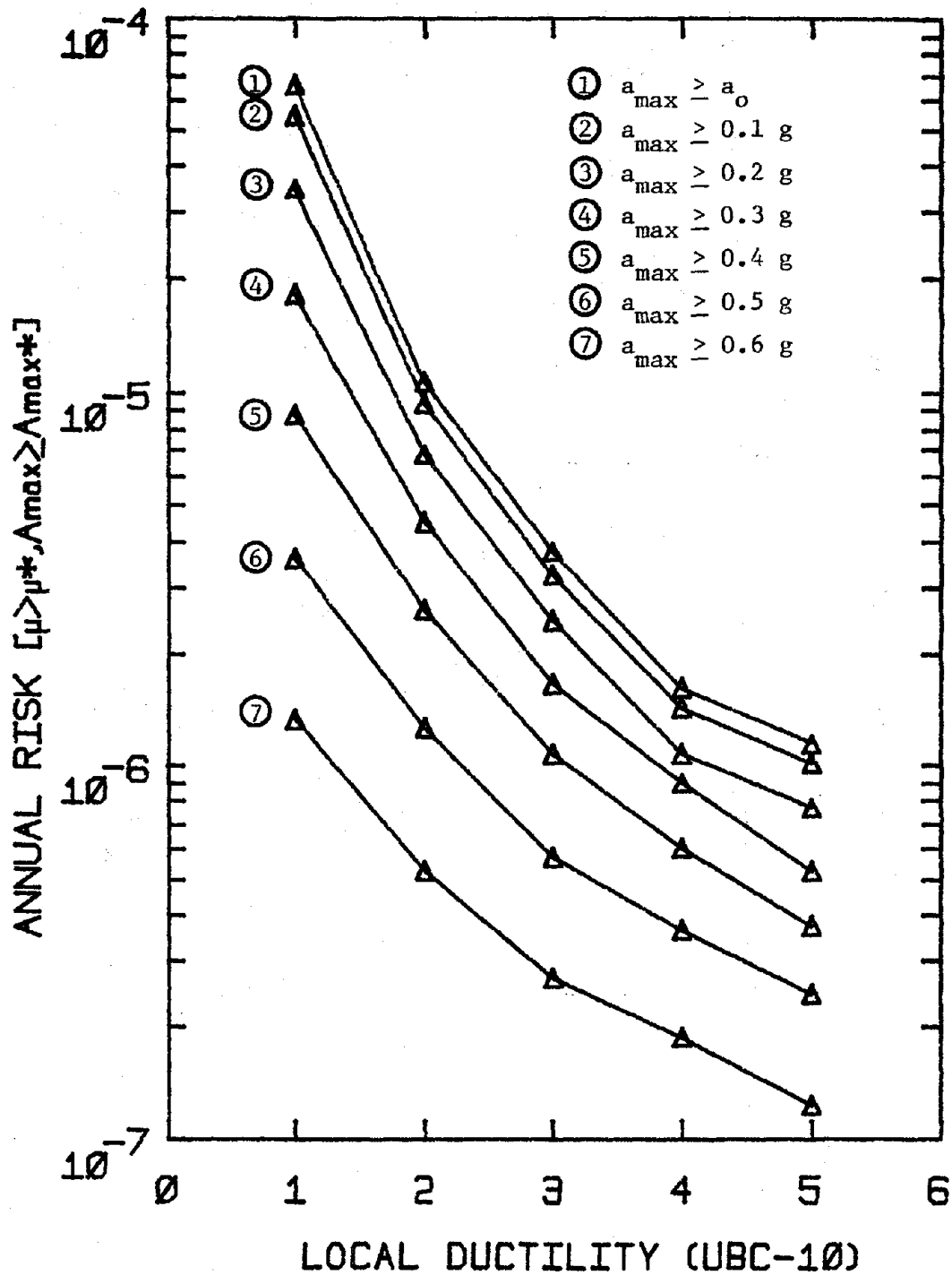

FIG. 6-28 ANNUAL EXCEEDANCE PROBABILITY OF 1st-STORY LOCAL DUCTILITY RATIO FOR DIFFERENT PEAK ACCELERATION THRESHOLDS (10-STORY UBC FRAME)

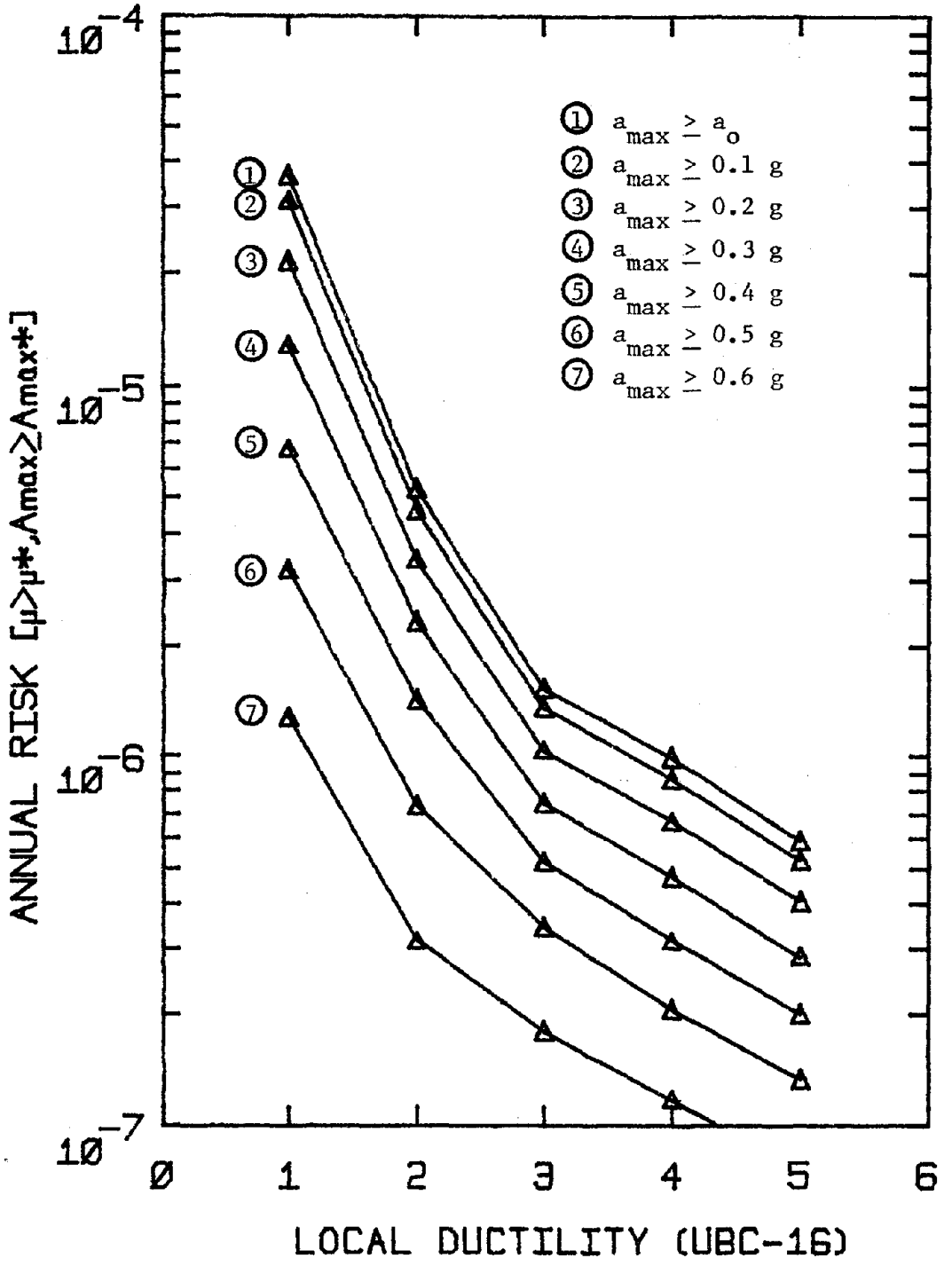

FIG. 6-29 ANNUAL EXCEEDANCE PROBABILITY OF 1st-STORY LOCAL DUCTILITY RATIO FOR DIFFERENT PEAK ACCELERATION THRESHOLDS (16-STORY UBC FRAME)

ance probability of the first-story local ductility ratio have been computed. The results are presented in Figures 6-30, 6-31 and 6-32 for the three IARS-designed steel frames. Notice that the annual exceedance probability has significant contributions due to high acceleration levels. This is most pronounced when the local ductility thresholds are large. Moreover, the location of the maximum contribution tends to shift toward a larger peak ground acceleration compared to the weighted seismic risk curve.

By summing individual contributions, the normalized annual exceedance probabilities for the local ductility ratio are determined; they are listed in Tables C-7, C-8 and C-9 of Appendix C for the three steel frames. The overall annual risk of exceeding various local ductility thresholds are listed in Table 6-5. The annual probability that the first story of the 4-story frame will at least have some local yielding (i.e., $\mu > 1$) is estimated at 4.34×10^{-4}, compared to 2.81×10^{-4} for the "weighted" seismic risk curve. The probabilities are 6.19×10^{-4} and 6.47×10^{-4} for the 10- and 16-story steel frames, respectively, compared to 4.21×10^{-4} and 4.4×10^{-4} for the weighted seismic risk curve. The values of the annual probability of exceeding the design local ductility ratio (i.e., $\mu = 4$) are 3.9×10^{-5}, 5.27×10^{-5} and 4.77×10^{-5} for the 4-, 10- and 16-story steel frames, respectively, (compared to 1.49×10^{-5}, 1.97×10^{-5} and 1.72×10^{-5}, respectively, when the "weighted" seismic risk curve is used).

Hence, it is concluded that the local inelastic response exceedance probabilities are quite sensitive to variations in the local seismic risk. For the case considered, the effect is most pronounced for high local ductility thresholds.

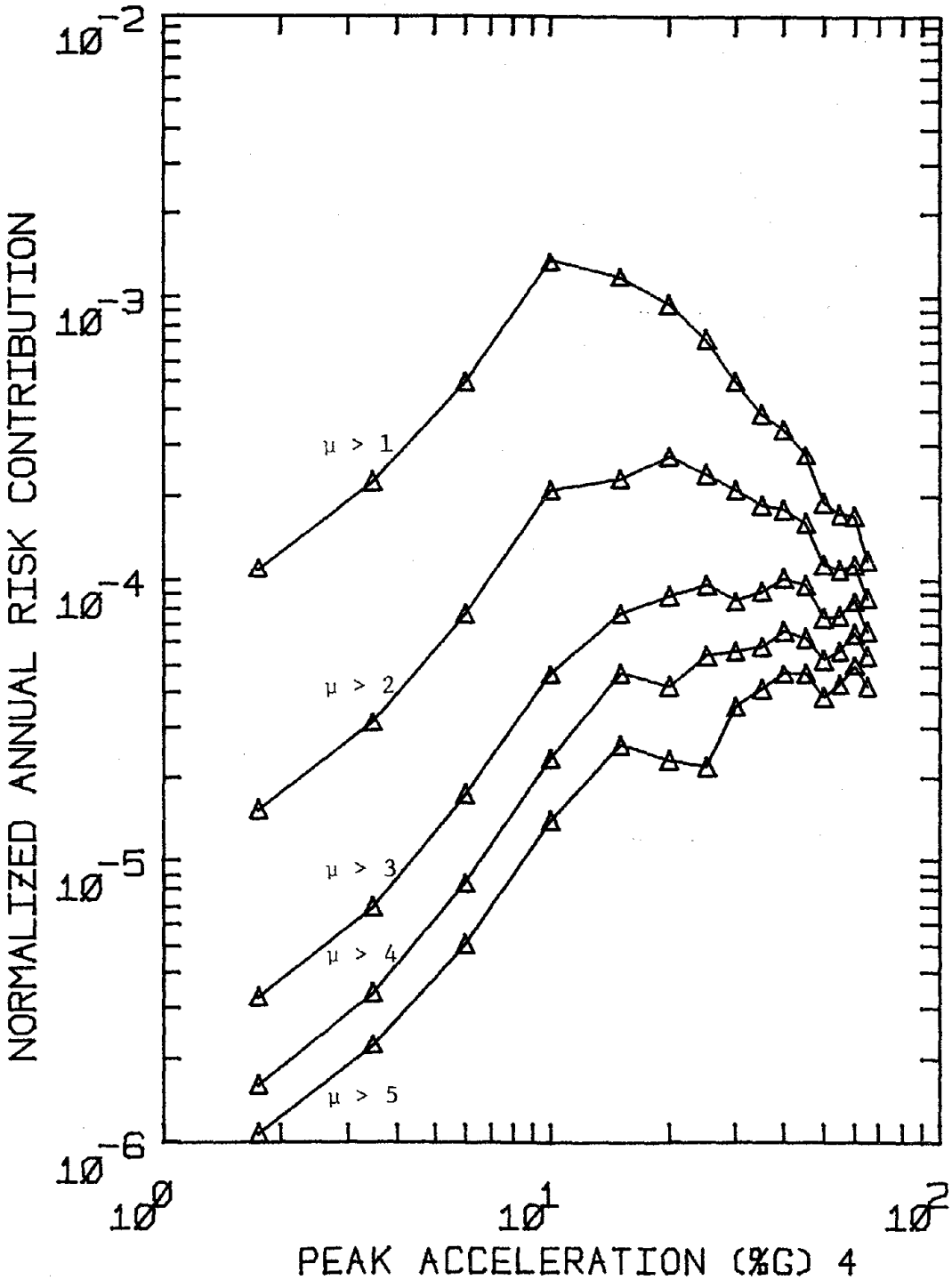

FIG. 6-30 NORMALIZED CONTRIBUTIONS TO ANNUAL EXCEEDANCE PROBABILITY OF 1st-STORY LOCAL DUCTILITY RATIO DUE TO DIFFERENT LEVELS OF PEAK ACCELERATION (4-STORY IARS FRAME, STRAIGHT-LINE SEISMIC RISK)

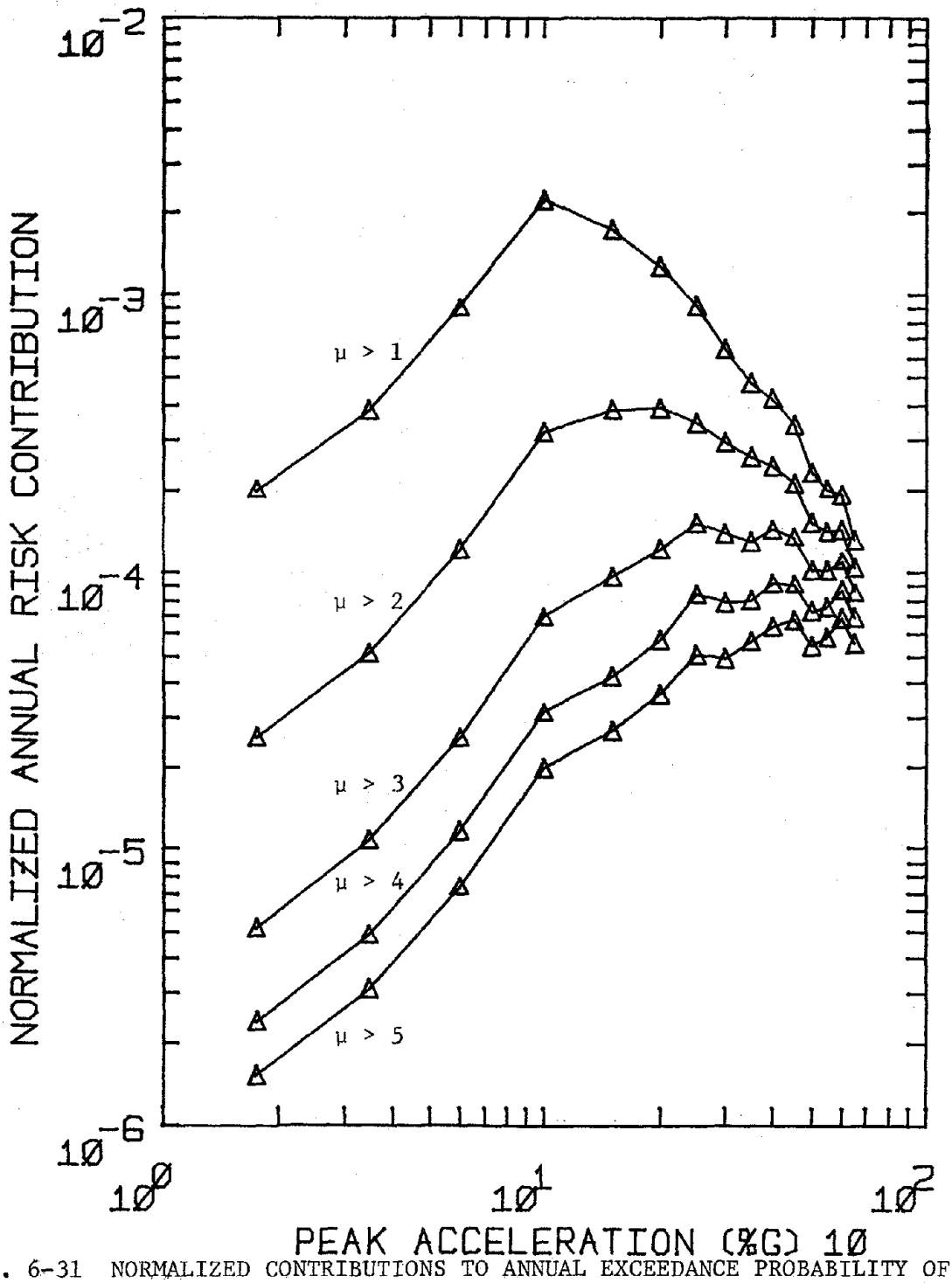

FIG. 6-31 NORMALIZED CONTRIBUTIONS TO ANNUAL EXCEEDANCE PROBABILITY OF 1st-STORY LOCAL DUCTILITY RATIO DUE TO DIFFERENT LEVELS OF PEAK ACCELERATION (10-STORY IARS FRAME, STRAIGHT-LINE SEISMIC RISK)

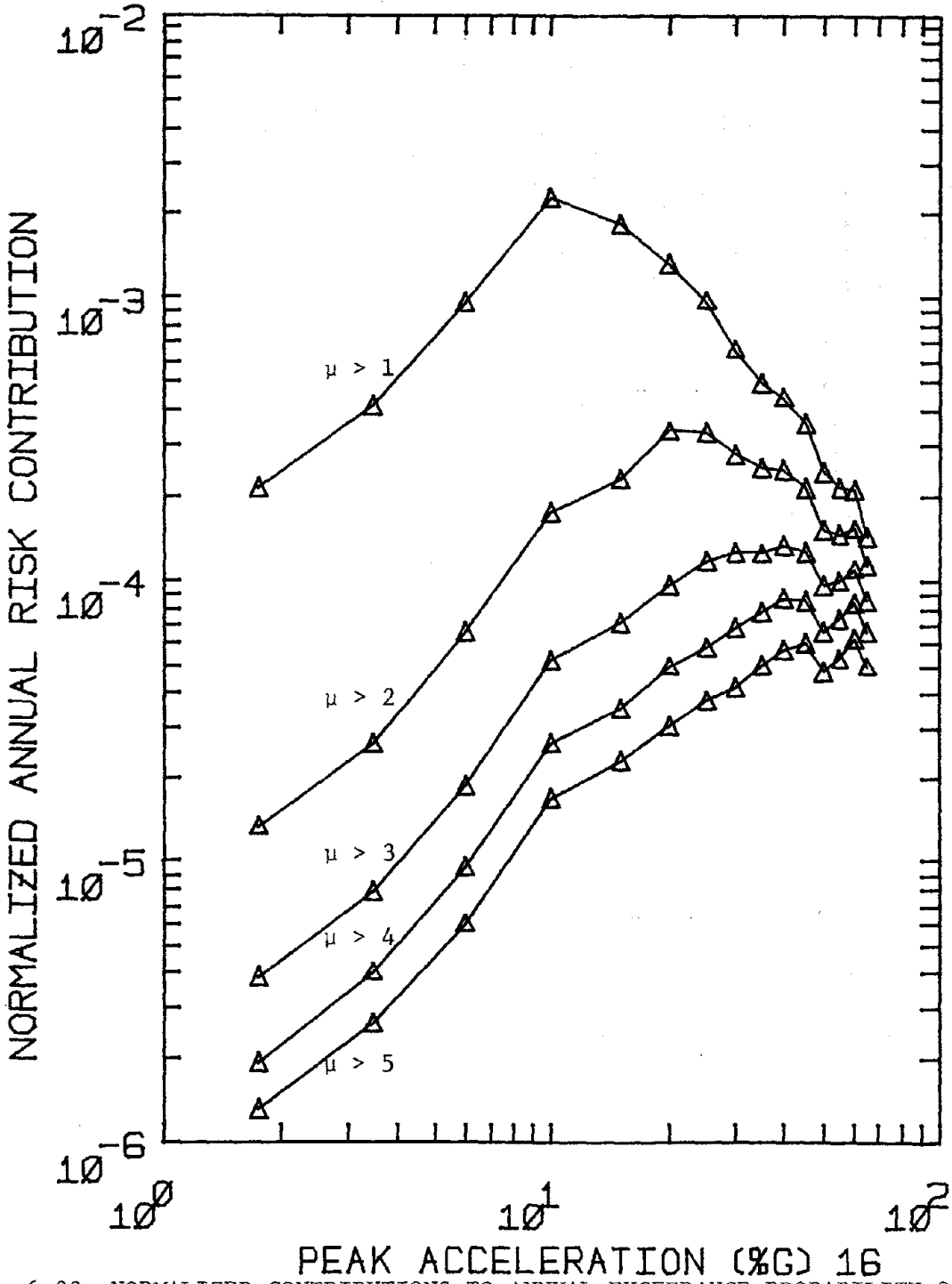

FIG. 6-32 NORMALIZED CONTRIBUTIONS TO ANNUAL EXCEEDANCE PROBABILITY OF 1st-STORY LOCAL DUCTILITY RATIO DUE TO DIFFERENT LEVELS OF PEAK ACCELERATION (16-STORY IARS FRAME, STRAIGHT-LINE SEISMIC RISK)

TABLE 6-5 ANNUAL EXCEEDANCE PROBABILITIES OF 1st-STORY LOCAL DUCTILITY RATIO FOR DIFFERENT FRAMES (STRAIGHT-LINE SEISMIC RISK)

LOCAL DUCTILITY		4-STORY FRAME	10-STORY FRAME	16-STORY FRAME
IARS DESIGN METHOD	$\mu > 1$	4.34×10^{-4}	6.19×10^{-4}	6.47×10^{-4}
	$\mu > 2$	1.34×10^{-4}	1.92×10^{-4}	1.65×10^{-4}
	$\mu > 3$	6.08×10^{-5}	8.56×10^{-5}	7.65×10^{-5}
	$\mu > 4$	3.90×10^{-5}	5.27×10^{-5}	4.77×10^{-5}
	$\mu > 5$	2.64×10^{-5}	3.71×10^{-5}	3.26×10^{-5}

TABLE 6-6 RELATIONSHIP BETWEEN DAMAGE FACTOR AND DUCTILITY RATIO FOR DIFFERENT FRAMES

FRAMES	$\mu = 1$	$\mu = 2$	$\mu = 3$	$\mu = 4$	$\mu = 5$
4-STORY	0	2.586×10^{-3}	1.188×10^{-2}	2.899×10^{-2}	5.459×10^{-2}
10- & 16-STORY	0	1.372×10^{-3}	1.097×10^{-2}	3.704×10^{-2}	8.779×10^{-2}

6.5.5 System Reliability of Local Inelastic Response

Based on the annual local ductility level exceedance probability for each story (denoted by $P[\mu_i > \mu^*, a_{max} \geq a_o]$), approximate bounds can be established on the "system reliability", i.e., the annual probability of no exceedance anywhere in the building [22]:

$$\max_{i=1}^{n} \left(P[\mu_i > \mu^*, a_{max} \geq a_o]\right) \leq P[\mu > \mu^*, a_{max} \geq a_o] \leq \sum_{i=1}^{n} P[\mu_i > \mu^*, a_{max} \geq a_o] \tag{6-13}$$

where n is the number of stories of the building and μ^* is any given local ductility threshold.

The lower bound is based on the assumption of perfect correlation among the inelastic responses of all stories, whereas the upper bound corresponds to the assumption of complete statistical independence among them. For each of the six moment-resisting steel frames under study, the annual probability for the first-story local inelastic response exceedance is generally larger than that for the other stories. Since the collapse (i.e., extremely severe local yielding) at the bottom story implies total failure of the entire building, it is conceivable that the system failure probability may be approximated by the annual exceedance probability of the first-story local response. Therefore, the first-story results presented in the preceding sections are used to characterize the overall seismic system reliability for each of the building frames (though it may be somewhat unconservative).

6.6 Correlation Between Local Ductility Ratio and Building Damage

Few attempts have been reported in the literature to assess quantitatively the building damage due to strong earthquake motions. For example, based on damage survey of actual buildings, Whitman [67] and Whitman et al. [68] suggested a set of the so-called "damage states" (related to the modified Mercalli intensity) for different types of buildings. The damage state is defined in two ways: i) by qualitative description of the degree of structural and non-structural damage and ii) by the damage ratio (i.e., the ratio of the repairing cost of seismic damage to the replacement cost of the building). In a recent study, by using a normalized dissipated energy and an element stiffness ratio (i.e., the initial stiffness divided by the final secant stiffness), Banon [6] proposed a stochastic model for predicting seismic damage in reinforced concrete frames.

In developing the so-called "spectral matrix method" for predicting building damage, Blume and Monroe [11] suggested a "damage factor" for relating the ductility ratio to the structural damage. The damage factor (DF) has been modified by Blume et al. as follows [12,52]:

$$DF = \left(\frac{\mu - 1}{\mu_{ult} - 1}\right)^{\kappa} = \frac{\text{Repair Cost}}{\text{Replacement Cost}} \tag{6-14}$$

where μ_{ult} is the ultimate ductility of the building (i.e., the point at which the structural deformation increases with decreasing shear force). The quantity κ is an empirical "economic factor" which varies with different types of buildings. Using this empirical relationship between structural (and non-structural) damage and the local ductility ratio, it becomes possible to consider the balance between replacement cost (or discounted initial cost) and the expected damage due to future earthquakes for a par-

ticular building frame at a specific site.

Consider first the 4-story IARS-designed steel frame for which an ultimate ductility ratio of 16 and an economic factor of 2.2 are assumed [12]. As listed in Table 6-6, the damage factors corresponding to various levels of local ductility ratio can be conveniently computed by Eq. 6-14. Hence, the annual exceedance probability of the local ductility ratio can be readily interpreted as the annual probability of exceeding a given damage factor. For example, the annual probability that the damage factor will exceed 5.46×10^{-2} (which corresponds to $\mu > 5$) is estimated at 8.8×10^{-6}. This is illustrated in Fig. 6-33. The results for the 4-story UBC-designed steel frame are also plotted in the figure.

For the middle-height (10-story) and high-rise (16-story) buildings, Scholl [52] suggested an ultimate ductility ratio of 10 and an empirical economic factor of 3. Based on these values, the damage ratios have been computed for different levels of local ductility ratios, and are listed in Table 6-6. The resulting annual probabilities of damage factor exceedance are plotted in Fig. 6-33 for the 10- and 16-story IARS- and UBC-designed steel frames. For example, the annual probability that the damage factor will exceed 8.8×10^{-2} (or $\mu > 5$) is 1.32×10^{-5} for the 10-story IARS-designed steel frame; it is 1.14×10^{-6} for the 10-story UBC-designed frame. The annual probability that the damage factor will exceed 8.8×10^{-2} (or $\mu > 5$) is 1.13×10^{-5} for the 16-story IARS-designed frame; for the 16-story UBC-designed frame, it is 5.91×10^{-7}.

Given the discounted initial building cost (or replacement cost), the annual probability of damage factor exceedance can be used to quantify the effectiveness of alternate design procedures for steel buildings in reducing the risk of damage due to earthquake loads. Since the complicated

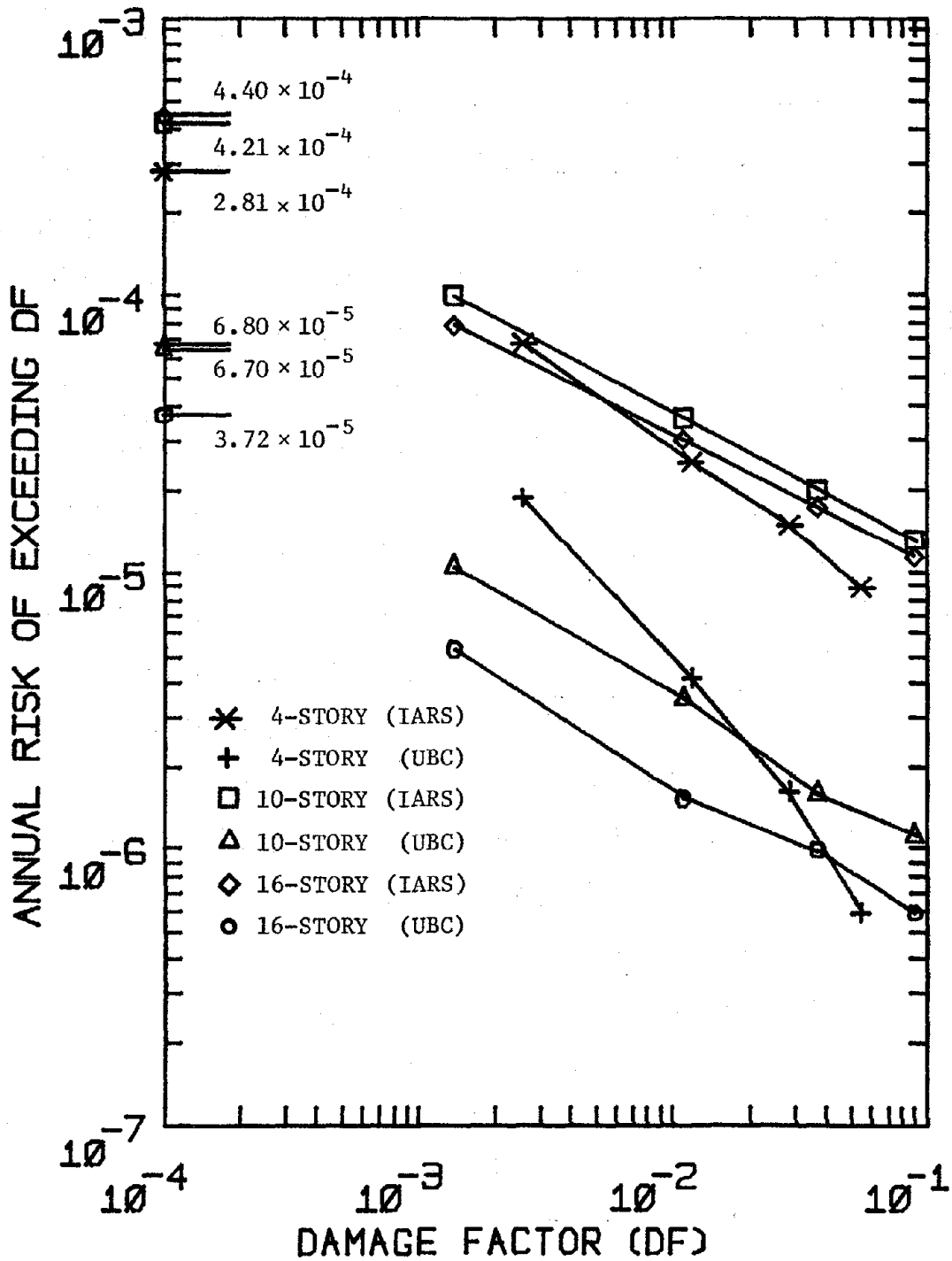

FIG. 6-33 ANNUAL EXCEEDANCE PROBABILITIES OF DAMAGE FACTOR FOR DIFFERENT FRAMES

cost issue of real buildings is beyond the scope of this research endeavor, no attempt has been made to pursue the cost-effectiveness investigation in greater depth.

6.7 Summary

Based on the investigation of three steel moment-resisting frames which represent real world low (4-story), middle-height (10-story) and high-rise (16-story) buildings, the degree of overall seismic safety has been compared for different building design methods. Specifically, the code-based design method (i.e., the Uniform Building Code) and the design method using the "Inelastic Acceleration Response Spectrum" were considered. For illustrative purposes, a "weighted" seismic risk curve for a hypothetical Boston site was employed. A straight-line approximation (on a log-log plot) to the risk curve has also been investigated. Major conclusions can be summarized as follows:

(1) Due to the fact that the local inelastic response is sensitive to the extremes of some pertinent random variables, in particular, the Kanai-Tajimi frequency, the local response statistics predicted by the mean value "First-Order Second-Moment" method is inadequate. The method of enumeration is found to be more desirable in computing the overall seismic response statistics.

(2) Based on the "weighted" seismic risk for the Boston site, and for the steel frames considered, the annual probability of having at least some local yielding (i.e., $\mu > 1$) in the first story is shown to have significant contributions due to low levels of peak ground acceleration. The dominant contributions to the probability of exceeding a

high local ductility threshold come from the intermediate ground acceleration range.

(3) The annual exceedance probability for the local inelastic response generally decreases with increasing local ductility threshold, as expected. It approaches asymptotically the site-specific seismic risk curve when the peak ground acceleration threshold becomes large.

(4) The annual probabilities of exceeding local ductility ratios are generally smaller for the three UBC-designed frames than for the corresponding IARS-designed steel frames. This is due to the fact that the equivalent story yielding strengths of the UBC-designed frames are greater than those of the IARS-designed steel frames.

(5) By using a straight-line approximation (on a log-log plot) to the weighted seismic risk curve for the Boston site, it is shown that the annual probability of local inelastic response exceedance is quite sensitive to the variation of the local seismic risk curve. The effect is most significant at high local ductility thresholds.

(6) Based on the annual exceedance probability of local inelastic response for each story level, bounds can be approximately established on the "system-reliability", i.e., the annual exceedance probability of local response of the entire building. The lower bound is based on the assumption of perfect correlation among the inelastic responses of all stories, whereas the upper bound corresponds to the assumption of complete statistical independence among them.

(7) By using empirical relationships between structural (and non-structural) damage and local ductility ratios, it becomes possible to consider in quantitative terms the balance between replacement cost and expected damage due to future earthquakes for a building frame.

CHAPTER 7

CONCLUSIONS AND RECOMMENDATIONS

7.1 Conclusions

In this investigation of the seismic safety of buildings, three major sources of uncertainty have been extensively examined: i) the representation of the earthquake environment, ii) the dynamic structural properties, and iii) the method of dynamic analysis. Based on an approximate multi-degree elasto-plastic random vibration methodology, the overall seismic safety analysis of buildings has been formulated. The degree of seismic safety has been assessed quantitatively for several multistory steel buildings designed by different methods. Specifically, the conventional code-based design method, i.e., the Uniform Building Code [58], and a more complicated design method based on the "Inelastic Acceleration Response Spectrum" [39] were considered. Three moment-resisting steel frames which represent real world low (4-story), middle-height (10-story) and high-rise (16-story) buildings have been studied. The major conclusions of this research endeavor are summarized as follows:

(1) If the frequency content of strong earthquake motion is characterized by the Kanai-Tajimi power spectral density function, the four ground

motion parameters for which the statistical description of the motion is needed are: i) peak ground acceleration, ii) strong-motion duration, iii) Kanai-Tajimi frequency and iv) Kanai-Tajimi damping. The latter three parameters are appoximately mutually independent. Both the strong-motion duration and the K-T frequency may be assumed Gamma-distributed, whereas the K-T damping is approximately Lognormal-distributed.

(2) The influence of the site condition on strong-motion duration is significant. The mean duration for records on soil is twice that for records on rock. The mean Kanai-Tajimi frequency for soil site records is smaller than that of rock site records. The mean K-T frequency for rock site records is 26.7 rad/sec, which is much higher than the value of 4π rad/sec often suggested in the literature [22,48,60].

(3) Based on an analysis of moving average statistics, it is concluded that the strong-motion duration and the peak ground acceleration are negatively correlated. This is attributable to their common dependence on epicentral distance and local magnitude. In particular, for an earthquake with given magnitude, as the epicentral distance increases, the peak ground acceleration tends to decrease, whereas the strong-motion duration tends to increase.

(4) For given earthquake local magnitude and epicentral distance, empirical relationships are suggested to predict strong-motion duration. Given the peak ground acceleration, the strong-motion duration can also be estimated. Based on a brief compatibility study, it is concluded that these proposed relationships lead to a reasonably consistent prediction of the strong-motion duration.

(5) Based on an extensive simulation study of one-degree elasto-plastic

systems, the Karnopp-Scharton energy conservation equation [35] is found to be valid only for high yielding thresholds. In the range of ductilities of earthquake engineering interest (say, about 5), a semi-empirical modification has been suggested. The same modification has been incorporated in the multi-degree elasto-plastic random vibration solution for shear-beam systems.

(6) The equivalent story stiffnesses of a structural frame can be satisfactorily determined by the "First Mode Approximation" method, whereas the "Biggs method" tends to lead to an unconservative estimate of the first-story stiffness and to conservative stiffnesses for the other stories. The "yielding strength factor" is introduced so as to correct the underestimation of equivalent story yielding strength computed from the upper bound approximation suggested by Anagnostopoulos [2]. The factor is found to be dependent on the actual stiffness distribution between columns and girders.

(7) For a close-coupled shear-beam system, the story response statistics predicted by the modified multi-degree elasto-plastic random vibration methodology are quite compatible with those obtained by multiple time-history analyses. But it may be somewhat overestimated when the ground motion is intense.

(8) By using the "local ductility correction factor", the "local" component response statistics of a structural frame can be satisfactorily related to the random vibration prediction of the "story" response characteristics for the corresponding equivalent shear-beam system. The effect of gravity loads on the local inelastic response has been implicitly accounted for by the local ductility correction factor.

(9) The average maximum story displacements estimated by multiple time-history analyses of a structural frame are quite compatible with those obtained for the equivalent shear-beam system. Useful approximate upper and lower bounds on the maximum story displacement can be determined by the simple summation (in absolute values) and the "SRSS" combination of the maximum story distortions predicted by the random vibration methodology.

(10) Through extensive sensitivity studies, the local inelastic response (conditional given the peak ground acceleration) of a structural frame is found to be relatively insensitive to the variations of the Kanai-Tajimi damping and the structural damping. But it is quite sensitive to the variabilities of the Kanai-Tajimi frequency and the local ductility correction factor. The local response is also significantly dependent on the fundamental natural frequency of the structural frame, and therefore, on the natural period ratio.

(11) The mean local ductility ratio increases with peak ground acceleration, as expected, and the increase is more pronounced in the bottom stories. This may be attributable to the fact that a great portion of the excitation energy is dissipated by severe plastic action in the bottom stories, resulting in smaller levels of inelastic response in the upper stories.

(12) The local inelastic response of a structural frame generally increases with increasing strong-motion duration. When the strong-motion duration and the peak ground acceleration are taken to be negatively correlated, the resulting local response is smaller than when no correlation is assumed between the duration and the peak acceleration. How-

ever, the effect is not very pronounced when evaluated in light of the sensitivity with respect to other parameters.

(13) By combining the uncertainties in the ground motion representation, the structural dynamic properties and the method of dynamic analysis, the "conditional reliability" (given the peak ground acceleration) of local inelastic response can be assessed for structural frames. The overall seismic safety can then be evaluated by introducing site-specific seismic risk, i.e., the relationship between average return period and peak ground acceleration. Based on a brief sensitivity study, the overall seismic safety is shown to be quite sensitive to the variability in the local seismic risk.

(14) Using a "weighted" seismic risk of a hypothetical Boston site, the annual probabilities of having at least some local yielding (i.e., $\mu > 1$) in the first story of the steel frames are found to have significant contributions due to low levels of peak ground acceleration. The contributions to the annual exceedance probability associated with a high local ductility threshold are more pronounced in the intermediate peak acceleration range.

(15) The annual probabilities of local inelastic response exceedance for the three (4-, 10- and 16-story) UBC-designed steel frames are generally smaller than those of the IARS-designed steel frames. This is due to the fact that the equivalent story yielding strengths of the UBC-designed frames are generally larger than those of the IARS-designed frames.

(16) Based on the annual local ductility exceedance probability for each story, approximate bounds can be established on the "system reliability", i.e., the annual probability of no exceedance anywhere in the buil-

ding. The lower bound is based on the assumption of perfect correlation among the inelastic responses of all stories, whereas the uppper bound corresponds to the assumption of complete statistical independence among them.

(17) By using empirical relationships between structural (and non-structural) damage and local ductility ratios, the annual risk of the "damage factor" (i.e., the ratio between expected losses due to future earthquakes and the replacement cost) is computed for each of the steel buildings under study. Given the actual replacement cost of a building, this information can then be used to quantify the effectiveness of alternative design procedures in reducing the risk of seismic damage.

7.2 Recommendations for Further Research

Further research is necessary to better quantify the overall safety of multistory buildings subjected to earthquake loads. In particular, the following studies are recommended:

(1) The multi-degree random vibration methodology used in the study was primarily for the elasto-plastic shear-beam systems. The random vibration modeling of other types of shear-spring characteristics, e.g., bilinear hysteretic, should be investigated.

(2) The peak ductility ratio measures only the maximum inelastic structural response, and it may not be an adequate indicator for structural damage. Within the context of seismic safety assessment, other possible inelastic response measures, e.g., the cumulative yielding ductility [39] or the normalized dissipated energy [6], need to be tested.

(3) In addition to the steel buildings studied, the overall seismic safety

of multistory reinforced concrete buildings, shear wall structures, and shear wall-frame combined systems should also be assessed.

(4) Due to the fact that the local inelastic response is sensitive to the extremes of some characteristics of the ground motion, e.g., the Kanai-Tajimi frequency, the local response statistics predicted by the mean value "First-Order Second-Moment" method is inadequate. Possible improvements in the FOSM technique need to be studied.

(5) The results reported herein are based on the seismic risk information of the hypothetical Boston site; other seismic risk curves for different earthquake-prone areas could also be incorporated. Since the overall seismic safety of a building is quite sensitive to the variability in the local seismic risk, the uncertainty of the seismic risk information itself may directly be included [43].

(6) The relationship between the overall "system reliability" and the "story reliability" of inelastic response under earthquake loads needs to be investigated in greater detail.

(7) The actual replacement cost of the six different steel frames considered in this research should be evaluated, so that the cost-effectiveness of measures to reduce the overall seismic risk of alternative design procedures could be assessed.

REFERENCES

1. Algermissen, S.T. and Perkins, D.M., "A Probabilistic Estimate of Maximum Acceleration in Rock in the Contiguous United States", U.S. Department of the Interior Geological Survey Open-File Report 76-416, 1976.

2. Anagnostopoulos, S.A., "Non-linear Dynamic Response and Ductility Requirements of Building Structures Subjected to Earthquakes", M.I.T. Department of Civil Engineering Research Report R72-54, September 1972.

3. Applied Technology Council, An Evaluation of a Response Spectrum Approach to Seismic Design of Buildings, A Study Report for Center for Building Technology, Institue of Applied Technology, National Bureau of Standards, September 1974.

4. Applied Technology Council, Tentative Provisions for the Development of Seismic Regulations for Buildings, National Bureau of Standards Special Publication 510, June 1978.

5. Arias, A., "A Measure of Earthquake Intensity", Seismic Design of Nuclear Power Plants, R. Hansen, Editor, M.I.T. Press, 1970.

6. Banon, H., "Prediction of Seismic Damage in Reinforced Concrete Frames", Ph.D. Thesis, M.I.T., June 1980.

7. Benfer, N.A. and Coffman, J.L., San Fernando, California, Earthquake of February 9, 1971, National Oceanic and Atmospheric Administration, U.S. Department of Commerce, Government Printing Office, Washington, D.C., 1973.

8. Benjamin, J.R. and Cornell, C.A., Probability, Statistics and Decision for Civil Engineers, McGraw-Hill, New York, 1970.

9. Binder, R., "Strong-Motion Durations and Spectral Density Functions for a Set of 39 Earthquake Ground Motions", M.I.T. Department of Civil Engineering, Seismic Safety of Buildings Internal Study Report No. 16, April 1978.

10. Binder, R., "Seismic Safety Analysis of Multi-Degree-of-Freedom Inelastic Structures", S.M. Thesis, M.I.T., June 1978.

11. Blume, J.A. and Monroe, R.F., "The Spectral Matrix Method of Predicting Damage from Ground Motion", John A. Blume and Associate Research Division, Nevada Operations Office, United States Atomic Energy Commission, Las Vegas, Nevada, 1971.

12. Blume, J.A., Wang, E.C., Scholl, R.E. and Shah, H.C., "Earthquake Damage Prediction: A Technological Assessment", Stanford University, Department of Civil Engineering Report 17, October 1975.

13. C.I.T. Earthquake Engineering Research Laboratory, Strong-Motion Earthquake Accelerograms - Digitized and Plotted Data, Vol. II, 1971.

14. Caughey, T.K., "Equivalent Linearization Techniques", Journal of the Acoustical Society of America, Vol. 35, No. 11, November 1963.

15. Construction Industry Research and Information Association, "Rationalization of Safety and Serviceability Factors in Structural Codes", CIRIA Report No. 63, London, July 1977.

16. Cornell, C.A., "Engineering Seismic Risk Analysis", Bulletin of the Seismological Society of America, Vol. 58, No. 5, October 1968.

17. Cornell, C.A. and Merz, H.A., "A Seismic Risk Analysis of Boston", M.I.T. Department of Civil Engineering Research Report R74-2, April 1974.

18. Crandall, S.H., "Perturbation Techniques for Random Vibration of Nonlinear Systems", Journal of the Acoustical Society of America, Vol. 35, No. 11, November 1963.

19. Crandall, S.H. and Mark, W.D., Random Vibration in Mechanical Systems, Academic Press, New York, 1973.

20. Esteva, L. and Villaverde, R., "Seismic Risk, Design Spectra and Structural Reliability", Proceedings of the 5th World Conference on Earthquake Engineering, Vol. II, Rome, Italy, 1973.

21. Gasparini, D.A. and Vanmarcke, E.H., "Simulated Earthquake Motion Compatible with Prescribed Response Spectra", M.I.T. Department of Civil Engineering Research Report R76-4, January 1976.

22. Gasparini, D.A., "On the Safety Provided by Alternate Seismic Design Methods", M.I.T. Department of Civil Engineering Research Report R77-22, July 1977.

23. Gates, N.C., "The Earthquake Reponse of Deteriorating Systems", Ph.D. Thesis, California Institute of Technology, Report No. EERL 77-03, 1977.

24. Gazetas, G., "Random Vibration Analysis of Inelastic Multi-Degree-of-Freedom Systems Subjected to Earthquake Ground Motions", M.I.T. Department of Civil Engineering Research Report R76-39, August 1976.

25. Grossmayer, R.L. and Iwan, W.D., "Some Observations on the Effective Period and Damping of Randomly Excited Yielding Systems", Proceedings of the Second National Conference on Earthquake Engineering, Stanford University, August 1979.

26. Gulkan, P. and Sozen, M.A., "Inelastic Responses of Reinforced Concrete Structures to Earthquake Motions", Journal of the American Concrete Institute, Vol. 71, No. 12, December 1974.

27. Gutenberg, B. and Richter, C., "Earthquake Magnitude, Intensity, Energy and Acceleration (Second Paper), Bulletin of the Seismological Society of America, Vol. 46, 1956.

28. Hart, G.C., Lew, M., and Di Julio, R., "High-Rise Building Response: Damping and Period Nonlinearities", Proceedings of the Fifth World Conference on Earthquake Engineering, Vol II, Rome, Italy, 1973.

29. Hart, G.C. and Vasudevan, R., "Earthquake Design of Buildings: Damping", Journal of the Structural Division, ASCE, Vol. 101, No. ST1, January 1975.

30. Haviland, R., "A Study of the Uncertainties in the Fundamental Translational Periods and Damping Values for Real Buildings", M.I.T. Department of Civil Engineering Research Report R76-12, February 1976.

31. Housner, G.W., "Intensity of Ground Shaking Near the Causative Fault", Proceedings of the 3rd World Conference on Earthquake Engineering, Vol. I, New Zealand, 1965.

32. Iwan, W.D. and Gates, N.C., "Estimating Earthquake Response of Simple Hysteretic Structures", Journal of the Engineering Mechanics Division, ASCE, Vol. 105, No. EM3, June 1979.

33. Iyengar, N.R. and Iyengar, J.K., "Stochastic Analysis of Yielding System", Journal of the Engineering Mechanics Division, ASCE, Vol. 104, No. EM2, April 1978.

34. Kanai, K., "An Empirical Formula for the Spectrum of Strong Earthquake Motions", Bulletin of the Earthquake Research Institute, University of Tokyo, Vol. 39, Tokyo, Japan, 1961.

35. Karnopp, D. and Scharton, T.D., "Plastic Deformation in Random Vibration", Journal of the Acoustical Society of America, Vol. 39, No. 6, June 1966.

36. Kaul, M.K. and Penzien, J., "Stochastic Seismic Analysis of Yielding Offshore Towers", Journal of the Engineering Mechanics Division, ASCE, Vol. 100, No. EM5, October 1974.

37. Kobori, T., Minai, R and Suzuki, Y., "Statistical Linearization Techniuqes of Hysteretic Structures to Earthquake Excitation", Bulletin of Disaster Prevention Research Institute, Kyoto University, Japan, Vol. 23, 1973.

38. Krinitzsky, E.L. and Chang, F.K., "Earthquake Intensity and the Selection of Ground Motions for Seismic Design", U.S. Army Engineer Waterways Experiment Station, State-of-the-Art for Assessing Earthquake Hazards in the United States Report No. 4, September 1975.

39. Lai, S.P., "On Inelastic Response Spectra for Aseismic Design", M.I.T. Department of Civil Engineering Research Report R78-18, July 1978.

40. Lai, S.P., "Ground Motion Parameters for Seismic Safety Assessment", M.I.T. Department of Civil Engineering, Seismic Safety of Buildings Internal Study Report No. 17, February 1979.

41. Lutes, L.D., "Equivalent Linearization for Random Vibration", Journal of the Engineering Mechanics Division, ASCE, Vol. 96, No. EM3, June 1970.

42. Luyties, W.H., Anagnostopoulos, S.A. and Biggs, J.M., "Studies on the Inelastic Dynamic Analysis and Design of Multistory Frames", M.I.T. Department of Civil Engineering Research Report R76-29, July 1976.

43. McGuire, R.K., "Effects of Uncertainty in Seismicity on Estimates of Seismic Hazard for the East Coast of the United States", Bulletin of the Seismological Society of America, Vol. 67, No. 3, June 1977.

44. McGuire, R.K. and Barnhard, J.A., "Magnitude, Distance and Intensity Data for C.I.T. Strong Motion Records", U.S. Geological Survey Journal of Research, Vol. 5, No. 4, July 1977.

45. Newmark, N.M. and Rosenblueth, E., Fundamentals of Earthquake Engineering, Prentice-Hall, Englewood Cliffs, New Jersey, 1971.

46. Newmark, N.M. and Hall, W.J., "Procedures and Criteria for Earthquake-Resistant Design", Building Practices for Disaster Mitigation, Building Science Series 46, National Bureau of Standards, February 1973.

47. Paez, T.L. and Yao, J.P., "Probabilistic Analysis of Elasto-Plastic Structures", Technical Report No. CE-STR-73-2, School of Civil Engineering, Purdue University, West Lafayette, Indiana, August 1973.

48. Penzien, J., Chapter 13 of Earthquake Engineering, Wiegel, R.L., Editor, Prentice-Hall, Englewood Cliffs, New Jersey, 1970.

49. Piqué, J.R., "On the Use of Simple Models in Nonlinear Dynamic Analysis", M.I.T. Department of Civil Engineering Research Report R76-43, September 1976.

50. Pulgrano, L.J. and Ablowitz, M., "The Response of Mechanical Systems to Bands of Random Excitation", The Shock and Vibration Bulletin, Vol. 39, January 1969.

51. Rackwitz, R., "Principles and Methods for a Practical Probabilistic Approach to Structural Safety", Sub-Committee for First Order Reliability Concepts for Design Codes of the Joint CEB-CECM-CIB-IIP-IABSE Committee on Structural Safety, CEB Bulletin, No. 112, July 1976.

52. Scholl, R.E., Editor, Effects Prediction Guidelines for Structures Subjected to Ground Motion, URS/John A. Blume and Associates, Engineers, July 1975.

53. Shibata, A. and Sozen, M.A., "Substitute-Structure Method for Seismic Design in R/C", Journal of the Structural Division, ASCE, Vol. 102, No. ST1, January 1976.

54. Sixsmith, E. and Roesset, J., "Statistical Properties of Strong Motion Earthquakes", M.I.T. Department of Civil Engineering Research Report R70-7, January 1970.

55. Tajimi, H., "A Statistical Method of Determining the Maximum Response of a Building Structure During an Earthquake", Proceedings of the 2nd World Conference on Earthquake Engineering, Vol. II, Tokyo, Japan, July 1960.

56. Tanaka, T., Yoshizawa, S., Osawa, Y. and Morishita, T., "Period and Damping of Vibration in Actual Buildings During Earthquakes", Bulletin of Earthquake Engineering Research Institute, University of Tokyo, Japan, Vol. 47, 1969.

57. Tong, W.H., Schumacker, B., Cornell, C.A. and Whitman, R.V., "Seismic Hazard Maps for Massachusetts", M.I.T. Department of Civil Engineering, Seismic Design Decision Analysis Internal Study Report No. 52, February 1975.

58. Uniform Building Code, International Conference of Building Officials, Whittier, California, 1973.

59. Vanmarcke, E.H., "First Passage and Other Failure Criteria in Narrow Band Random Vibration: A Discrete State Approach", M.I.T. Department of Civil Engineering Research Report R69-68, October 1969.

60. Vanmarcke, E.H., Chapter 8 of Seismic Risk and Engineering Decisions, Lomnitz, C. and Rosenblueth, E., Editors, Elsevier Publishing Co., 1977.

61. Vanmarcke, E.H. and Lai, S.P., "Strong-Motion Duration of Earthquakes", M.I.T. Department of Civil Engineering Research Report R77-16, July 1977.

62. Vanmarcke, E.H. and Lai, S.P., "Prediction of Inelastic Response Spectra Using Random Vibration", Proceedings of ASCE Engineering Mechanics Division Specialty Conference, Austin, Texas, September 1979.

63. Vanmarcke, E.H. and Lai, S.P., "Strong-Motion Duration and R.M.S. Amplitude of Earthquake Records", Bulletin of the Seismological Society of America, to be printed in August 1980.

64. Vanmarcke, E.H. and Veneziano, D., "Probabilistic Seismic Response of Simple Inelastic Systems", Proceedings of the 5th World Conference on Earthquake Engineering, Vol. II, Rome, Italy, 1973.

65. Vanmarcke, E.H., Yanev, P.I. and De Estrada, M.B., "Response of Simple Hysteretic Systems to Random Excitation", M.I.T. Department of Civil Engineering Research Report R70-66, September 1970.

66. Wen, Yi-Kwei, "Stochastic Seismic Response Analysis of Hysteretic Multi-Degree-of-Freedom Structures", Journal of Earthquake Engineering and Structural Dynamics, Vol. 7, No. 2, March 1979.

67. Whitman, R.V., "Damage Probability Matrices for Prototype Buildings", M.I.T. Department of Civil Engineering Research Report R73-57, Seismic Design Decision Analysis Series No. 8, October 1973.

68. Whitman, R.V., Biggs, J.M., Brennan, J.E., Cornell, C.A., de Neufville, R.L. and Vanmarcke, E.H., "Seismic Design Decision Analysis", Journal of the Structural Division, ASCE, Vol. 101, No. ST5, May 1975.

69. Wood, J.H., "Analysis of the Earthquake Response of a Nine-Story Steel Frame Building During the San Fernando Earthquake", California Institute of Technology Report No. EERL 72-04, 1972.

70. Yanev, P.I., "Response of Simple Inelastic Systems to Random Excitation", S.M. Thesis, M.I.T., June 1970.

APPENDICES

APPENDIX A

$$J_o(\Omega) = \frac{1}{\pi}\tan^{-1}\left(\frac{2\zeta_g\Omega}{1-\Omega^2}\right) + \frac{\zeta_g}{2\pi\sqrt{1-\zeta_g^2}}\ \ell n\left(\frac{1+2\Omega\sqrt{1-\zeta_g^2}+\Omega^2}{1-2\Omega\sqrt{1-\zeta_g^2}+\Omega^2}\right) \tag{A-1}$$

$$J_1(\Omega) = \frac{1}{\pi\sqrt{1-\zeta_g^2}}\tan^{-1}\left(\frac{2\zeta_g\sqrt{1-\zeta_g^2}}{1-2\zeta_g^2-\Omega^2}\right) \tag{A-2}$$

$$J_2(\Omega) = \frac{1}{\pi}\tan^{-1}\left(\frac{2\zeta_g\Omega}{1-\Omega^2}\right) - \frac{\zeta_g}{2\pi\sqrt{1-\zeta_g^2}}\ \ell n\left(\frac{1+2\Omega\sqrt{1-\zeta_g^2}+\Omega^2}{1-2\Omega\sqrt{1-\zeta_g^2}+\Omega^2}\right) \tag{A-3}$$

$$J_3(\Omega) = \frac{\zeta_g}{\pi}\ \ell n\left[(1-\Omega^2)^2 + 4\zeta_g^2\Omega^2\right] + \frac{1-2\zeta_g^2}{\pi\sqrt{1-\zeta_g^2}}\ \tan^{-1}\left(\frac{2\zeta_g\sqrt{1-\zeta_g^2}}{1-2\zeta_g^2-\Omega^2}\right) \tag{A-4}$$

$$J_4(\Omega) = \frac{4\zeta_g}{\pi}\,\Omega + 2(1-2\zeta_g)^2 J_2 - J_o \tag{A-5}$$

$$\Omega = \omega/\omega_g \tag{A-6}$$

APPENDIX B

TABLE B-1 MOMENT CAPACITIES FOR 4-STORY FRAME [LAI,39]

STORY	COLUMN (kip-inch)		GIRDER (kip-inch)	
	EXTERIOR	INTERIOR	EXTERIOR	INTERIOR
1	1100	1524	965	899
2	794	1333	960*	839
3	597	964	960*	602
4	419	582	960*	540*

* Controlled by $wL_G^2/8$

TABLE B-2 MOMENT CAPACITIES FOR 10-STORY FRAME [LAI,39]

STORY	COLUMN (kip-inch)		GIRDER (kip-inch)	
	EXTERIOR	INTERIOR	EXTERIOR	INTERIOR
1	2092	3216	1034	1002
2	1674	2778	1028	1017
3	1518	2465	984	974
4	1326	2230	960*	960*
5	1176	1971	960*	960*
6	1015	1713	960*	960*
7	795	1513	960*	960*
8	619	1249	960*	960*
9	570	865	960*	960*
10	408	547	960*	960*

* Controlled by $wL_G^2/8$

TABLE B-3 MOMENT CAPACITIES FOR 16-STORY FRAME [LAI,39]

STORY	COLUMN (kip-inch)		GIRDER (kip-inch)	
	EXTERIOR	INTERIOR	EXTERIOR	INTERIOR
1	3289	4669	1552	1486
2	2778	4239	1560	1544
3	2613	3939	1407	1419
4	2398	3681	1353	1400
5	2207	3423	1227	1307
6	2019	3199	1214	1295
7	1877	2941	1124	1199
8	1693	2714	1076	1174
9	1509	2475	1042	1156
10	1338	2236	960*	1010
11	1183	1999	960*	999
12	1024	1747	960*	960*
13	814	1523	960*	960*
14	636	1275	960*	960*
15	590	886	960*	960*
16	432	547	960*	960*

* Controlled by $wL_G^2/8$

TA3LE B-4 PARAMETERS FOR 4-STORY EQUIVALENT SHEAR-BEAM SYSTEM

STORY	LATERAL STIFFNESS (kip/inch)		YIELDING STRENGTH (kip)	
	LAI (IARS)	PIQUE (UBC)	LAI (IARS)	PIQUE (UBC)
1	107.4	107.5	65.43	106
2	74.8	74.8	56.62	96.5
3	65.9	65.9	45.16	78
4	60.9	60.9	32.08	70

TABLE B-5 PARAMETERS FOR 10-STORY EQUIVALENT SHEAR-BEAM SYSTEM

STORY	LATERAL STIFFNESS (kip/inch)		YIELDING STRENGTH (kip)	
	LAI (IARS)	PIQUE (UBC)	LAI (IARS)	PIQUE (UBC)
1	111.1	111.1	63.65	137
2	102.7	102.4	61.03	135
3	93.5	93.9	59.30	130
4	87.2	87.5	56.00	122.5
5	76.3	76.3	52.59	114
6	74.7	74.5	48.63	101
7	62.9	63.2	43.61	87.5
8	62.0	61.8	38.58	93
9	42.3	42.4	31.95	69.5
10	36.7	36.6	25.85	62

TABLE B-6 PARAMETERS FOR 16-STORY EQUIVALENT SHEAR-BEAM SYSTEM

STORY	LATERAL STIFFNESS (kip/inch)		YIELDING STRENGTH (kip)	
	LAI (IARS)	PIQUE (UBC)	LAI (IARS)	PIQUE (UBC)
1	224.2	224.3	85.88	225
2	209.6	209.6	84.22	224
3	176.3	176.5	78.10	201
4	163.5	163.8	72.91	190.5
5	145.2	145.4	68.37	184.5
6	135.7	135.8	65.10	173.5
7	122.4	122.6	60.48	164
8	115.6	115.8	58.	153
9	106.9	107.0	55.91	146
10	96.3	96.5	51.7	134.5
11	80.7	80.8	48.58	120.6
12	74.2	74.3	45.93	107.6
13	58.4	58.4	42.08	92
14	55.6	55.5	37.97	88
15	37.8	37.8	32.55	66
16	30.5	30.4	24.97	60

TABLE B-7 MODAL PROPERTIES OF 4-STORY EQUIVALENT SHEAR-BEAM SYSTEM

STORY	1st MODAL SHAPE T = 0.967 sec	2nd MODAL SHAPE T = 0.352 sec	3rd MODAL SHAPE T = 0.234 sec	4th MODAL SHAPE T = 0.191 sec
4	1.432	-1.225	0.824	-0.252
3	1.201	0.268	-1.447	0.793
2	0.805	1.343	0.192	-1.323
1	0.35	0.939	1.199	1.340

TABLE B-8 MODAL PROPERTIES OF 10-STORY EQUIVALENT SHEAR-BEAM SYSTEM

STORY	1st MODAL SHAPE T = 2.322 sec	2nd MODAL SHAPE T = 0.872 sec	3rd MODAL SHAPE T = 0.545 sec	4th MODAL SHAPE T = 0.396 sec
10	0.939	-1.013	0.915	-0.757
9	0.891	-0.648	0.067	0.572
8	0.809	-0.123	-0.721	0.833
7	0.728	0.261	-0.853	0.126
6	0.626	0.591	-0.512	-0.703
5	0.524	0.751	0.015	-0.781
4	0.411	0.788	0.523	-0.183
3	0.303	0.685	0.758	0.479
2	0.196	0.493	0.691	0.758
1	0.095	0.257	0.397	0.527

TABLE B-9 MODAL PROPERTIES OF 16-STORY EQUIVALENT SHEAR-BEAM SYSTEM

STORY	1st MODAL SHAPE T = 2.935 sec	2nd MODAL SHAPE T = 1.170 sec	3rd MODAL SHAPE T = 0.727 sec	4th MODAL SHAPE T = 0.533 sec
16	0.812	-0.950	0.919	-0.826
15	0.780	-0.693	0.356	0.131
14	0.731	-0.375	-0.290	0.763
13	0.682	-0.124	-0.638	0.691
12	0.621	0.130	-0.758	0.195
11	0.563	0.337	-0.650	-0.280
10	0.502	0.501	-0.387	-0.592
9	0.444	0.602	-0.086	-0.623
8	0.387	0.645	0.200	-0.436
7	0.330	0.630	0.429	-0.126
6	0.273	0.570	0.573	0.204
5	0.219	0.481	0.618	0.452
4	0.167	0.378	0.576	0.566
3	0.119	0.273	0.469	0.541
2	0.074	0.170	0.318	0.401
1	0.036	0.083	0.161	0.211

TABLE B-10 MODAL PROPERTIES OF 4-STORY MOMENT-RESISTING FRAME [LAI,39]

STORY	1st MODAL SHAPE T = 0.967 sec	2nd MODAL SHAPE T = 0.32 sec	3rd MODAL SHAPE T = 0.186 sec	4th MODAL SHAPE T = 0.134 sec
4	1.432	-1.213	0.826	-0.297
3	1.201	0.249	-1.397	0.883
2	0.805	1.337	0.084	-1.340
1	0.350	0.968	1.266	1.255

TABLE B-11 MODAL PROPERTIES OF 10-STORY MOMENT-RESISTING FRAME [LAI,39]

STORY	1st MODAL SHAPE T = 2.322 sec	2nd MODAL SHAPE T = 0.835 sec	3rd MODAL SHAPE T = 0.496 sec	4th MODAL SHAPE T = 0.339 sec
10	0.939	-0.993	0.892	-0.744
9	0.891	-0.653	0.121	0.482
8	0.809	-0.135	-0.696	0.880
7	0.728	0.251	-0.858	0.199
6	0.626	0.579	-0.544	-0.669
5	0.524	0.752	-0.025	-0.799
4	0.411	0.789	0.496	-0.244
3	0.303	0.701	0.760	0.436
2	0.196	0.511	0.714	0.764
1	0.095	0.265	0.419	0.556

TABLE B-12 MODAL PROPERTIES OF 16-STORY MOMENT-RESISTING FRAME [LAI,39]

STORY	1st MODAL SHAPE T = 2.935 sec	2nd MODAL SHAPE T = 1.112 sec	3rd MODAL SHAPE T = 0.659 sec	4th MODAL SHAPE T = 0.649 sec
16	0.812	-0.868	0.836	-0.753
15	0.780	-0.688	0.406	-0.033
14	0.731	-0.401	-0.189	0.669
13	0.682	-0.151	-0.532	0.734
12	0.621	0.114	-0.696	0.359
11	0.563	0.313	-0.649	-0.105
10	0.502	0.471	-0.446	-0.496
9	0.444	0.571	-0.182	-0.646
8	0.387	0.619	0.095	-0.546
7	0.330	0.624	0.339	-0.268
6	0.273	0.589	0.516	0.084
5	0.219	0.522	0.597	0.384
4	0.167	0.430	0.585	0.562
3	0.119	0.326	0.494	0.577
2	0.074	0.212	0.345	0.452
1	0.036	0.105	0.178	0.247

APPENDIX C

TABLE C-1 NORMALIZED ANNUAL EXCEEDANCE PROBABILITY OF 1st-STORY LOCAL DUCTILITY RATIO $P[\mu > \mu^*, a_{max} \geq a^*_{max}]$ (4-STORY IARS FRAME)

$a_{max} \geq$ (g)	$\mu > 1$	$\mu > 2$	$\mu > 3$	$\mu > 4$	$\mu > 5$
0.0175	4.669×10^{-3}	1.131×10^{-3}	4.169×10^{-4}	2.475×10^{-4}	1.463×10^{-4}
0.035	4.558×10^{-3}	1.115×10^{-3}	4.136×10^{-4}	2.458×10^{-4}	1.463×10^{-4}
0.06	4.318×10^{-3}	1.082×10^{-3}	4.061×10^{-4}	2.422×10^{-4}	1.428×10^{-4}
0.1	3.802×10^{-3}	1.004×10^{-3}	3.886×10^{-4}	2.337×10^{-4}	1.377×10^{-4}
0.15	2.625×10^{-3}	8.248×10^{-4}	3.487×10^{-4}	2.137×10^{-4}	1.257×10^{-4}
0.2	1.697×10^{-3}	6.452×10^{-4}	2.888×10^{-4}	1.767×10^{-4}	1.127×10^{-4}
0.25	1.055×10^{-3}	4.596×10^{-4}	2.295×10^{-4}	1.483×10^{-4}	9.724×10^{-5}
0.3	6.709×10^{-4}	3.315×10^{-4}	1.771×10^{-4}	1.192×10^{-4}	8.560×10^{-5}
0.35	4.408×10^{-4}	2.366×10^{-4}	1.387×10^{-4}	9.378×10^{-5}	6.920×10^{-5}
0.4	2.688×10^{-4}	1.561×10^{-4}	9.843×10^{-5}	6.817×10^{-5}	5.09×10^{-5}
0.45	1.656×10^{-4}	1.024×10^{-4}	6.810×10^{-5}	4.841×10^{-5}	3.693×10^{-5}
0.5	1.006×10^{-4}	6.510×10^{-5}	4.539×10^{-5}	3.386×10^{-5}	2.587×10^{-5}
0.55	6.086×10^{-5}	4.109×10^{-5}	2.996×10^{-5}	2.295×10^{-5}	1.769×10^{-5}
0.6	3.426×10^{-5}	2.404×10^{-5}	1.811×10^{-5}	1.422×10^{-5}	1.103×10^{-5}
0.65	1.349×10^{-5}	1.004×10^{-5}	7.652×10^{-6}	6.217×10^{-6}	4.878×10^{-6}

TABLE C-2 NORMALIZED ANNUAL EXCEEDANCE PROBABILITY OF 1st-STORY LOCAL DUCTILITY RATIO $P[\mu > \mu^*, a_{max} \geq a^*_{max}]$ (10-STORY IARS FRAME)

$a_{max} \geq$ (g)	$\mu > 1$	$\mu > 2$	$\mu > 3$	$\mu > 4$	$\mu > 5$
0.0175	7.000×10^{-3}	1.687×10^{-3}	5.953×10^{-4}	3.272×10^{-4}	2.191×10^{-4}
0.035	6.801×10^{-3}	1.662×10^{-3}	5.901×10^{-4}	3.248×10^{-4}	2.175×10^{-4}
0.06	6.382×10^{-3}	1.606×10^{-3}	5.786×10^{-4}	3.196×10^{-4}	2.141×10^{-4}
0.1	5.454×10^{-3}	1.482×10^{-3}	5.528×10^{-4}	3.077×10^{-4}	2.067×10^{-4}
0.15	3.538×10^{-3}	1.203×10^{-3}	4.929×10^{-4}	2.808×10^{-4}	1.897×10^{-4}
0.2	2.191×10^{-3}	9.032×10^{-4}	4.181×10^{-4}	2.479×10^{-4}	1.687×10^{-4}
0.25	1.323×10^{-3}	6.377×10^{-4}	3.356×10^{-4}	2.092×10^{-4}	1.442×10^{-4}
0.3	8.279×10^{-4}	4.515×10^{-4}	3.542×10^{-4}	1.644×10^{-4}	1.168×10^{-4}
0.35	5.373×10^{-4}	3.186×10^{-4}	1.914×10^{-4}	1.294×10^{-4}	9.475×10^{-5}
0.4	3.251×10^{-4}	2.052×10^{-4}	1.347×10^{-4}	9.461×10^{-5}	7.005×10^{-5}
0.45	1.982×10^{-4}	1.325×10^{-4}	9.198×10^{-5}	6.687×10^{-5}	5.089×10^{-5}
0.5	1.184×10^{-4}	8.365×10^{-5}	6.055×10^{-5}	4.569×10^{-5}	3.529×10^{-5}
0.55	7.000×10^{-5}	5.185×10^{-5}	3.926×10^{-5}	3.046×10^{-5}	2.392×10^{-5}
0.6	3.881×10^{-5}	2.981×10^{-5}	2.346×10^{-5}	1.861×10^{-5}	1.477×10^{-5}
0.65	1.511×10^{-5}	1.196×10^{-5}	9.756×10^{-6}	7.843×10^{-6}	6.313×10^{-6}

TABLE C-3 NORMALIZED ANNUAL EXCEEDANCE PROBABILITY OF 1st-STORY LOCAL DUCTILITY RATIO $P[\mu > \mu^*, a_{max} \geq a^*_{max}]$ (16-STORY IARS FRAME)

$a_{max} \geq$ (g)	$\mu > 1$	$\mu > 2$	$\mu > 3$	$\mu > 4$	$\mu > 5$
0.0175	7.309×10^{-3}	1.294×10^{-3}	5.024×10^{-4}	2.859×10^{-4}	1.885×10^{-4}
0.035	7.094×10^{-3}	1.280×10^{-3}	4.985×10^{-4}	2.840×10^{-4}	1.872×10^{-4}
0.06	6.645×10^{-3}	1.252×10^{-3}	4.899×10^{-4}	2.796×10^{-4}	1.844×10^{-4}
0.1	5.666×10^{-3}	1.185×10^{-3}	4.709×10^{-4}	2.699×10^{-4}	1.782×10^{-4}
0.15	3.710×10^{-3}	1.035×10^{-3}	4.260×10^{-4}	2.469×10^{-4}	1.637×10^{-4}
0.2	2.273×10^{-3}	8.554×10^{-4}	3.703×10^{-4}	2.193×10^{-4}	1.457×10^{-4}
0.25	1.384×10^{-3}	6.285×10^{-4}	3.058×10^{-4}	1.858×10^{-4}	1.251×10^{-4}
0.3	8.597×10^{-4}	4.481×10^{-4}	2.418×10^{-4}	1.544×10^{-4}	1.047×10^{-4}
0.35	5.617×10^{-4}	3.203×10^{-4}	1.842×10^{-4}	1.233×10^{-4}	8.552×10^{-5}
0.4	3.422×10^{-4}	2.105×10^{-4}	1.289×10^{-4}	8.927×10^{-5}	6.320×10^{-5}
0.45	2.101×10^{-4}	1.366×10^{-4}	8.898×10^{-5}	6.332×10^{-5}	4.583×10^{-5}
0.5	1.263×10^{-4}	8.658×10^{-5}	5.941×10^{-5}	4.342×10^{-5}	3.186×10^{-5}
0.55	7.560×10^{-5}	5.465×10^{-5}	3.899×10^{-5}	2.938×10^{-5}	2.175×10^{-5}
0.6	4.234×10^{-5}	3.178×10^{-5}	2.339×10^{-5}	1.795×10^{-5}	1.343×10^{-5}
0.65	1.664×10^{-5}	1.301×10^{-5}	9.852×10^{-6}	7.652×10^{-6}	5.739×10^{-6}

TABLE C-4 NORMALIZED ANNUAL EXCEEDANCE PROBABILITY OF 1st-STORY LOCAL DUCTILITY RATIO $P[\mu > \mu^*, a_{max} \geq a^*_{max}]$ (4-STORY UBC FRAME)

$a_{max} \geq$ (g)	$\mu > 1$	$\mu > 2$	$\mu > 3$	$\mu > 4$	$\mu > 5$
0.0175	1.131×10^{-3}	3.085×10^{-4}	6.903×10^{-5}	2.690×10^{-5}	9.834×10^{-6}
0.035	1.115×10^{-3}	2.940×10^{-4}	6.838×19^{-5}	2.687×10^{-5}	9.834×10^{-6}
0.06	1.082×10^{-3}	2.752×10^{-4}	6.711×10^{-5}	2.679×10^{-5}	9.834×10^{-6}
0.1	1.004×10^{-3}	2.484×10^{-4}	6.443×10^{-5}	2.653×10^{-5}	9.830×10^{-6}
0.15	8.248×10^{-4}	2.075×10^{-4}	5.884×10^{-5}	2.567×10^{-5}	9.802×10^{-6}
0.2	6.452×10^{-4}	1.710×10^{-4}	5.225×10^{-5}	2.429×10^{-5}	9.712×10^{-6}
0.25	4.596×10^{-4}	1.349×10^{-4}	4.503×10^{-5}	2.231×10^{-5}	9.506×10^{-6}
0.3	3.315×10^{-4}	1.029×10^{-4}	3.805×10^{-5}	1.998×10^{-5}	9.157×10^{-6}
0.35	2.366×10^{-4}	7.968×10^{-5}	3.183×10^{-5}	1.772×10^{-5}	8.648×10^{-6}
0.4	1.561×10^{-4}	5.663×10^{-5}	2.433×10^{-5}	1.424×10^{-5}	7.880×10^{-6}
0.45	1.024×10^{-4}	3.966×10^{-5}	1.834×10^{-5}	1.125×10^{-5}	6.881×10^{-6}
0.5	6.510×10^{-5}	2.686×10^{-5}	1.328×10^{-5}	8.570×10^{-6}	5.485×10^{-6}
0.55	4.109×10^{-5}	1.781×10^{-5}	9.485×10^{-6}	6.508×10^{-6}	4.221×10^{-6}
0.6	2.404×10^{-5}	1.075×10^{-5}	6.159×10^{-6}	4.221×10^{-6}	2.973×10^{-6}
0.65	1.004×10^{-5}	4.591×10^{-6}	2.774×10^{-6}	1.913×10^{-6}	1.435×10^{-6}

TABLE C-5 NORMALIZED ANNUAL EXCEEDANCE PROBABILITY OF 1st-STORY LOCAL DUCTILITY RATIO $P[\mu > \mu^*, a_{max} \geq a^*_{max}]$ (10-STORY UBC FRAME)

$a_{max} \geq$ (g)	$\mu > 1$	$\mu > 2$	$\mu > 3$	$\mu > 4$	$\mu > 5$
0.0175	1.114×10^{-3}	1.793×10^{-4}	6.204×10^{-5}	2.670×10^{-5}	1.891×10^{-5}
0.035	1.076×10^{-3}	1.747×10^{-4}	6.058×10^{-5}	2.616×10^{-5}	1.853×10^{-5}
0.06	1.019×10^{-3}	1.676×10^{-4}	5.833×10^{-5}	2.531×10^{-5}	1.793×10^{-5}
0.1	9.208×10^{-4}	1.552×10^{-4}	5.447×10^{-5}	2.376×10^{-5}	1.685×10^{-5}
0.15	7.611×10^{-4}	1.342×10^{-4}	4.748×10^{-5}	2.087×10^{-5}	1.485×10^{-5}
0.2	5.815×10^{-4}	1.133×10^{-4}	4.060×10^{-5}	1.787×10^{-5}	1.276×10^{-5}
0.25	4.139×10^{-4}	9.265×10^{-5}	3.363×10^{-5}	1.756×10^{-5}	1.057×10^{-5}
0.3	3.033×10^{-4}	7.461×10^{-5}	2.758×10^{-5}	1.477×10^{-5}	8.704×10^{-6}
0.35	2.168×10^{-4}	5.934×10^{-5}	2.249×10^{-5}	1.247×10^{-5}	7.514×10^{-6}
0.4	1.454×10^{-4}	4.361×10^{-5}	1.774×10^{-5}	9.904×10^{-6}	6.233×10^{-6}
0.45	9.550×10^{-5}	3.103×10^{-5}	1.314×10^{-5}	7.908×10^{-6}	5.235×10^{-6}
0.5	6.058×10^{-5}	2.114×10^{-5}	9.419×10^{-6}	6.046×10^{-6}	4.070×10^{-6}
0.55	3.796×10^{-5}	1.415×10^{-5}	6.758×10^{-6}	4.582×10^{-6}	3.073×10^{-6}
0.6	2.216×10^{-5}	8.749×10^{-6}	4.471×10^{-6}	3.127×10^{-6}	2.033×10^{-6}
0.65	9.087×10^{-6}	3.826×10^{-6}	2.009×10^{-6}	1.435×10^{-6}	9.565×10^{-7}

TABLE C-6 NORMALIZED ANNUAL EXCEEDANCE PROBABILITY OF 1st-STORY LOCAL DUCTILITY RATIO $P[\mu > \mu^*, a_{max} \geq a^*_{max}]$ (16-STORY UBC FRAME)

$a_{max} \geq$ (g)	$\mu > 1$	$\mu > 2$	$\mu > 3$	$\mu > 4$	$\mu > 5$
0.0175	6.182×10^{-4}	8.774×10^{-5}	2.537×10^{-5}	1.645×10^{-5}	9.824×10^{-6}
0.035	5.997×10^{-4}	8.563×10^{-5}	2.482×10^{-5}	1.604×10^{-5}	9.594×10^{-6}
0.06	5.72×10^{-4}	8.241×10^{-5}	2.397×10^{-5}	1.546×10^{-5}	9.264×10^{-6}
0.1	5.256×10^{-4}	7.674×10^{-5}	2.247×10^{-5}	1.445×10^{-5}	8.697×10^{-6}
0.15	4.438×10^{-4}	6.676×10^{-5}	1.988×10^{-5}	1.272×10^{-5}	7.699×10^{-6}
0.2	3.630×10^{-4}	5.688×10^{-5}	1.724×10^{-5}	1.098×10^{-5}	6.682×10^{-6}
0.25	2.858×10^{-4}	4.709×10^{-5}	1.467×10^{-5}	9.252×10^{-6}	5.651×10^{-6}
0.3	2.159×10^{-4}	3.859×10^{-5}	1.234×10^{-5}	7.739×10^{-6}	4.778×10^{-6}
0.35	1.611×10^{-4}	3.180×10^{-5}	1.047×10^{-5}	6.495×10^{-6}	4.043×10^{-6}
0.4	1.135×10^{-4}	2.375×10^{-5}	8.570×10^{-6}	5.251×10^{-6}	3.311×10^{-6}
0.45	7.862×10^{-5}	1.737×10^{-5}	6.973×10^{-6}	4.253×10^{-6}	2.712×10^{-6}
0.5	5.301×10^{-5}	1.213×10^{-5}	5.692×10^{-6}	3.438×10^{-6}	2.223×10^{-6}
0.55	3.512×10^{-5}	8.337×10^{-6}	4.429×10^{-6}	2.773×10^{-6}	1.824×10^{-6}
0.6	2.139×10^{-5}	5.219×10^{-6}	2.973×10^{-6}	1.941×10^{-6}	1.408×10^{-6}
0.65	9.087×10^{-6}	2.296×10^{-6}	1.435×10^{-6}	9.565×10^{-7}	6.696×10^{-7}

TABLE C-7 NORMALIZED ANNUAL EXCEEDANCE PROBABILITY OF 1st-STORY LOCAL DUCTILITY RATIO $P[\mu > \mu^*, a_{max} \geq a^*_{max}]$ (4-STORY IARS FRAME, STRAIGHT-LINE SEISMIC RISK)

$a_{max} \geq$ (g)	$\mu > 1$	$\mu > 2$	$\mu > 3$	$\mu > 4$	$\mu > 5$
0.0175	7.223×10^{-3}	2.229×10^{-3}	1.011×10^{-3}	6.492×10^{-4}	4.382×10^{-4}
0.035	7.112×10^{-3}	2.213×10^{-3}	1.007×10^{-3}	6.476×10^{-4}	4.371×10^{-4}
0.06	6.888×10^{-3}	2.182×10^{-3}	1.000×10^{-3}	6.442×10^{-4}	4.348×10^{-4}
0.1	6.381×10^{-3}	2.106×10^{-3}	9.832×10^{-4}	6.358×10^{-4}	4.298×10^{-4}
0.15	5.017×10^{-3}	1.898×10^{-3}	9.369×10^{-4}	6.127×10^{-4}	4.159×10^{-4}
0.2	3.832×10^{-3}	1.668×10^{-3}	8.604×10^{-4}	5.653×10^{-4}	3.901×10^{-4}
0.25	2.879×10^{-3}	1.393×10^{-3}	7.725×10^{-4}	5.232×10^{-4}	3.671×10^{-4}
0.3	2.166×10^{-3}	1.155×10^{-3}	6.752×10^{-4}	4.692×10^{-4}	3.455×10^{-4}
0.35	1.658×10^{-3}	9.455×10^{-4}	5.904×10^{-4}	4.130×10^{-4}	3.093×10^{-4}
0.4	1.267×10^{-3}	7.626×10^{-4}	4.989×10^{-4}	3.548×10^{-4}	2.677×10^{-4}
0.45	9.233×10^{-4}	5.836×10^{-4}	3.978×10^{-4}	2.890×10^{-4}	2.211×10^{-4}
0.5	6.449×10^{-4}	4.240×10^{-4}	3.005×10^{-4}	2.266×10^{-4}	1.737×10^{-4}
0.55	4.559×10^{-4}	3.099×10^{-4}	2.272×10^{-4}	1.748×10^{-4}	1.349×10^{-4}
0.6	2.856×10^{-4}	2.008×10^{-4}	1.513×10^{-4}	1.189×10^{-4}	9.230×10^{-5}
0.65	1.172×10^{-4}	8.731×10^{-5}	6.652×10^{-5}	5.405×10^{-5}	4.241×10^{-5}

TABLE C-8 NORMALIZED ANNUAL EXCEEDANCE PROBABILITY OF 1st-STORY LOCAL DUCTILITY RATIO $P[\mu > \mu^*, a_{max} \geq a^*_{max}]$ (10-STORY IARS FRAME, STRAIGHT-LINE SEISMIC RISK)

$a_{max} \geq$ (g)	$\mu > 1$	$\mu > 2$	$\mu > 3$	$\mu > 4$	$\mu > 5$
0.0175	1.029×10^{-2}	3.188×10^{-3}	1.423×10^{-3}	8.761×10^{-4}	6.171×10^{-4}
0.035	1.010×10^{-2}	3.163×10^{-3}	1.417×10^{-3}	8.737×10^{-4}	6.156×10^{-4}
0.06	9.703×10^{-3}	3.111×10^{-3}	1.407×10^{-3}	8.688×10^{-4}	6.125×10^{-4}
0.1	8.790×10^{-3}	2.989×10^{-3}	1.381×10^{-3}	8.572×10^{-4}	6.051×10^{-4}
0.15	6.570×10^{-3}	2.666×10^{-3}	1.312×10^{-3}	8.260×10^{-4}	5.855×10^{-4}
0.2	4.849×10^{-3}	2.283×10^{-3}	1.216×10^{-3}	7.839×10^{-4}	5.587×10^{-4}
0.25	3.560×10^{-3}	1.889×10^{-3}	1.094×10^{-3}	7.265×10^{-4}	5.224×10^{-4}
0.3	2.641×10^{-3}	1.543×10^{-3}	9.425×10^{-4}	6.433×10^{-4}	4.715×10^{-4}
0.35	2.000×10^{-3}	1.250×10^{-3}	8.040×10^{-4}	5.660×10^{-4}	4.230×10^{-4}
0.4	1.518×10^{-3}	9.924×10^{-4}	6.751×10^{-4}	4.870×10^{-4}	3.668×10^{-4}
0.45	1.095×10^{-3}	7.502×10^{-4}	5.328×10^{-4}	3.945×10^{-4}	3.029×10^{-4}
0.5	7.531×10^{-4}	5.407×10^{-4}	3.981×10^{-4}	3.037×10^{-4}	2.361×10^{-4}
0.55	5.230×10^{-4}	3.896×10^{-4}	2.969×10^{-4}	2.313×10^{-4}	1.820×10^{-4}
0.6	3.235×10^{-4}	2.486×10^{-4}	1.958×10^{-4}	1.555×10^{-4}	1.235×10^{-4}
0.65	1.314×10^{-4}	1.039×10^{-4}	8.481×10^{-5}	6.818×10^{-5}	5.488×10^{-5}

TABLE C-9 NORMALIZED ANNUAL EXCEEDANCE PROBABILITY OF 1st-STORY LOCAL DUCTILITY RATIO $P[\mu > \mu^*, a_{max} \geq a^*_{max}]$ (16-STORY IARS FRAME, STRAIGHT-LINE SEISMIC RISK)

$a_{max} \geq$ (g)	$\mu > 1$	$\mu > 2$	$\mu > 3$	$\mu > 4$	$\mu > 5$
0.0175	1.076×10^{-2}	2.736×10^{-3}	1.273×10^{-3}	7.932×10^{-4}	5.426×10^{-4}
0.035	1.054×10^{-2}	2.723×10^{-3}	1.269×10^{-3}	7.913×10^{-4}	5.413×10^{-4}
0.06	1.012×10^{-2}	2.696×10^{-3}	1.261×10^{-3}	7.782×10^{-4}	5.386×10^{-4}
0.1	9.157×10^{-3}	2.630×10^{-3}	1.243×10^{-3}	7.776×10^{-4}	5.325×10^{-4}
0.15	6.891×10^{-3}	2.457×10^{-3}	1.190×10^{-3}	7.510×10^{-4}	5.158×10^{-4}
0.2	5.055×10^{-3}	2.227×10^{-3}	1.119×10^{-3}	7.158×10^{-4}	4.928×10^{-4}
0.25	3.736×10^{-3}	1.891×10^{-3}	1.024×10^{-3}	6.661×10^{-4}	4.622×10^{-4}
0.3	2.762×10^{-3}	1.555×10^{-3}	9.048×10^{-4}	6.077×10^{-4}	4.244×10^{-4}
0.35	2.105×10^{-3}	1.273×10^{-3}	7.775×10^{-4}	5.391×10^{-4}	3.820×10^{-4}
0.4	1.606×10^{-3}	1.024×10^{-3}	6.520×10^{-4}	4.617×10^{-4}	3.312×10^{-4}
0.45	1.166×10^{-3}	7.778×10^{-4}	5.189×10^{-4}	3.753×10^{-4}	2.734×10^{-4}
0.5	8.066×10^{-4}	5.633×10^{-4}	3.922×10^{-4}	2.899×10^{-4}	2.135×10^{-4}
0.55	5.659×10^{-4}	4.116×10^{-4}	2.952×10^{-4}	2.233×10^{-4}	1.655×10^{-4}
0.6	3.530×10^{-4}	2.653×10^{-4}	1.954×10^{-4}	1.501×10^{-4}	1.123×10^{-4}
0.65	1.447×10^{-4}	1.131×10^{-4}	8.564×10^{-5}	6.652×10^{-5}	4.989×10^{-5}